Vaccines for T Cell Induction in Malignant and Infectious Disease

Dissertation

der Mathematisch-Naturwissenschaftlichen Fakultät
der Eberhard Karls Universität Tübingen
zur Erlangung des Grades eines
Doktors der Naturwissenschaften
(Dr. rer. nat.)

vorgelegt von

M.Sc. Yacine Ileana Maringer

aus Saarbrücken

Tübingen

2023

Gedruckt mit Genehmigung der Mathematisch-Naturwissenschaftlichen Fakultät der Eberhard Karls Universität Tübingen.

Tag der mündlichen Qualifikation:	05.07.2024
Dekan:	Prof. Dr. Thilo Stehle
1. Berichterstatterin:	Prof. Dr. Juliane S. Walz
2. Berichterstatter:	Prof. Dr. Hans-Georg Rammensee
3. Berichterstatter:	Prof. Dr. Oliver Planz
4. Berichterstatter:	Prof. Dr. Markus P. Radsak

Contents

Publications

Nelde A, Schuster H, Heitmann JS, Bauer J, **Maringer Y,** Zwick M, Volkmer J-P, Chen JY, Paczulla Stanger AM, Lehmann A, Appiah B, Märklin M, Rücker-Braun E, Salih HR, Roerden M, Schroeder SM, Häring M-F, Schlosser A, Schetelig J, Schmitz M, Boerries M, Köhler N, Lengerke C, Majeti R, Weissman IL, Rammensee H-G, Walz JS. Immune Surveillance of Acute Myeloid Leukemia Is Mediated by HLA-Presented Antigens on Leukemia Progenitor Cells. ***Blood Cancer Discov*** 2023 OF1-OF22

Heitmann JS, Tandler C, Marconato M, Nelde A, Habibzada T, Rittig SM, Tegeler CM, **Maringer Y,** Jaeger SU, Denk M, Richter M, Oezbek MT, Wiesmüller K-H, Bauer J, Rieth J, Wacker M, Schroeder SM, Hoenisch Gravel N, Scheid J, Märklin M, Henrich A, Klimovich B, Clar KL, Lutz M, Holzmayer S, Hörber S, Peter A, Meisner C, Fischer I, Löffler MW, Peuker CA, Habringer S, Goetze TO, Jäger E, Rammensee H-G, Salih HR, Walz JS**.** Phase I/II trial of a peptide-based COVID-19 T-cell activator in patients with B-cell deficiency. ***Nat Commun****.* 2023 Aug 18;14(1):5032

Hackenbruch C, **Maringer Y,** Tegeler CM, Walz JS, Nelde A, Heitmann JS. Elevated SARS-CoV-2-Specific Antibody Levels in Patients with Post-COVID Syndrome. ***Viruses*** 2023;15(3), 701

Maringer Y,** Nelde A, Schroeder SM, Schuhmacher J, Hörber S, Peter A, Karbach J, Jäger E, Walz JS Durable spike-specific T cell responses after different COVID-19 vaccination regimens are not further enhanced by booster vaccination. ***Sci Immunol. 2022 Nov 1;eadd3899

Bauer J, Köhler N, **Maringer Y,** Bucher P, Bilich T, Zwick M, Dicks S, Nelde A, Dubbelaar M, Scheid J, Wacker M, Heitmann JS, Schroeder S, Rieth J, Denk M, Richter M, Klein R, Bonzheim I, Luibrand J, Holzer U, Ebinger M, Brecht IB, Bitzer M, Boerries M, Feucht J, Salih HR, Rammensee H-G, Hailfinger S, Walz JS. The oncogenic fusion protein DNAJB1-PRKACA can be specifically targeted by peptide-based immunotherapy in fibrolamellar hepatocellular carcinoma. ***Nat Commun.*** 2022 Oct 27;13(1):6401

Marconato M, **Maringer Y,** Walz JS, Nelde A, Heitmann JS. Immunopeptidome Diversity in Chronic Lymphocytic Leukemia Identifies Patients with Favorable Disease Outcome. ***Cancers*** 2022 Sep;*14*(19), 4659

Tegeler CM, Bilich T, **Maringer Y,** Salih HR, Walz JS, Nelde A, Heitmann JS. Prevalence of COVID-19-associated symptoms during acute infection in relation to SARS-CoV-2-directed humoral and cellular immune responses in a mild-diseased convalescent cohort. ***Int J Infect Dis****.* 2022 Jul;120:187-195

Junker D, Becker M, Wagner TR, Kaiser PD, Maier S, Grimm TM, Griesbaum J, Marsall P, Gruber J, Traenkle B, Heinzel C, Pinilla YT, Held J, Fendel R, Kreidenweiss A, Nelde A, **Maringer Y,** Schroeder S, Walz JS, Althaus K, Uzun G, Mikus M, Bakchoul T, Schenke-Layland K, Bunk S, Haeberle H, Göpel S, Bitzer M, Renk H, Remppis J, Engel C, Franz AR, Harries M, Kessel B, Lange B, Strengert M, Krause G, Zeck A, Rothbauer U, Dulovic A, Schneiderhan-Marra N. Antibody binding and ACE2 binding inhibition is significantly reduced for both the BA1 and BA2 omicron variants. ***Clin Infect Dis.*** 2022 Jun 19;ciac498.

Heitmann JS, Bilich T, Tandler C, Nelde A, **Maringer Y,** Marconato M, Reusch J, Jäger S, Denk M, Richter M, Anton L, Weber LM, Roerden M, Bauer J, Rieth J, Wacker M, Hörber S, Peter A, Meisner C, Fischer I, Löffler MW, Karbach J, Jäger E, Klein R, Rammensee H-G, Salih HR, Walz JS. A COVID-19 peptide vaccine for the induction of SARS-CoV-2 T cell immunity. ***Nature*****.** 2022 Jan;601(7894):617-622

Maringer Y, Walz JS. Tumorvakzinierung –Strategien und Timing. ***Internist (Berl).*** 2021 Sep;62(9):991-997. Review.

Bilich T, Roerden M, **Maringer Y,** Nelde A, Heitmann JS, Dubbelaar ML, Peter A, Sebastian Hörber S, Bauer J, Rieth J, Wacker M, Berner F, Flatz L, Held S, Brossart P, Märklin M, Wagner P, Erne E, Klein R, Rammensee H-G, Salih HR, Walz JS. Preexisting and Post-COVID-19 Immune Responses to SARS-CoV-2 in Patients with Cancer. ***Cancer Discov.*** 2021 Aug;11(8):1982-1995

*Nelde A[#], **Maringer Y[#],** Bilich T, Salih HR, Roerden M, Heitmann JS, Marcu A, Bauer J, Neidert MC, Denzlinger C, Illerhaus G, Aulitzky WE, Rammensee H-G, Walz JS. Immunopeptidomics-Guided Warehouse Design for Peptide-Based Immunotherapy in Chronic Lymphocytic Leukemia ***Front Immunol.*** 2021 Jul 8;12:705974

Simnica D, Schultheiß C, Mohme M, Paschold L, Willscher E, Fitzek A, Püschel K, Matschke J, Ciesek S, Sedding DG, Zhao Y, Gagliani N, **Maringer Y,** Walz JS, Heide J, Schulze-Zur-Wiesch J, Binder M. Landscape of T-cell repertoires with public COVID-19-associated T-cell receptors in pre-pandemic risk cohorts. ***Clin Transl Immunology.*** 2021 Aug 28;10(9):e1340

Maringer Y, Walz JS. Tumorvakzinierung –Strategien und Timing. ***Gastroenterologe.*** 2021 Jun; 16:241-248. Review.

Bilich T, Nelde A, Heitmann JS, **Maringer Y,** Roerden M, Bauer J, Rieth J, Wacker M, Peter A, Hörber S, Rachfalski D, Märklin M, Stevanović S, Rammensee H-G, Salih HR, Walz JS. T cell and antibody kinetics delineate SARS-CoV-2 peptides mediating long-term immune responses in COVID-19 convalescent individuals. ***Sci Transl Med.*** 2021 Apr 21;13(590):eabf7517

Nelde A, Bilich T, Heitmann JS, **Maringer Y,** Salih HR, Roerden M, Lübke M, Bauer J, Rieth J, Wacker M, Peter A, Hörber S, Traenkle B, Kaiser PD, Rothbauer U, Becker M, Junker D, Krause G, Strengert M, Schneiderhan-Marra N, Templin MF, Joos TO, Kowalewski DJ, Stos-Zweifel V, Fehr M, Rabsteyn A, Mirakaj V, Karbach J, Jäger E, Graf M, Gruber L-C, Rachfalski D, Preuß B, Hagelstein I, Märklin M, Bakchoul T, Gouttefangeas C, Kohlbacher O, Klein R, Stevanović S, Rammensee H-G, Walz JS. SARS-CoV-2-derived peptides define heterologous and COVID-19-induced T cell recognition. ***Nat Immunol.*** 2021 Jan;22(1):74-85

* The publication is presented in this thesis.

[#] The first authorship is shared and the authors contributed equally to this work.

Summary

For centuries, vaccines have played an important role to induce protective immune responses against infectious diseases. Over the past decade, therapeutic vaccines have been developed to direct the immune system against cancer cells. Whereas, prophylactic vaccination focusses largely on the induction of pathogen-specific B-cell derived antibodies, therapeutic vaccination mainly aims to induce cancer-specific T cell responses. With the COVID-19 pandemic, T cells have however also gained increasing significance in infectious disease.

In this thesis, characterization of antigen-specific T cell responses was applied to (i) define a peptide warehouse for clinical application in chronic lymphocytic leukemia (CLL), (ii) to develop an optimized protocol for $CD4^+$ T cell priming using monocyte-derived dendritic cells (MoDCs) and (iii) to uncover Severe Acute Respiratory Syndrome Coronavirus 2 (SARS-CoV-2) spike-specific T cell responses following different Coronavirus disease 2019 (COVID-19) vaccination regimens.

(i), Naturally and frequently presented CLL-specific human leukocyte antigen (HLA)-restricted peptides were identified by comparative mass spectrometry-based immunopeptidome analyses of primary patient samples. The resulting CLL-specific antigens were shown to be recognized by preexisting, and *de novo* induced T cells in CLL patients and healthy volunteers, respectively. This tumor antigen selection process allowed for the generation of a premanufactured warehouse for the construction of personalized HLA class I- and HLA class II-restricted multi-peptide vaccines that are being evaluated in a first clinical trial for the treatment of CLL (NCT04688385). The presented workflow may provide the basis for the development of broad personalized T cell-based immunotherapy approaches as it is easily transferable to other tumor entities.

(ii) To prove immunogenicity of HLA class II-restricted peptides, the second chapter of this thesis focused on the optimization of the *de novo* priming of $CD4^+$ T cells using MoDCs. A preliminary protocol was available in our group; however, it was not yet set up functionally. Through modifications in the MoDC maturation cocktail, the time of MoDC coincubation with peptides and the setup for the $CD4^+$ T cell stimulation with MoDCs, successful *de novo* priming of specific $CD4^+$ T cells was achieved for all tested peptides and donors.

(iii) With the COVID-19 pandemic, several vaccines were rapidly developed to protect the population against severe disease outcome after infection with SARS-CoV-2. The last chapter of this thesis focused on the characterization of induced T cell responses after vaccination with different vaccination regimens after 4 weeks and 6 months, as well as the effect of a booster vaccine dose compared with SARS-CoV-2 T cell responses in convalescents and prepandemic donors. Frequent, divers and multifunctional spike-specific T cell responses were shown for donors of all vaccination regimens that

were comparable to responses seen in convalescent donors and were significantly increased compared to cross-reactive T cell responses in prepandemic donors. T cell responses remained stable over time and did not significantly benefit from a booster vaccination dose. However, after decreasing over 6 months after vaccination, anti-spike antibody titers significantly increased through the application of a booster vaccine dose.

Together, within this thesis, an extensive analysis was conducted to characterize antigen-specific T cell responses within the frame of both prophylactic and therapeutic vaccination, providing a comprehensive elucidation of cellular immune responses pertaining to diverse COVID-19 vaccine schedules as well as the validation of a peptide warehouse facilitating its prospective evaluation in a therapeutic vaccine trial for CLL patients.

Zusammenfassung

Impfstoffe spielen seit Jahrhunderten eine wichtige Rolle, um schützende Immunreaktionen gegen Infektionskrankheiten auszulösen. In den letzten zehn Jahren wurden therapeutische Impfstoffe als entwickelt, um das Immunsystem gegen Krebszellen zu richten. Während sich die prophylaktische Impfung weitgehend auf die Induktion erregerspezifischer Antikörper konzentriert, zielt die therapeutische Impfung hauptsächlich auf die Induktion krebsspezifischer T-Zell-Antworten ab. Mit der COVID-19 Pandemie haben T-Zellen jedoch auch gegen Infektionskrankheiten zunehmend an Bedeutung gewonnen.

In dieser Arbeit wurde die Charakterisierung Antigen-spezifischer T-Zell-Antworten genutzt, um (i) ein Peptid-Warenhaus für die klinische Anwendung bei chronischer lymphatischer Leukämie (CLL) zu definieren, (ii) ein optimiertes Protokoll für das Priming von $CD4^+$ T-Zellen unter Verwendung von Monozyten-abgeleiteten dendritischen Zellen (MoDCs) zu entwickeln und (iii) Schweres Akutes Respiratorisches Syndrom-Coronavirus-2 (SARS-CoV-2) spike-spezifische T-Zell-Antworten nach verschiedenen Impfschemata gegen die Coronavirus-Krankheit-2019 (englisch Coronavirus Disease 2019, COVID-19) aufzudecken.

(i) Durch vergleichende massenspektrometrische Immunopeptidomanalysen von primären Patientenproben wurden natürlich und häufig vorkommende, auf humane Leukozytenantigene (HLA) präsentierte Peptide identifiziert, die für CLL spezifisch sind. Die daraus resultierenden CLL-spezifischen Antigene wurden sowohl von bereits vorhandenen als auch von *de novo* induzierten T-Zellen bei CLL-Patienten bzw. gesunden Freiwilligen erkannt. Dieses Verfahren zur Auswahl von Tumorantigenen ermöglichte die Erstellung eines vorgefertigten Warenhauses für die Generierung von personalisierten HLA-Klasse-I- und HLA-Klasse-II-restringierten Multi-Peptid-Impfstoffen, die in einer ersten klinischen Studie zur Behandlung von CLL untersucht werden (NCT04688385). Der hier vorgestellte Arbeitsablauf könnte die Grundlage für die Entwicklung einer breit angelegten personalisierten T-Zell-basierten Immuntherapie bilden, da er leicht auf andere Tumorentitäten übertragbar ist.

(ii) Zum Nachweis der Immunogenität von HLA-Klasse-II-restringierten Peptiden lag der Fokus des zweiten Kapitels dieser Arbeit auf der Optimierung des *de novo* Primings von $CD4^+$ T-Zellen unter Verwendung von MoDCs. In unserer Gruppe stand ein vorläufiges Protokoll zur Verfügung, das jedoch noch nicht funktionell anwendbar war. Durch die Optimierung des MoDC-Reifungscocktails, der Dauer der Koinkubation von MoDCs mit Peptiden und des Setups für die Stimulation von $CD4^+$ T-Zellen mit MoDCs konnte für alle getesteten Peptide und Spender ein erfolgreiches *de novo* Priming spezifischer $CD4^+$ T-Zellen erreicht werden.

(iii) Nach dem Ausbruch der COVID-19-Pandemie wurden in kurzer Zeit mehrere Impfstoffe entwickelt, um die Bevölkerung vor schweren Krankheitsfolgen nach einer Infektion mit SARS-CoV-2 zu schützen. Das letzte Kapitel dieser Arbeit befasste sich mit der Charakterisierung der induzierten T-Zell-Reaktionen nach der Impfung mit verschiedenen Impfschemata nach 4 Wochen und 6 Monaten sowie mit der Wirkung einer Auffrischungsimpfstoffdosis im Vergleich zu den SARS-CoV-2-T-Zell-Reaktionen bei Rekonvaleszenten und präpandemischen Spendern. Bei Spendern aller Impfschemata wurden häufige, vielfältige und multifunktionale spike-spezifische T-Zell-Antworten nachgewiesen, die mit den bei rekonvaleszenten Spendern beobachteten Antworten vergleichbar waren und im Vergleich zu den kreuzreaktiven T-Zell-Antworten bei präpandemischen Spendern signifikant erhöht waren. Die T-Zell-Reaktionen blieben im Laufe der Zeit stabil und profitierten nicht signifikant von einer Auffrischungsimpfung. Nachdem die T-Zell-Antworten über 6 Monate nach der Impfung abgenommen hatten, stiegen die Anti-Spike-Antikörper Titer jedoch durch eine Auffrischungsimpfung signifikant an.

Im Rahmen dieser Arbeit wurde eine umfassende Analyse zur Charakterisierung der antigenspezifischen T-Zell-Antworten sowohl im Rahmen einer prophylaktischen als auch einer therapeutischen Impfung durchgeführt. Dies ermöglichte eine umfassende Aufklärung der zellulären Immunantworten im Zusammenhang mit verschiedenen COVID-19-Impfschemata sowie die Validierung eines Peptid-Warenhauses, das dessen prospektive Bewertung in einer therapeutischen Impfstoffstudie für CLL-Patienten erleichtert.

Introduction

The immune system

The human body is constantly confronted with cellular alterations and pathogens able to induce disease. The immune system, with its many different cell types and molecules, is responsible for the protection against malignancies and pathogen-induced infections. To successfully defend the body, the immune system orchestrates the detection of the pathogens or altered cells followed by a protective response, synergistically mediated by the innate and adaptive immunity (*1, 2*).

The innate immunity provides the first line of defense against a variety of pathogens, such as viruses, bacteria, and fungi. It reacts rapidly within minutes to hours, but therefore has the disadvantage of being pathogen-unspecific in its response. The innate immune system includes physical (e.g., the skin, mucosal membranes) and chemical barriers (e.g., lysozyme, defensins in body fluids), the complement system, lymphoid cell recruitment to the site of infection through chemokines and cytokines, and their activation following pathogen detection through conserved pattern recognition (*3*).

The adaptive immune system is crucial to target arising malignant cells or pathogens that overcame the innate immune system. Whereas, the adaptive immune response requires more time, it is very specific, can recognize a broader spectrum of pathogens and alterations, and is able to develop an immunologic memory, leading to a faster response in case of re-exposure. The main acting components of the adaptive immune system are the B and T lymphocytes. Following maturation in the bone marrow, B cells express unique B cell receptors (BCR) and are activated once their specific antigen is detected. Subsequently, proliferation is induced as well as the differentiation into memory B cells and antibody-producing plasma cells. Due to their ability to produce antibodies, B cells are key players of the humoral immune response. T cells on the other hand are the important players of the cell-mediated immune response. They originate from the bone marrow and mature in the thymus. T cells are activated and able to rapidly proliferate when a specific antigen-derived peptide, presented by an antigen-presenting cell (APC) or an infected cell, is recognized by the T cell receptor (TCR) (*4, 5*).

For successful antigen presentation to the T cells, cells express surface proteins called major histocompatibility complex (MHC), in humans also known as human leukocyte antigen (HLA). HLA molecules can be divided into two categories due to their structure and functionality: HLA class I (including HLA-A, HLA-B, and HLA-C) present peptides from endogenous proteins and are expressed by every nucleated cell (*6*), while HLA class II molecules (including HLA-DP, HLA-DQ and HLA-DR) present peptides originating from exogenous antigens and are traditionally described to be expressed on professional APCs (*7*). For enhanced diversity all individuals carry two allelic variants, also known as

allotypes, for each of the HLA class I and HLA class II genes. The different HLA allotypes allow for the binding of peptides with different sequence motifs defined by specific anchor amino acids (aas) (*5, 8*).

HLA class I molecules are composed of a three-domain heavy chain and a β_2-microglobulin light chain. The molecules are loaded with antigenic peptides of 8-12 aas derived from proteasomal degradation of cytoplasmic proteins in the endoplasmatic reticulum and transported to the cell surface, where they can be recognized by peptide-specific TCRs of $CD8^+$ cytotoxic T lymphocytes (CTLs; Fig.1). HLA class II molecules on the other hand are heterodimers formed by the α and the β chain. Following exogenous antigen endocytosis and fusion with a lysosome, the antigen is cleaved by proteases. The resulting peptide containing vesicles fuse with vesicles containing HLA class II molecules that are blocked by an invariant chain. The peptides (generally 9-25 aas) then take the place of the invariant chain and fold into the HLA binding groove. The now loaded MHC class II molecules in the vesicles are transported to and fuse with the cell membrane (Fig. 1). This HLA class II-peptide complex is recognized by the TCR of $CD4^+$ T helper (T_H) cells (*5, 9, 10*).

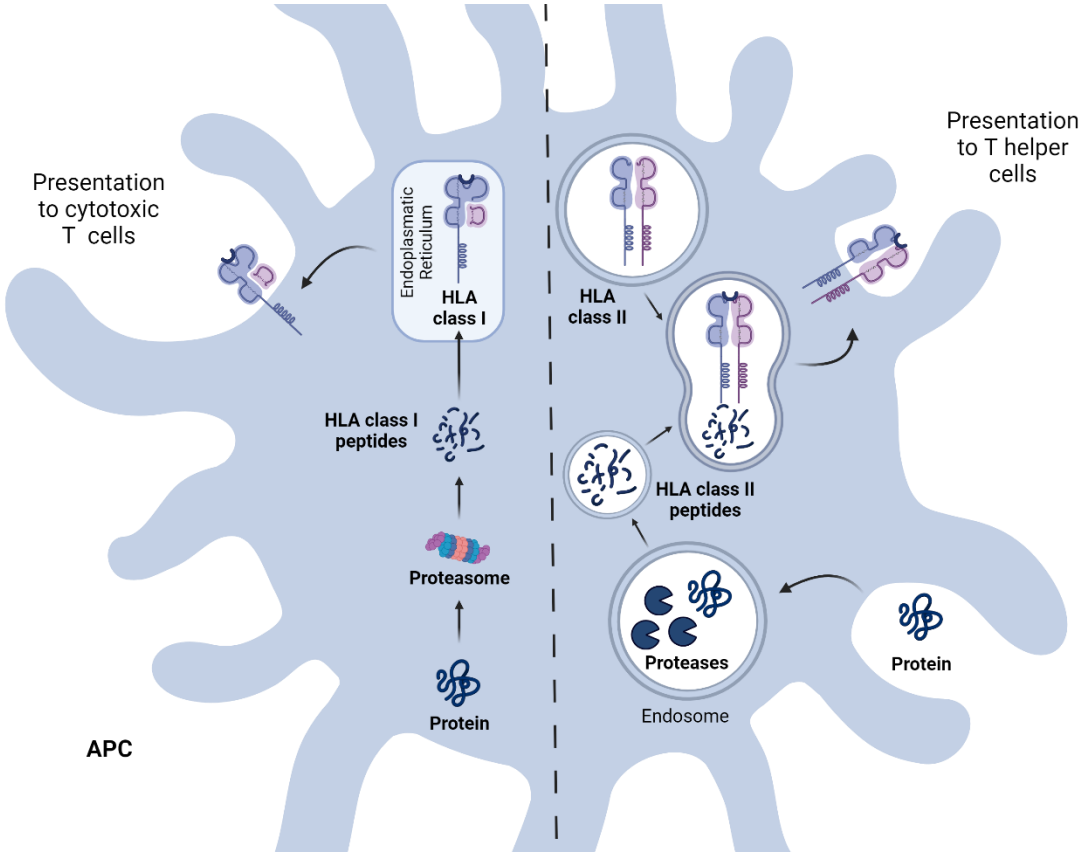

Figure 1: Protein processing and peptide loading onto HLA class I and HLA class II molecules. Endogenous proteins are degraded into short peptides by proteasomes and loaded onto human leukocyte antigen (HLA) class I molecules then transported to the antigen presenting cell (APC) surface for antigen presentation to cytotoxic T cells. Extracellular proteins are engulfed and cleaved into peptides by proteases in the endosome. After the fusion with compartments containing HLA class II, the peptides are loaded onto the molecules and transported to the cell surface for presentation to T helper cells. This figure was created with BioRender.

For successful activation, T cells require several signals from APCs, such as dendritic cells (DCs). The first signal is the antigen recognition of HLA-presented peptides by specific TCRs. The second signal is mediated by the interaction of co-stimulatory molecules, such as CD28 present on the T cell surface with CD80 or CD86 found on the surface of APCs (*1*). The final signal essential for T cell activation is obtained through cytokine secretion (e.g., type I interferons (IFNs) and interleukin (IL)-12) of the APCs (*11*). Once all three signals are present, T cells can proliferate and differentiate into the different effector phenotypes, which mediate immune regulation and cytotoxicity (Fig. 2).

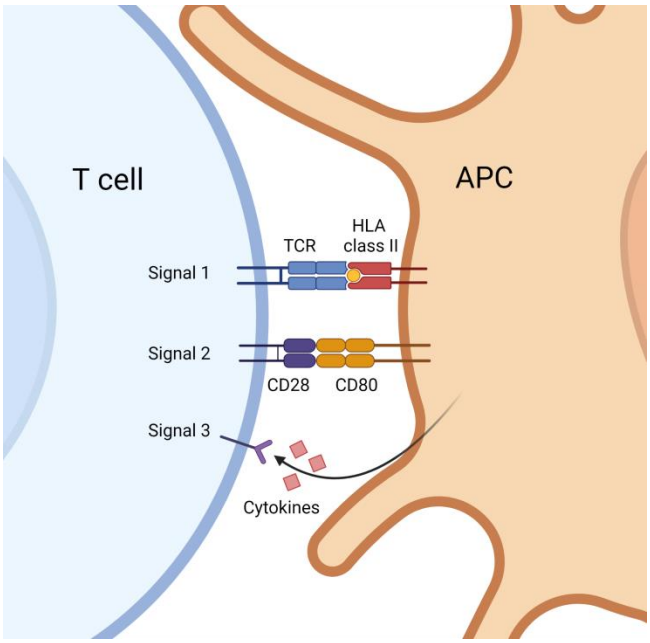

Figure 2: Three signals are required for T cell activation. The first signal consists of the interaction of the T cell receptor (TCR) with the peptide-loaded human leukocyte antigen (HLA) molecule and is the main activating signal. Costimulatory molecules, such as CD28 on T cells and CD80 on antigen presenting cells (APC) make up the secondary signal required for cell survival. The third signal necessary for T cell differentiation is mediated by cytokines (e.g., IL-12) released by the APC and sensed by the T cell. This figure was created with BioRender.

Immune response to malignant and infectious diseases

Tumor immunology

Cancer is the most frequent cause of human death after cardiovascular diseases, with continuously increasing numbers of newly diagnosed patients every year due to changing demographics and environmental factors. Cancer originates from malignant cellular transformation followed by uncontrollable proliferation and is driven by either endogenous or exogenous factors. Endogenous causes arise through genome instability at cellular and molecular level, while exogenous mutagens include environmental factors such as alcohol, smoking and obesity as well as virus infections (e.g., human papilloma virus) and ionizing radiation (*12*). The “hallmarks of cancer” as postulated by Hanahan consist of ten main physiological changes and requirements for tumorigenesis. The latter comprise sustaining proliferative signaling, evading growth suppressors, deregulating cellular

metabolism, resisting cell death, enabling replicative immortality, inducing or accessing vasculature, activating invasion and metastasis, avoiding immune destruction, genome instability and mutation, and tumor promoting inflammation (*13*).

First observations in the field of tumor immunology were made in 1900 by Paul Ehrlich, postulating that the body possesses a safety mechanism able to recognize and eliminate pathogens and malignant cells (*13, 14*). Almost 50 years later, Burnet and Thomas proposed the concept of immunosurveillance describing that "small accumulations of tumor cells" could be recognized and eliminated by the immune system (*15, 16*). This theory was later confirmed and extended by Dunn et al., who introduced the concept of immunoediting (*17*). The latter comprises three stages: elimination, equilibrium and escape. The elimination phase corresponds to the above mentioned immunosurveillance, where the immune system can efficiently defend against malignancies. However, single mutated cells overcome that process and evade the anti-tumor immune response. The equilibrium phase can last for years, while some tumor-cell precursors are eliminated, others more resistant to the immune system can arise. During the escape phase, the resistant cells that cannot be contained by the immune system start proliferating uncontrollably.

Immunotherapy for malignant disease

Once cancer is diagnosed several therapies are available for treatment. The three classical "pillars" of cancer therapy include i) surgery, ii) radiation therapy and iii) chemotherapy. i) Surgery arose after the invention of anesthesia in 1846 and was the first therapeutic method to remove entire tumors together with the lymph nodes; its success however was limited by cancer metastasis (*18*). ii) Radiation therapy was used for cancer diagnosis and treatment following the "X-ray" discovery by Roentgen in the late 19th century (*19*). iii) Chemotherapy is cytotoxic for neoplastic cells, but its success is limited by drug resistance of the tumor cells (*20*). Those three treatment methods are often applied in combination, and chemotherapy as well as radiation approaches have greatly improved since their first therapeutic application. However, the lack of specificity is a major disadvantage, and the accompanying off-target damage of healthy tissues inevitably causes strong side effects in already weak patients (*21*).

Immunotherapy makes the fourth pillar of cancer therapy. Research advances in the field of immunology have allowed for new ways to direct immune responses against cancer to avoid off-target effects. Several classes of immunotherapies are available that include i) cytokines, ii) monospecific and bispecific antibodies, iii) immune checkpoint inhibitors (ICI), iv) engineered T cells (e.g., chimeric antigen receptor (CAR) T cells), and v) cancer vaccines (*22*). i) The application of the recombinant cytokine IFN-α was the first kind of immunotherapy used in the clinics for the treatment of hairy cell

leukemia, followed by recombinant IL-2 for metastatic renal cancer. Cytokines induce lymphocyte activation and directly limit tumor growth through their anti-proliferative or pro-apoptotic activity (*23*). The exclusive application of cytokine has shown limited success and is therefore often combined with other immunotherapeutic approaches. ii) Monospecific antibodies, such as the anti-CD20 antibody Rituximab used for the treatment of B-cell malignancies, first approved in 1997, can mediate complement-dependent cytotoxicity and antibody-dependent cellular cytotoxicity once binding their target molecule (*24, 25*). Bispecific antibodies mainly intend to direct T cells to tumor cells by binding an extracellular molecule of the T cell as well as an antigen on the tumor cell surface thereby facilitating tumor recognition and T cell activation (*26*). The first approved bispecific antibody was Blinatumomab for the treatment of acute lymphoblastic leukemia that combines binding of CD3 on T cells with binding to CD19 expressed on B cells (*27*). iii) ICI are immunomodulators able to block the immune checkpoints such as programmed cell death 1 protein (PD-1) and cytotoxic T lymphocyte-associated protein 4 (CTLA-4). The first approved checkpoint inhibitor was Ipilimumab, an anti-CTLA-4 monoclonal antibody, followed by the monoclonal antibodies Pembrolizumab and Nivolumab targeting PD-1 (*28*). iv) Engineered T cells are autologous T cells from a patient that are isolated and either genetically modified for improved tumor recognition, e.g., anti-CD19 CAR T cells, or simply expanded *in vitro*, e.g., TIL (tumor infiltrating lymphocyte) cell therapy for melanoma, before being transferred back to the patients (*23, 29*). v) Cancer vaccines include several methods to prime the immune system to recognize tumor antigens and will be addressed in more detail later in this introduction.

Most immunotherapeutic approaches depend on the identification and selection of suitable tumor antigens, which can be either i) HLA-independent or ii) HLA-dependent. i) HLA-independent tumor antigens are generally molecules that are overexpressed or expressed exclusively on the surface of malignant cells, e.g. CD19 or CD20 in B cell malignancies. These antigens are relevant as targets for therapeutic approaches such as monospecific or bispecific antibodies as well as CAR T cells (*30*). ii) The HLA-dependent tumor antigens are presented as peptides on malignant cells via HLA. Such antigens should ideally be tumor specific, *i.e.*, not presented on healthy somatic cells. Furthermore, they must be recognized by T cells in order to induce a strong T cell response in the patient. Tumor antigens can be divided into three groups: 1. Tumor-associated antigens (TAAs) from non-mutated gene products that arise in tumor cells through altered gene expression or protein processing (*31, 32*). 2. Neoantigens derived from tumor-specific mutations (*32, 33*) and 3. Oncoviral antigens derived from viral proteins that exhibit oncogenic properties (*32*).

Different strategies are available for the identification of tumor antigens. Whereas, the so-called reverse immunology, based on genome and transcriptome analyses (*34*), predicts algorithm-based HLA-presented tumor antigens, the isolation of HLA ligands and their mass-spectrometric analysis (the

so-called immunopeptidome analysis) allows for a direct investigation of tumor antigens on the cell surface (*35*). Since numerous studies in recent years have shown that changes at the genome or transcriptome level are not directly reflected in the immunopeptidome (*36*), a direct identification of the HLA-presented antigens provides insights on the natural occurrence of the targets for immunotherapeutic approaches on the tumor cells.

Neoantigens are relevant since they are completely tumor exclusive and peripheral tolerance has no influence on the T cells recognizing these antigens (*37*). Peripheral tolerance is the suppression of an immune response to self-antigens, which serves to prevent autoimmune diseases (*5*) but also hinders cancer immunity. However, the disadvantage of neoantigens is, on the one hand, their individual, patient-specific presentation (*38*), since only a few tumor entities have a universal mutation pattern. On the other hand, only a fraction of tumor-specific mutations is presented as neoantigens via HLA molecules on the cell surface and is therefore visible and targetable by the immune system (*36*). In contrast to neoantigens and oncoviral antigens that are highly immunogenic as foreign antigens (*39*), non-mutated TAAs usually require the addition of adjuvants or costimulants to overcome the peripheral tolerance of T cells to these overexpressed tumor antigens (*40*).

Immunology of infectious disease

Pathogens spread through different modes of transmission, such as for example droplet spread (e.g., common cold), bodily fluids (e.g., human immunodeficiency virus (HIV)) or spores (e.g., Bacillus anthracis) (*41, 42*). Mucosal surfaces are the most abundant point of entry for those pathogens that can either colonize on epithelial surfaces after adhesion or pass through them to infect the underlying tissues. While many microorganisms are cleared by the innate immune response, the adaptive immune system takes over once the innate defenses are overpowered to induce a stronger, more pathogen-specific response to prevent pathogen spreading or even acute infection. The innate immune system keeps supporting the adaptive immune response by presenting pathogen-specific antigens and generating an inflammatory milieu through the production of cytokines. To resolve an infection, phagocytes and opsonizing antibodies clear extracellular infectious particles, while effector T cells remove intracellular infectious residues (*1, 5*).

After an effective adaptive immune response, most pathogen-induced infections resolve without enduring pathology. Nevertheless, some infectious agents can persist and establish latency, giving them the ability to resurface once the immune system is weakened or in response to different stimuli (*5, 43*). This is observed for the Herpes simplex virus type 1 for example, that replicates in mucosal epithelial cells following first infection, then infiltrates sensory neurons, and ultimately persists latently in neuronal cell bodies invisible to the patrolling immune system (*44*).

To clear the body from a pathogen, the interplay of both effector mechanisms, the cellular and the humoral response of the adaptive immune system, is required. The induction of antibody secretion is important in removing viruses and preventing them from entering host cells (*5*). In case of Ebola virus infected patients for example, an early and strong antiviral antibody response is crucial for survival, irrespective of T cell responses (*45*). In other cases, such as for *Mycobacterium tuberculosis* that resides inside infected macrophages, T cells are essential for pathogen clearance (*46*). Determining which of the effector mechanisms plays a greater role in host protection against different pathogens is paramount for protective measures, such as immunization to prevent infection.

Vaccination in malignant and infectious diseases

For centuries, vaccinations have played an essential role in the prevention of infectious diseases by training the adaptive immune system, generally B cells that produce antibodies, to recognize and clear certain pathogens (*5*). Nowadays, this principle is also used to specifically induce T cells that target tumor cells (*47*). An important role is attributed to the HLA molecules presenting peptides from intracellular and extracellular foreign or altered proteins, e.g., in the case of an infection or in a tumor cell. In general, tumor vaccines are therapeutic, whereas vaccines for infectious diseases are prophylactic (*48*).

Historically, to develop vaccines for the prevention of infectious diseases, researchers screened for organisms with attenuated pathogenicity (e.g., rabies vaccine), or used neutralized organisms (e.g., polio vaccine), trying to induce a protective immune response thus avoiding disease contraction. Later on, vaccines were applied using more processes including inactivated toxins (e.g., bacterial), viral vectors, subunit and conjugate vaccines (containing a part of the target pathogen). Nowadays, many different vaccination concepts are available to administer the selected infectious and malignant disease antigens for specific stimulation of the immune system (*5, 49*).

Ribonucleic acid vaccines

One possible delivery vehicle for tumor and infectious disease antigens is through messenger RNA (mRNA) vaccination. The mRNA, encoding the corresponding antigens, can be injected using carriers, such as lipid nanoparticles, to improve stability (*50*). These can be taken up by APCs through endocytosis. In the successfully transfected cells, the RNA is translated and transcribed to the encoded target antigens. The antigens are then further processed into peptides by the cells and presented to T cells via HLAs, resulting in an antigen-specific immune response (*51*). RNA does not migrate into the nucleus but remains in the cytoplasm of the cells, thus it cannot be integrated into the genome, which minimizes the risk of vaccine-induced cell degeneration. RNA vaccines are easy and relatively inexpensive to produce and therefore offer the possibility of personalized vaccine production (*51, 52*).

One example for targeting malignant disease, is a personalized neoantigen-based RNA vaccine that is being tested in patients with locally advanced or metastatic tumors in combination with the ICI Atezolizumab in a phase I trial (NCT03289962). After the start of the COVID-19 pandemic at the end of 2019, the first mRNA vaccine was available under emergency use authorization in December 2021 (*53*), encoding for the prefusion-stabilized spike protein of SARS-CoV-2 (*54, 55*).

Vector-based vaccines

To make use of the natural immunogenicity of viruses, replication-incompetent virus vectors can be engineered to infect APCs to make them express either tumor antigens or infectious disease proteins. Through the subsequent presentation of tumor or infectious disease antigens to the immune system, antigen-specific B and T cells can be induced to combat tumor cells or prevent infection. Several viruses have been engineered for use as vectors over the past years, including adenoviruses, poxviruses, cytomegaloviruses, herpesviruses, and retroviruses (*56-58*). A current example for the application of a vector-based vaccine approach in cancer is a clinical trial evaluating a chimpanzee adenovirus vector encoding 20 patient-specific tumor neoantigens for patients with advanced solid tumors (NCT03639714). Vector-based vaccines were also broadly applied to combat COVID-19, with the use of the AZD1222 chimpanzee adenovirus-vector vaccine that expresses the spike protein gene of SARS-CoV-2 (*59*).

Peptide-based vaccines

Peptide vaccination, *i.e.*, the direct application of HLA-presented tumor- or pathogen-specific antigens, offers several advantages. Firstly, the peptides, which are only 9-20 amino acids long, are easy and inexpensive to produce, and secondly, no additional processing of the peptides needs to take place in the patient. Multiple peptides can be applied simultaneously to cover multiple tumor or pathogenic antigens and prevent a so-called "immune escape" due to loss of individual antigens (*60*). Since each person expresses individual HLA molecules, it should be noted that the peptide selection must be adapted to the patient-individual HLA allotypes. In addition to the production of vaccines restricted to certain HLA allotypes, there is the possibility of a completely personalized vaccine, *i.e.*, each patient receives a personalized peptide mixture. Pre-produced peptide warehouses according to a modular system allow for a cost-effective and less time-consuming assembly of completely individualized vaccines (*61, 62*). Both HLA class I- and class II-restricted peptides can be included in the vaccine formulation, and a combination of both is possible and reasonable to activate both cytotoxic and helper T cells equally and provide an efficient immune response (*60*). Multivalent long peptide sequences can also be vaccinated which can be further processed *in vivo* by APCs to both HLA class I and class II epitopes.

The efficacy of a peptide vaccine depends strongly on the adjuvant administered together with the selected antigens, since peptides alone show poor immunogenicity (*63*). The role of an adjuvant includes protection of the peptide and prevention of immediate degradation, efficient uptake by APCs, and activation of APCs for optimal subsequent antigen-specific T cell activation and expansion (*60*). The prevention of early degradation of the peptide can be achieved by application in oil solutions, liposomes, or nanoparticles. Commonly used adjuvants that optimize peptide uptake and activation of APCs are granulocyte-macrophage colony-stimulating factor (GM-CSF) as well as Toll-like receptor agonists (*60*).

Peptide-based vaccination concepts have been evaluated in recent years for numerous tumor entities and viral diseases (*61, 64, 65*). A wide variety of peptide antigens and adjuvants have been used. For example, studies in melanoma and glioblastoma investigating the use of personalized peptide vaccines based on neoepitopes demonstrated the induction of strong T cell responses and first indications of clinical efficacy (*61, 62*). In addition, a phase I peptide vaccination study using an HLA-A*02-restricted peptide derived from IDO5 demonstrated long-lasting disease stabilization in patients with metastatic non-small cell lung cancer (*66*). For viral diseases, such as Influenza and COVID-19, strong induction of T cell responses that are essential for disease control were observed in several studies (*64, 65*).

Specific considerations on therapeutic cancer vaccines

Vaccines for the prevention of infectious diseases are generally highly immunogenic and are usually administered to healthy people. For tumor vaccines however, the immunogenicity is reduced and the immune system of the patients receiving the vaccine is often weakened. Therefore, in addition to the selection of optimal tumor antigens, adjuvants, and application strategies, the timing of application in the context of tumor treatment is crucial for the success of tumor vaccines.

An optimal effector-to-target cell ratio is central for vaccine efficacy in malignant disease. Meaning that sufficient functional T cells must be available to eliminate the tumor cells present (*67*). In particular, the adjuvant situation in which a large proportion of tumor cells have been eliminated after previous surgery, chemotherapy, or radiation, is a promising setting (*68, 69*). Activation of the patient's immune system after vaccination can combat residual tumor cells and thus prevent recurrence. Regarding the required functionality of the immune system, the general immunosuppression caused by the tumor, but also the immunosuppressive effects of many tumor therapies should be considered. Radiation and chemotherapy, for example, have been described to reduce T cell populations by up to 80% (*70, 71*). In this case, a sufficient time interval between initial neoadjuvant treatment and immunotherapy, an assessment of the immune status prior to vaccination are necessary. Over the past

years, combinatorial approaches have been gaining research interest, using immunostimulatory agents or ICI together with cancer vaccines (*72, 73*).

Tumor vaccination offers the potential of targeted immunotherapy allowing for personalization with few side effects. Especially in the adjuvant setting after initial reduction of tumor burden, tumor vaccines can make a decisive contribution to cancer therapy and prevention of recurrences in the future. Furthermore, an optimized selection of suitable tumor antigens, adjuvants, and application strategies will improve the clinical efficacy of tumor vaccines in the future and enable their introduction into clinical routine.

Malignant and infectious diseases addressed in this thesis

Chronic lymphocytic leukemia (CLL)

CLL is a hematological malignancy that affects the lymphoid lineage and is one of the most common types of leukemia. CLL commonly affects elderly patients with a median age of onset of 70 years, and males are more susceptible than females. The disease is characterized by the accumulation and clonal proliferation of mature $CD5^+$ B cells in the blood, lymph nodes, and bone marrow (*74*). The 5-year survival rate has improved to 86.1 % due to novel treatment methods and is higher than for most other cancer types (*75*).

Chromosomal alterations are often observed in CLL patients, with around 80% of patients carrying a trisomy 12 or deletions in chromosome 13 (del(13q14), approx. 55% of patients), 11 (del(11q)) or 17 (del(17p)). High-risk patients include patients with TP53 mutation and del(17p) mutations. Another mutation that is relevant in CLL patients affects the immunoglobulin heavy-chain variable region gene (IGHV). Patients with leukemic clones that have a mutated IGHV (M-CLL), have an improved prognosis compared to patients with unmutated IGHV (U-CLL) clones (*76*).

Two clinical staging models are available for CLL called Rai and Binet classification. Both describe three prognostic groups with low-, intermediate- and high-risk disease. However, nowadays, the CLL International Prognostic Index (CLL-IPI), integrating genetic alterations, has become the most important prognostic score, using four categories with different 5-year overall survival (OS). For the low-risk group treatment-free monitoring is indicated (watch and wait strategy) with a 5-year OS of 93.2%. The intermediate-risk group has a 5-year OS of 79.3% and is not recommended to receive treatment except for highly symptomatic cases. For the high-risk group with a 5-year OS of 63.3%, therapeutic intervention is recommended with the exception for asymptomatic cases. And finally, the very high-risk group with a low 5-year OS of 23.3% is advised to be treated using novel antibody or small molecule approaches instead of chemotherapy (*74, 77*).

Standard therapy changed from conventional chemoimmunotherapy regimens to inhibitors that directly inhibit CLL cell signaling, such as the Bruton's tyrosine kinase (BTK) inhibitor Ibrutinib (*77, 78*). This change led to increased OS, however many patients still experience relapse originating from few persisting CLL cells, also known as minimal residual disease (MRD). Many trials are ongoing to find a curative treatment by eliminating MRD to further increase life-expectancy while maintaining life-quality.

Severe acute respiratory syndrome coronavirus 2 (SARS-CoV-2)

SARS-CoV-2 emerged in December 2019 causing a global pandemic with unprecedented transmission. The positive-sense single-stranded ribonucleic acid (RNA) virus belonging to the family of coronaviruses, expresses spike proteins on its surface that are essential for host cell penetration by binding to the angiotensin-converting enzyme 2 (ACE2) receptor expressed in human cells in various tissues (*79*). Following receptor binding and cellular infiltration, the virus seizes control of the host's cellular machinery to further replicate and spread to surrounding cells (Fig. 3) (*80*).

The associated coronavirus disease 2019 (COVID-19) leads to symptoms that resemble common cold symptoms, such as fever, sore throat, shortness of breath, cough, and fatigue, but also unique symptoms including loss of taste or smell. Increased neutrophil counts and reactive oxygen species release, cytokine release syndrome, as well as higher antibody titers targeting different components of SARS-CoV-2 have been shown to be associated with severe COVID-19 cases (*81*). Severe disease can lead to pneumonia and acute respiratory distress syndrome (ARDS) that are potentially followed by organ failure and death (*82*). High-risk individuals include the elderly, as well as people with underlying medical conditions including diabetes, immunosuppression and heart conditions (*83*).

Many public health measures were taken to reduce the spread of SARS-CoV-2 such as the mandatory wearing of a medical face mask (*84*), and social distancing (*85*). In order to treat patients with severe COVID-19 or avoid severe disease in high risk groups, the Food & Drug Administration (FDA) approved drugs such as Remdesivir, targeting the RNA polymerase and thereby inhibiting viral RNA transcription, or Paxlovid, inhibiting the SARS-CoV-2 main protease and subsequently viral replication (*86*). Great progress was made in vaccine development, leading to the approval of first vaccines targeting the spike protein of SARS-CoV-2 with new technologies one year after the outbreak. These vaccines were broadly applied and approved to reduce COVID-19 severity, transmission, and infection (*87*). Despite the great achievements through vaccination and treatment options, it is still crucial to understand the nature of the immune responses against SARS-CoV-2 after vaccination and infection.

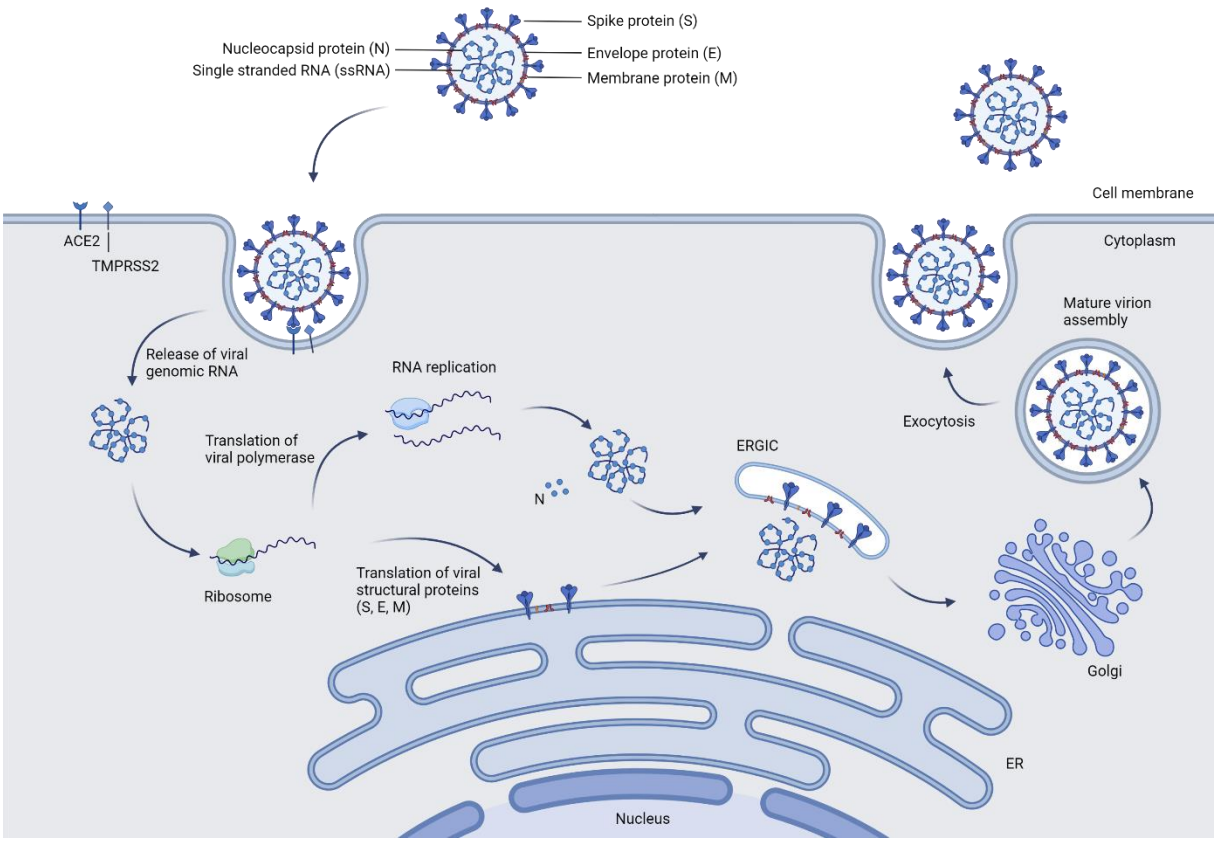

Figure 3: Infection and replication mechanism of SARS-CoV-2. After the spike protein binds the host receptor angiotensin-converting enzyme 2 (ACE2) and host factor TMPRSS2, viral uptake is promoted and viral genomic RNA is uncoated and released. This results in the immediate translation of viral proteins. The viral polymerase protein replicase replicates the viral RNA, while the structural proteins are translocated into the endoplasmatic reticulum (ER) following translation. The replicated positive sense RNA that binds nucleocapsid proteins found in the cytoplasm can then bud into the ER-Golgi intermediate compartment (ERGIC) that already carries the structural proteins. The infected cell secretes assembled mature virions through exocytosis(*80, 88*). This figure was created with BioRender.

Aim of the thesis

The immune system is essential to prevent malignant and infectious diseases. Different vaccine approaches allow to prime the immune system to recognize and remove either tumor cells or infected cells. For CLL, therapeutic success has greatly improved over the past years with small molecules like Bruton's tyrosine kinase inhibitors entering clinical routine, however MRD still leads to early disease relapse. Thus, the development of new low side effect immunotherapeutic approaches targeting MRD are indispensable. One aim of this thesis was to design a peptide warehouse, composed of CLL-associated T cell epitopes, for peptide-based immunotherapy in CLL. Therefore, novel CLL-associated HLA class I- and HLA class II-restricted peptides were identified by mass spectrometry-based immunopeptidome analysis of CLL cells and tested for immunogenicity. Since HLA class II:peptide complexes cannot be easily refolded *in vitro* to functional monomers for *de novo* $CD4^+$T cell priming experiments to prove immunogenicity of potential peptide warehouse candidates, the second aim of this thesis was to establish a monocyte-derived DC priming protocol.

During the COVID-19 pandemic, several different vaccine products were developed resulting in different vaccination regimens for the population. These vaccines, aiming for reduced transmission and infection rates, relied on known (e.g., vector vaccines) as well as new (mRNA vaccine) vaccination concepts, most of them targeting the spike protein of SARS-CoV-2. The third aim of this thesis was to analyze the differences in SARS-CoV-2-specific T cell responses depending on the vaccination regimen and number of received vaccine doses in healthy volunteers.

In this thesis, the main focus was laid on the characterization of T cell responses induced by peptide candidates for peptide-based vaccination in CLL or by vaccination with different COVID-19 vaccines**.**

References

1. D. D. Chaplin, Overview of the immune response. *J Allergy Clin Immunol* **125**, S3-23 (2010).
2. H. Gonzalez, C. Hagerling, Z. Werb, Roles of the immune system in cancer: from tumor initiation to metastatic progression. *Genes Dev* **32**, 1267-1284 (2018).
3. J. S. Marshall, R. Warrington, W. Watson, H. L. Kim, An introduction to immunology and immunopathology. *Allergy Asthma Clin Immunol* **14**, 49 (2018).
4. F. A. Bonilla, H. C. Oettgen, Adaptive immunity. *J Allergy Clin Immunol* **125**, S33-40 (2010).
5. K. Murphy, P. Travers, M. Walport, C. Janeway, *Janeway's immunobiology*. (Garland Science, New York, ed. 8th, 2012), pp. xix, 868 p.
6. L. Maggs, A. Sadagopan, A. S. Moghaddam, S. Ferrone, HLA class I antigen processing machinery defects in antitumor immunity and immunotherapy. *Trends Cancer* **7**, 1089-1101 (2021).
7. B. Seliger, M. Kloor, S. Ferrone, HLA class II antigen-processing pathway in tumors: Molecular defects and clinical relevance. *Oncoimmunology* **6**, e1171447 (2017).
8. K. Falk, O. Rotzschke, S. Stevanovic, G. Jung, H. G. Rammensee, Allele-specific motifs revealed by sequencing of self-peptides eluted from MHC molecules. *Nature* **351**, 290-296 (1991).
9. J. M. Vyas, A. G. Van der Veen, H. L. Ploegh, The known unknowns of antigen processing and presentation. *Nat Rev Immunol* **8**, 607-618 (2008).
10. S. Burgdorf, A. Kautz, V. Bohnert, P. A. Knolle, C. Kurts, Distinct pathways of antigen uptake and intracellular routing in CD4 and CD8 T cell activation. *Science* **316**, 612-616 (2007).
11. N. L. Pham, V. P. Badovinac, J. T. Harty, Differential role of "Signal 3" inflammatory cytokines in regulating CD8 T cell expansion and differentiation in vivo. *Front Immunol* **2**, 4 (2011).
12. A. L. Brown, M. Li, A. Goncearenco, A. R. Panchenko, Finding driver mutations in cancer: Elucidating the role of background mutational processes. *PLoS Comput Biol* **15**, e1006981 (2019).
13. D. Hanahan, Hallmarks of Cancer: New Dimensions. *Cancer Discov* **12**, 31-46 (2022).
14. P. Ehrlich, Ueber den jetzigen Stand der Karzinomforschung. *Nederlands Tijdschrift voor Geneeskunde* **5**, 273-290 (1909).
15. M. Burnet, Cancer: a biological approach. III. Viruses associated with neoplastic conditions. IV. Practical applications. *Br Med J* **1**, 841-847 (1957).
16. L. Thomas, On immunosurveillance in human cancer. *Yale J Biol Med* **55**, 329-333 (1982).
17. G. P. Dunn, A. T. Bruce, H. Ikeda, L. J. Old, R. D. Schreiber, Cancer immunoediting: from immunosurveillance to tumor escape. *Nat Immunol* **3**, 991-998 (2002).
18. A. Sudhakar, History of Cancer, Ancient and Modern Treatment Methods. *J Cancer Sci Ther* **1**, 1-4 (2009).
19. W. C. Rontgen, On a New Kind of Rays. *Science* **3**, 227-231 (1896).
20. R. W. Johnstone, A. A. Ruefli, S. W. Lowe, Apoptosis: a link between cancer genetics and chemotherapy. *Cell* **108**, 153-164 (2002).
21. K. D. Miller, R. L. Siegel, C. C. Lin, A. B. Mariotto, J. L. Kramer, J. H. Rowland, K. D. Stein, R. Alteri, A. Jemal, Cancer treatment and survivorship statistics, 2016. *CA Cancer J Clin* **66**, 271-289 (2016).
22. R. S. Riley, C. H. June, R. Langer, M. J. Mitchell, Delivery technologies for cancer immunotherapy. *Nat Rev Drug Discov* **18**, 175-196 (2019).
23. P. Berraondo, M. F. Sanmamed, M. C. Ochoa, I. Etxeberria, M. A. Aznar, J. L. Perez-Gracia, M. E. Rodriguez-Ruiz, M. Ponz-Sarvise, E. Castanon, I. Melero, Cytokines in clinical cancer immunotherapy. *Br J Cancer* **120**, 6-15 (2019).
24. T. M. Pierpont, C. B. Limper, K. L. Richards, Past, Present, and Future of Rituximab-The World's First Oncology Monoclonal Antibody Therapy. *Front Oncol* **8**, 163 (2018).
25. T. van Meerten, R. S. van Rijn, S. Hol, A. Hagenbeek, S. B. Ebeling, Complement-induced cell death by rituximab depends on CD20 expression level and acts complementary to antibody-dependent cellular cytotoxicity. *Clin Cancer Res* **12**, 4027-4035 (2006).

26. C. Ordonez-Reyes, J. E. Garcia-Robledo, D. F. Chamorro, A. Mosquera, L. Sussmann, A. Ruiz-Patino, O. Arrieta, L. Zatarain-Barron, L. Rojas, A. Russo, D. de Miguel-Perez, C. Rolfo, A. F. Cardona, Bispecific Antibodies in Cancer Immunotherapy: A Novel Response to an Old Question. *Pharmaceutics* **14**, (2022).
27. E. Y. Jen, Q. Xu, A. Schetter, D. Przepiorka, Y. L. Shen, D. Roscoe, R. Sridhara, A. Deisseroth, R. Philip, A. T. Farrell, R. Pazdur, FDA Approval: Blinatumomab for Patients with B-cell Precursor Acute Lymphoblastic Leukemia in Morphologic Remission with Minimal Residual Disease. *Clin Cancer Res* **25**, 473-477 (2019).
28. C. Robert, A decade of immune-checkpoint inhibitors in cancer therapy. *Nat Commun* **11**, 3801 (2020).
29. A. D. Fesnak, C. H. June, B. L. Levine, Engineered T cells: the promise and challenges of cancer immunotherapy. *Nat Rev Cancer* **16**, 566-581 (2016).
30. J. Bauer, A. Nelde, T. Bilich, J. S. Walz, Antigen Targets for the Development of Immunotherapies in Leukemia. *Int J Mol Sci* **20**, (2019).
31. C. C. Liu, H. Yang, R. Zhang, J. J. Zhao, D. J. Hao, Tumour-associated antigens and their anti-cancer applications. *Eur J Cancer Care (Engl)* **26**, (2017).
32. S. Feola, J. Chiaro, B. Martins, V. Cerullo, Uncovering the Tumor Antigen Landscape: What to Know about the Discovery Process. *Cancers (Basel)* **12**, (2020).
33. T. Jiang, T. Shi, H. Zhang, J. Hu, Y. Song, J. Wei, S. Ren, C. Zhou, Tumor neoantigens: from basic research to clinical applications. *J Hematol Oncol* **12**, 93 (2019).
34. D. Mennonna, C. Maccalli, M. C. Romano, C. Garavaglia, F. Capocefalo, R. Bordoni, M. Severgnini, G. De Bellis, J. Sidney, A. Sette, A. Gori, R. Longhi, M. Braga, L. Ghirardelli, L. Baldari, E. Orsenigo, L. Albarello, E. Zino, K. Fleischhauer, G. Mazzola, N. Ferrero, A. Amoroso, G. Casorati, G. Parmiani, P. Dellabona, T cell neoepitope discovery in colorectal cancer by high throughput profiling of somatic mutations in expressed genes. *Gut* **66**, 454-463 (2017).
35. S. P. Haen, M. W. Loffler, H. G. Rammensee, P. Brossart, Towards new horizons: characterization, classification and implications of the tumour antigenic repertoire. *Nat Rev Clin Oncol* **17**, 595-610 (2020).
36. T. Bilich, A. Nelde, L. Bichmann, M. Roerden, H. R. Salih, D. J. Kowalewski, H. Schuster, C. C. Tsou, A. Marcu, M. C. Neidert, M. Lubke, J. Rieth, M. Schemionek, T. H. Brummendorf, V. Vucinic, D. Niederwieser, J. Bauer, M. Marklin, J. K. Peper, R. Klein, O. Kohlbacher, L. Kanz, H. G. Rammensee, S. Stevanovic, J. S. Walz, The HLA ligandome landscape of chronic myeloid leukemia delineates novel T-cell epitopes for immunotherapy. *Blood* **133**, 550-565 (2019).
37. T. N. Schumacher, R. D. Schreiber, Neoantigens in cancer immunotherapy. *Science* **348**, 69-74 (2015).
38. R. E. Hollingsworth, K. Jansen, Turning the corner on therapeutic cancer vaccines. *NPJ Vaccines* **4**, 7 (2019).
39. N. Xie, G. Shen, W. Gao, Z. Huang, C. Huang, L. Fu, Neoantigens: promising targets for cancer therapy. *Signal Transduct Target Ther* **8**, 9 (2023).
40. W. W. Overwijk, Cancer vaccines in the era of checkpoint blockade: the magic is in the adjuvant. *Curr Opin Immunol* **47**, 103-109 (2017).
41. R. N. Shepard, J. Schock, K. Robertson, D. C. Shugars, J. Dyer, P. Vernazza, C. Hall, M. S. Cohen, S. A. Fiscus, Quantitation of human immunodeficiency virus type 1 RNA in different biological compartments. *J Clin Microbiol* **38**, 1414-1418 (2000).
42. J. M. van Seventer, N. S. Hochberg, Principles of Infectious Diseases: Transmission, Diagnosis, Prevention, and Control. *International Encyclopedia of Public Health*, 22–39 (2017).
43. S. H. Speck, D. Ganem, Viral latency and its regulation: lessons from the gamma-herpesviruses. *Cell Host Microbe* **8**, 100-115 (2010).
44. M. P. Nicoll, J. T. Proenca, S. Efstathiou, The molecular basis of herpes simplex virus latency. *FEMS Microbiol Rev* **36**, 684-705 (2012).
45. S. Baize, E. M. Leroy, M. C. Georges-Courbot, M. Capron, J. Lansoud-Soukate, P. Debre, S. P. Fisher-Hoch, J. B. McCormick, A. J. Georges, Defective humoral responses and extensive

intravascular apoptosis are associated with fatal outcome in Ebola virus-infected patients. *Nat Med* **5**, 423-426 (1999).
46. A. O'Garra, P. S. Redford, F. W. McNab, C. I. Bloom, R. J. Wilkinson, M. P. Berry, The immune response in tuberculosis. *Annu Rev Immunol* **31**, 475-527 (2013).
47. S. Thomas, G. C. Prendergast, Cancer Vaccines: A Brief Overview. *Methods Mol Biol* **1403**, 755-761 (2016).
48. R. E. Vance, M. J. Eichberg, D. A. Portnoy, D. H. Raulet, Listening to each other: Infectious disease and cancer immunology. *Sci Immunol* **2**, (2017).
49. A. Saleh, S. Qamar, A. Tekin, R. Singh, R. Kashyap, Vaccine Development Throughout History. *Cureus* **13**, e16635 (2021).
50. A. Heine, S. Juranek, P. Brossart, Clinical and immunological effects of mRNA vaccines in malignant diseases. *Mol Cancer* **20**, 52 (2021).
51. M. A. McNamara, S. K. Nair, E. K. Holl, RNA-Based Vaccines in Cancer Immunotherapy. *J Immunol Res* **2015**, 794528 (2015).
52. S. Kreiter, M. Vormehr, N. van de Roemer, M. Diken, M. Lower, J. Diekmann, S. Boegel, B. Schrors, F. Vascotto, J. C. Castle, A. D. Tadmor, S. P. Schoenberger, C. Huber, O. Tureci, U. Sahin, Mutant MHC class II epitopes drive therapeutic immune responses to cancer. *Nature* **520**, 692-696 (2015).
53. U. S. F. D. Administration. FDA Approves First COVID-19 Vaccine. https://www.fda.gov/news-events/press-announcements/fda-approves-first-covid-19-vaccine. (2021).
54. F. P. Polack, S. J. Thomas, N. Kitchin, J. Absalon, A. Gurtman, S. Lockhart, J. L. Perez, G. Perez Marc, E. D. Moreira, C. Zerbini, R. Bailey, K. A. Swanson, S. Roychoudhury, K. Koury, P. Li, W. V. Kalina, D. Cooper, R. W. Frenck, Jr., L. L. Hammitt, O. Tureci, H. Nell, A. Schaefer, S. Unal, D. B. Tresnan, S. Mather, P. R. Dormitzer, U. Sahin, K. U. Jansen, W. C. Gruber, C. C. T. Group, Safety and Efficacy of the BNT162b2 mRNA Covid-19 Vaccine. *N Engl J Med* **383**, 2603-2615 (2020).
55. L. R. Baden, H. M. El Sahly, B. Essink, K. Kotloff, S. Frey, R. Novak, D. Diemert, S. A. Spector, N. Rouphael, C. B. Creech, J. McGettigan, S. Khetan, N. Segall, J. Solis, A. Brosz, C. Fierro, H. Schwartz, K. Neuzil, L. Corey, P. Gilbert, H. Janes, D. Follmann, M. Marovich, J. Mascola, L. Polakowski, J. Ledgerwood, B. S. Graham, H. Bennett, R. Pajon, C. Knightly, B. Leav, W. Deng, H. Zhou, S. Han, M. Ivarsson, J. Miller, T. Zaks, C. S. Group, Efficacy and Safety of the mRNA-1273 SARS-CoV-2 Vaccine. *N Engl J Med* **384**, 403-416 (2021).
56. M. S. Gebre, L. A. Brito, L. H. Tostanoski, D. K. Edwards, A. Carfi, D. H. Barouch, Novel approaches for vaccine development. *Cell* **184**, 1589-1603 (2021).
57. F. Sakurai, M. Tachibana, H. Mizuguchi, Adenovirus vector-based vaccine for infectious diseases. *Drug Metab Pharmacokinet* **42**, 100432 (2022).
58. C. Larocca, J. Schlom, Viral vector-based therapeutic cancer vaccines. *Cancer J* **17**, 359-371 (2011).
59. M. N. Ramasamy, A. M. Minassian, K. J. Ewer, A. L. Flaxman, P. M. Folegatti, D. R. Owens, M. Voysey, P. K. Aley, B. Angus, G. Babbage, S. Belij-Rammerstorfer, L. Berry, S. Bibi, M. Bittaye, K. Cathie, H. Chappell, S. Charlton, P. Cicconi, E. A. Clutterbuck, R. Colin-Jones, C. Dold, K. R. W. Emary, S. Fedosyuk, M. Fuskova, D. Gbesemete, C. Green, B. Hallis, M. M. Hou, D. Jenkin, C. C. D. Joe, E. J. Kelly, S. Kerridge, A. M. Lawrie, A. Lelliott, M. N. Lwin, R. Makinson, N. G. Marchevsky, Y. Mujadidi, A. P. S. Munro, M. Pacurar, E. Plested, J. Rand, T. Rawlinson, S. Rhead, H. Robinson, A. J. Ritchie, A. L. Ross-Russell, S. Saich, N. Singh, C. C. Smith, M. D. Snape, R. Song, R. Tarrant, Y. Themistocleous, K. M. Thomas, T. L. Villafana, S. C. Warren, M. E. E. Watson, A. D. Douglas, A. V. S. Hill, T. Lambe, S. C. Gilbert, S. N. Faust, A. J. Pollard, C. V. T. G. Oxford, Safety and immunogenicity of ChAdOx1 nCoV-19 vaccine administered in a prime-boost regimen in young and old adults (COV002): a single-blind, randomised, controlled, phase 2/3 trial. *Lancet* **396**, 1979-1993 (2021).
60. A. Nelde, H. G. Rammensee, J. S. Walz, The Peptide Vaccine of the Future. *Mol Cell Proteomics* **20**, 100022 (2021).

61. N. Hilf, S. Kuttruff-Coqui, K. Frenzel, V. Bukur, S. Stevanovic, C. Gouttefangeas, M. Platten, G. Tabatabai, V. Dutoit, S. H. van der Burg, P. Thor Straten, F. Martinez-Ricarte, B. Ponsati, H. Okada, U. Lassen, A. Admon, C. H. Ottensmeier, A. Ulges, S. Kreiter, A. von Deimling, M. Skardelly, D. Migliorini, J. R. Kroep, M. Idorn, J. Rodon, J. Piro, H. S. Poulsen, B. Shraibman, K. McCann, R. Mendrzyk, M. Lower, M. Stieglbauer, C. M. Britten, D. Capper, M. J. P. Welters, J. Sahuquillo, K. Kiesel, E. Derhovanessian, E. Rusch, L. Bunse, C. Song, S. Heesch, C. Wagner, A. Kemmer-Bruck, J. Ludwig, J. C. Castle, O. Schoor, A. D. Tadmor, E. Green, J. Fritsche, M. Meyer, N. Pawlowski, S. Dorner, F. Hoffgaard, B. Rossler, D. Maurer, T. Weinschenk, C. Reinhardt, C. Huber, H. G. Rammensee, H. Singh-Jasuja, U. Sahin, P. Y. Dietrich, W. Wick, Actively personalized vaccination trial for newly diagnosed glioblastoma. *Nature* **565**, 240-245 (2019).
62. P. A. Ott, Z. Hu, D. B. Keskin, S. A. Shukla, J. Sun, D. J. Bozym, W. Zhang, A. Luoma, A. Giobbie-Hurder, L. Peter, C. Chen, O. Olive, T. A. Carter, S. Li, D. J. Lieb, T. Eisenhaure, E. Gjini, J. Stevens, W. J. Lane, I. Javeri, K. Nellaiappan, A. M. Salazar, H. Daley, M. Seaman, E. I. Buchbinder, C. H. Yoon, M. Harden, N. Lennon, S. Gabriel, S. J. Rodig, D. H. Barouch, J. C. Aster, G. Getz, K. Wucherpfennig, D. Neuberg, J. Ritz, E. S. Lander, E. F. Fritsch, N. Hacohen, C. J. Wu, An immunogenic personal neoantigen vaccine for patients with melanoma. *Nature* **547**, 217-221 (2017).
63. H. Khong, W. W. Overwijk, Adjuvants for peptide-based cancer vaccines. *J Immunother Cancer* **4**, 56 (2016).
64. J. S. Heitmann, T. Bilich, C. Tandler, A. Nelde, Y. Maringer, M. Marconato, J. Reusch, S. Jager, M. Denk, M. Richter, L. Anton, L. M. Weber, M. Roerden, J. Bauer, J. Rieth, M. Wacker, S. Horber, A. Peter, C. Meisner, I. Fischer, M. W. Loffler, J. Karbach, E. Jager, R. Klein, H. G. Rammensee, H. R. Salih, J. S. Walz, A COVID-19 peptide vaccine for the induction of SARS-CoV-2 T cell immunity. *Nature* **601**, 617-622 (2022).
65. S. Romeli, S. S. Hassan, W. B. Yap, Multi-Epitope Peptide-Based and Vaccinia-Based Universal Influenza Vaccine Candidates Subjected to Clinical Trials. *Malays J Med Sci* **27**, 10-20 (2020).
66. T. Z. Iversen, L. Engell-Noerregaard, E. Ellebaek, R. Andersen, S. K. Larsen, J. Bjoern, C. Zeyher, C. Gouttefangeas, B. M. Thomsen, B. Holm, P. Thor Straten, A. Mellemgaard, M. H. Andersen, I. M. Svane, Long-lasting disease stabilization in the absence of toxicity in metastatic lung cancer patients vaccinated with an epitope derived from indoleamine 2,3 dioxygenase. *Clin Cancer Res* **20**, 221-232 (2014).
67. R. Le Dieu, D. C. Taussig, A. G. Ramsay, R. Mitter, F. Miraki-Moud, R. Fatah, A. M. Lee, T. A. Lister, J. G. Gribben, Peripheral blood T cells in acute myeloid leukemia (AML) patients at diagnosis have abnormal phenotype and genotype and form defective immune synapses with AML blasts. *Blood* **114**, 3909-3916 (2009).
68. J. Nakata, Y. Nakae, M. Kawakami, S. Morimoto, D. Motooka, N. Hosen, F. Fujiki, H. Nakajima, K. Hasegawa, S. Nishida, A. Tsuboi, Y. Oji, Y. Oka, A. Kumanogoh, H. Sugiyama, Wilms tumour 1 peptide vaccine as a cure-oriented post-chemotherapy strategy for patients with acute myeloid leukaemia at high risk of relapse. *Br J Haematol* **182**, 287-290 (2018).
69. T. A. Brown, 2nd, E. A. Mittendorf, D. F. Hale, J. W. Myers, 3rd, K. M. Peace, D. O. Jackson, J. M. Greene, T. J. Vreeland, G. T. Clifton, A. Ardavanis, J. K. Litton, N. M. Shumway, J. Symanowski, J. L. Murray, S. Ponniah, E. A. Anastasopoulou, N. F. Pistamaltzian, C. N. Baxevanis, S. A. Perez, M. Papamichail, G. E. Peoples, Prospective, randomized, single-blinded, multi-center phase II trial of two HER2 peptide vaccines, GP2 and AE37, in breast cancer patients to prevent recurrence. *Breast Cancer Res Treat* **181**, 391-401 (2020).
70. B. Petrini, J. Wasserman, U. Glas, H. Blomgren, T lymphocyte subpopulations in blood following radiation therapy for breast cancer. *Eur J Cancer Clin Oncol* **18**, 921-924 (1982).
71. L. Zitvogel, L. Apetoh, F. Ghiringhelli, G. Kroemer, Immunological aspects of cancer chemotherapy. *Nat Rev Immunol* **8**, 59-73 (2008).
72. A. Mougel, M. Terme, C. Tanchot, Therapeutic Cancer Vaccine and Combinations With Antiangiogenic Therapies and Immune Checkpoint Blockade. *Front Immunol* **10**, 467 (2019).

73. M. D. Kerr, D. A. McBride, A. K. Chumber, N. J. Shah, Combining therapeutic vaccines with chemo- and immunotherapies in the treatment of cancer. *Expert Opin Drug Discov* **16**, 89-99 (2021).
74. M. Hallek, Chronic lymphocytic leukemia: 2020 update on diagnosis, risk stratification and treatment. *Am J Hematol* **94**, 1266-1287 (2019).
75. R. L. Siegel, K. D. Miller, H. E. Fuchs, A. Jemal, Cancer Statistics, 2021. *CA Cancer J Clin* **71**, 7-33 (2021).
76. T. J. Hamblin, Z. Davis, A. Gardiner, D. G. Oscier, F. K. Stevenson, Unmutated Ig V(H) genes are associated with a more aggressive form of chronic lymphocytic leukemia. *Blood* **94**, 1848-1854 (1999).
77. M. Hallek, O. Al-Sawaf, Chronic lymphocytic leukemia: 2022 update on diagnostic and therapeutic procedures. *Am J Hematol* **96**, 1679-1705 (2021).
78. L. Iovino, M. Shadman, Novel Therapies in Chronic Lymphocytic Leukemia: A Rapidly Changing Landscape. *Curr Treat Options Oncol* **21**, 24 (2020).
79. M. Y. Li, L. Li, Y. Zhang, X. S. Wang, Expression of the SARS-CoV-2 cell receptor gene ACE2 in a wide variety of human tissues. *Infect Dis Poverty* **9**, 45 (2020).
80. H. F. Florindo, R. Kleiner, D. Vaskovich-Koubi, R. C. Acurcio, B. Carreira, E. Yeini, G. Tiram, Y. Liubomirski, R. Satchi-Fainaro, Immune-mediated approaches against COVID-19. *Nat Nanotechnol* **15**, 630-645 (2020).
81. H. Nasrollahi, A. G. Talepoor, Z. Saleh, M. Eshkevar Vakili, P. Heydarinezhad, N. Karami, M. Noroozi, S. Meri, K. Kalantar, Immune responses in mildly versus critically ill COVID-19 patients. *Front Immunol* **14**, 1077236 (2023).
82. J. Zheng, J. Miao, R. Guo, J. Guo, Z. Fan, X. Kong, R. Gao, L. Yang, Mechanism of COVID-19 Causing ARDS: Exploring the Possibility of Preventing and Treating SARS-CoV-2. *Front Cell Infect Microbiol* **12**, 931061 (2022).
83. J. Holstiege, M. K. Akmatov, C. Kohring, L. Dammertz, F. Ng, T. Czihal, D. von Stillfried, J. Batzing, Patients at high risk for a severe clinical course of COVID-19 - small-area data in support of vaccination and other population-based interventions in Germany. *BMC Public Health* **21**, 1769 (2021).
84. G. Leech, C. Rogers-Smith, J. T. Monrad, J. B. Sandbrink, B. Snodin, R. Zinkov, B. Rader, J. S. Brownstein, Y. Gal, S. Bhatt, M. Sharma, S. Mindermann, J. M. Brauner, L. Aitchison, Mask wearing in community settings reduces SARS-CoV-2 transmission. *Proc Natl Acad Sci U S A* **119**, e2119266119 (2022).
85. F. D. F. Freitas, A. C. Q. de Medeiros, F. A. Lopes, Effects of Social Distancing During the COVID-19 Pandemic on Anxiety and Eating Behavior-A Longitudinal Study. *Front Psychol* **12**, 645754 (2021).
86. C. Ho, P. C. Lee, COVID-19 Treatment-Current Status, Advances, and Gap. *Pathogens* **11**, (2022).
87. X. Chen, H. Huang, J. Ju, R. Sun, J. Zhang, Impact of vaccination on the COVID-19 pandemic in U.S. states. *Sci Rep* **12**, 1554 (2022).
88. P. V'Kovski, A. Kratzel, S. Steiner, H. Stalder, V. Thiel, Coronavirus biology and replication: implications for SARS-CoV-2. *Nat Rev Microbiol* **19**, 155-170 (2021).

Chapter 1

Immunopeptidomics-guided warehouse design for peptide-based immunotherapy in chronic lymphocytic leukemia

Annika Nelde[1,2,3,†], Yacine Maringer[1,2,3,†], Tatjana Bilich[1,2,3], Helmut R. Salih[1,3], Malte Roerden[2,3,4], Jonas S. Heitmann[1,3], Ana Marcu[2], Jens Bauer[1,2], Marian C. Neidert[5], Claudio Denzlinger[6], Gerald Illerhaus[7], Walter Erich Aulitzky[8], Hans-Georg Rammensee[2,3,9], Juliane S. Walz[1,2,3,10]

[1] Clinical Collaboration Unit Translational Immunology, German Cancer Consortium (DKTK), Department of Internal Medicine, University Hospital Tübingen, Tübingen, Germany

[2] Institute for Cell Biology, Department of Immunology, University of Tübingen, Tübingen, Germany

[3] Cluster of Excellence iFIT (EXC2180) "Image-Guided and Functionally Instructed Tumor Therapies", University of Tübingen, Tübingen, Germany

[4] Department of Hematology, Oncology, Clinical Immunology and Rheumatology, University Hospital Tübingen, Tübingen, Germany

[5] Department of Neurosurgery, Cantonal Hospital St. Gallen, St. Gallen, Switzerland

[6] Marienhospital, Stuttgart, Germany

[7] Clinic for Hematology and Oncology, Klinikum Stuttgart, Stuttgart, Germany

[8] Department of Hematology, Oncology and Palliative Medicine, Robert-Bosch-Krankenhaus Stuttgart, Stuttgart, Germany

[9] German Cancer Consortium (DKTK) and German Cancer Research Center (DKFZ), partner site Tübingen, Tübingen, Germany

[10] Dr. Margarete Fischer-Bosch Institute of Clinical Pharmacology and Robert Bosch Center for Tumor Diseases (RBCT), Stuttgart, Germany

[†] These authors have contributed equally to this work and share first authorship.

Front Immunol. 2021 Jul 8;12:705974. PMID: 34305947
doi: 10.3389/fimmu.2021.705974.

Disclosure and author contributions

YM and AN contributed equally to this publication. YM participated in the study design. YM conducted and planned *in vitro* T cell experiments and analyzed the obtained data. YM conceived all tables and figures describing T cell-based assay, including Table 1, Figure 3 and Supplementary Figure 4. The manuscript was drafted by YM, JSW and AN. For more information, please refer to the statement provided in the "Author Contributions" section at the end of this chapter.

Abstract

Antigen-specific immunotherapies, in particular peptide vaccines, depend on the recognition of naturally presented antigens derived from mutated and unmutated gene products on human leukocyte antigens, and represent a promising low-side-effect concept for cancer treatment. So far, the broad application of peptide vaccines in cancer patients is hampered by challenges of time- and cost-intensive personalized vaccine design, and the lack of neoepitopes from tumor-specific mutations, especially in low-mutational burden malignancies. In this study, we developed an immunopeptidome-guided workflow for the design of tumor-associated off-the-shelf peptide warehouses for broadly applicable personalized therapeutics. Comparative mass spectrometry-based immunopeptidome analyses of primary chronic lymphocytic leukemia (CLL) samples, as representative example of low-mutational burden tumor entities, and a dataset of benign tissue samples enabled the identification of high-frequent non-mutated CLL associated antigens. These antigens were further shown to be recognized by pre-existing and *de novo* induced T cells in CLL patients and healthy volunteers, and were evaluated as pre-manufactured warehouse for the construction of personalized multi-peptide vaccines in a first clinical trial for CLL (NCT04688385). This workflow for the design of peptide warehouses is easily transferable to other tumor entities and can provide the foundation for the development of broad personalized T cell-based immunotherapy approaches.

Introduction

The breakthrough clinical success of T cell-based immunotherapy approaches, including immune checkpoint inhibitors, CAR T cells, bispecific antibodies, and adoptive T cell transfer, has recently revolutionized the treatment of solid tumors and hematological malignancies. However, some patients do not respond to available therapies at all, others only temporarily calling for further efficacy improvement of T cell-centered immunotherapies. Peptide-based approaches, which rely on the specific immune recognition of tumor-associated human leukocyte antigen (HLA)-presented peptides, represent promising alternatives with low side effects. Targeting mutation-derived neoepitopes by vaccination in melanoma – a high-mutational burden tumor entity – has demonstrated immunogenicity and first clinical efficacy (*1*). However, only a minority of mutations at the DNA level is translated and naturally processed to HLA-presented neoepitopes targetable for T cells (*2, 3*). Non-

mutated tumor-associated antigens, arising through differential gene expression or protein processing in tumor cells, might supplement or even substitute neoepitope targeting in low-mutational burden malignancies. Whereas a huge number of clinical studies have shown immune responses, including strong $CD8^+$ T cell responses, to vaccines targeting non-mutated tumor antigens, so far, all performed trials failed to show meaningful clinical results (*4-10*). Nonetheless, several studies showed a pathophysiological relevance of these tumor antigens, correlating spontaneous, pre-existing as well as immune checkpoint inhibitor-induced T cell responses, targeting non-mutated tumor antigens with improved clinical outcome of malignancies (*11-14*). Therefore, the usage of novel technologies and methods, to unravel and resolve the underlying issues and limitations of non-mutated antigen-based vaccines, might enable that T cell responses, induced or boosted by these vaccines, may result in clinical effectiveness in the future (*15*).

One issue of former peptide-vaccine trials was the selection of non-mutated tumor antigens that were not proven to be naturally presented on the tumor cell surface of the individual patients. For multiple of the applied "classical" tumor antigens novel analyses showed a distorted correlation of tumor-associated presentation on mRNA level, and limited or even lacking presentation on cell surface HLA (*16-22*).

In recent years, characterization of naturally presented mutated and non-mutated tumor antigens was refined using direct, mass spectrometry-based analyses of the entirety of HLA ligands termed the immunopeptidome (*13, 20-25*). While mass spectrometric identification of neoepitopes remains rare with inter-individual heterogeneity and requires a time- and cost-intensive fully personalized vaccine design (*1*), distinct panels of high-frequent non-mutated tumor-associated antigens have been previously identified (*13, 20-24*). Such panels could enable the construction of off-the-shelf pre-manufactured peptide warehouses for the design of broadly applicable personalized therapeutics, such as multi-peptide vaccines or products for adoptive T cell transfer, that could be assembled based on patient-individual characteristics. To evaluate this concept in chronic lymphocytic leukemia (CLL) as representative example of an immunogenic, low-mutational burden malignancy (*26, 27*), we here developed a widely applicable workflow for the immunopeptidomics-guided design of such a warehouse, that provides the basis for the selection of personalized multi-peptide vaccine cocktails for a first-in-man clinical trial (NCT04688385).

Materials and Methods

Patients and Blood Samples

Peripheral blood mononuclear cells (PBMCs) from CLL patients as well as PBMCs from healthy volunteers (HVs) were isolated by density gradient centrifugation and stored at -80°C until further use for subsequent HLA immunoprecipitation or T cell-based assays. For immunopeptidome analysis,

PBMCs from CLL patients with white blood cell counts ≥ 20,000 per µl were used. Informed consent was obtained in accordance with the Declaration of Helsinki protocol. The study was performed according to the guidelines of the local ethics committees (373/2011B02, 454/2016B02, 406/2019BO2). HLA typing of CLL patient samples was carried out by the Department of Hematology and Oncology, Tübingen, Germany. Patient characteristics of the immunopeptidome cohort (n = 61) are provided in Table S1. Sample characteristics of the immunogenicity cohort (n = 51) are provided in Table S2.

Isolation of HLA Ligands

HLA class I and HLA class II molecules were isolated by standard immunoaffinity purification (*28*) using the pan-HLA class I-specific monoclonal antibody W6/32, the pan-HLA class II-specific monoclonal antibody Tü-39, and the HLA-DR-specific monoclonal antibody L243 (all produced in-house) to extract HLA ligands.

Analysis of HLA Ligands by Liquid Chromatography-Coupled Tandem Mass Spectrometry (LC-MS/MS)

Isolated peptide samples were analyzed as described previously (*13, 29*). Peptides were separated by nanoflow high-performance liquid chromatography. Eluted peptides were analyzed in an online-coupled LTQ Orbitrap XL or Orbitrap Fusion Lumos mass spectrometer (both Thermo Fisher, Waltham, Massachusetts, USA).

Data Processing

Data processing was performed as described previously (*13, 29*). The Proteome Discoverer (v1.3, Thermo Fisher) was used to integrate the search results of the SequestHT search engine (University of Washington) (*30*) against the human proteome (Swiss-Prot database, 20 279 reviewed protein sequences, September 27th 2013) accompanied with recurrent somatic CLL-associated mutations in 61 different proteins (Table S3) as described in the literature (*31, 32*) and assigned in the COSMIC database (http://cancer.sanger.ac.uk) (*33*) without enzymatic restriction. Precursor mass tolerance was set to 5 ppm. Fragment mass tolerance was set to 0.5 Da for ion trap spectra (LTQ Orbitrap XL) and 0.02 Da for orbitrap spectra (Orbitrap Fusion Lumos). Oxidized methionine was allowed as dynamic modification. The false discovery rate (FDR), estimated by the Percolator algorithm 2.04 (*34*) was limited to 5% for HLA class I- and 1% for HLA class II-presented peptides. HLA class I annotation was performed using SYFPEITHI 1.0 (*35*) and NetMHCpan 4.0 (*36, 37*).

Peptide Synthesis

Peptides were produced by the peptide synthesizer Liberty Blue (CEM, Kamp-Lintfort, Germany) using the 9-fluorenylmethyl-oxycarbonyl/tert-butyl strategy (*38*). Peptides for the peptide warehouse were selected with regard to a subsequent good manufacturing practice (GMP) and manufacturing license

conform production process, including peptide length restriction of 20 amino acids, avoiding cysteine-containing peptides as well as peptides with histidine or proline at the C-terminus.

Spectrum Validation

Spectrum validation of the experimentally eluted peptides was performed by computing the similarity of the spectra with corresponding synthetic peptides measured in a complex matrix. The spectral correlation was calculated between the MS/MS spectra of the eluted and the synthetic peptide (*39*).

Amplification of Peptide-Specific T Cells and Interferon-γ (IFN-γ) Enzyme-Linked Immunospot (ELISpot) Assay

PBMCs from CLL patients were treated with 1 µg/ml anti-human PD-1 monoclonal antibody (CD279, catalog no.14-2799-80, Invitrogen, Carlsbad, CA, USA) and 1 µg/ml anti-human CTLA-4 monoclonal antibody (CD152, catalog no.16-1529-82, Invitrogen) for one hour before pulsing with 1 µg/ml or 5 µg/ml per HLA class I or HLA class II peptide, respectively. Negative control peptides with the respective HLA restrictions were also used for stimulation: YLLPAIVHI for HLA-A*02 (source protein: DDX5_HUMAN), KYPENFFLL for HLA-A*24 (source protein: PP1G_HUMAN), TPGPGVRYPL for HLA-B*07 (source protein: NEF_HV1BR) and ETVITVDTKAAGKGK for HLA class II (source protein: FLNA_HUMAN). Cells were cultured for 12 days adding 20 U/ml IL-2 (Novartis, Basel, Switzerland) on days 2, 5, and 7 (*13, 22*). Peptide-stimulated PBMCs were analyzed by IFN-γ ELISpot assay on day 12 (*23, 40*). Spots were counted using an ImmunoSpot S6 analyzer (CTL, Cleveland, OH, USA) and T cell responses were considered positive when > 10 spots/500,000 cells were counted, and the mean spot count was at least three-fold higher than the mean spot count of the negative control.

Refolding

Biotinylated HLA:peptide complexes were manufactured as described previously (*41*) and tetramerized using PE-conjugated streptavidin (Invitrogen) at a 4:1 molar ratio.

Induction of Peptide-Specific $CD8^+$ T Cells with Artificial Antigen-Presenting Cells (aAPCs)

Priming of peptide-specific cytotoxic T lymphocytes was conducted using aAPCs as described previously (*42*). In detail, 800,000 streptavidin-coated microspheres (Bangs Laboratories, Fishers, Indiana, USA) were loaded with 200 ng biotinylated HLA:peptide monomer and 600 ng biotinylated anti-human CD28 monoclonal antibody (clone 9.3, in-house production). $CD8^+$ T cells were cultured with 4.8 U/µl IL 2 (R&D Systems, Minneapolis, MN, USA) and 1.25 ng/ml IL 7 (PromoKine, Heidelberg, Germany). Weekly stimulation with aAPCs (200, 000 aAPCs per 1×10^6 $CD8^+$ T cells) and 5 ng/ml IL-12 (PromoKine) was performed four times.

Cytokine and Tetramer Staining

The functionality of peptide-specific $CD8^+$ T cells was analyzed by intracellular cytokine staining (ICS) as described previously (*40, 43*). Cells were pulsed with 10 µg/ml of individual peptide and incubated with FITC anti-human CD107a (BioLegend, San Diego, CA, USA) for one hour before incubating with 10 µg/ml Brefeldin A (Sigma-Aldrich, Saint Louis, MO, USA) and 10 µg/ml GolgiStop (BD, Franklin Lakes, NJ, USA) for 12-16 h. Staining was performed using aqua fluorescent reactive dye (Invitrogen), Cytofix/Cytoperm (BD), PE-Cy7 anti-human CD8 (Beckman Coulter, Brea, CA, USA), Pacific Blue anti-human tumor necrosis factor (TNF), and PE anti-human IFN-γ (Biolegend) monoclonal antibodies. PMA and ionomycin (Sigma-Aldrich) served as positive control. Negative control peptides were used as described for the ELISpot assays. The frequency of peptide-specific $CD8^+$ T cells after aAPC-based priming was determined by PE-Cy7 anti-human CD8 monoclonal antibody and HLA:peptide tetramer-PE staining. Cells of the same donor primed with an irrelevant control peptide and stained with the tetramer containing the test peptide were used as negative control. The priming was considered successful if the frequency of peptide-specific $CD8^+$ T cells was ≥ 0.1% of $CD8^+$ T cells within the viable single cell population and at least three-fold higher than the frequency of peptide-specific $CD8^+$ T cells in the negative control. The same evaluation criteria were applied for ICS results. Samples were analyzed on a FACS Canto II cytometer (BD).

Software and Statistical Analysis

An in-house Python script was used for the calculation of FDRs of CLL-associated peptides at different presentation frequencies (*13*). Overlap analysis was performed using BioVenn (*44*). The population coverage of HLA allotypes was calculated by the IEDB population coverage tool (www.iedb.org) (*45, 46*). Flow cytometric data was analyzed using FlowJo 10.0.8 (Treestar, Ashland, Oregon, USA). All figures and statistical analyses were generated using GraphPad Prism 9.0.2 (GraphPad Software, San Diego, CA, USA).

Results

Mass Spectrometry-Based Identification of Naturally Presented CLL-Associated Antigens

In the first step of our workflow for the definition of an off-the-shelf peptide warehouse (Fig. 1A), we comprehensively mapped the immunopeptidome of 61 primary CLL samples (n = 52 for HLA class I, n = 49 for HLA class II; Table S1). We identified a total of 58,554 unique HLA class I ligands representing 10,854 source proteins, obtaining 96% of the estimated maximum attainable source protein coverage (Fig. 1B). The number of identified unique peptides per patient ranged from 527 to 9,530 (mean 3,035; Table S4). For HLA class II, we identified 70,525 different peptides (range 575-10,392, mean 3,842 per sample; Table S4) derived from 6,074 source proteins, achieving 85% of maximum attainable coverage (Fig. S1A).

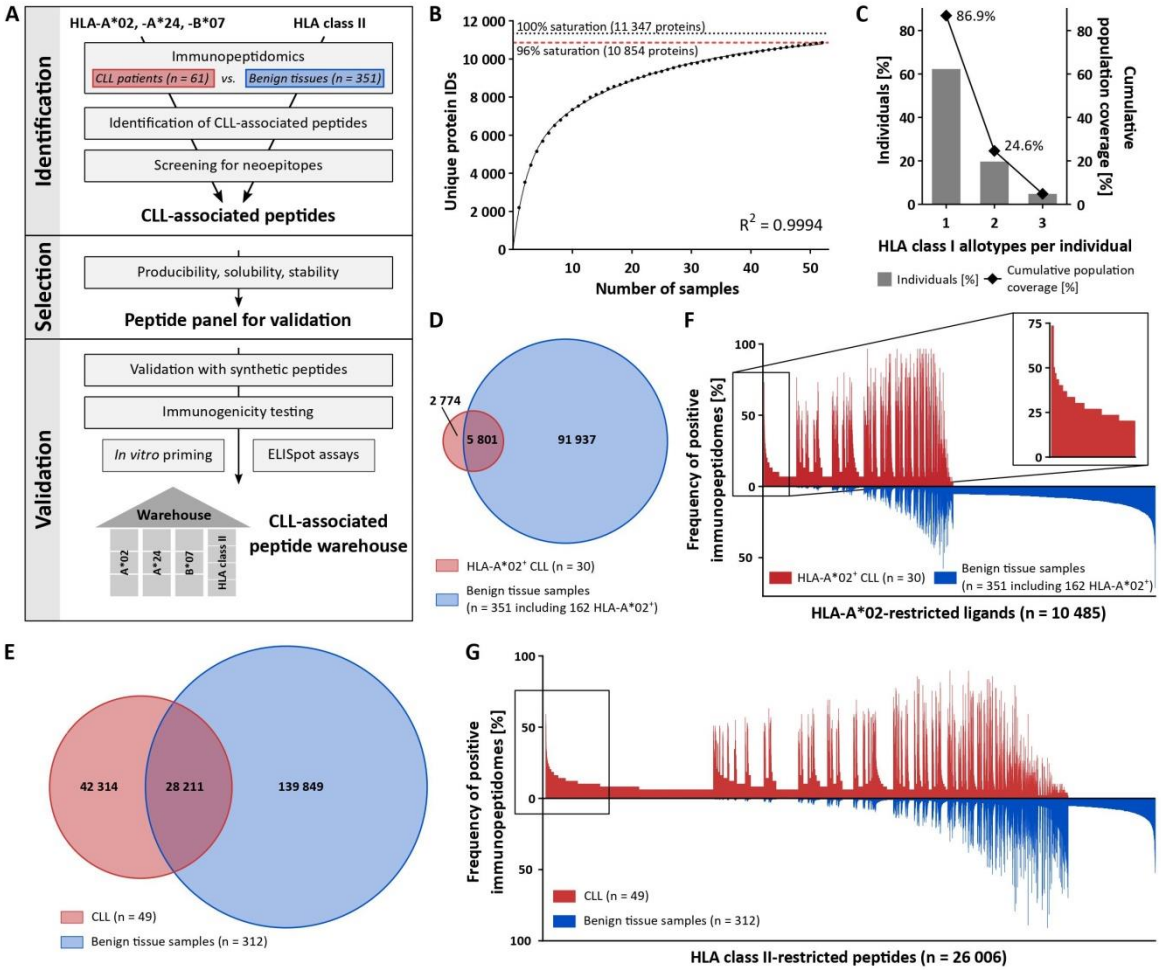

Figure 1: Comparative immunopeptidome profiling identifies CLL-associated antigens. (A) Mass spectrometry-based workflow for the design of a CLL-associated immunopeptidome-derived peptide warehouse. **(B)** Saturation analysis of source proteins of HLA class I-presented peptides. Number of unique source protein identifications shown as a function of cumulative immunopeptidome analysis of CLL samples (n = 52). Exponential regression allowed for the robust calculation of the maximum attainable number of different source protein identifications (dotted line). The dashed red line depicts the source proteome coverage achieved in the CLL cohort. **(C)** HLA-A*02, -A*24, and -B*07 allotype coverage within the CLL cohort (n = 61). The frequencies of individuals within the CLL cohort carrying up to three HLA allotypes (x-axis) are indicated as gray bars on the left y-axis. The cumulative percentage of population coverage is depicted as black dots on the right y-axis. **(D, E)** Overlap analysis of **(D)** HLA-A*02- and **(E)** HLA class II-restricted peptide identifications of primary CLL samples (D, n = 30; E, n = 49) and benign tissue samples (D, n = 351 including 162 HLA-A*02$^+$; E, n = 312). **(F, G)** Comparative immunopeptidome profiling of **(F)** HLA-A*02- and **(G)** HLA class II-presented peptides based on the frequency of HLA-restricted presentation in immunopeptidomes of CLL and benign tissue samples. Frequencies of positive immunopeptidomes for the respective HLA-presented peptides (x-axis) are indicated on the y-axis. To allow for better readability, HLA-presented peptides identified in < 5% of the samples within the respective cohort were not depicted. The box on the left highlights the subset of CLL associated antigens that show CLL-exclusive high-frequent presentation. IDs, identifications.

For the identification of broadly applicable non-mutated CLL-associated antigens, we focused on antigens presented by the common allotypes HLA-A*02, -A*24, and -B*07. In total, 87% (53/61, 61% A*02$^+$, 28% A*24$^+$, 28% B*07$^+$) of CLL patients in our cohort carry at least one of the selected HLA class I allotypes (Fig. 1C). In comparison, 76% of patients included in a previous CLL peptide vaccination trial (NCT02802943), 68% of the European population, and 61% of the world population carry one or more of these HLA allotypes (Fig. S1B-D). Allotype-specific immunopeptidome analysis revealed 8,575

unique HLA-A*02- (range 82-3,723, mean 1,121 per sample), 5,280 unique HLA-A*24- (range 134-1,926, mean 1,042 per sample), and 5,780 unique HLA-B*07-restricted (range 223-2,933, mean 1,140 per sample) peptides derived from 5,020, 3,813, and 3,886 source proteins achieving 89%, 85%, and 86% of the estimated maximum attainable protein coverage, respectively (Fig. S1E-G and Table S4). For comparative immunopeptidome profiling we utilized a dataset of benign hematological and non-hematological (www.hla-ligand-atlas.org) tissue samples (n = 351 for HLA class I, n = 312 for HLA class II) including 162 HLA-A*02$^+$, 39 HLA-A*24$^+$, and 63 HLA-B*07$^+$ samples, comprising 97,738 unique HLA class I- and 168,060 HLA class II-presented peptides. Overlap analysis of the total HLA class I immunopeptidome of the CLL cohort with the benign tissue cohort revealed 23,676 peptides to be exclusively presented on CLL samples and never on benign tissue samples (Fig. S1H). Allotype-specific overlap analysis with the entirety of benign tissue-derived immunopeptidomes revealed 2,774 HLA-A*02-, 1,440 HLA-A*24-, and 1,450 HLA-B*07-presented peptides detected exclusively on CLL samples (Fig. 1D and Fig. S1I,J). For HLA class II, overlap analysis identified 42,314 peptides to be CLL-exclusive (Fig. 1E). At a target-definition FDR of < 1%, a total of 393 HLA A*02-, 168 HLA-A*24-, and 127 HLA-B*07-restricted ligands with allotype-specific representation frequencies up to 73%, 81%, and 60%, respectively, and 3,970 HLA class II-restricted peptides with frequencies up to 59% were identified (Fig. 1F,G, Fig. S1K,L and Fig. S2).

The Role of Neoantigens in the Immunopeptidome of CLL

In addition to the identification of high-frequent non-mutated tumor-associated peptides, we screened our CLL cohort for naturally presented neoepitopes derived from common CLL-associated point and frameshift mutations (95 point and 3 frameshift mutations within 61 different genes representing 85 different mutation sites, Table S3). Even though these mutations potentially provide HLA binding motifs for several HLA allotypes, no naturally HLA-presented neoepitopes were identified in our immunopeptidome analyses. Of note, we were able to identify wild-type peptides derived from 57/61 (93%) mutation-bearing proteins in benign and/or CLL immunopeptidomes with an average of 15 and 11 HLA class I- and HLA class II-presented peptides per protein, respectively. However, only 17/85 (20%) mutation sites are covered directly by wild-type peptides as most of the recurrent CLL-associated mutations are located in “dark spots” of the immunopeptidome, defined as protein regions without any detectable HLA-presented peptides (Fig. 2A,B).

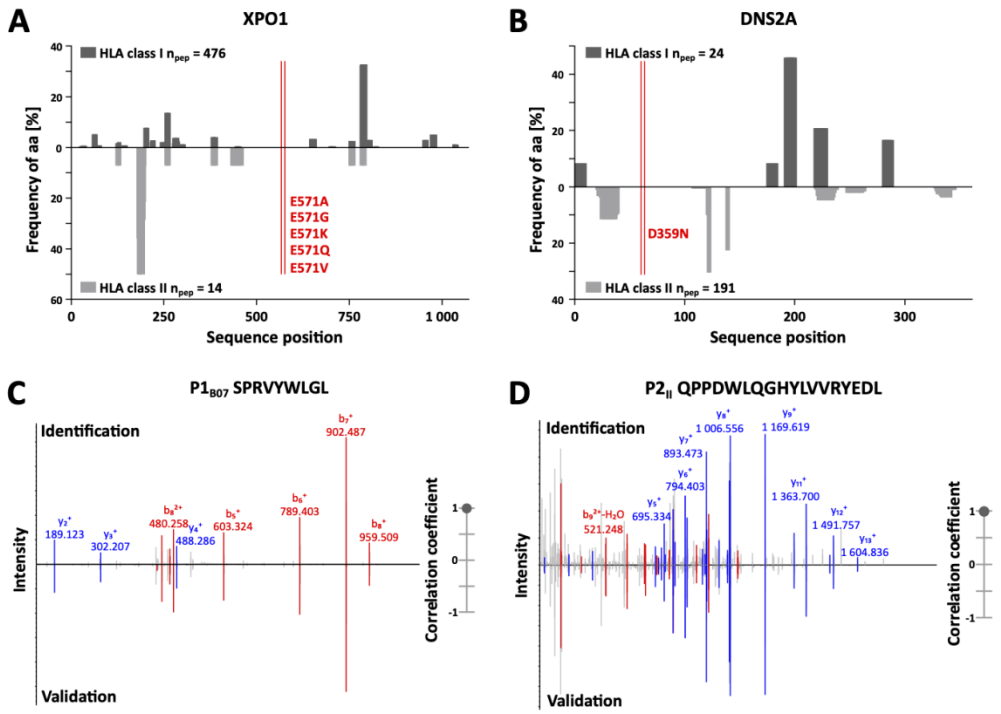

Figure 2: Immunopeptidome coverage of common CLL mutation sites and spectral validation of CLL-associated peptides. **(A, B)** Hotspot and dark spot analysis by HLA class I (above x-axis) and HLA class II (below x-axis) peptide clustering. All identified HLA class I- and HLA class II-presented peptides of the CLL and benign tissue immunopeptidomes were mapped to their amino acid positions within the respective source protein. Representative examples are shown for **(A)** XPO1 and **(B)** DNS2A. Representation frequencies of amino acid counts for the respective amino acid position (x-axis) were calculated and are indicated on the y-axis. The red lines highlight the analyzed mutation sites of recurrent CLL-associated mutations. **(C, D)** Representative examples of the validation of the experimentally eluted **(C)** HLA class I-restricted peptide $P1_{B07}$ and **(D)** the HLA class II-restricted peptide $P2_{II}$ using synthetic isotope-labeled peptides. Comparison of fragment spectra (m/z on the x-axis) of peptides eluted from primary CLL patient samples (identification) to their corresponding synthetic peptides (validation). The spectra of the synthetic peptides are mirrored on the x-axis. Identified b- and y-ions are marked in red and blue, respectively. The calculated spectral correlation coefficients are depicted on the right graph, respectively. aa, amino acid; n_{pep}, number of peptides.

Definition of Peptide Warehouse

For the setup of a broadly applicable peptide warehouse, we focused on the 532 non-mutated peptides presented by ≥ 20% of (HLA-matched) CLL samples comprising 82 HLA-A*02-, 105 HLA-A*24-, 127 HLA B*07-, and 218 HLA class II-restricted peptides (Tables S5-S8). For HLA class II, 184/218 (84%) peptides showed length variants (> 50% overlap) that were presented on benign samples and were therefore omitted.

To enable the peptide warehouse production for clinical application, further selection steps, including approval of producibility, solubility, and stability of target antigens under GMP conditions, delineated a 14-peptide panel (Table 1) comprising 9 HLA class I- (3 for each allotype) and 5 HLA class II-restricted CLL-exclusive high-frequent target antigens. Experimentally acquired spectra of the selected peptide identifications were validated by comparison of mass spectrometric fragment spectra using isotope-labeled synthetic peptides (Fig. 2C,D and Fig. S3).

Table 1: Immunogenicity of CLL-associated warehouse peptides.

Peptide ID	Sequence	Source protein	HLA restriction	Peptide length	Allotype-specific frequency	T cell response in CLL	*In vitro* $CD8^+$ T cell priming in HVs	Functionality of peptide-specific T cells after *in vitro* priming
$P1_{A02}$	VIAELPPKV	IGHM	A*02	9	47%	0/19 (0%)	3/3	TNF^+
$P2_{A02}$	ALHRPDVYL	IGHM	A*02	9	40%	0/19 (0%)	3/3	TNF^+
$P3_{A02}$	TLDTSKLYV	RGRF1	A*02	9	37%	0/19 (0%)	3/3	IFN-γ^+ TNF^+
$P1_{A24}$	GYMPYLNRF	SWP70	A*24	9	56%	0/14 (0%)	3/3	IFN-γ^+ TNF^+
$P2_{A24}$	KYSKALIDYF	AFF3	A*24	10	50%	0/14 (0%)	2/3	IFN-γ^+ TNF^+
$P3_{A24}$	RHTGALPLF	SI1L3	A*24	9	50%	0/14 (0%)	3/3	IFN-γ^+ TNF^+ $CD107a^+$
$P1_{B07}$	SPRVYWLGL	CL17A	B*07	9	53%	4/14 (29%)	3/3	IFN-γ^+ TNF^+ $CD107a^+$
$P2_{B07}$	RPSNKAPLL	EHMT1	B*07	9	47%	0/14 (0%)	3/3	IFN-γ^+ TNF^+ $CD107a^+$
$P3_{B07}$	LPRLEALDL	TLR9	B*07	9	40%	4/14 (29%)	3/3	IFN-γ^+ TNF^+ $CD107a^+$
$P1_{II}$	GSSFFGELFNQNPE	CHST2	class II	14	59%	4/10 (40%)	-	-
$P2_{II}$	QPPDWLQGHYLVVRYEDL	CHST2	class II	18	29%	5/10 (50%)	-	-
$P3_{II}$	YPDRPGWLRYIQRTPYSDG	SGCE	class II	19	27%	2/10 (20%)	-	-
$P4_{II}$	DHAQLVAIKTLKDYNNPQ	ROR1	class II	18	24%	0/10 (0%)	-	-
$P5_{II}$	LLLILRDPSERVLSDY	HS3S1	class II	16	24%	3/10 (30%)	-	-

ID, identification; HVs, healthy volunteers.

Warehouse Peptides Show Pre-Existing and *De Novo* Inducible Immune Responses in CLL Patients and HVs

In the final step, selected peptide targets were analyzed for their immunogenicity, *i.e.*, their potential to induce antigen-specific T cell responses. Using aAPC-based *in vitro* priming of naive $CD8^+$ T cells of HLA-matched HVs, we confirmed induction of peptide-specific $CD8^+$ T cells for all 9 HLA class I peptides in at least 2/3 HVs (Fig. 3A, Fig. S4A,B, Table 1). Intracellular cytokine and degranulation marker staining revealed induction of multifunctional peptide-specific T cells for 7/9 (78%) peptides (Fig. 3B, Fig. S4C,D, Table 1). Moreover, IFN-γ ELISpot assays, using PBMCs from HLA-matched CLL patients, revealed preexisting peptide-specific memory T cells targeting 2/9 (22%) and 4/5 (80%) HLA class I- and HLA class II-restricted warehouse peptides in up to 29% and 50% of CLL patient samples, respectively (Fig. 3C,D, Fig. S5 and Table 1). In total, we validated 13/14 (93%) of the preselected naturally presented CLL associated HLA class I- and HLA class II-restricted peptides as immunogenic, with either pre-existing or *de novo* inducible immune responses, unveiling these as ideal targets for peptide-based immunotherapy approaches.

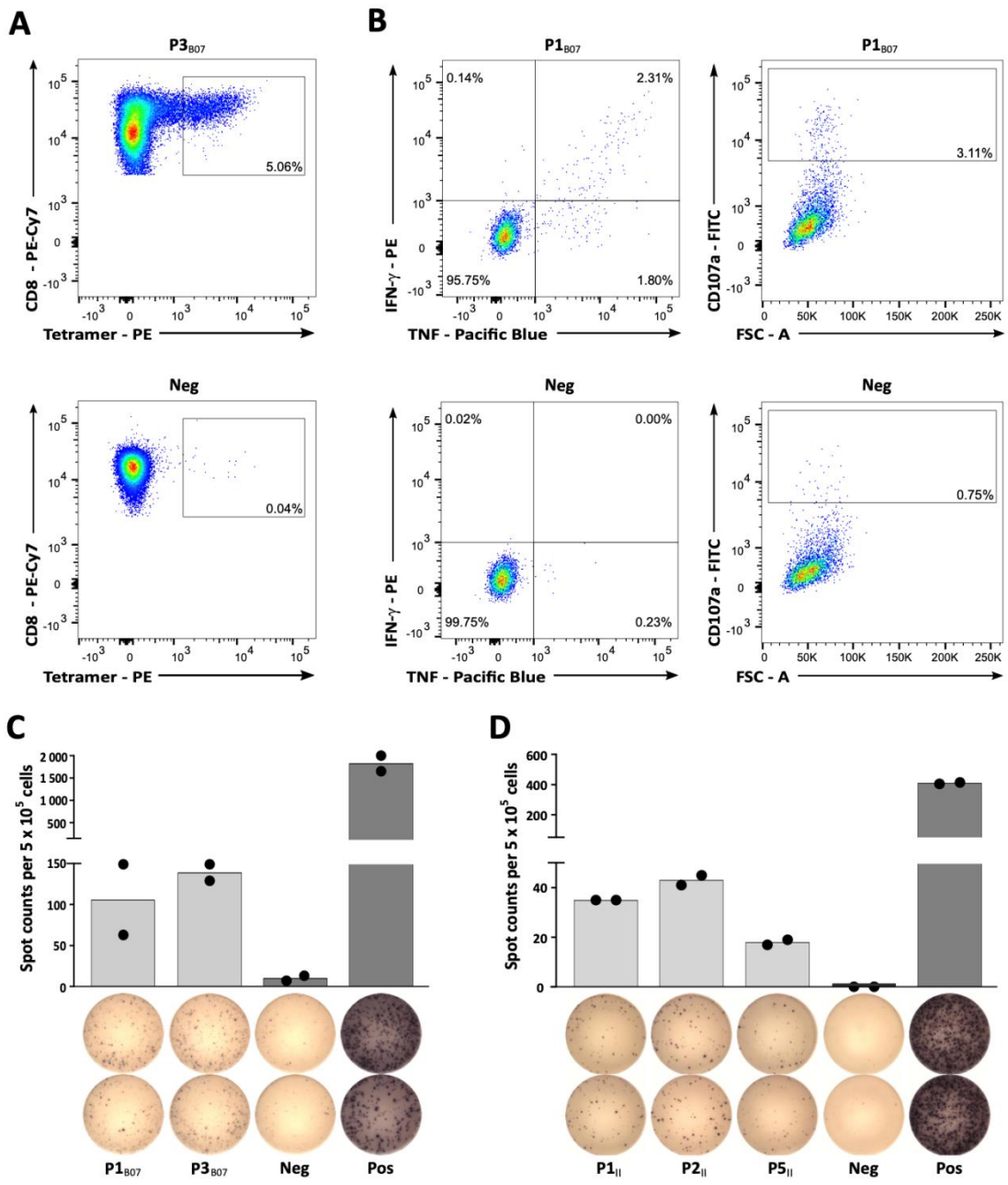

Figure 3: Immunogenicity analyses of CLL-associated peptides. (A) Representative example of $P3_{B07}$-specific tetramer staining of $CD8^+$ T cells after 4 cycles of aAPC-based *in vitro* priming. Graphs show single, viable cells stained for CD8 and PE-conjugated multimers of indicated specificity. The upper panel displays $P3_{B07}$-tetramer staining of T cells primed with $P3_{B07}$. The lower panel (negative control) depicts $P3_{B07}$-tetramer staining of T cells from the same donor primed with an HLA-matched irrelevant control peptide. **(B)** Functional characterization of induced $P1_{B07}$-specific $CD8^+$ T cells after *in vitro* aAPC-based priming by intracellular cytokine (IFN-γ, TNF) and degranulation marker (CD107a) staining. Representative example of IFN-γ and TNF production as well as CD107a expression after stimulation with the peptide $P1_{B07}$ compared to an HLA-matched negative control peptide. **(C, D)** Representative examples of preexisting T cell responses to **(C)** HLA-B*07- and **(D)** HLA class II-restricted peptides as evaluated by IFN-γ ELISpot assays after 12-day *in vitro* expansion using PBMC samples of CLL patients (C, UPN064; D, UPN066). Data are presented as scatter dot plot with mean. FSC, forward scatter; Neg, negative control; Pos, positive control.

Discussion

We present a novel workflow for the immunopeptidomics-guided design of off-the-shelf peptide warehouses, here applied to CLL as a representative of low-mutational burden tumor entities. The

mass spectrometry-based characterization of high-frequent, non-mutated, tumor-associated, and immunogenic antigens naturally presented on primary CLL samples enables the development of a personalized peptide-based immunotherapy in a time- and cost-effective manner and can be easily transferred to other tumor entities.

The treatment landscape for CLL has faced profound changes with the development and clinical success of targeted therapies in the past years (*47, 48*), including the Bruton's tyrosine kinase (BTK) inhibitor ibrutinib (*49*). However, beside the combination of anti-CD20 antibodies and venetoclax, all novel substances require continuous treatment bearing the risk of therapy resistance and accumulation of side effects. Current efforts are now focusing on the further and earlier elimination of minimal residual disease (MRD) to allow for reduced treatment duration and the therewith associated side effects, as well as the achievement of long-lasting remission and potential cure in the future. The favorable immune effector-to-target cell ratios in the MRD setting and the immunogenicity of CLL (*26, 27*) suggest that this malignancy might be effectively targeted by peptide-based immunotherapy.

For the clinical application of such approaches three different strategies have been proposed. (i) Stratification, applying an invariant drug product to every patient, seems unsuitable due to the patient-individual HLA allotypes. Therefore, such an approach must focus on very common HLA allotypes thereby excluding a substantial proportion of patients. In addition, as shown by us and others, even in allotype-matched patients of the same entity, presentation of tumor-associated peptides is not given in 100% of tumors, calling for more personalized approaches of target selection (*21, 50*). However, the broad applicability of (ii) completely individualized peptide vaccine concepts is hampered, since these are based on time- and cost-intensive patient-specific identification and selection processes and on-demand *de novo* drug production (*1, 5, 51*). The approach of (iii) peptide warehouse design, comprising a collection of pre-defined and pre-manufactured high-frequent tumor-associated peptides, enables the subsequent composition of patient-specific vaccine cocktails based on individual characteristics (*5, 10, 52*).

In recent years, multiple peptide vaccination approaches were focused on the targeting of neoepitopes from tumor mutations as prime tumor-specific targets. For tumor entities with high mutational burden, such as melanoma, high immunogenicity and first signs of clinical efficacy have been demonstrated (*1, 53*). However, only a minority of mutations at the DNA sequence level is translated and processed to naturally presented HLA-restricted neoepitopes that can be targeted by T cells (*2, 16, 54, 55*). This is in line with our data demonstrating the lack of naturally presented neoantigens in the immunopeptidome of CLL. Together with recent immunopeptidomic studies (*16, 21, 56*) we showed that HLA-presented peptides are not randomly distributed across protein sequences but rather show "hotspot" locations of presentation. Most of the recurrent CLL-associated mutations are located in "dark spots" of the immunopeptidome, defined as protein regions without any detectable

HLA-presented peptides, explaining the rare detection of neoepitopes especially in low mutational burden entities. The underlying reasons for the occurrence of such hotspots and corresponding dark spots still remain ambiguous but might include differential proteasomal cleavage, peptide processing, and HLA-binding (*16, 56, 57*). Thus, the role of neoantigen-based T cell responses in tumor entities with low-mutational burden remains obscure, calling for the application of alternative targets in peptide-based immunotherapy approaches (*1-3*). Non-mutated tumor peptides, arising through altered gene expression or protein processing in the tumor cells have been suggested as vaccine targets for many years (*4-10, 13, 58, 59*). However, although numerous clinical trials reported peptide-specific T cell induction upon vaccination with non-mutated tumor antigens, no correlation with clinical activity was shown and no meaningful clinical results were achieved (*4-10*). Nevertheless, there are two main points that prompt us and others, despite former disappointing clinical data, to use novel technologies and methods to unravel and resolve the underlying issues and limitations of non-mutated antigen-based vaccines: (i) Several studies report on the existence of spontaneous preexisting T cell responses targeting non-mutated tumor antigens and their correlation with beneficial clinical outcome, suggesting a pathophysiological relevance of these immune responses *in vivo* (*11-14*) and (ii) recent data show that immune checkpoint inhibitor-mediated T cell responses are not only targeting neoepitopes but also non-mutated tumor antigens (*60-62*).

Several unmet issues that hamper the development of effective peptide vaccines have been identified in recent years and need to be considered and addressed during future peptide vaccine design. These include target antigen selection, time points of application, and selection of combinatorial drugs (*15, 63*). Within this study we aimed to address one obvious and often discussed issue of former vaccination trials, where peptide selection included non-mutated tumor antigens that were never proven to be naturally presented on the tumor cell surface of the individual patients. For multiple of the applied "classical" tumor antigens novel analyses showed a distorted correlation of tumor-associated presentation on mRNA level, and limited or even lacking presentation on the immunopeptidome level (*16-22*) highlighting that the immunopeptidome is an independent complex layer formed by the antigen presentation machinery, and does not necessarily mirror the transcriptome or proteome. Therefore, it is essential to use direct methods of peptide target identification (*64*). This can be realized by mass spectrometry-based analysis of the entirety of naturally presented HLA ligands, termed the HLA ligandome or immunopeptidome of cancer cells (*65*). In recent years, we and others worked intensively on the characterization of such naturally presented tumor-associated peptides based on the direct isolation of HLA class I- and class II-presented ligands from tumor cells and the subsequent identification by mass spectrometry (*21-24, 66, 67*). Our approach allowed the identification of distinct panels of high-frequent non-mutated tumor peptides across multiple donors.

In addition to cytotoxic $CD8^+$ T cells, $CD4^+$ T cells play important direct and indirect roles in anti-cancer immunity (*68*) and therefore are indispensable for vaccination approaches. Consequently, the here described workflow comprises target selection of multiple HLA class I- and HLA class II-presented peptides to prevent antigen loss and reduce the risk of immune escape, which often occurs under therapeutic pressure (*69, 70*). Furthermore, the promiscuous binding motifs of HLA class II molecules enable a broad allotype-independent application of these peptides.

Moreover, the detection of preexisting memory T cell responses targeting our warehouse peptides underscores the pathophysiological relevance of our selected antigen targets for immune surveillance in CLL.

Further limitations of peptide vaccines in general, and in particular of non-mutated antigen vaccine peptides, comprise tumor evasion, immune-editing and immune cell exhaustion (*71*). Increased numbers of regulatory T cells (T_{reg}) have been associated with a worse outcome of vaccination, both in mice and patients (*72, 73*). In addition, peripheral tolerance limits the available T cell repertoire capable of recognizing cancer cells with high affinity. T cell recruitment is often impaired by an immunosuppressive tumor environment (*74*) and the aberrant tumor vasculature actively suppresses the access of cancer-specific T cells (*75*), which limits therapeutic vaccine efficacy. Therefore, combinatorial approaches to further improve vaccine-induced effects are currently being investigated. These include strategies to deplete or modulate T_{regs} (*7, 76-80*) as well as the development of modified, so-called heteroclitic, vaccine peptides to enhance low-affinity T cells (*81, 82*). Furthermore, to overcome limited T cell function and recruitment, combinatorial approaches with immune checkpoint inhibitors (*83, 84*) as well as with direct or indirect microenvironment modifiers, such as MEK or PARP inhibitors as well as VEGF-targeting antibody- or inhibitor-based therapies, are already evaluated (*85*). The importance of a rational selection of combinatorial drugs was recently demonstrated in a phase III peptide vaccination study (*86*), which failed to confirm the vaccine-induced immune responses and clinical outcome reported in the preceding phase II trial (*7*). Here, the combination of the peptide vaccine with the tyrosine kinase inhibitor sunitinib, for which a negative impact on T cell responses was described (*87*), was suggested as an underlying reason. In contrast, a supporting and positive effect on T cell functionality was proven for other tyrosine kinase inhibitors, such as ibrutinib (*88-90*), suggesting this BTK inhibitor as a potential combination drug for peptide vaccines in CLL patients.

Together, this study presents a mass spectrometry-based workflow for the design of an immunopeptidome-derived off-the-shelf CLL-associated peptide warehouse, which is currently being evaluated within a first personalized multi-peptide vaccine trial in combination with the novel adjuvant XS15 (*91*) in CLL patients under ibrutinib treatment (iVAC-XS15-CLL01, NCT04688385). Integrating next generation developments and insights, in terms of antigen selection, interaction of tumor cells with the immune system and rational selection of combination therapies, we aim to contribute a further

step on the way to clinically effective peptide vaccinations with this study. Our warehouse design concept is further easily transferable to other tumor entities, enabling the construction of broadly applicable peptide warehouses, which provide the foundation for the development of time- and cost-effective personalized T cell-based immunotherapy approaches.

Conflict of Interest

H-G.R. is shareholder of Immatics Biotechnologies GmbH, Synimmune GmbH, and Curevac AG, and holds a patent application on an adjuvant, XS15. A.N., H-G.R., and J.S.W. are listed as inventors on patents related to peptides described in this manuscript.

The remaining authors declare that the research was conducted in the absence of any commercial or financial relationships that could be construed as a potential conflict of interest.

Author Contributions

AN, YM, H-GR, and JSW designed the study. AN, AM, and JB performed immunopeptidome experiments. YM. and TB conducted *in vitro* T cell experiments. HRS, MR, JSH, MCN, WEA, CD, GI, and JSW provided new reagents/analytic tools/samples. HRS, MR, JSH, MCN, WEA, CD, GI, and JSW collected patient data. AN, YM, and JSW analyzed data. AN, YM, and JSW wrote the manuscript. All authors revised the manuscript. H-GR and JSW supervised the study. All authors contributed to the article and approved the submitted version.

Funding

This work was supported by the Deutsche Forschungsgemeinschaft (DFG, German Research Foundation, Grant WA 4608/1-2), the Deutsche Forschungsgemeinschaft under Germany's Excellence Strategy (Grant EXC2180-390900677), the German Cancer Consortium (DKTK), the Wilhelm Sander Stiftung (Grant 2016.177.2), the José Carreras Leukämie-Stiftung (Grant DJCLS 05 R/2017), and the Fortüne Program of the University of Tübingen (Fortüne number 2451-0-0 and 2581 0 0).

Acknowledgements

We thank Ulrike Schmidt, Sabrina Sauter, Hannah Zug, Claudia Falkenburger, Beate Pömmerl, and Ulrich Wulle for technical support.

Data availability

The mass spectrometry data have been deposited to the ProteomeXchange Consortium (http://proteomecentral.proteomexchange.org) via the PRIDE (*92*) partner repository with the dataset identifier PXD024871.

Reviewer account to the ProteomeXchange Consortium via the PRIDE partner repository:

Username: reviewer_pxd024871@ebi.ac.uk

Password: yel1NVF2

Footnotes

Received 2021 May 6, Accepted 2021 Jun 24.

The published online version of this article contains the full Supplementary Materials.

References

1. P. A. Ott, Z. Hu, D. B. Keskin, S. A. Shukla, J. Sun, D. J. Bozym, W. Zhang, A. Luoma, A. Giobbie-Hurder, L. Peter, C. Chen, O. Olive, T. A. Carter, S. Li, D. J. Lieb, T. Eisenhaure, E. Gjini, J. Stevens, W. J. Lane, I. Javeri, K. Nellaiappan, A. M. Salazar, H. Daley, M. Seaman, E. I. Buchbinder, C. H. Yoon, M. Harden, N. Lennon, S. Gabriel, S. J. Rodig, D. H. Barouch, J. C. Aster, G. Getz, K. Wucherpfennig, D. Neuberg, J. Ritz, E. S. Lander, E. F. Fritsch, N. Hacohen, C. J. Wu, An immunogenic personal neoantigen vaccine for patients with melanoma. *Nature* **547**, 217-221 (2017).
2. M. Yadav, S. Jhunjhunwala, Q. T. Phung, P. Lupardus, J. Tanguay, S. Bumbaca, C. Franci, T. K. Cheung, J. Fritsche, T. Weinschenk, Z. Modrusan, I. Mellman, J. R. Lill, L. Delamarre, Predicting immunogenic tumour mutations by combining mass spectrometry and exome sequencing. *Nature* **515**, 572-576 (2014).
3. O. J. Finn, H. G. Rammensee, Is It Possible to Develop Cancer Vaccines to Neoantigens, What Are the Major Challenges, and How Can These Be Overcome? Neoantigens: Nothing New in Spite of the Name. *Cold Spring Harb Perspect Biol* **10**, (2018).
4. M. Schmitt, A. Schmitt, M. T. Rojewski, J. Chen, K. Giannopoulos, F. Fei, Y. Yu, M. Gotz, M. Heyduk, G. Ritter, D. E. Speiser, S. Gnjatic, P. Guillaume, M. Ringhoffer, R. F. Schlenk, P. Liebisch, D. Bunjes, H. Shiku, H. Dohner, J. Greiner, RHAMM-R3 peptide vaccination in patients with acute myeloid leukemia, myelodysplastic syndrome, and multiple myeloma elicits immunologic and clinical responses. *Blood* **111**, 1357-1365 (2008).
5. N. Hilf, S. Kuttruff-Coqui, K. Frenzel, V. Bukur, S. Stevanovic, C. Gouttefangeas, M. Platten, G. Tabatabai, V. Dutoit, S. H. van der Burg, P. Thor Straten, F. Martinez-Ricarte, B. Ponsati, H. Okada, U. Lassen, A. Admon, C. H. Ottensmeier, A. Ulges, S. Kreiter, A. von Deimling, M. Skardelly, D. Migliorini, J. R. Kroep, M. Idorn, J. Rodon, J. Piro, H. S. Poulsen, B. Shraibman, K. McCann, R. Mendrzyk, M. Lower, M. Stieglbauer, C. M. Britten, D. Capper, M. J. P. Welters, J. Sahuquillo, K. Kiesel, E. Derhovanessian, E. Rusch, L. Bunse, C. Song, S. Heesch, C. Wagner, A. Kemmer-Bruck, J. Ludwig, J. C. Castle, O. Schoor, A. D. Tadmor, E. Green, J. Fritsche, M. Meyer, N. Pawlowski, S. Dorner, F. Hoffgaard, B. Rossler, D. Maurer, T. Weinschenk, C. Reinhardt, C. Huber, H. G. Rammensee, H. Singh-Jasuja, U. Sahin, P. Y. Dietrich, W. Wick, Actively personalized vaccination trial for newly diagnosed glioblastoma. *Nature* **565**, 240-245 (2019).
6. Y. Oka, A. Tsuboi, T. Taguchi, T. Osaki, T. Kyo, H. Nakajima, O. A. Elisseeva, Y. Oji, M. Kawakami, K. Ikegame, N. Hosen, S. Yoshihara, F. Wu, F. Fujiki, M. Murakami, T. Masuda, S. Nishida, T. Shirakata, S. Nakatsuka, A. Sasaki, K. Udaka, H. Dohy, K. Aozasa, S. Noguchi, I. Kawase, H. Sugiyama, Induction of WT1 (Wilms' tumor gene)-specific cytotoxic T lymphocytes by WT1 peptide vaccine and the resultant cancer regression. *Proc Natl Acad Sci U S A* **101**, 13885-13890 (2004).
7. S. Walter, T. Weinschenk, A. Stenzl, R. Zdrojowy, A. Pluzanska, C. Szczylik, M. Staehler, W. Brugger, P. Y. Dietrich, R. Mendrzyk, N. Hilf, O. Schoor, J. Fritsche, A. Mahr, D. Maurer, V. Vass, C. Trautwein, P. Lewandrowski, C. Flohr, H. Pohla, J. J. Stanczak, V. Bronte, S. Mandruzzato, T. Biedermann, G. Pawelec, E. Derhovanessian, H. Yamagishi, T. Miki, F. Hongo, N. Takaha, K. Hirakawa, H. Tanaka, S. Stevanovic, J. Frisch, A. Mayer-Mokler, A. Kirner, H. G. Rammensee, C. Reinhardt, H. Singh-Jasuja, Multipeptide immune response to cancer vaccine IMA901 after single-dose cyclophosphamide associates with longer patient survival. *Nat Med* **18**, 1254-1261 (2012).

8. P. F. Brunsvig, J. A. Kyte, C. Kersten, S. Sundstrom, M. Moller, M. Nyakas, G. L. Hansen, G. Gaudernack, S. Aamdal, Telomerase peptide vaccination in NSCLC: a phase II trial in stage III patients vaccinated after chemoradiotherapy and an 8-year update on a phase I/II trial. *Clin Cancer Res* **17**, 6847-6857 (2011).
9. J. M. Hubbard, C. Cremolini, R. P. Graham, R. Moretto, J. L. Mitchell, J. Wessling, E. R. Toke, Z. Csiszovszki, O. Lőrincz, L. Molnar, E. Somogyi, M. Megyesi, K. Pantya, J. Tóth, P. Páles, I. Miklós, A. Falcone, Evaluation of safety, immunogenicity, and preliminary efficacy of PolyPEPI1018 off-the-shelf vaccine with fluoropyrimidine/bevacizumab maintenance therapy in metastatic colorectal cancer (mCRC) patients. *Journal of Clinical Oncology* **38**, 4048-4048 (2020).
10. K. Yoshimura, T. Minami, M. Nozawa, T. Kimura, S. Egawa, H. Fujimoto, A. Yamada, K. Itoh, H. Uemura, A Phase 2 Randomized Controlled Trial of Personalized Peptide Vaccine Immunotherapy with Low-dose Dexamethasone Versus Dexamethasone Alone in Chemotherapy-naive Castration-resistant Prostate Cancer. *Eur Urol* **70**, 35-41 (2016).
11. R. Casalegno-Garduno, A. Schmitt, A. Spitschak, J. Greiner, L. Wang, I. Hilgendorf, C. Hirt, A. D. Ho, M. Freund, M. Schmitt, Immune responses to WT1 in patients with AML or MDS after chemotherapy and allogeneic stem cell transplantation. *Int J Cancer* **138**, 1792-1801 (2016).
12. M. Hojjat-Farsangi, M. Jeddi-Tehrani, A. H. Daneshmanesh, F. Mozaffari, A. Moshfegh, L. Hansson, S. M. Razavi, R. A. Sharifian, H. Rabbani, A. Osterborg, H. Mellstedt, F. Shokri, Spontaneous Immunity Against the Receptor Tyrosine Kinase ROR1 in Patients with Chronic Lymphocytic Leukemia. *PLoS One* **10**, e0142310 (2015).
13. D. J. Kowalewski, H. Schuster, L. Backert, C. Berlin, S. Kahn, L. Kanz, H. R. Salih, H. G. Rammensee, S. Stevanovic, J. S. Stickel, HLA ligandome analysis identifies the underlying specificities of spontaneous antileukemia immune responses in chronic lymphocytic leukemia (CLL). *Proc Natl Acad Sci U S A* **112**, E166-E175 (2015).
14. Y. Godet, E. Fabre, M. Dosset, M. Lamuraglia, E. Levionnois, P. Ravel, N. Benhamouda, A. Cazes, F. Le Pimpec-Barthes, B. Gaugler, P. Langlade-Demoyen, X. Pivot, P. Saas, B. Maillere, E. Tartour, C. Borg, O. Adotevi, Analysis of spontaneous tumor-specific CD4 T-cell immunity in lung cancer using promiscuous HLA-DR telomerase-derived epitopes: potential synergistic effect with chemotherapy response. *Clin Cancer Res* **18**, 2943-2953 (2012).
15. A. Nelde, H. G. Rammensee, J. S. Walz, The Peptide Vaccine of the Future. *Mol Cell Proteomics* **20**, 100022 (2021).
16. M. Bassani-Sternberg, E. Braunlein, R. Klar, T. Engleitner, P. Sinitcyn, S. Audehm, M. Straub, J. Weber, J. Slotta-Huspenina, K. Specht, M. E. Martignoni, A. Werner, R. Hein, H. B. D, C. Peschel, R. Rad, J. Cox, M. Mann, A. M. Krackhardt, Direct identification of clinically relevant neoepitopes presented on native human melanoma tissue by mass spectrometry. *Nat Commun* **7**, 13404 (2016).
17. A. O. Weinzierl, C. Lemmel, O. Schoor, M. Muller, T. Kruger, D. Wernet, J. Hennenlotter, A. Stenzl, K. Klingel, H. G. Rammensee, S. Stevanovic, Distorted relation between mRNA copy number and corresponding major histocompatibility complex ligand density on the cell surface. *Mol Cell Proteomics* **6**, 102-113 (2007).
18. M. H. Fortier, E. Caron, M. P. Hardy, G. Voisin, S. Lemieux, C. Perreault, P. Thibault, The MHC class I peptide repertoire is molded by the transcriptome. *J Exp Med* **205**, 595-610 (2008).
19. M. Bassani-Sternberg, S. Pletscher-Frankild, L. J. Jensen, M. Mann, Mass spectrometry of human leukocyte antigen class I peptidomes reveals strong effects of protein abundance and turnover on antigen presentation. *Mol Cell Proteomics* **14**, 658-673 (2015).
20. M. C. Neidert, D. J. Kowalewski, M. Silginer, K. Kapolou, L. Backert, L. K. Freudenmann, J. K. Peper, A. Marcu, S. S. Wang, J. S. Walz, F. Wolpert, H. G. Rammensee, R. Henschler, K. Lamszus, M. Westphal, P. Roth, L. Regli, S. Stevanovic, M. Weller, G. Eisele, The natural HLA ligandome of glioblastoma stem-like cells: antigen discovery for T cell-based immunotherapy. *Acta Neuropathol* **135**, 923-938 (2018).
21. T. Bilich, A. Nelde, L. Bichmann, M. Roerden, H. R. Salih, D. J. Kowalewski, H. Schuster, C. C. Tsou, A. Marcu, M. C. Neidert, M. Lubke, J. Rieth, M. Schemionek, T. H. Brummendorf, V.

Vucinic, D. Niederwieser, J. Bauer, M. Marklin, J. K. Peper, R. Klein, O. Kohlbacher, L. Kanz, H. G. Rammensee, S. Stevanovic, J. S. Walz, The HLA ligandome landscape of chronic myeloid leukemia delineates novel T-cell epitopes for immunotherapy. *Blood* **133**, 550-565 (2019).

22. C. Berlin, D. J. Kowalewski, H. Schuster, N. Mirza, S. Walz, M. Handel, B. Schmid-Horch, H. R. Salih, L. Kanz, H. G. Rammensee, S. Stevanovic, J. S. Stickel, Mapping the HLA ligandome landscape of acute myeloid leukemia: a targeted approach toward peptide-based immunotherapy. *Leukemia* **29**, 647-659 (2015).
23. S. Walz, J. S. Stickel, D. J. Kowalewski, H. Schuster, K. Weisel, L. Backert, S. Kahn, A. Nelde, T. Stroh, M. Handel, O. Kohlbacher, L. Kanz, H. R. Salih, H. G. Rammensee, S. Stevanovic, The antigenic landscape of multiple myeloma: mass spectrometry (re)defines targets for T-cell-based immunotherapy. *Blood* **126**, 1203-1213 (2015).
24. H. Schuster, J. K. Peper, H. C. Bösmüller, K. Rohle, L. Backert, T. Bilich, B. Ney, M. W. Loffler, D. J. Kowalewski, N. Trautwein, A. Rabsteyn, T. Engler, S. Braun, S. P. Haen, J. S. Walz, B. Schmid-Horch, S. Y. Brucker, D. Wallwiener, O. Kohlbacher, F. Fend, H. G. Rammensee, S. Stevanovic, A. Staebler, P. Wagner, The immunopeptidomic landscape of ovarian carcinomas. *Proc Natl Acad Sci U S A* **114**, E9942-E9951 (2017).
25. A. Reustle, M. Di Marco, C. Meyerhoff, A. Nelde, J. S. Walz, S. Winter, S. Kandabarau, F. Buttner, M. Haag, L. Backert, D. J. Kowalewski, S. Rausch, J. Hennenlotter, V. Stuhler, M. Scharpf, F. Fend, A. Stenzl, H. G. Rammensee, J. Bedke, S. Stevanovic, M. Schwab, E. Schaeffeler, Integrative -omics and HLA-ligandomics analysis to identify novel drug targets for ccRCC immunotherapy. *Genome Med* **12**, 32 (2020).
26. J. M. Ribera, N. Vinolas, A. Urbano-Ispizua, T. Gallart, E. Montserrat, C. Rozman, "Spontaneous" complete remissions in chronic lymphocytic leukemia: report of three cases and review of the literature. *Blood cells* **12**, 471-483 (1987).
27. J. G. Gribben, D. Zahrieh, K. Stephans, L. Bartlett-Pandite, E. P. Alyea, D. C. Fisher, A. S. Freedman, P. Mauch, R. Schlossman, L. V. Sequist, R. J. Soiffer, B. Marshall, D. Neuberg, J. Ritz, L. M. Nadler, Autologous and allogeneic stem cell transplantations for poor-risk chronic lymphocytic leukemia. *Blood* **106**, 4389-4396 (2005).
28. A. Nelde, D. J. Kowalewski, S. Stevanovic, Purification and Identification of Naturally Presented MHC Class I and II Ligands. *Methods Mol Biol* **1988**, 123-136 (2019).
29. A. Nelde, D. J. Kowalewski, L. Backert, H. Schuster, J. O. Werner, R. Klein, O. Kohlbacher, L. Kanz, H. R. Salih, H. G. Rammensee, S. Stevanovic, J. S. Walz, HLA ligandome analysis of primary chronic lymphocytic leukemia (CLL) cells under lenalidomide treatment confirms the suitability of lenalidomide for combination with T-cell-based immunotherapy. *Oncoimmunology* **128**, 3234 (2018).
30. J. K. Eng, A. L. McCormack, J. R. Yates, An approach to correlate tandem mass spectral data of peptides with amino acid sequences in a protein database. *J Am Soc Mass Spectrom* **5**, 976-989 (1994).
31. M. Hernandez-Sanchez, J. Kotaskova, A. E. Rodriguez, L. Radova, D. Tamborero, M. Abaigar, K. Plevova, R. Benito, N. Tom, M. Quijada-Alamo, V. Bikos, A. A. Martin, K. Pal, A. Garcia de Coca, M. Doubek, N. Lopez-Bigas, J. M. Hernandez-Rivas, S. Pospisilova, CLL cells cumulate genetic aberrations prior to the first therapy even in outwardly inactive disease phase. *Leukemia* **33**, 518-558 (2019).
32. N. A. Amin, S. N. Malek, Gene mutations in chronic lymphocytic leukemia. *Semin Oncol* **43**, 215-221 (2016).
33. J. G. Tate, S. Bamford, H. C. Jubb, Z. Sondka, D. M. Beare, N. Bindal, H. Boutselakis, C. G. Cole, C. Creatore, E. Dawson, P. Fish, B. Harsha, C. Hathaway, S. C. Jupe, C. Y. Kok, K. Noble, L. Ponting, C. C. Ramshaw, C. E. Rye, H. E. Speedy, R. Stefancsik, S. L. Thompson, S. Wang, S. Ward, P. J. Campbell, S. A. Forbes, COSMIC: the Catalogue Of Somatic Mutations In Cancer. *Nucleic Acids Res* **47**, D941-D947 (2019).
34. L. Kall, J. D. Canterbury, J. Weston, W. S. Noble, M. J. MacCoss, Semi-supervised learning for peptide identification from shotgun proteomics datasets. *Nat Methods* **4**, 923-925 (2007).

35. M. M. Schuler, M. D. Nastke, S. Stevanovic, SYFPEITHI: database for searching and T-cell epitope prediction. *Methods Mol Biol* **409**, 75-93 (2007).
36. I. Hoof, B. Peters, J. Sidney, L. E. Pedersen, A. Sette, O. Lund, S. Buus, M. Nielsen, NetMHCpan, a method for MHC class I binding prediction beyond humans. *Immunogenetics* **61**, 1-13 (2009).
37. V. Jurtz, S. Paul, M. Andreatta, P. Marcatili, B. Peters, M. Nielsen, NetMHCpan-4.0: Improved Peptide-MHC Class I Interaction Predictions Integrating Eluted Ligand and Peptide Binding Affinity Data. *J Immunol* **199**, 3360-3368 (2017).
38. T. Sturm, T. Leinders-Zufall, B. Macek, M. Walzer, S. Jung, B. Pommerl, S. Stevanovic, F. Zufall, P. Overath, H. G. Rammensee, Mouse urinary peptides provide a molecular basis for genotype discrimination by nasal sensory neurons. *Nat Commun* **4**, 1616 (2013).
39. U. H. Toprak, L. C. Gillet, A. Maiolica, P. Navarro, A. Leitner, R. Aebersold, Conserved peptide fragmentation as a benchmarking tool for mass spectrometers and a discriminating feature for targeted proteomics. *Mol Cell Proteomics* **13**, 2056-2071 (2014).
40. M. Widenmeyer, H. Griesemann, S. Stevanovic, S. Feyerabend, R. Klein, S. Attig, J. Hennenlotter, D. Wernet, D. V. Kuprash, A. Y. Sazykin, S. Pascolo, A. Stenzl, C. Gouttefangeas, H. G. Rammensee, Promiscuous survivin peptide induces robust CD4+ T-cell responses in the majority of vaccinated cancer patients. *Int J Cancer* **131**, 140-149 (2012).
41. J. D. Altman, P. A. Moss, P. J. Goulder, D. H. Barouch, M. G. McHeyzer-Williams, J. I. Bell, A. J. McMichael, M. M. Davis, Phenotypic analysis of antigen-specific T lymphocytes. *Science* **274**, 94-96 (1996).
42. J. K. Peper, H. C. Bosmuller, H. Schuster, B. Guckel, H. Horzer, K. Roehle, R. Schafer, P. Wagner, H. G. Rammensee, S. Stevanovic, F. Fend, A. Staebler, HLA ligandomics identifies histone deacetylase 1 as target for ovarian cancer immunotherapy. *Oncoimmunology* **5**, e1065369 (2016).
43. A. Neumann, H. Horzer, N. Hillen, K. Klingel, B. Schmid-Horch, H. J. Buhring, H. G. Rammensee, H. Aebert, S. Stevanovic, Identification of HLA ligands and T-cell epitopes for immunotherapy of lung cancer. *Cancer immunology, immunotherapy : CII* **62**, 1485-1497 (2013).
44. T. Hulsen, J. de Vlieg, W. Alkema, BioVenn - a web application for the comparison and visualization of biological lists using area-proportional Venn diagrams. *BMC Genomics* **9**, 488 (2008).
45. H. H. Bui, J. Sidney, K. Dinh, S. Southwood, M. J. Newman, A. Sette, Predicting population coverage of T-cell epitope-based diagnostics and vaccines. *BMC Bioinform* **7**, 153 (2006).
46. R. Vita, J. A. Overton, J. A. Greenbaum, J. Ponomarenko, J. D. Clark, J. R. Cantrell, D. K. Wheeler, J. L. Gabbard, D. Hix, A. Sette, B. Peters, The immune epitope database (IEDB) 3.0. *Nucleic Acids Res* **43**, D405-D412 (2015).
47. J. A. Burger, P. M. Barr, T. Robak, C. Owen, P. Ghia, A. Tedeschi, O. Bairey, P. Hillmen, S. E. Coutre, S. Devereux, S. Grosicki, H. McCarthy, D. Simpson, F. Offner, C. Moreno, S. Dai, I. Lal, J. P. Dean, T. J. Kipps, Long-term efficacy and safety of first-line ibrutinib treatment for patients with CLL/SLL: 5 years of follow-up from the phase 3 RESONATE-2 study. *Leukemia* **34**, 787-798 (2020).
48. J. F. Seymour, T. J. Kipps, B. Eichhorst, P. Hillmen, J. D'Rozario, S. Assouline, C. Owen, J. Gerecitano, T. Robak, J. De la Serna, Venetoclax–rituximab in relapsed or refractory chronic lymphocytic leukemia. *New England Journal of Medicine* **378**, 1107-1120 (2018).
49. J. A. Woyach, A. S. Ruppert, N. A. Heerema, W. Zhao, A. M. Booth, W. Ding, N. L. Bartlett, D. M. Brander, P. M. Barr, K. A. Rogers, S. A. Parikh, S. Coutre, A. Hurria, J. R. Brown, G. Lozanski, J. S. Blachly, H. G. Ozer, B. Major-Elechi, B. Fruth, S. Nattam, R. A. Larson, H. Erba, M. Litzow, C. Owen, C. Kuzma, J. S. Abramson, R. F. Little, S. E. Smith, R. M. Stone, S. J. Mandrekar, J. C. Byrd, Ibrutinib Regimens versus Chemoimmunotherapy in Older Patients with Untreated CLL. *N Engl J Med* **379**, 2517-2528 (2018).
50. N. Ternette, M. J. M. Olde Nordkamp, J. Muller, A. P. Anderson, A. Nicastri, A. V. S. Hill, B. M. Kessler, D. Li, Immunopeptidomic Profiling of HLA-A2-Positive Triple Negative Breast Cancer Identifies Potential Immunotherapy Target Antigens. *Proteomics* **18**, e1700465 (2018).

51. Y. Fang, F. Mo, J. Shou, H. Wang, K. Luo, S. Zhang, N. Han, H. Li, S. Ye, Z. Zhou, R. Chen, L. Chen, L. Liu, H. Wang, H. Pan, S. Chen, A Pan-cancer Clinical Study of Personalized Neoantigen Vaccine Monotherapy in Treating Patients with Various Types of Advanced Solid Tumors. *Clin Cancer Res* **26**, 4511-4520 (2020).
52. Y. Narita, Y. Arakawa, F. Yamasaki, R. Nishikawa, T. Aoki, M. Kanamori, M. Nagane, T. Kumabe, Y. Hirose, T. Ichikawa, H. Kobayashi, T. Fujimaki, H. Goto, H. Takeshima, T. Ueba, H. Abe, T. Tamiya, Y. Sonoda, A. Natsume, T. Kakuma, Y. Sugita, N. Komatsu, A. Yamada, T. Sasada, S. Matsueda, S. Shichijo, K. Itoh, M. Terasaki, A randomized, double-blind, phase III trial of personalized peptide vaccination for recurrent glioblastoma. *Neuro Oncol* **21**, 348-359 (2019).
53. U. Sahin, E. Derhovanessian, M. Miller, B. P. Kloke, P. Simon, M. Lower, V. Bukur, A. D. Tadmor, U. Luxemburger, B. Schrors, T. Omokoko, M. Vormehr, C. Albrecht, A. Paruzynski, A. N. Kuhn, J. Buck, S. Heesch, K. H. Schreeb, F. Muller, I. Ortseifer, I. Vogler, E. Godehardt, S. Attig, R. Rae, A. Breitkreuz, C. Tolliver, M. Suchan, G. Martic, A. Hohberger, P. Sorn, J. Diekmann, J. Ciesla, O. Waksmann, A. K. Bruck, M. Witt, M. Zillgen, A. Rothermel, B. Kasemann, D. Langer, S. Bolte, M. Diken, S. Kreiter, R. Nemecek, C. Gebhardt, S. Grabbe, C. Holler, J. Utikal, C. Huber, C. Loquai, O. Tureci, Personalized RNA mutanome vaccines mobilize poly-specific therapeutic immunity against cancer. *Nature* **547**, 222-226 (2017).
54. L. K. Freudenmann, A. Marcu, S. Stevanovic, Mapping the tumour human leukocyte antigen (HLA) ligandome by mass spectrometry. *Immunology* **154**, 331-345 (2018).
55. N. van Rooij, M. M. van Buuren, D. Philips, A. Velds, M. Toebes, B. Heemskerk, L. J. van Dijk, S. Behjati, H. Hilkmann, D. El Atmioui, M. Nieuwland, M. R. Stratton, R. M. Kerkhoven, C. Kesmir, J. B. Haanen, P. Kvistborg, T. N. Schumacher, Tumor exome analysis reveals neoantigen-specific T-cell reactivity in an ipilimumab-responsive melanoma. *J Clin Oncol* **31**, e439-442 (2013).
56. H. Pearson, T. Daouda, D. P. Granados, C. Durette, E. Bonneil, M. Courcelles, A. Rodenbrock, J. P. Laverdure, C. Cote, S. Mader, S. Lemieux, P. Thibault, C. Perreault, MHC class I-associated peptides derive from selective regions of the human genome. *J Clin Invest* **126**, 4690-4701 (2016).
57. F. Marino, A. Semilietof, J. Michaux, H. S. Pak, G. Coukos, M. Muller, M. Bassani-Sternberg, Biogenesis of HLA Ligand Presentation in Immune Cells Upon Activation Reveals Changes in Peptide Length Preference. *Front Immunol* **11**, 1981 (2020).
58. V. Mailander, C. Scheibenbogen, E. Thiel, A. Letsch, I. W. Blau, U. Keilholz, Complete remission in a patient with recurrent acute myeloid leukemia induced by vaccination with WT1 peptide in the absence of hematological or renal toxicity. *Leukemia* **18**, 165-166 (2004).
59. V. F. Van Tendeloo, A. Van de Velde, A. Van Driessche, N. Cools, S. Anguille, K. Ladell, E. Gostick, K. Vermeulen, K. Pieters, G. Nijs, B. Stein, E. L. Smits, W. A. Schroyens, A. P. Gadisseur, I. Vrelust, P. G. Jorens, H. Goossens, I. J. de Vries, D. A. Price, Y. Oji, Y. Oka, H. Sugiyama, Z. N. Berneman, Induction of complete and molecular remissions in acute myeloid leukemia by Wilms' tumor 1 antigen-targeted dendritic cell vaccination. *Proc Natl Acad Sci U S A* **107**, 13824-13829 (2010).
60. F. Berner, D. Bomze, S. Diem, O. H. Ali, M. Fassler, S. Ring, R. Niederer, C. J. Ackermann, P. Baumgaertner, N. Pikor, C. G. Cruz, W. van de Veen, M. Akdis, S. Nikolaev, H. Laubli, A. Zippelius, F. Hartmann, H. W. Cheng, G. Honger, M. Recher, J. Goldman, A. Cozzio, M. Fruh, J. Neefjes, C. Driessen, B. Ludewig, A. N. Hegazy, W. Jochum, D. E. Speiser, L. Flatz, Association of Checkpoint Inhibitor-Induced Toxic Effects With Shared Cancer and Tissue Antigens in Non-Small Cell Lung Cancer. *JAMA Oncol* **5**, 1043-1047 (2019).
61. J. A. Lo, M. Kawakubo, V. R. Juneja, M. Y. Su, T. H. Erlich, M. W. LaFleur, L. V. Kemeny, M. Rashid, M. Malehmir, S. A. Rabi, R. Raghavan, J. Allouche, G. Kasumova, D. T. Frederick, K. E. Pauken, Q. Y. Weng, M. Pereira da Silva, Y. Xu, A. A. J. van der Sande, W. Silkworth, E. Roider, E. P. Browne, D. J. Lieb, B. Wang, L. A. Garraway, C. J. Wu, K. T. Flaherty, C. E. Brinckerhoff, D. W. Mullins, D. J. Adams, N. Hacohen, M. P. Hoang, G. M. Boland, G. J. Freeman, A. H. Sharpe, D. Manstein, D. E. Fisher, Epitope spreading toward wild-type melanocyte-lineage antigens rescues suboptimal immune checkpoint blockade responses. *Sci Transl Med* **13**, (2021).

62. J. Zhou, J. Li, I. Guleria, T. Chen, A. Giobbie-Hurder, J. Stevens, M. Gupta, X. Wu, R. C. Brennick, M. P. Manos, F. S. Hodi, Immunity to X-linked inhibitor of apoptosis protein (XIAP) in malignant melanoma and check-point blockade. *Cancer immunology, immunotherapy : CII* **68**, 1331-1340 (2019).
63. D. Shae, J. J. Baljon, M. Wehbe, K. W. Becker, T. L. Sheehy, J. T. Wilson, At the bench: Engineering the next generation of cancer vaccines. *J Leukoc Biol* **108**, 1435-1453 (2020).
64. M. Di Marco, J. K. Peper, H. G. Rammensee, Identification of Immunogenic Epitopes by MS/MS. *Cancer J* **23**, 102-107 (2017).
65. K. Falk, O. Rotzschke, S. Stevanovic, G. Jung, H. G. Rammensee, Allele-specific motifs revealed by sequencing of self-peptides eluted from MHC molecules. *Nature* **351**, 290-296 (1991).
66. D. J. Kowalewski, S. Walz, L. Backert, H. Schuster, O. Kohlbacher, K. Weisel, S. M. Rittig, L. Kanz, H. R. Salih, H. G. Rammensee, S. Stevanovic, J. S. Stickel, Carfilzomib alters the HLA-presented peptidome of myeloma cells and impairs presentation of peptides with aromatic C-termini. *Blood cancer journal* **6**, e411 (2016).
67. F. Heidenreich, E. Rucker-Braun, J. S. Walz, A. Eugster, D. Kuhn, S. Dietz, A. Nelde, A. Tunger, R. Wehner, C. S. Link, J. M. Middeke, F. Stolzel, T. Tonn, S. Stevanovic, H. G. Rammensee, E. Bonifacio, M. Bachmann, M. Zeis, G. Ehninger, M. Bornhauser, J. Schetelig, M. Schmitz, Mass spectrometry-based identification of a naturally presented receptor tyrosine kinase-like orphan receptor 1-derived epitope recognized by CD8(+) cytotoxic T cells. *Haematologica* **102**, e460-e464 (2017).
68. E. M. Janssen, E. E. Lemmens, T. Wolfe, U. Christen, M. G. von Herrath, S. P. Schoenberger, CD4+ T cells are required for secondary expansion and memory in CD8+ T lymphocytes. *Nature* **421**, 852-856 (2003).
69. C. C. Chang, S. Ferrone, Immune selective pressure and HLA class I antigen defects in malignant lesions. *Cancer immunology, immunotherapy : CII* **56**, 227-236 (2007).
70. H. T. Khong, Q. J. Wang, S. A. Rosenberg, Identification of multiple antigens recognized by tumor-infiltrating lymphocytes from a single patient: tumor escape by antigen loss and loss of MHC expression. *J Immunother* **27**, 184-190 (2004).
71. Z. Zhang, S. Liu, B. Zhang, L. Qiao, Y. Zhang, Y. Zhang, T Cell Dysfunction and Exhaustion in Cancer. *Front Cell Dev Biol* **8**, 17 (2020).
72. M. J. Welters, G. G. Kenter, P. J. de Vos van Steenwijk, M. J. Lowik, D. M. Berends-van der Meer, F. Essahsah, L. F. Stynenbosch, A. P. Vloon, T. H. Ramwadhdoebe, S. J. Piersma, J. M. van der Hulst, A. R. Valentijn, L. M. Fathers, J. W. Drijfhout, K. L. Franken, J. Oostendorp, G. J. Fleuren, C. J. Melief, S. H. van der Burg, Success or failure of vaccination for HPV16-positive vulvar lesions correlates with kinetics and phenotype of induced T-cell responses. *Proc Natl Acad Sci U S A* **107**, 11895-11899 (2010).
73. G. Zhou, C. G. Drake, H. I. Levitsky, Amplification of tumor-specific regulatory T cells following therapeutic cancer vaccines. *Blood* **107**, 628-636 (2006).
74. Y. R. Murciano-Goroff, A. B. Warner, J. D. Wolchok, The future of cancer immunotherapy: microenvironment-targeting combinations. *Cell Res* **30**, 507-519 (2020).
75. M. B. Schaaf, A. D. Garg, P. Agostinis, Defining the role of the tumor vasculature in antitumor immunity and immunotherapy. *Cell Death Dis* **9**, 115 (2018).
76. A. J. Rech, R. Mick, S. Martin, A. Recio, N. A. Aqui, D. J. Powell, Jr., T. A. Colligon, J. A. Trosko, L. I. Leinbach, C. H. Pletcher, C. K. Tweed, A. DeMichele, K. R. Fox, S. M. Domchek, J. L. Riley, R. H. Vonderheide, CD25 blockade depletes and selectively reprograms regulatory T cells in concert with immunotherapy in cancer patients. *Sci Transl Med* **4**, 134ra162 (2012).
77. M. Sharma, H. Khong, F. Fa'ak, S. E. Bentebibel, L. M. E. Janssen, B. C. Chesson, C. A. Creasy, M. A. Forget, L. M. S. Kahn, B. Pazdrak, B. Karki, Y. Hailemichael, M. Singh, C. Vianden, S. Vennam, U. Bharadwaj, D. J. Tweardy, C. Haymaker, C. Bernatchez, S. Huang, K. Rajapakshe, C. Coarfa, M. E. Hurwitz, M. Sznol, P. Hwu, U. Hoch, M. Addepalli, D. H. Charych, J. Zalevsky, A. Diab, W. W. Overwijk, Bempegaldesleukin selectively depletes intratumoral Tregs and potentiates T cell-mediated cancer therapy. *Nat Commun* **11**, 661 (2020).

78. D. Alizadeh, N. Larmonier, Chemotherapeutic targeting of cancer-induced immunosuppressive cells. *Cancer Res* **74**, 2663-2668 (2014).
79. A. Tanaka, S. Sakaguchi, Regulatory T cells in cancer immunotherapy. *Cell Res* **27**, 109-118 (2017).
80. G. Zeng, L. Jin, Q. Ying, H. Chen, M. C. Thembinkosi, C. Yang, J. Zhao, H. Ji, S. Lin, R. Peng, M. Zhang, D. Sun, Regulatory T Cells in Cancer Immunotherapy: Basic Research Outcomes and Clinical Directions. *Cancer Manag Res* **12**, 10411-10421 (2020).
81. M. Gigoux, R. Zappasodi, J. J. Park, S. Pourpe, A. Ghosh, C. C. Bozkus, L. M. B. Mangarin, D. Redmond, S. Verma, S. Schad, W. Duke, M. Leventhal, M. Jan, V. Ho, G. Hobbs, T. A. Knudsen, V. Skov, L. Kjær, T. S. Larsen, D. L. Hansen, R. C. Lindsley, H. Hasselbalch, J. H. Grauslund, M. H. Andersen, M. O. Holmström, T. Chan, R. Rampal, O. Abdel-Wahab, N. Bhardwaj, J. D. Wolchok, A. Mullally, T. Merghoub, Heteroclitic peptide cancer vaccine counters MHC-I skewing in mutant calreticulin-positive myeloproliferative neoplasms. *The Journal of Immunology* **204**, 239.234-239.234 (2020).
82. T. Dao, T. Korontsvit, V. Zakhaleva, C. Jarvis, P. Mondello, C. Oh, D. A. Scheinberg, An immunogenic WT1-derived peptide that induces T cell response in the context of HLA-A* 02: 01 and HLA-A* 24: 02 molecules. *Oncoimmunology* **6**, e1252895 (2017).
83. A. Ribas, J. D. Wolchok, Cancer immunotherapy using checkpoint blockade. *Science* **359**, 1350-1355 (2018).
84. A. Martínez-Usatorre, A. Donda, D. Zehn, P. Romero, PD-1 blockade unleashes effector potential of both high-and low-affinity tumor-infiltrating T cells. *The Journal of Immunology* **201**, 792-803 (2018).
85. M. S. Pelster, R. N. Amaria, Combined targeted therapy and immunotherapy in melanoma: a review of the impact on the tumor microenvironment and outcomes of early clinical trials. *Ther Adv Med Oncol* **11**, 1758835919830826 (2019).
86. B. I. Rini, A. Stenzl, R. Zdrojowy, M. Kogan, M. Shkolnik, S. Oudard, S. Weikert, S. Bracarda, S. J. Crabb, J. Bedke, J. Ludwig, D. Maurer, R. Mendrzyk, C. Wagner, A. Mahr, J. Fritsche, T. Weinschenk, S. Walter, A. Kirner, H. Singh-Jasuja, C. Reinhardt, T. Eisen, IMA901, a multipeptide cancer vaccine, plus sunitinib versus sunitinib alone, as first-line therapy for advanced or metastatic renal cell carcinoma (IMPRINT): a multicentre, open-label, randomised, controlled, phase 3 trial. *Lancet Oncol* **17**, 1599-1611 (2016).
87. Y. Gu, W. Zhao, F. Meng, B. Qu, X. Zhu, Y. Sun, Y. Shu, Q. Xu, Sunitinib impairs the proliferation and function of human peripheral T cell and prevents T-cell-mediated immune response in mice. *Clin Immunol* **135**, 55-62 (2010).
88. Q. Yin, M. Sivina, H. Robins, E. Yusko, M. Vignali, S. O'Brien, M. J. Keating, A. Ferrajoli, Z. Estrov, N. Jain, W. G. Wierda, J. A. Burger, Ibrutinib Therapy Increases T Cell Repertoire Diversity in Patients with Chronic Lymphocytic Leukemia. *J Immunol* **198**, 1740-1747 (2017).
89. C. Cubillos-Zapata, J. Avendano-Ortiz, R. Cordoba, E. Hernandez-Jimenez, V. Toledano, R. Perez de Diego, E. Lopez-Collazo, Ibrutinib as an antitumor immunomodulator in patients with refractory chronic lymphocytic leukemia. *Oncoimmunology* **5**, e1242544 (2016).
90. I. Sagiv-Barfi, H. E. Kohrt, L. Burckhardt, D. K. Czerwinski, R. Levy, Ibrutinib enhances the antitumor immune response induced by intratumoral injection of a TLR9 ligand in mouse lymphoma. *Blood* **125**, 2079-2086 (2015).
91. H. G. Rammensee, K. H. Wiesmuller, P. A. Chandran, H. Zelba, E. Rusch, C. Gouttefangeas, D. J. Kowalewski, M. Di Marco, S. P. Haen, J. S. Walz, Y. C. Gloria, J. Bodder, J. M. Schertel, A. Tunger, L. Muller, M. Kiessler, R. Wehner, M. Schmitz, M. Jakobi, N. Schneiderhan-Marra, R. Klein, K. Laske, K. Artzner, L. Backert, H. Schuster, J. Schwenck, A. N. R. Weber, B. J. Pichler, M. Kneilling, C. la Fougere, S. Forchhammer, G. Metzler, J. Bauer, B. Weide, W. Schippert, S. Stevanovic, M. W. Loffler, A new synthetic toll-like receptor 1/2 ligand is an efficient adjuvant for peptide vaccination in a human volunteer. *J Immunother Cancer* **7**, 307 (2019).
92. J. A. Vizcaino, E. W. Deutsch, R. Wang, A. Csordas, F. Reisinger, D. Rios, J. A. Dianes, Z. Sun, T. Farrah, N. Bandeira, P. A. Binz, I. Xenarios, M. Eisenacher, G. Mayer, L. Gatto, A. Campos, R. J.

Chalkley, H. J. Kraus, J. P. Albar, S. Martinez-Bartolome, R. Apweiler, G. S. Omenn, L. Martens, A. R. Jones, H. Hermjakob, ProteomeXchange provides globally coordinated proteomics data submission and dissemination. *Nat Biotechnol* **32**, 223-226 (2014).

Chapter 2

Optimization of CD4$^+$ T cell priming using monocyte-derived dendritic cells

Introduction

In order to combat cancer, several immunotherapeutic approaches have been developed over the years to direct the immune system against tumor cells (*1*). One low-side effect approach to induce tumor-targeting T cells is peptide-based vaccination. However, to induce clinically effective responses the antigen selection is crucial. To determine if HLA class I- and HLA class II-restricted peptides are suitable targets for peptide-based vaccination approaches, immunogenicity, i.e., recognition of the peptide by T cells needs to be proven (*2, 3*). As described in the first chapter of this thesis, IFN-γ ELISpot assays after 12-day *in vitro* expansion using PBMCs of cancer patients as well as of healthy volunteers represent one approach for immunogenicity screening to reveal pre-existing peptide-specific memory T cells. Another approach is the *de novo* induction of peptide-specific T cells from naïve T cells. For HLA class I-restricted peptides, *in vitro* priming with aAPCs allow to demonstrate immunogenicity of a specific peptide by *de novo* induction of peptide-specific CD8$^+$ T cells.

In contrast to HLA class I, HLA class II molecules show high promiscuity with regard to peptide binding, that results in a broader peptide presentation with less strict HLA restriction (*2, 4*). Thus, one HLA class II peptide could induce CD4$^+$ T cell responses in patients with different HLA class II allotypes. Since HLA class II typing of healthy volunteer and patient samples is a time and cost factor, and commercially available MHC class II monomers are restricted to a limited number of alleles not guaranteeing TCR cross-recognition (*5*), an alternative option consists in the priming of naïve CD4$^+$ T cells using autologous monocyte-derived dendritic cells (MoDCs).

This chapter focuses on the establishment of a MoDC-based priming protocol for the induction of *de novo* peptide-specific CD4$^+$ T cells, to prove the immunogenicity of a fusion protein-derived peptide.

Materials and Methods

Preliminary MoDC Priming Protocol

PBMC Isolation and CD14$^+$ Cell Separation

On day one, PBMCs from healthy donors were isolated by density gradient centrifugation and CD14$^+$ cells were separated by performing magnetic activated cell sorting (MACS) using CD14 MircoBeads (Miltenyi Biotec) as described by the manufacturer. CD14$^-$ cells were cultured in T cell medium (TCM; IMDM with 1% penicillin-streptomycin, 0.05 % gentamycin, 0.05% 0.1 M ß-mercaptoethanol, 5 % Seraclot Human Serum) containing 10 U/ml IL-2 (R&D Systems) and 2.5 ng/ml IL-7 (PromoCell). While CD14$^+$ cells were cultured in TCM containing 100 ng/ml granulocyte-macrophage colony stimulating factor (GM-CSF) and 40 ng/ml IL-4 (MoDC CytoBox, Miltenyi Biotec).

Isolation of naïve CD4$^+$ T cells

On day 3, the CD14$^-$ cells were harvested before performing a CD4$^+$ T cell MACS using the naïve CD4$^+$ T cell isolation kit II (Miltenyi Biotec) as described by the manufacturer. In one well of a 12-well plate, 1x10^7 CD4$^+$ T cells were cultured in 1 ml of TCM containing 10 U/ml IL-2 (R&D Systems) and 2.5 ng/ml IL-7 (PromoCell). The CD4$^-$ cell fraction was frozen and stored at -80°C for the use as APCs in case MoDCs were insufficient for a total of 4 rounds of stimulation.

Differentiation and maturation of MoDCs

On day 4, CD14$^+$ cells were differentiated by restimulation with the MoDC Cytobox cytokines, adding 100 ng/ml GM-CSF and 40 ng/ml IL-4 (Myltenyi Biotec). On day 8, MoDCs were matured. For maturation, the CD14$^+$ cells were harvested, centrifuged and cultured in TCM containing 100 ng/ml GM-CSF, 50 ng/ml IL-4 (Myltenyi Biotec), 10 ng/ml TNF (PromoCell), 1 µg/ml Protaglandin E_2 (PGE_2, R&D Systems) and 5 µg/ml Resiquimod (R848, R&D Systems) for 18-24h.

Culture of CD4$^+$ T cells

On days 5, 8, 12, 19, 26 and 33, CD4$^+$ T cells were fed with 1 ml of TCM containing 10 U/ml IL-2 (R&D Systems) and 2.5 ng/ml IL-7 (PromoCell).

Loading of MoDCs with peptide and CD4$^+$ T cell stimulation

On day 9, the matured MoDCs were harvested and counted to calculate the required amount of MoDCs for T cell stimulation. Different MoDC to T cell ratios were used, 1:10 and 1:100, for the stimulation with one peptide. The calculated amount of mature MoDCs was resuspended in 1 ml TCM containing 10 µg of the test peptide and incubated for 24 h. The remaining MoDCs were frozen for the repeating stimulations.

On days 15, 22 and 29, MoDCs were thawed in thawing medium (IMDM with 1% penicillin-streptomycin, 0.05 % gentamycin, 0.05% 0.1 M ß-mercaptoethanol, 3µg/ml DNAse), centrifuged and incubated for at least 10 minutes in fresh thawing medium before resuspension in TCM and incubation for 24h. If not enough MoDCs were available, $CD4^-$ cells were thawed to be used for the last peptide stimulation. On days 16, 23 and 30, MoDCs were loaded with peptides as described for day 9. When using $CD4^-$ cells, cells were irradiated with 20 Gy prior to peptide loading.

On days 10, 17, 24 and 31, peptide-loaded MoDCs were washed twice with TCM before resuspension in 1 ml of TCM containing 5 ng/ml IL-12 (PromoCell). The MoDCs were transferred to the 12-well plate containing the $CD4^+$ T cells for stimulation. Figure 1 represents a schematic summary of the MoDC priming protocol.

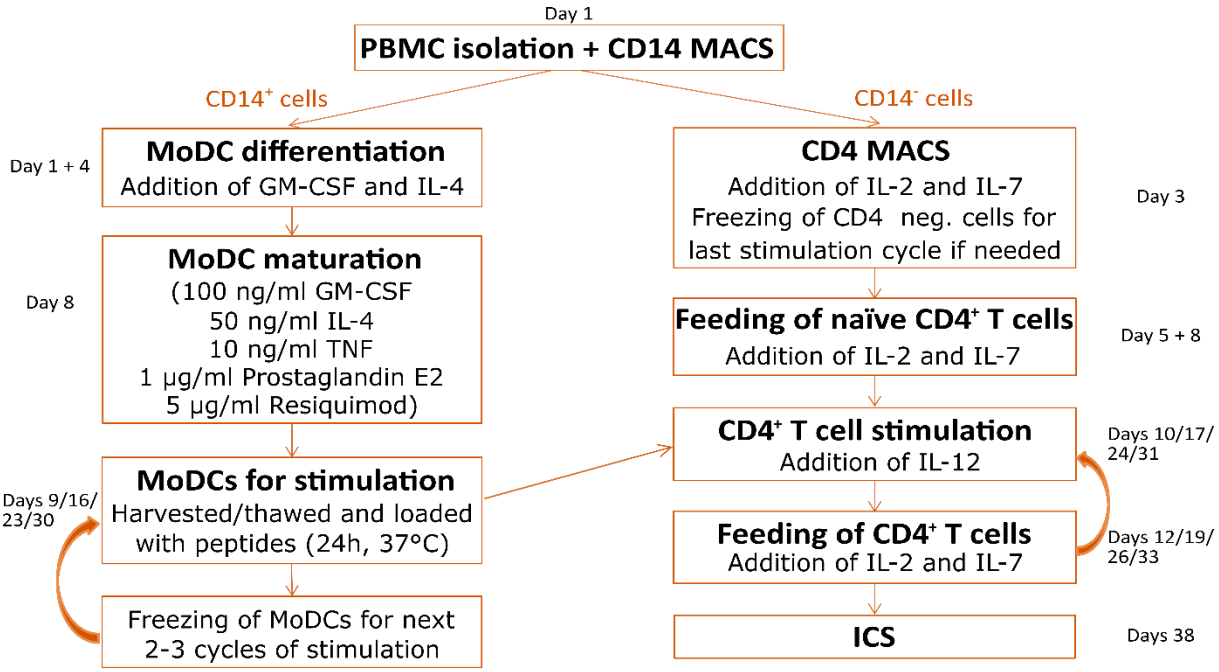

Figure 1: Schematic summary of the MoDC priming protocol.

MoDC Inspector FACS Staining

In order to assess if the differentiation and maturation of MoDCs was successful, $2x10^6$ MoDCs were collected before and after addition and incubation with the MoDC maturation cocktail. Staining was performed using Zombie Aqua (1:200 dilution, BioLegend), Human Fc Block (BD Biosciences, Franklin Lakes, USA), Alexa Fluor 700 anti-human CD14 (1:40 dilution), APC/Cy7 anti-human CD40 (1:100 dilution), FITC anti-human CD80 (1:40 dilution), Brilliant Violet 605 anti-human CD86 (1:400 dilution) and Brilliant Violet 711 anti-human HLA-DR (1:100 dilution, BioLegend). A fluorescence minus one (FMO) control was included for each fluorochrome and condition. MoDC samples were analyzed on a FACS LSRFortessa (BD) and data analyzed using FlowJo 10.7.1 (BD). The gating strategy is depicted in Figure S1.

Intracellular Cytokine Staining and Surface Marker Staining of MoDC-primed CD4⁺ T cells

The *de novo* induced peptide-specific CD4⁺ T cells were characterized by intracellular cytokine and cell surface marker staining. $2x10^5$ - $1x10^6$ cells were transferred to a 96-well plate, pulsed with 10 µg/ml of peptide and incubated with FITC anti-human CD107a (1:100 dilution, BioLegend) for one hour before adding 10 µg/ml Brefeldin A (Sigma-Aldrich, Saint Louis, USA) and 10 µg/ml GolgiStop (BD) and incubating for 12-16h. Staining was performed using aqua fluorescent reactive dye (1:400, Invitrogen), Cytofix/Cytoperm (BD), APC/Cy7 anti-human CD4 (1:100 dilution), PE/Cy7 anti-human IL-2 (1:400 dilution), PE anti-human IFN-γ (1:200 dilution), Pacific Blue anti-human TNF (1:120 dilution) and APC anti-human CD154 (1:100 dilution, BioLegend). PMA and ionomycin (Sigma-Aldrich) served as positive control. As negative control, the HLA class II-restricted FLNA_HUMAN-derived peptide ETVITVDTKAAGKGK was used. The priming was considered successful if the frequency of peptide-specific CD4⁺ cytokine-secreting or cell surface marker expressing T cells was ≥ 0.1% of CD4⁺ T cells within the viable single cell population and at least three-fold higher than the frequency of cytokine-secreting CD4⁺ T cells in the negative control. Samples were analyzed on a FACS Canto II cytometer (BD) and data was analyzed using FlowJo 10.7.1 (BD). The gating strategy is depicted in Figure S2.

Results

CD4⁺ T Cell Priming Using the Preliminary MoDC Priming Protocol

For the application of the HLA class II-restricted, fusion protein-derived peptide KREIFDRYGEEVKEFLAKAKED (DNAJB1-PRKACA) in a clinical trial, its immunogenicity had to be proven. Therefore, MoDC priming was performed in 4 healthy donors using the preliminary priming protocol. To confirm protocol functionality, the mutated peptide KLKKMWKSPNGTIQNILGGTVF (IDH2 R140Q), which had proven to be immunogenic in previously performed ELISpot assays (*6*), was applied as positive control. However, in none of the priming experiments, independent of MoDC to T cell ratio, an induction of peptide-specific CD4⁺ T cells could be observed (Table 1 and Fig. 2).

Table 1: Tested peptides, responses and donors with the preliminary MoDC priming protocol.

	KREIFDRYGEEVKEFLAKAKED		KLKKMWKSPNGTIQNILGGTVF	
Donor	**MoDC:T cell 1:10**	**MoDC:T cell 1:100**	**MoDC:T cell 1:10**	**MoDC:T cell 1:100**
J341	-	negative	negative	negative
J342	-	-	-	negative
J347	negative	negative	-	-
J350	-	negative	-	-
J353	negative	negative	negative	negative

After priming with MoDCs loaded with KREIFDRYGEEVKEFLAKAKED, cytokine and surface marker staining revealed background cytokine secretion in the negative control, that was detectable independently of the MoDC to T cell ratio of 1:10 and 1:100 (Fig. 2A and B, respectively) with no visible peptide-specific cytokine secretion as exemplarily shown in Figure 2.

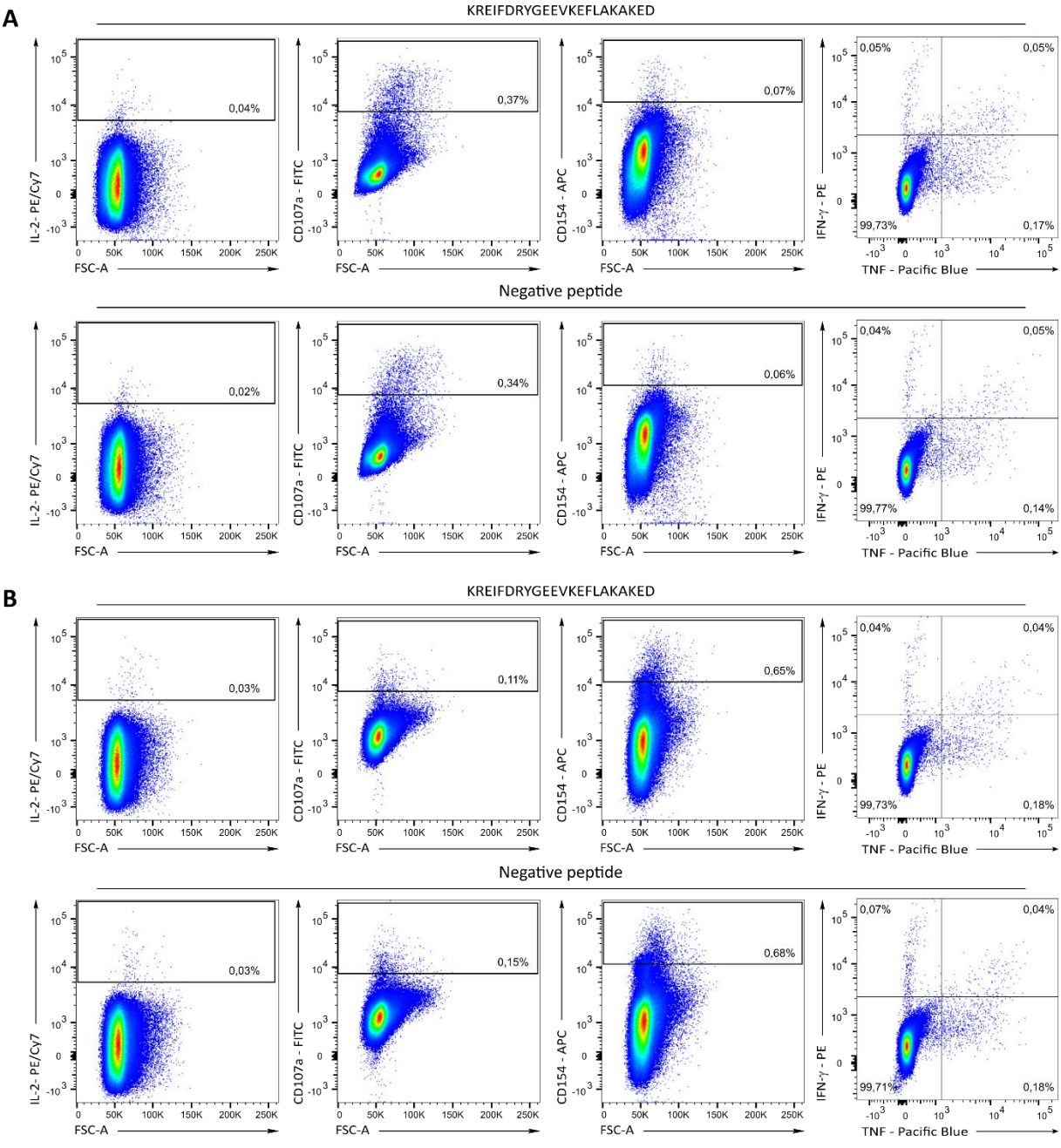

Figure 2: Intracellular cytokine and surface marker staining of a MoDC priming with the peptide KREIFDRYGEEVKEFLAKAKED. A, B, Representative example of the flow cytometry-based analysis of $CD4^+$ T cells from a healthy volunteer primed with MoDCs loaded with KREIFDRYGEEVKEFLAKAKED (upper panels) using the preliminary priming protocol. Results are shown for $CD4^+$ T cells primed with a MoDC to T cell ratio of 1:10 (**A**) and 1:100 (**B**). The lower panels show the negative controls consisting of KREIFDRYGEEVKEFLAKAKED-primed $CD4^+$ T cells stimulated with a negative peptide.

Since the performed MoDC priming assays using the previously described method did not result in *de novo* induction of peptide-specific $CD4^+$ T cells after several attempts, different aspects of the priming experiment were adapted for protocol optimization.

Optimization of MoDC Maturation Cocktail

The generation of functional MoDCs is the most relevant factor for successful priming of $CD4^+$ T cells. After the separation of the $CD14^+$ cells from PBMCs, the obtained monocytes are stimulated with GM-CSF and IL-4 to differentiate them into immature DCs as commonly done. The maturation of MoDCs however, can be achieved by activating several different pathways that facilitate maturation (*7*). The alternatively tested maturation cocktail only included 100 ng/ml GM-CSF, 50 ng/ml IL-4 and 100 ng/ml lipopolysaccharide (LPS, Invivogen) compared to the preliminary protocol including 100 ng/ml GM-CSF, 50 ng/ml IL-4, 10 ng/ml TNF, 1µg/ml PGE_2 and 5µg/ml Resiquimod. To validate the maturation of MoDCs the expression of different cell surface markers (CD14, CD40, CD80, CD86, HLA-DR; Table 2) were analyzed in differentiated immature, and mature MoDCs matured with the two different cocktails.

Table 2: Cell surface marker expression expected in differentiated immature and mature MoDCs.

Marker	Expression on differentiated MoDCs	Expression on mature MoDCs
CD14	Positive	Positive (low)
CD40	Positive	Positive
CD80	Negative	Positive (low)
CD86	Positive (high)	Positive (high)
HLA-DR	Positive	Positive

In mature MoDCs the expression of CD14 is decreased compared to the expression in differentiated MoDCs, independent of maturation protocol (Fig. 3A). CD40 is known to be upregulated on activated DCs (*8*). Interestingly, its expression is highest in MoDCs matured with LPS, followed by the differentiated MoDCs, whereas MoDCs matured with the preliminary protocol have the lowest CD40 expression level (Fig. 3B). The co-stimulatory molecule CD80 is expressed on the mature MoDCs, although maturation with LPS shows a slight advantage compared to the preliminary maturation protocol (Fig. 3C). The costimulatory molecule CD86 was only expressed highly in LPS matured MoDCs compared to the differentiated MoDCs, while MoDCs matured with the preliminary protocol did not show any expression level (Fig. 3D). HLA-DR expression was observed for all MoDCs, while it was increased in mature MoDCs in particular when using LPS for maturation (Fig. 3E). These observations indicate an advantage in using LPS for MoDC maturation compared to the preliminary maturation cocktail.

Optimization of MoDC Peptide-Loading

When MoDCs start the maturation process, they develop the ability of improved antigen uptake until it decreases again after 20 to 40h (*9*). Following the preliminary protocol, MoDCs received the maturation cocktail for 18 to 24h and were subsequently loaded with peptides for 24h. Therefore, the optimal timing of antigen uptake for the MoDCs might be exceeded, which could be further improved. Other groups evaluated several MoDC coincubation timeframes with peptides, reporting T cell activation already after a coincubation of one hour (*10*). We therefore decided to decrease the duration of coincubation to 2h to avoid the loss of antigen uptake ability of the MoDCs.

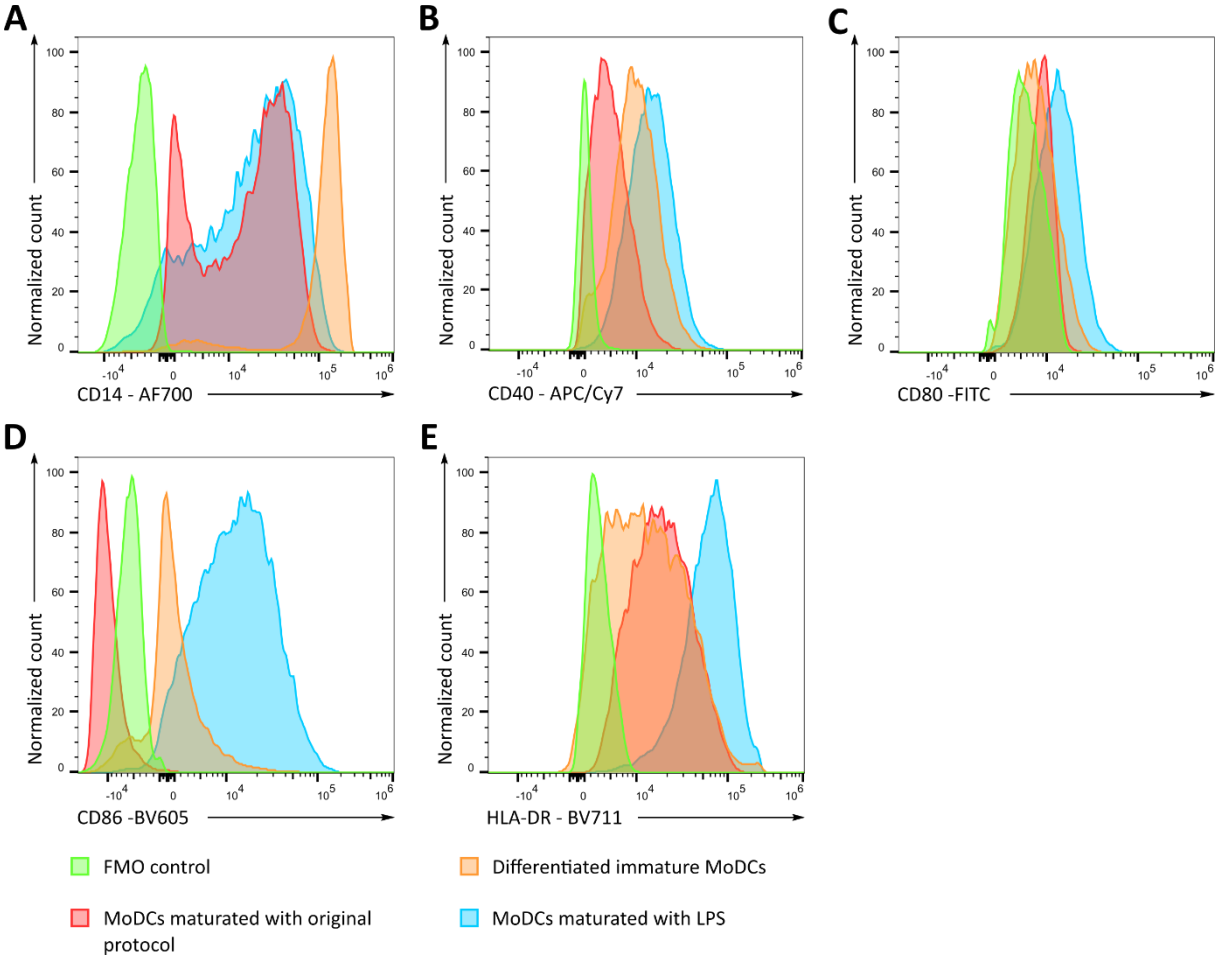

Figure 3: Cell surface marker expression in MoDCs matured with different maturation cocktails. The differences in cell surface marker expression including CD14 (**A**), CD40 (**B**), CD80 (**C**), CD86 (**D**) and HLA-DR (**E**) were assessed by flow cytometry using the MoDC Inspector staining, to distinguish differentiated immature MoDCs (orange) from MoDCs matured with the preliminary protocol (red) or with LPS (blue) in comparison to fluorescence minus one (FMO) controls with the indicated surface markers.

After four stimulations with MoDCs matured either with the preliminary protocol or using LPS, and loaded with peptides during 2h, the priming of $CD4^+$ T cells still failed. Nevertheless, the intracellular cytokine and cell surface marker staining revealed that the frequency of peptide-specific $CD4^+$ cytokine-secreting T cells did increase up to two-fold (Fig. 4). However, this increase observed using

LPS for MoDC maturation did not reach the three-fold increase in frequency of peptide-specific cytokine-secreting $CD4^+$ T cells in the negative control required to fulfill the criteria for successful priming.

The obtained results showed the advantage of using LPS for MoDC maturation, as well as shorter duration of MoDC coincubation with peptides, compared to the preliminary protocol. Nonetheless further optimization appeared to be necessary to complete the criteria for a successful priming.

Optimization of Stimulation Settings

Since adjusting the MoDC maturation protocol and the duration of peptide loading showed only limited improvement, the stimulation setting was reconsidered. The preliminary protocol required the experiment to be performed in a 12-well plate, however, these plates have a great volume and might not be the optimal priming environment. For aAPC-based $CD8^+$ T cell priming experiments, as described in the first chapter of this thesis, the stimulation of the $CD8^+$ T cells is performed in round bottom 96-well plates, allowing for better contact between the aAPCs and the T cells due to the smaller volume and stacking resulting from the round bottom. This knowledge, together with reports from other groups (*11, 12*) also using 96-well plates for MoDC experiments, led to the change of layout, from 12- to 96-well plates for the stimulation of $CD4^+$ T cells. Two different $CD4^+$ T cell densities were tested with either 100.000 or 500.000 cells seeded per well. The MoDC to T cell ratios previously used (1:10 and 1:100) were conserved, with the additional testing of a 1:50 ratio. The use of 96-well plates also allowed for the stimulation in multiple replicates.

Intracellular cytokine and cell surface marker staining analysis of $CD4^+$ T cells stimulated with peptide loaded MoDCs in a 96-well plate showed successful *de novo* priming of peptide-specific $CD4^+$ T cells (Fig. 5, Fig.6, Fig. S3, Fig. S4 and Table 3). For KREIFDRYGEEVKEFLAKAKED, the priming was successful independent of the used MoDC to $CD4^+$ T cell ratios. The results for the setting with a MoDC to T cell ratio of 1:10 were enhanced in the setting with a 1:100 ratio, with most cytokine secretion and cell surface marker expression seen for the 1:50 ratio ($CD107a^+$: 1.94%, 2.58% and 5.38%, respectively; $CD154^+$: 1.34%, 2.18% and 1.73%, respectively; IFN-γ^+: 0.06%, 0.81% and 0.71%, respectively; IFN-γ^+/TNF^+: 0.04%, 0.47% and 0.49%, respectively; TNF^+: 0.74%, 1.41% and 1.61%, respectively; Fig.5 and Fig. 6).

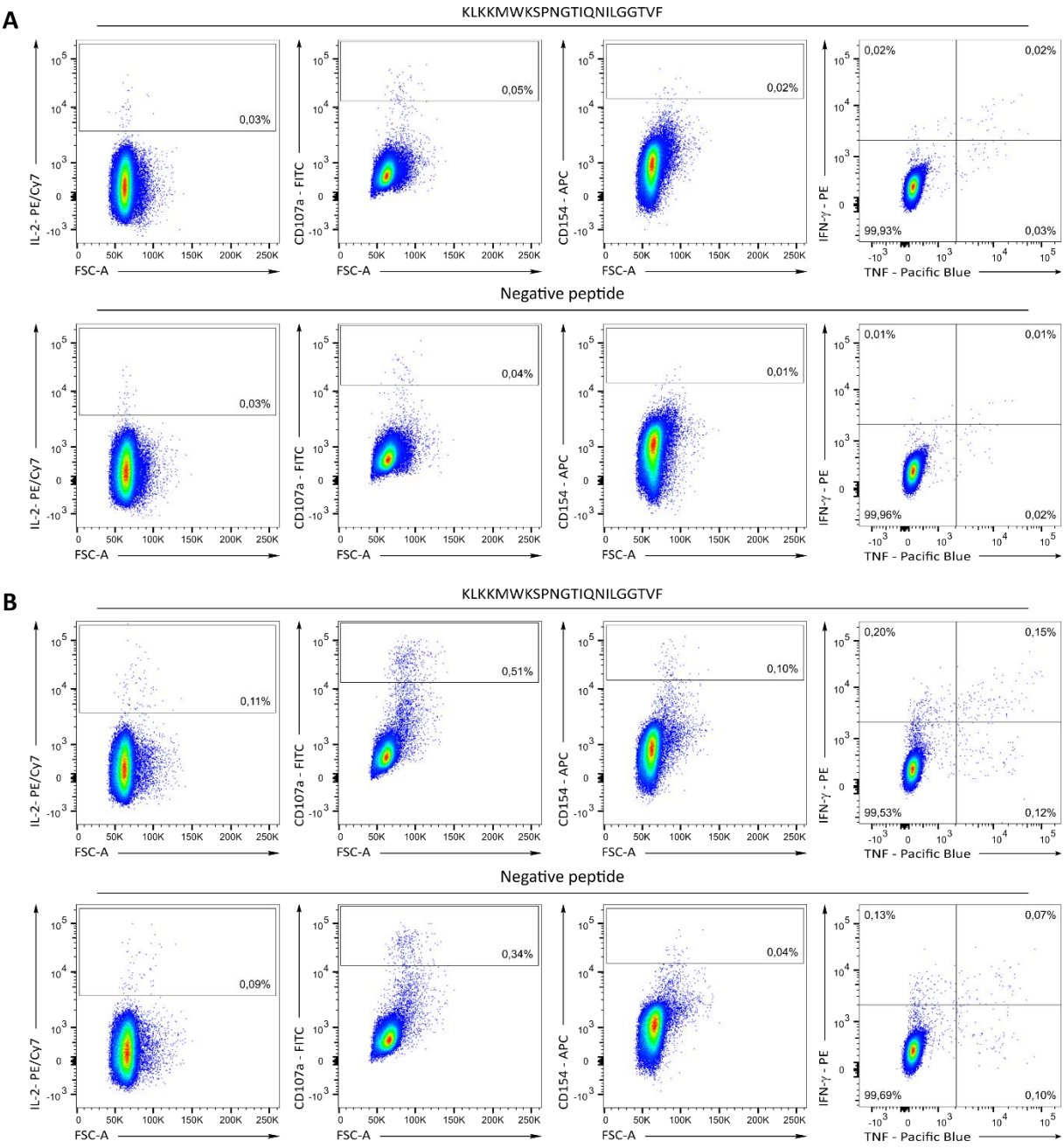

Figure 4: Intracellular cytokine and surface marker staining of a MoDC priming with the peptide KLKKMWKSPNGTIQNILGGTVF. A, B, Exemplary flow cytometry-based analysis of $CD4^+$ T cells from a healthy volunteer primed with MoDCs loaded with KLKKMWKSPNGTIQNILGGTVF (upper panels) using the preliminary priming protocol (**A**) or LPS for MoDC maturation (**B**). Results are shown for $CD4^+$ T cells primed with a MoDC to T cell ratio of 1:100. The lower panels show the negative controls consisting of KLKKMWKSPNGTIQNILGGTVF-primed $CD4^+$ T cells stimulated with a negative peptide.

For $CD4^+$ T cell priming using MoDCs loaded with KLKKMWKSPNGTIQNILGGTVF, the 1:100 MoDC to T cell ratio did not result in peptide-specific cytokine secretion (Table 3, Fig.6, Fig. S3 and S4). Interestingly, peptide-specific cytokine secretion was seen for the 1:10 T cell to MoDC ratio only when using 500.000 $CD4^+$ T cells per stimulated well and not when using only 100.000 $CD4^+$ T cells. In general, priming with MoDCs loaded with KLKKMWKSPNGTIQNILGGTVF resulted in the rather weak and monofunctional induction of $CD4^+$ T cells (Table 3, Fig.6, Fig. S3 and Fig. S4).

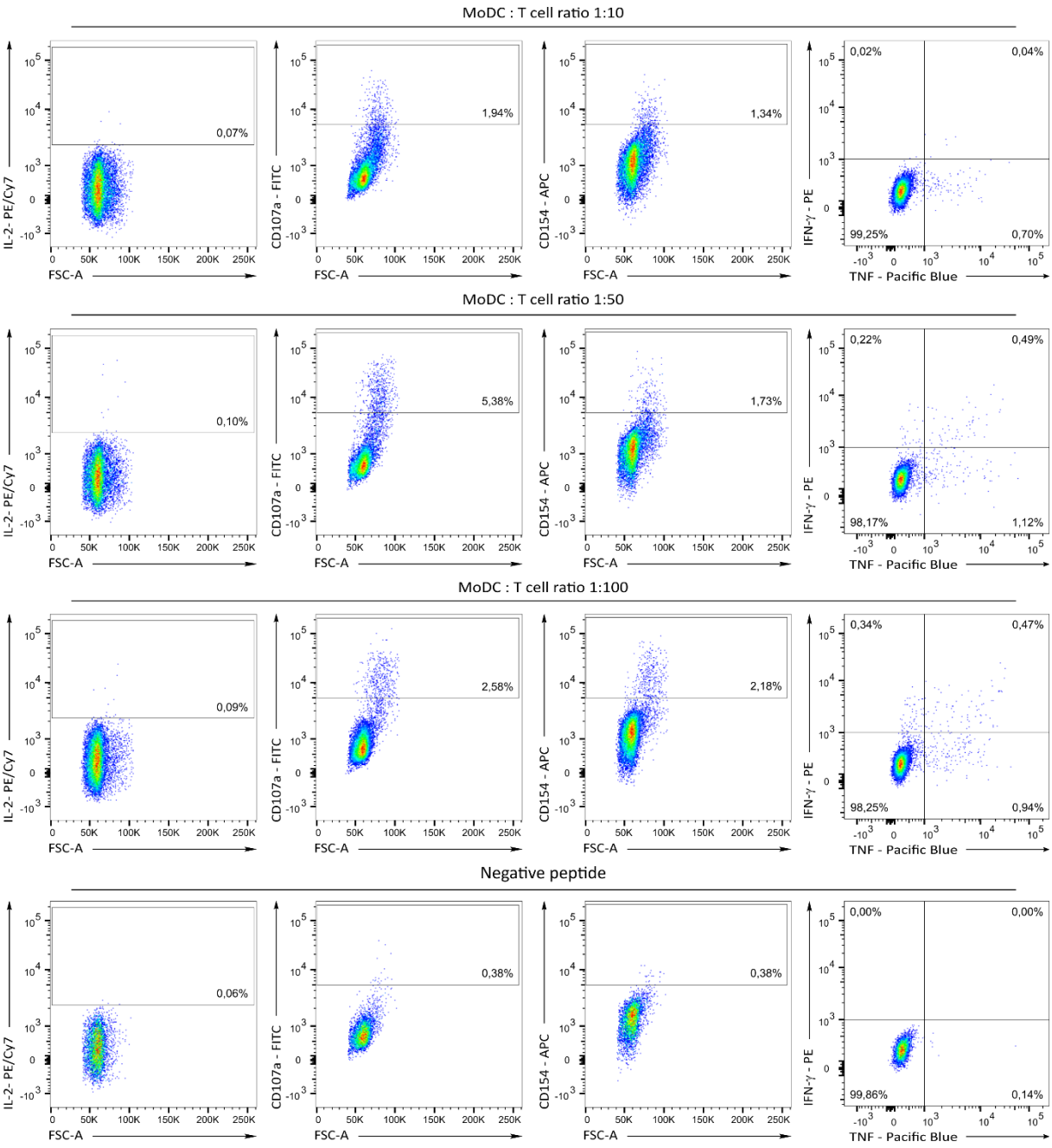

Figure 5: Intracellular cytokine and surface marker staining of a MoDC priming with the peptide KREIFDRYGEEVKEFLAKAKED performed in a 96-well plate. Representative example of the flow cytometry-based analysis of $CD4^+$ T cells from a healthy volunteer primed with MoDCs loaded with KREIFDRYGEEVKEFLAKAKED (upper three panels stimulated with indicated MoDC to T cell ratios) using the optimized priming protocol, including LPS in the MoDC maturation cocktail, the shorter coincubation of MoDCs with peptides and the stimulation of 100.000 $CD4^+$ T cells in a 96-well plate. The lower panels show the negative controls consisting of KREIFDRYGEEVKEFLAKAKED-primed $CD4^+$ T cells stimulated with a negative peptide.

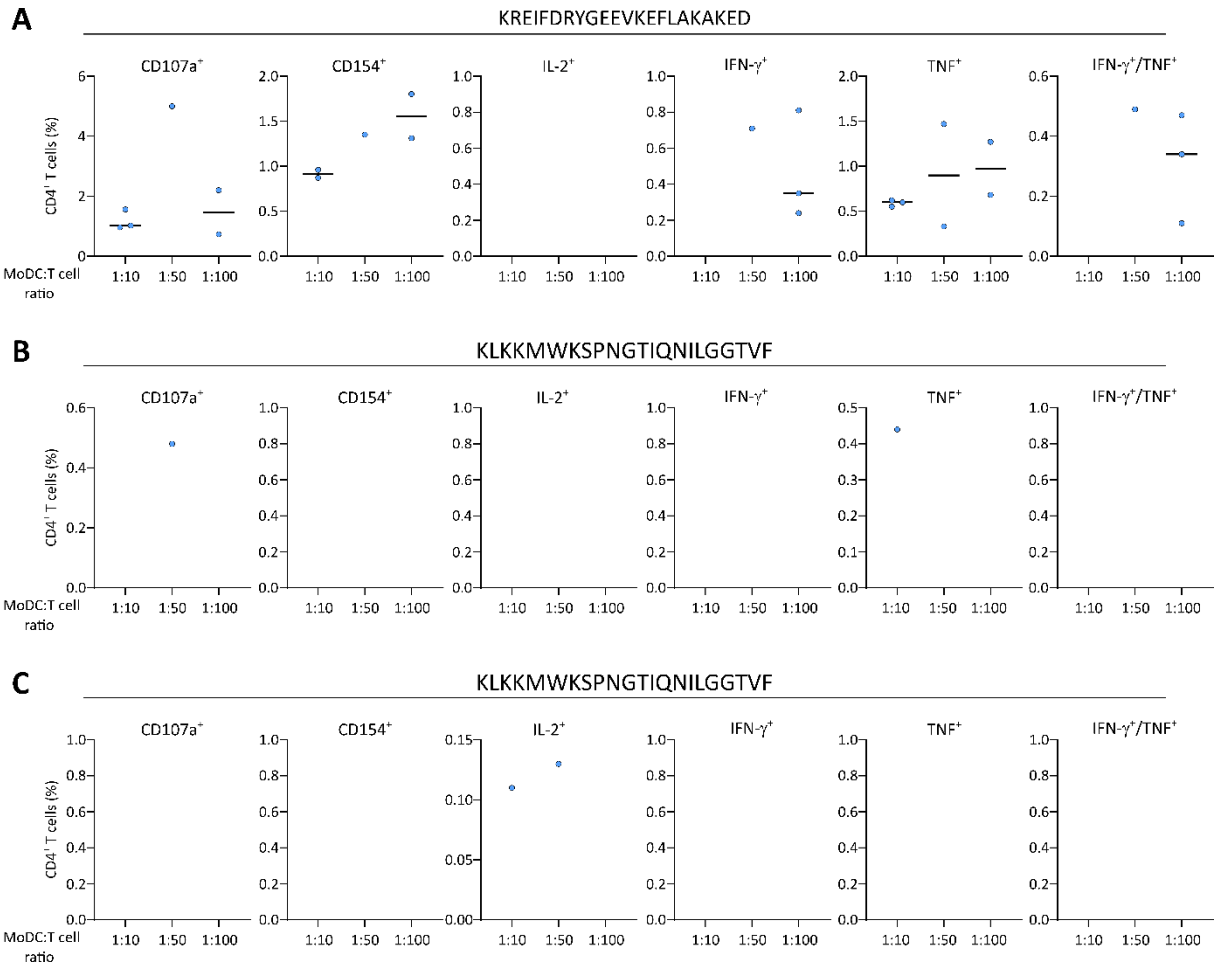

Figure 6: Frequencies and functionality of de novo primed CD4⁺ T cells using MoDCs in a 96-well plate. A-C, Functional characterization of de novo induced CD4⁺ T cells after 4 rounds of priming with MoDCs loaded with (**A**) KREIFDRYGEEVKEFLAKAKED and (**B, C**) KLKKMWKSPNGTIQNILGGTVF in a 96-well plate stimulating 100.000 (**A, B**) or 500.000 (**C**) CD4⁺ T cells per well, respectively, using surface marker (CD107a and CD154) as well as intracellular cytokine staining (IL-2, IFN-γ and TNF). Scatter dot plots show the calculated frequencies of surface marker expressing or cytokine secreting CD4⁺ T cells for healthy volunteer J371 for wells stimulated with a MoDC to T cell ratio of 1:10, 1:50 and 1:100. Each dot depicts the calculated frequency for one positive test well. Each setting was tested in 3 wells.

Table 3: Peptides and responses after priming of CD4⁺ T cells with the optimized protocol for donor J371.

	KREIFDRYGEEVKEFLAKAKED			KLKKMWKSPNGTIQNILGGTVF		
	MoDC:T cell ratio			MoDC:T cell ratio		
CD4⁺ T cells	**1:10**	**1:50**	**1:100**	**1:10**	**1:50**	**1:100**
100.000/well	positive	positive	positive	negative	positive	negative
500.000/well	-	-	-	positive	positive	negative

The use of LPS for MoDC maturation, the shorter coincubation of MoDCs with peptide together with the stimulation of CD4⁺ T cells in 96-well plates instead of 12-well plates allowed for the successful *de novo* induction of peptide-specific CD4⁺ T cells. However, this result was obtained in a single donor with only two test peptides and therefore required further validation.

Validation of the Novel MoDC Priming Protocol

To validate that the optimization of the MoDC priming protocol led to improved $CD4^+$ T cell priming compared to the preliminary protocol, it was tested with another donor using two other test peptides. The optimized priming protocol comprised the seeding of 500.000 $CD4^+$ T cells per well in a 96-well plate on day 3 after isolation, the use of 100 ng/ml GM-CSF, 50 ng/ml IL-4 and 100 ng/ml LPS as maturation cocktail for the MoDCs on day 8 and the loading of the MoDCs with peptide for only 2h on days 9,16,23 and 30 right before T cell stimulation (Fig. 7). All other steps, as well as cytokine dilutions and media were used as described in the preliminary protocol.

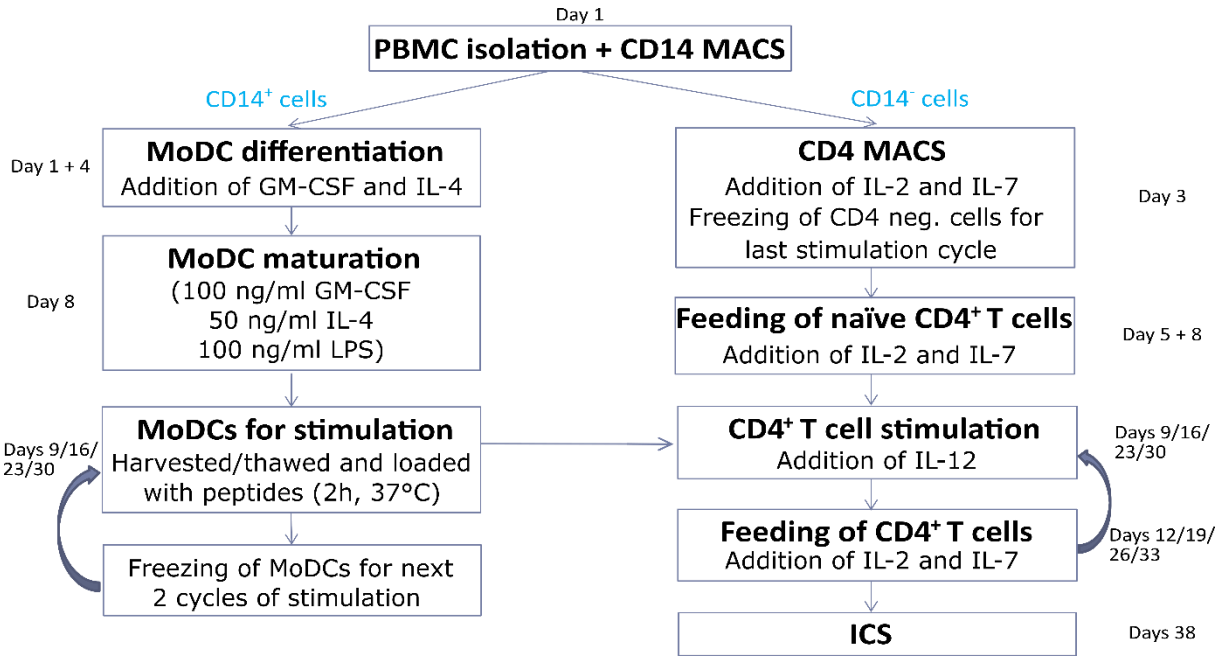

Figure 7: Schematic summary of the optimized MoDC priming protocol.

The test peptides were the prostate-specific HLA-class II-restricted peptides DTGQVFQVSHSFPHPLY (PSA) and MLLRLSEPAELTD (PSA). The priming was performed using the previously tested $CD4^+$ T cell to MoDC ratios of 1:10, 1:50 and 1:100, and resulted in successful *de novo* priming of peptide-specific $CD4^+$ T cells for the ratio of 1:10 for both peptides and for the ratio of 1:100 for MLLRLSEPAEKTD (Fig. 8, Table 4). As exemplarily shown for DTGQVFQVSHSFPHPLY, using a MoDC to $CD4^+$ T cell ratio of 1:10 during stimulation, peptide-specific cytokine-secreting and cell surface marker expressing $CD4^+$ T cells reached high frequencies, with 1.07% of IL-2^+, 3.24% of $CD107a^+$, 6.86% of $CD154^+$, 7.32% IFN-γ^+, 14.33% TNF^+ and 7.28% of IFN-γ^+/TNF^+ cells (Fig.9). These results allowed to validate the optimized MoDC priming protocol.

Table 4: Donor and peptides used for the validation of the optimized MoDC priming protocol.

	DTGQVFQVSHSFPHPLY			MLLRLSEPAELTD		
	MoDC: T cell ratio			MoDC: T cell ratio		
Donor	**1:10**	**1:50**	**1:100**	**1:10**	**1:50**	**1:100**
J420	positive	negative	negative	positive	negative	positive

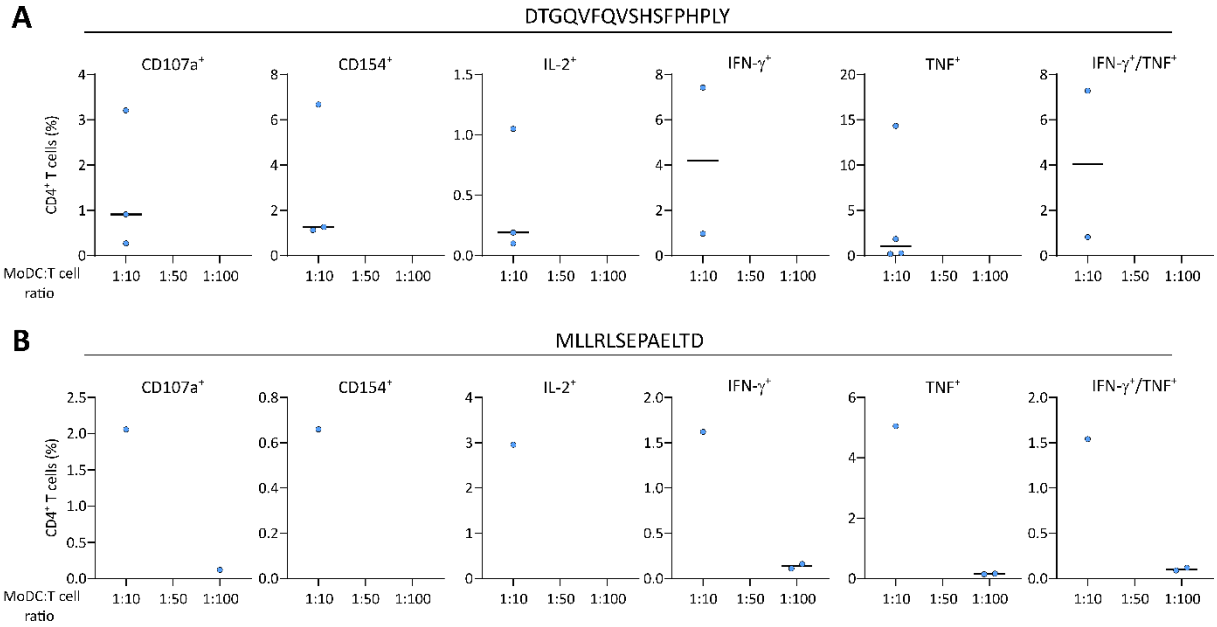

Figure 3: Frequencies and functionality of de novo primed CD4⁺ T cells using the optimized MoDC priming protocol. A, B, Functional characterization of de novo induced CD4⁺ T cells after 4 rounds of priming with MoDCs loaded with (**A**) DTGQVFQVSHSFPHPLY and (**B**) MLLRLSEPAELTD in a 96-well plate stimulating 500.000 CD4⁺ T cells per well, using surface marker (CD107a and CD154) as well as intracellular cytokine staining (IL-2, IFN-γ, and TNF). Scatter dot plots show the calculated frequencies of surface marker expressing or cytokine secreting CD4⁺ T cells for healthy volunteer J420 for wells stimulated with a MoDC to T cell ratio of 1:10 (n=4), 1:50 (n=3) and 1:100 (n=17). Each dot depicts the calculated frequency for one positive test well.

Discussion

Proving the immunogenicity of a peptide is essential for the selection of suitable targets for peptide-based vaccination approaches. For HLA class I-restricted peptides, as described in the first section of this thesis, aAPCs are used. For HLA class II-restricted peptides, MoDC-based priming experiments are a broadly applicable, cost-effective and autologous approach for the induction of *de novo* peptide-specific CD4⁺ T cells. This method was tested in our laboratory; however, it was not extensively set up and did therefore require optimization.

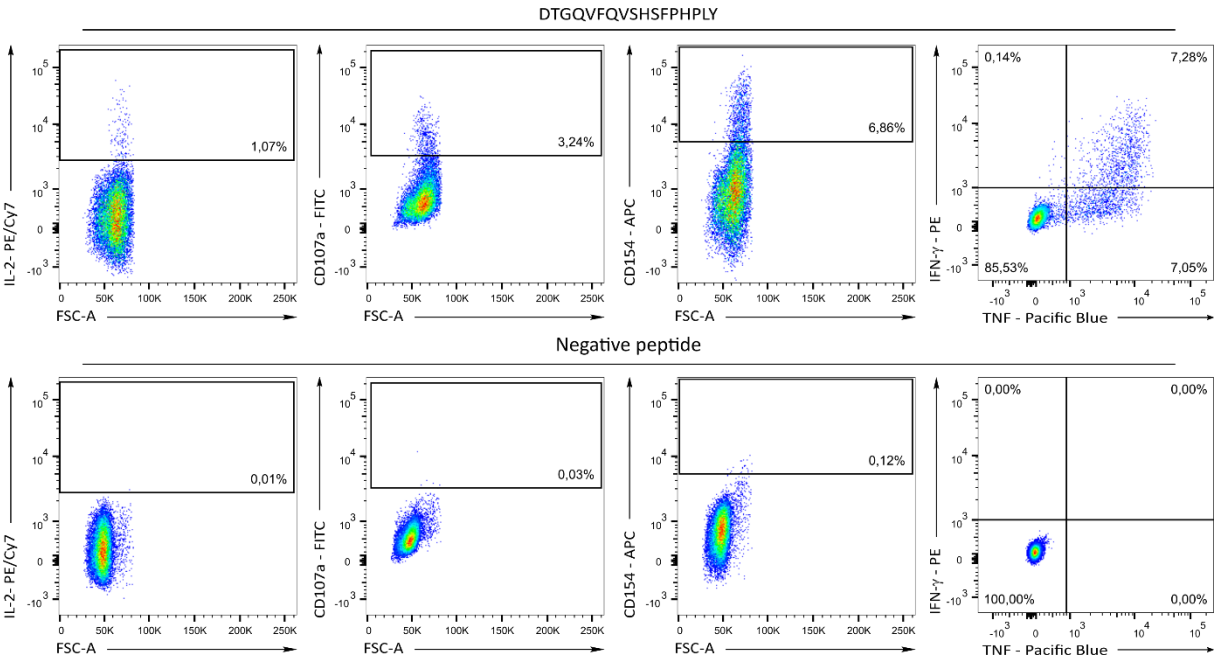

Figure 9: Validating the optimized MoDC priming protocol. Representative example of the flow cytometry-based analysis of CD4⁺ T cells from a healthy volunteer primed with MoDCs loaded with DTGQVFQVSHSFPHPLY (upper panels) using the optimized priming, using 500.000 CD4⁺ T cells/well in a 96-well plate. The CD4⁺ T cell to MoDC ratio is of 1:10. The lower panels show the negative controls consisting of DTGQVFQVSHSFPHPLY-primed CD4⁺ T cells stimulated with a negative peptide.

Whereas the preliminary MoDC priming protocol for CD4⁺ T cells was tested several times to prove the immunogenicity of the fusion protein-derived peptide KREIFDRYGEEVKEFLAKAKED, no peptide-specific CD4⁺ T cell induction could be seen using intracellular cytokine and surface marker staining. As a control for protocol functionality, the peptide KLKKMWKSPNGTIQNILGGTVF previously shown to be immunogenic in ELISpot assays (*6*) was used in the same MoDC priming assays but also failed to induce *de novo* peptide-specific CD4⁺ T cells. This confirmed the necessity of protocol optimization.

Using a preliminary protocol as base for optimization, several aspects were modified. In literature, it is common to start with the separation of CD14⁺ cells from PBMCs, and to stimulate the obtained monocytes with GM-CSF and IL-4 to differentiate them into immature DCs (*7*). For this step, protocols only differ in differentiation factor concentrations and duration of stimulation (*13-16*). However, many different approaches are used to turn differentiated MoDCs into mature MoDCs (*7, 13, 17, 18*), allowing for antigen presentation and T cell co-stimulation. Therefore, we started focusing on the maturation cocktail used for the MoDCs. LPS, an abundant antigen originating from the cell surface of gram-negative bacteria, is known to induce DC maturation and activation and is widely used for the generation of mature MoDCs (*7, 18-20*). As it appeared to be an interesting alternative to use in the maturation cocktail, it was tested in comparison to the cocktail used in the preliminary protocol, including TNF, Prostaglandin E2 and Resiquimod, and showed to induce higher costimulatory cell surface marker expression as well as increased HLA-DR expression on mature MoDCs. The reagents used in the preliminary protocol were therefore replaced by LPS in the maturation cocktail.

A further aspect to optimize MoDC priming of $CD4^+$ T cells, was the duration of coincubation of MoDCs with peptides, as MoDCs start losing their ability for antigen presentation 20 to 40h after starting the maturation process (*9*). In the preliminary protocol, MoDCs were matured for 18 to 24h before coincubation with peptide for additional 24 h. This timeline, requiring up to 48h between start of maturation and stimulation of $CD4^+$ T cells with peptide-loaded MoDCs, was therefore shortened. DC coincubation with peptides for only one hour already leads to $CD4^+$ T cell activation, that can be further increased when prolonging the duration of coincubation (*10*). To reduce the timeline of the preliminary protocol, the MoDC coincubation with peptides was shortened to 2 h. This modification led to improved frequencies of peptide-specific $CD4^+$ T cells.

The third aspect for method optimization was the overall stimulation setting. 12-well plates have greater volumes and surfaces compared to 96-well plates that are also more widely used in assays using MoDCs (*11, 12*). Performing MoDC priming of $CD4^+$ T cells in a 96-well plate finally allowed for the induction of KREIFDRYGEEVKEFLAKAKED-specific $CD4^+$ T cells, confirming its immunogenicity. The optimized protocol was also validated by priming cells of another donor and using other peptides.

Taken together, the MoDC priming protocol was optimized by modifying the maturation cocktail for the MoDCs, the duration of MoDC coincubation with peptides and the $CD4^+$ T cell stimulation setting. Optimization allowed for the *de novo* induction of peptide-specific $CD4^+$ T cells, enabling to prove immunogenicity for potential HLA class II-restricted peptide vaccine candidates.

References

1. A. D. Waldman, J. M. Fritz, M. J. Lenardo, A guide to cancer immunotherapy: from T cell basic science to clinical practice. *Nat Rev Immunol* **20**, 651-668 (2020).
2. A. Nelde, H. G. Rammensee, J. S. Walz, The Peptide Vaccine of the Future. *Mol Cell Proteomics* **20**, 100022 (2021).
3. J. K. Peper, S. Stevanovic, A combined approach of human leukocyte antigen ligandomics and immunogenicity analysis to improve peptide-based cancer immunotherapy. *Cancer immunology, immunotherapy : CII* **64**, 1295-1303 (2015).
4. S. Southwood, J. Sidney, A. Kondo, M. F. del Guercio, E. Appella, S. Hoffman, R. T. Kubo, R. W. Chesnut, H. M. Grey, A. Sette, Several common HLA-DR types share largely overlapping peptide binding repertoires. *J Immunol* **160**, 3363-3373 (1998).
5. J. Hennecke, D. C. Wiley, Structure of a complex of the human alpha/beta T cell receptor (TCR) HA1.7, influenza hemagglutinin peptide, and major histocompatibility complex class II molecule, HLA-DR4 (DRA*0101 and DRB1*0401): insight into TCR cross-restriction and alloreactivity. *J Exp Med* **195**, 571-581 (2002).
6. A. Nelde, H. Schuster, J. S. Heitmann, J. Bauer, Y. Maringer, M. Zwick, J. P. Volkmer, J. Y. Chen, A. M. P. Stanger, A. Lehmann, B. Appiah, M. Marklin, E. Rucker-Braun, H. R. Salih, M. Roerden, S. M. Schroeder, M. F. Haring, A. Schlosser, J. Schetelig, M. Schmitz, M. Boerries, N. Kohler, C. Lengerke, R. Majeti, I. L. Weissman, H. G. Rammensee, J. S. Walz, Immune Surveillance of Acute Myeloid Leukemia Is Mediated by HLA-Presented Antigens on Leukemia Progenitor Cells. *Blood Cancer Discov*, OF1-OF22 (2023).

7. L. Castiello, M. Sabatino, P. Jin, C. Clayberger, F. M. Marincola, A. M. Krensky, D. F. Stroncek, Monocyte-derived DC maturation strategies and related pathways: a transcriptional view. *Cancer immunology, immunotherapy : CII* **60**, 457-466 (2011).
8. D. Y. Ma, E. A. Clark, The role of CD40 and CD154/CD40L in dendritic cells. *Semin Immunol* **21**, 265-272 (2009).
9. A. Alloatti, F. Kotsias, J. G. Magalhaes, S. Amigorena, Dendritic cell maturation and cross-presentation: timing matters! *Immunol Rev* **272**, 97-108 (2016).
10. R. A. Rosalia, E. D. Quakkelaar, A. Redeker, S. Khan, M. Camps, J. W. Drijfhout, A. L. Silva, W. Jiskoot, T. van Hall, P. A. van Veelen, G. Janssen, K. Franken, L. J. Cruz, A. Tromp, J. Oostendorp, S. H. van der Burg, F. Ossendorp, C. J. Melief, Dendritic cells process synthetic long peptides better than whole protein, improving antigen presentation and T-cell activation. *Eur J Immunol* **43**, 2554-2565 (2013).
11. H. Tanaka, C. E. Demeure, M. Rubio, G. Delespesse, M. Sarfati, Human monocyte-derived dendritic cells induce naive T cell differentiation into T helper cell type 2 (Th2) or Th1/Th2 effectors. Role of stimulator/responder ratio. *J Exp Med* **192**, 405-412 (2000).
12. K. Schlienger, N. Craighead, K. P. Lee, B. L. Levine, C. H. June, Efficient priming of protein antigen-specific human CD4(+) T cells by monocyte-derived dendritic cells. *Blood* **96**, 3490-3498 (2000).
13. G. Angelini, S. Gardella, M. Ardy, M. R. Ciriolo, G. Filomeni, G. Di Trapani, F. Clarke, R. Sitia, A. Rubartelli, Antigen-presenting dendritic cells provide the reducing extracellular microenvironment required for T lymphocyte activation. *Proc Natl Acad Sci U S A* **99**, 1491-1496 (2002).
14. M. Hiasa, M. Abe, A. Nakano, A. Oda, H. Amou, S. Kido, K. Takeuchi, K. Kagawa, K. Yata, T. Hashimoto, S. Ozaki, K. Asaoka, E. Tanaka, K. Moriyama, T. Matsumoto, GM-CSF and IL-4 induce dendritic cell differentiation and disrupt osteoclastogenesis through M-CSF receptor shedding by up-regulation of TNF-alpha converting enzyme (TACE). *Blood* **114**, 4517-4526 (2009).
15. T. Q. Chometon, M. D. S. Siqueira, J. C. Sant Anna, M. R. Almeida, M. Gandini, A. C. Martins de Almeida Nogueira, P. R. Z. Antas, A protocol for rapid monocyte isolation and generation of singular human monocyte-derived dendritic cells. *PLoS One* **15**, e0231132 (2020).
16. V. Marzaioli, M. Canavan, A. Floudas, S. C. Wade, C. Low, D. J. Veale, U. Fearon, Monocyte-Derived Dendritic Cell Differentiation in Inflammatory Arthritis Is Regulated by the JAK/STAT Axis via NADPH Oxidase Regulation. *Front Immunol* **11**, 1406 (2020).
17. F. Moschella, A. Maffei, R. P. Catanzaro, K. P. Papadopoulos, D. Skerrett, C. S. Hesdorffer, P. E. Harris, Transcript profiling of human dendritic cells maturation-induced under defined culture conditions: comparison of the effects of tumour necrosis factor alpha, soluble CD40 ligand trimer and interferon gamma. *Br J Haematol* **114**, 444-457 (2001).
18. I. Baltathakis, O. Alcantara, D. H. Boldt, Expression of different NF-kappaB pathway genes in dendritic cells (DCs) or macrophages assessed by gene expression profiling. *J Cell Biochem* **83**, 281-290 (2001).
19. K. Abdi, N. J. Singh, P. Matzinger, Lipopolysaccharide-activated dendritic cells: "exhausted" or alert and waiting? *J Immunol* **188**, 5981-5989 (2012).
20. P. Jin, T. H. Han, J. Ren, S. Saunders, E. Wang, F. M. Marincola, D. F. Stroncek, Molecular signatures of maturing dendritic cells: implications for testing the quality of dendritic cell therapies. *J Transl Med* **8**, 4 (2010).

Chapter 3

Durable spike-specific T cell responses after different COVID-19 vaccination regimens are not further enhanced by booster vaccination

Yacine Maringer[1,2,3], Annika Nelde[1,2,3], Sarah M. Schroeder[1,2,4], Juliane Schuhmacher[1,3], Sebastian Hörber[5], Andreas Peter[5], Julia Karbach[6], Elke Jäger[6], Juliane S. Walz[1,2,3,7]

[1] Department of Peptide-based Immunotherapy, University and University Hospital Tübingen, Tübingen, Germany

[2] Institute for Cell Biology, Department of Immunology, University of Tübingen, Tübingen, Germany

[3] Cluster of Excellence iFIT (EXC2180) "Image-Guided and Functionally Instructed Tumor Therapies", University of Tübingen, Tübingen, Germany

[4] Department of Otorhinolaryngology, Head and Neck Surgery, University Hospital Tübingen, Tübingen, Germany.

[5] Institute for Clinical Chemistry and Pathobiochemistry, Department for Diagnostic Laboratory Medicine, University Hospital Tübingen, Tübingen, Germany.

[6] Department of Oncology and Hematology, Krankenhaus Nordwest, Frankfurt, Germany

[7] Clinical Collaboration Unit Translational Immunology, German Cancer Consortium (DKTK), Department of Internal Medicine, University Hospital Tübingen, Tübingen, Germany

Sci Immunol. 2022 Dec 23;7(78):eadd3899. PMID: 36318037
doi: 10.1126/sciimmunol.add3899

Disclosure and Author Contributions

YM participated in the study design. YM conducted and planned *ex vivo* and *in vitro* T cell experiments and analyzed the obtained data. YM conceived all tables and figures. The manuscript was drafted by YM, JSW and AN. For more information please refer to the statement provided in the "Author contributions" section at the end of this chapter.

Abstract:

Several COVID-19 vaccines are approved to prevent severe disease outcome following SARS-CoV-2 infection. Whereas induction and functionality of antiviral antibody response are largely studied, the induction of T cells upon vaccination with the different approved COVID-19 vaccines is less studied. Here, we report on T cell immunity 4 weeks and 6 months after different vaccination regimens and 4 weeks after an additional booster vaccination in comparison with SARS-CoV-2 T cell responses in convalescents and prepandemic donors using interferon-gamma ELISpot assays and flow cytometry. Increased T cell responses and cross-recognition of B.1.1.529 Omicron variant-specific mutations were observed *ex vivo* in mRNA- and heterologous-vaccinated donors compared with vector-vaccinated donors. Nevertheless, potent expandability of T cells targeting the spike protein was observed for all vaccination regimens, with frequency, diversity, and the ability to produce several cytokines of vaccine-induced T cell responses comparable with those in convalescent donors. T cell responses for all vaccinated donors significantly exceeded preexisting cross-reactive T cell responses in prepandemic donors. Booster vaccination led to a significant increase in anti-spike IgG responses, which showed a marked decline 6 month after complete vaccination. In contrast, T cell responses remained stable over time after complete vaccination with no significant effect of booster vaccination on T cell responses and cross-recognition of Omicron BA.1 and BA.2 mutations. This suggested that booster vaccination is of particular relevance for the amelioration of antibody response. Together, our work shows that different vaccination regimens induce broad and long-lasting spike-specific $CD4^+$ and $CD8^+$ T cell immunity to SARS-CoV-2.

Introduction:

During the Coronavirus Disease 2019 (COVID-19) pandemic, caused by the severe acute respiratory syndrome coronavirus 2 (SARS-CoV-2), several vaccines have been successfully developed, reducing transmission and preventing billions of people from severe disease outcome (*1-4*). Among the currently approved COVID-19 vaccines, the ChAdOx1 nCoV-19 adenovirus-based vector vaccine ChAdOx1, the human adenovirus type 26 (Ad26)-based vector vaccine Ad26.COV2.S, and the two mRNA vaccines BNT162b2 and mRNA-1273 are the most widely used in Europe and North America (*5-7*). Vaccination schedules comprise two doses of ChAdOx1, BNT162b2 and mRNA-1273 and one dose of Ad26.COV2.S for complete vaccination status (*1-4*). After reports of thromboembolic events after

ChAdOx1 vaccination (*8*), several European governments recommended completing vaccination with an mRNA vaccine after the first dose of ChAdOx1 (heterologous vaccination). To overcome waning vaccine immunity over time (*9*), the administration of an additional booster vaccine dose was approved in many countries 3 to 6 months after completion of vaccination (*10*).

COVID-19 vaccination induces both humoral immunity, mediated by B cell-derived antibodies, and cellular immunity, mediated by T cells (*2*). Although it is undisputed that neutralizing antibodies provide the first line of antiviral defense (*11, 12*), T cell immunity is crucial to combat acute SARS-CoV-2 infection and for the development of long-term immunity (*13*). Whereas antibody titers tend to wane quickly and show limited neutralizing activity to newly arising variants of concern (VOCs), T cell memory is largely conserved against VOCs after prior SARS-CoV-2 infection (*14, 15*) .

So far, research on SARS-CoV-2 vaccine-induced immunity is largely focused on anti-spike antibody titers and their ability to neutralize virus particles (*16*). Spike-specific T cell responses induced upon different vaccination regimens are studied to a lesser extent, with first reports showing the induction of both $CD4^+$ and $CD8^+$ T cell responses after complete vaccination with different vaccination regimens. Moreover, T cell responses are shown to be largely conserved against different SARS-CoV-2 variants, including early B.1.1.529 (Omicron) variants now dominant globally (*12, 17*).

In this work, we provided an analysis of spike-specific T cell responses and their cross-recognition of B.1.1.529 Omicron BA.1 and BA.2 variant-specific mutations after complete vaccination with mRNA, vector, and heterologous vaccine regimens in comparison with COVID-19 convalescents and prepandemic donors. In addition, we provided insight on the effects of a third mRNA booster vaccination after homologous and heterologous vaccination regimens on T cell and antibody immunity.

Results:

SARS-CoV-2 Spike-Specific T Cell Responses after Complete Vaccination with Different Vaccination Regimens

To assess spike-specific T cell responses after complete vaccination (two doses of BNT162b2, mRNA-1273, or ChAdOx1; one dose of Ad26.COV2.S; or one dose of vector vaccine ChAdOx1 followed by one dose of an mRNA vaccine for heterologous vaccine regimens), we performed interferon-γ (IFN-γ) enzyme-linked immunospot (ELISpot) assays 3 to 12 weeks (median, 4 weeks) after the complete vaccination dose (Table 1). Results were obtained using three different peptide pools covering various parts of the spike protein, with Prot_S1 covering the complete N-terminal S1 domain, Prot_S+ covering part of the C-terminal S2 domain, and Prot_S comprising selected immunodominant sequence domains (Fig. 1A,B). Asymptomatic infections during the study period were excluded by testing for nucleocapsid antibodies (Fig. S1).

Spike-specific IFN-γ T cell responses were observed *ex vivo* for 100% of mRNA- (n = 24) and heterologous-vaccinated donors (n = 15; Fig. 1C and Table 1). The cohort of vector-vaccinated donors (n = 9) showed a significantly reduced response rate (67%) compared with the other vaccination regimens (Fig. 1C). In COVID-19 convalescent donors (n = 16), spike-specific IFN-γ T cell responses were detected in 88% of the donors. A total of 16% of prepandemic donors never exposed to SARS-CoV-2 (Pre, n = 31; Fig. 1C) showed low-intensity cross-reactive spike-specific T cell responses (Fig. 1D). Intensity of spike-specific T cell responses did not significantly differ between the three vaccination cohorts and convalescent donors (Fig. 1D). However, mRNA- (median calculated spot counts, 71) and heterologous-vaccinated donors (median, 69) exhibited a two- to threefold increased T cell response intensity compared with vector-vaccinated (median, 24) and convalescent donors (median, 24; Fig. 1D). No correlation was observed between the time point of sample collection after complete vaccination (Fig. S2A); demographic donor characteristics comprising body mass index (BMI), age, sex, or side effects after vaccination as well as clinical symptoms of COVID-19 (as assessed by questionnaires) of complete vaccination (Table 1 and Fig. S2B-E) and convalescent (Table 2 and Fig. S2F-H) individuals, respectively; and the intensity of spike-specific IFN-γ T cell responses.

After 12-day T cell expansion (Fig. S3A), the percentage of donors with detectable spike-specific T cell responses was increased to 100% for all vaccinated groups and the convalescent cohort and to 97% for prepandemic donors (Fig. S3B). Significantly increased intensity of IFN-γ T cell responses for vaccinated donors (median mRNA, 1286; vector, 1281; heterologous, 2602) and convalescent donors (median, 2946) was observed compared with prepandemic donors (median, 112; Fig. S3C) and with *ex vivo* responses (fold change mRNA, 18; vector, 53; heterologous, 38; Fig. S3D). This indicates potent expandability of vaccine-induced T cells upon SARS-CoV-2 exposure.

Table 1: Characteristics of healthy volunteer cohorts after heterologous-, mRNA- or vector-based vaccination.

	mRNA vaccine cohort	vector vaccine cohort	heterologous vaccination cohort
Number of donors	35	10	17
Age [years]			
Median	38	n.a.	31
Range	25 -71	n.a	24 - 52
Sex [n (%)]			
Female	19 (54.3)	n.a.	11 (64.7)
Male	16 (45.7)	n.a.	6 (35.3)
Comorbidities [n (%)]			
High blood pressure	3 (12.5)	n.a.	1 (5.9)
Cardiovascular disease	1 (4.2)	n.a.	1 (5.9)
Blood sugar disorder	2 (8.3)	n.a.	0 (0.0)
Chronic lung disease	0 (0.0)	n.a.	1 (5.9)
Cancer disease	1 (4.2)	n.a.	0 (0.0)
n.a.	11	n.a.	0
Vaccination schemes (CV)			
BNT162b2 x BNT162b2	20 (83.3)		
mRNA-1273 x mRNA-1273	4 (16.7)		
ChadOx1 x ChadOx1		6 (60.0)	
Ad26.COV2.S		4 (40.0)	
ChadOx1 x BNT16b2			7 (46.7)
ChadOx1 x mRNA-1273			8 (53.3)
<u>Time points</u>			
Prevaccination			
Donors	-	-	9
After the first vaccination			
Donors	-	-	8
Weeks after vaccination			
Median	-	-	10
Range	-	-	9 -10
After complete vaccination			
Donors	24	10	15
Weeks after vaccination			
Median	3	4	6
Range	3 – 10	3 – 8	3 – 12
Awareness of side effects [n (%)]			
Yes	9 (69.2)	n.a.	5 (50.0)
No	4 (30.8)	n.a.	5 (50.0)
n.a.	11	n.a.	5
6 months after complete vaccination	11	-	17
Donors			
Weeks after vaccination	26	-	26
Median	21 -32	-	24 - 28
Range			
After booster vaccination			
Donors	13	-	17
Weeks after vaccination			
Median	4	-	4
Range	2 – 7	-	3 – 6
Awareness of side effects [n (%)]			
Yes	2 (18.2)	-	6 (35.3)
No	9 (81.8)	-	11 (64.7)
n.a.	2	-	0

The mRNA-based vaccine cohort includes healthy volunteers vaccinated two (complete vaccination) to three times (booster vaccination) either with mRNA-1273 or BNT162b2. Donors of the vector-based vaccine either received two doses of ChadOx1 (complete vaccination) or one dose of Ad26.COV2.S (complete vaccination). The heterologous vaccination group received one dose of ChadOx1 followed by one (complete vaccination) or two doses (booster vaccination) of either mRNA-1273 or BNT162b2. For mRNA- and heterologous-vaccinated donors, we analyzed two different time points after complete vaccination, the time point of complete vaccination 3 to 12 weeks after complete vaccination and the time point 6 months after complete vaccination (21-32 weeks after complete vaccination). Figures 1 to 3 show T cell responses after complete vaccination, and analysis over different time points are shown in Figure 4. Figure 4 includes the identical results for the time point of complete vaccination for mRNA- and heterologous-vaccinated donors as shown in Figures 1 to 3. Experiments were not always conducted with all donors, depending on available cell numbers. n, number; n.a., not applicable; CV, complete vaccination.

There are differences in SARS-CoV-2 T cell cross-reactivity to common cold human coronaviruses (HCoVs) of the N-terminal (less HCoV homologous) and C-terminal domain of the spike protein (*18*). To assess whether these differences affect vaccine-induced T cell responses, we performed IFN-γ ELISpot assays individually for the three different spike pools (Fig. 1E and Fig. S3E). In the mRNA-vaccinated, heterologous-vaccinated, and convalescent cohort, the most frequently recognized peptide pool was the Prot_S1 pool, with 96, 100 and 75% of individuals showing an *ex vivo* response against this pool, respectively (Fig. 1E). In the vector-vaccinated cohort, the Prot_S+ pool was recognized by T cells from the majority of donors (67%, not reaching level of significance compared with the other peptide pools; Fig. 1E). After 12-day T cell expansion, the differences in pool-specific recognition rates within the cohorts were upheld (Fig. S3E). Most individuals vaccinated with mRNA (75%) or a heterologous scheme (80%) showed *ex vivo* T cell responses against all three spike pools, whereas only 33% of vector-vaccinated individuals recognized all pools (Fig. 1F). A total of 44% of convalescent donors exhibited T cell responses against all pools (Fig. 1F). After 12-day T cell expansion, at least 78% of vaccinated donors recognized all peptide pools independent of vaccination regimen (Fig. S3F). For the prepandemic cohort, we detected no relevant differences in the recognition rate (up to 10% *ex vivo*, 66% after 12-day expansion) and intensity of cross-reactive T cell responses for the three peptide pools (Fig. 1E,F, and Fig. S3E,F).

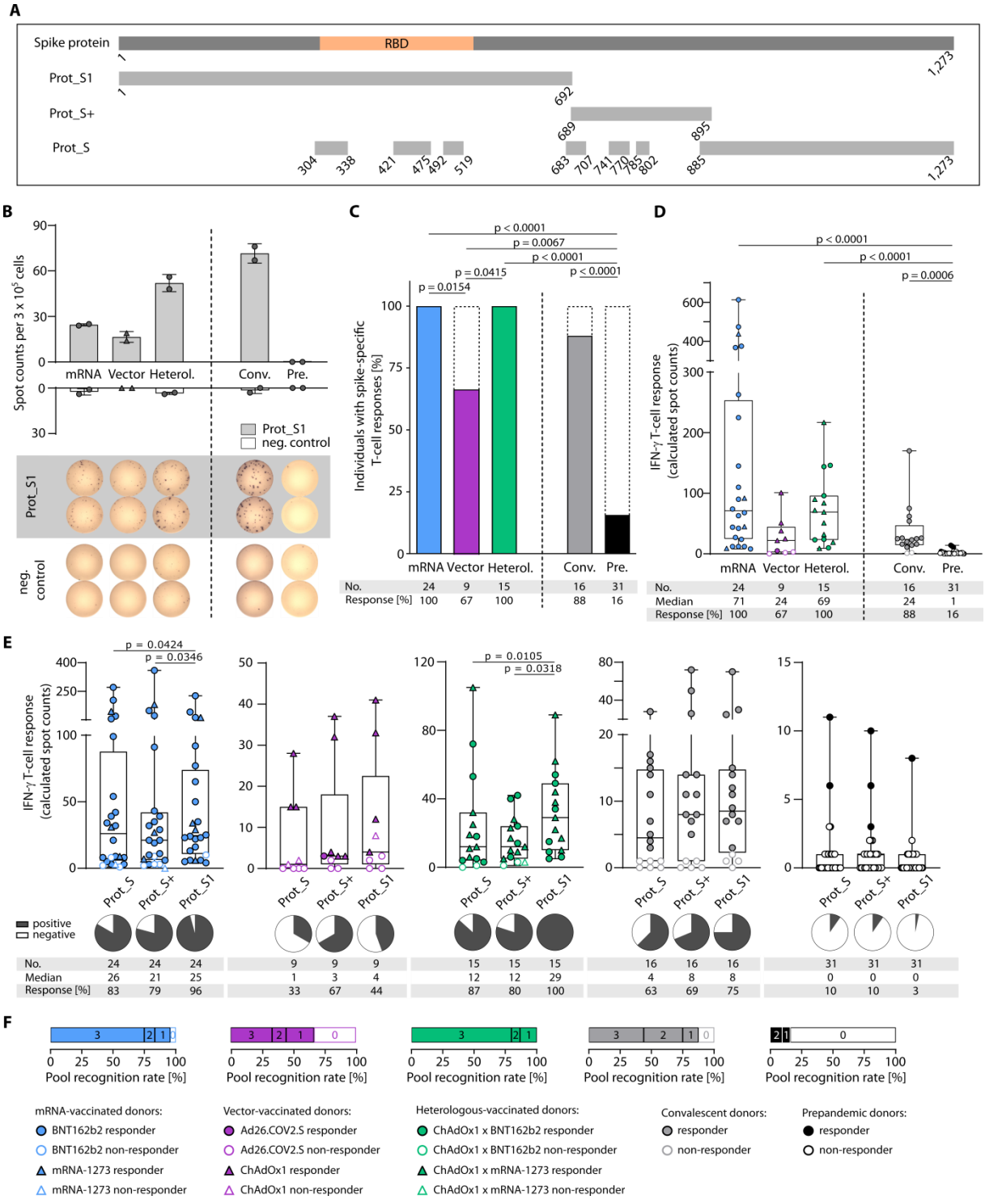

Figure 1: *Ex vivo* immune responses to SARS-CoV-2 spike protein peptide pools after complete vaccination. **A,** Schematic depiction of the SARS-CoV-2 spike protein, and protein section coverage by the peptide pools (Prot_S1, Prot_S+, Prot_S) used for immunogenicity testing. **B-F,** *Ex vivo* T cell responses after complete vaccination [two doses of BNT162b2, mRNA-1273, or ChAdOx1; one dose of Ad26.COV2.S; or one dose of the vector vaccine ChAdOx1 followed by one dose of an mRNA vaccine for heterologous (Heterol.) vaccine regimens] compared with COVID-19 convalescents (Conv.) and prepandemic (Pre.) donors were assessed by IFN-γ ELISpot assays 3 to 12 weeks (median 4 weeks) after the last vaccine dose (sample collection after complete vaccination, Table 1). **B,** Representative example of *ex vivo* IFN-γ T cell responses to the Prot_S1 peptide pool compared with a negative (neg.) control peptide, showing duplicates for one donor of each cohort. **C,D,** Percentage of individuals with *ex vivo* IFN-γ ELISpot T cell responses (**C**), and intensities of IFN-γ T cell responses in terms of calculated spot counts against the spike-specific peptide pools (**D**) after mRNA, vector or heterologous vaccination compared with convalescents and prepandemic donors (summarized responses against the three spike-specific peptide pools). **E,** Intensities of *ex vivo* IFN-γ T cell responses shown for the distinct spike protein peptide pools. **F,** Proportion of individuals (cohorts as indicated by color code) with responses to all three, two, one or none of the spike peptide pools. Responders are represented

by colored symbols, and nonresponders are represented by clear symbols. Symbol shapes indicate the different vaccine products received by the donors. **D,E,** Box plots represent the median with the 25th and 75th percentiles with minimum and maximum whiskers. **C,** Fisher's exact test was used. **D,** Kruskal-Wallis test was used, **E,** Friedman test was used. If P values are not shown, then results were not significant. RBD, receptor-binding domain; No., number.

T cell cross-recognition of the current dominant Omicron variant-specific mutations in the spike protein was assessed by ELISpot assays with spike-derived Omicron BA.1 and BA.2 variant-specific pools (Fig. 2A and Table S2). Cross-recognition of the BA.1- and BA.2-mutated regions by vaccine-induced T cells was observed for the majority of mRNA-vaccinated (69 and 85% for BA.1, 69 and 85% for BA.2) and heterologous-vaccinated (80 and 90% for BA.1, 60 and 100% for BA.2) donors *ex vivo* and after 12-day T cell expansion, respectively. T cell cross-recognition of BA.1- and BA.2-mutated regions of the spike protein was reduced in the vector-vaccinated cohort, with 20 and 0% recognition *ex vivo* and 25 and 25% recognition after 12-day T cell expansion, respectively (Fig. 2B-E and Fig. S4). In summary, our results showed induction of broad spike-specific T cell responses, particularly for mRNA- and heterologous-vaccinated individuals, that resembled the responses observed in convalescent donors.

Table 2: Characteristics of SARS-CoV-2 convalescent donors.

		Convalescent donor cohort
Number of donors		16
Age [years]		
	Median	46
	Range	19 - 83
Sex [n (%)]		
	Female	11 (68.8)
	Male	5 (31.2)
Comorbidities [n (%)]		
	High blood pressure	6 (37.5)
	Cardiovascular disease	0 (0.0)
	Blood sugar disorder	2 (12.5)
	Chronic lung disease	0 (0.0)
	Cancer disease	0 (0.0)
Sample collection date		July 2020
Interval positive test to sample collection (weeks)		
	Median	17
	Range	13 -19
Awareness of symptoms [n (%)]		
	No	3 (18.75)
	Mild	2 (12.5)
	Moderate	6 (37.5)
	Severe	5 (31.25)
Febrile illness (≥ 38.0°C)		
	No	10 (62.5)
	Yes	6 (37.5)

Convalescents showed asymptomatic to mild COVID-19. By the time of sample collection, the wild-type SARS-CoV-2 was circulating, and VOCs emerged at a later time point. None of the donors were hospitalized or required oxygen treatment. Awareness of disease symptoms was assessed by questionnaire. n, number.

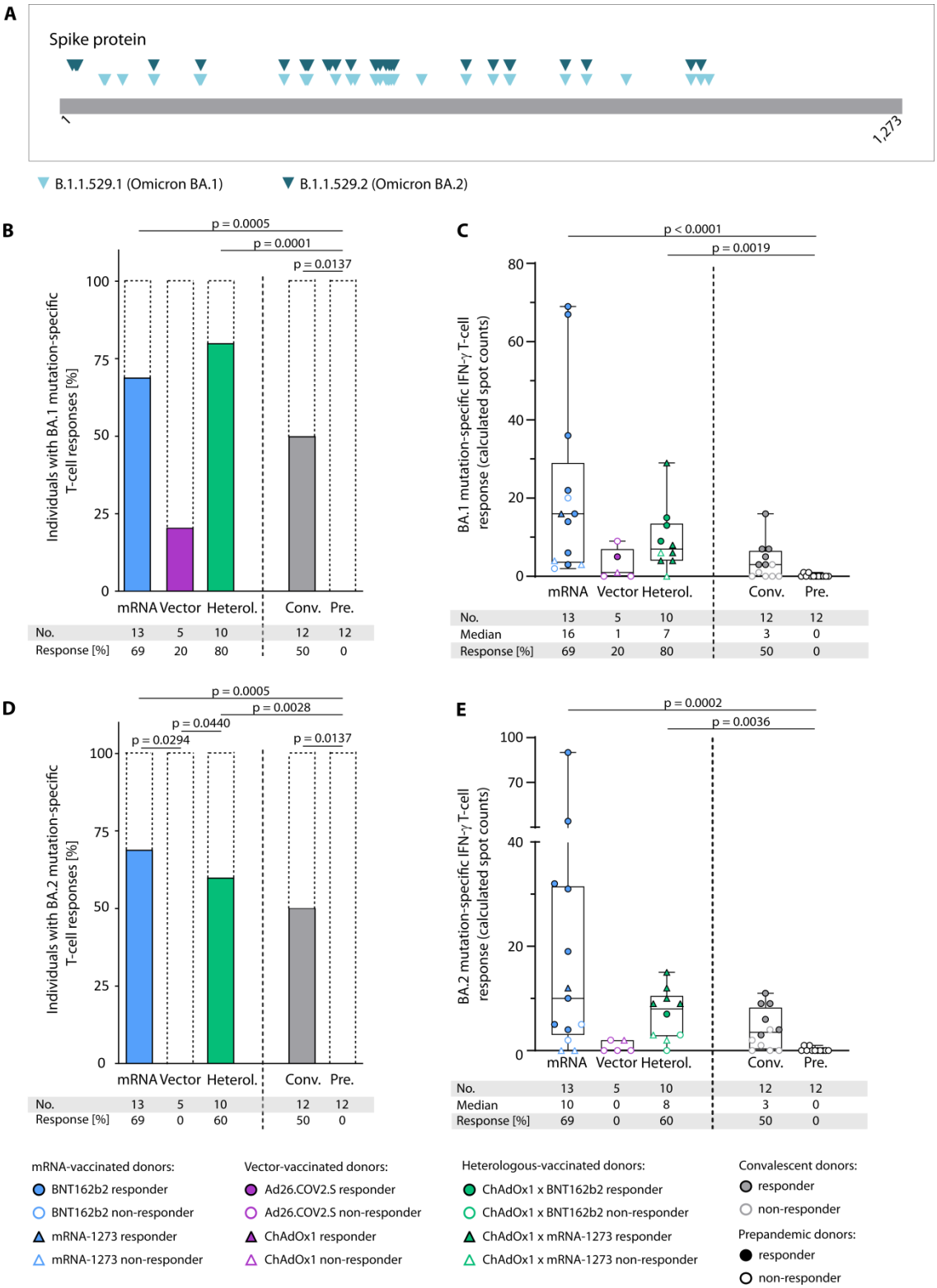

Figure 2: *Ex vivo* IFN-γ responses to SARS-CoV-2 BA.1 and BA.2 mutation pools. A, Overview of variant-defining mutations in the spike protein described for the different VOCs. **B-E,** Variant mutation-specific T cell responses after complete vaccination (two doses of BNT162b2, mRNA-1273 and ChAdOx1 or one dose of Ad26.COV2.S; for heterologous (Heterol.) vaccine regimens, one dose of the vector vaccine ChAdOx1 followed by one dose of an mRNA vaccine), were assessed by IFN-γ ELISpot assays. **B,** Percentage of individuals with BA.1 mutation pool-specific *ex vivo* IFN-γ T cell responses, and **C,** intensities of IFN-γ T cell responses in terms of calculated spot counts after mRNA, vector or heterologous vaccination, compared with COVID-19 convalescents (Conv.) and prepandemic (Pre.) donors. **D,** Percentage of individuals with BA.2 mutation pool-specific *ex vivo* IFN-γ T cell responses, and **E,** intensities of IFN-γ T cell responses in terms of calculated spot counts. Responders are represented by colored symbols, and nonresponders are represented by clear symbols. Symbol shapes indicate the different vaccine products received by the donors. **C,E,** Box plots represent the median with the 25th and 75th percentiles with

minimum and maximum whiskers. **B,D,** Fisher's exact test was used. **C,E,** Kruskal-Wallis test was used. If P values are not shown, then results were not significant.

Characterization of SARS-CoV-2 Spike-Specific T Cell Responses after Complete Vaccination

Ex vivo intracellular cytokine and surface marker staining revealed vaccine-induced spike-specific $CD4^+$ T cell responses for the majority of vaccinated donors of all regimens and in convalescent donors (86% for mRNA-vaccinated, 71% for vector-vaccinated, 70% for heterologous-vaccinated, and 75% for convalescents). The percentages of donors with $CD8^+$ (57% for mRNA-vaccinated, 71% for vector-vaccinated, 30% for heterologous-vaccinated, and 42% for convalescents) as well as with both $CD4^+$ and $CD8^+$ T cell responses (57% for mRNA-vaccinated, 57% for vector-vaccinated, 30% for heterologous-vaccinated, and 33% for convalescents) were generally lower compared with $CD4^+$ T cell responses (Fig. 3A). The low frequency of cross-reactive T cell responses detected in the prepandemic cohort in the IFN-γ ELISpot assay was mediated by $CD8^+$ T cells (0% $CD4^+$ T cells, 17% $CD8^+$ T cells; Fig. 3A). Vaccine-induced $CD4^+$ T cells displayed a T helper 1 (T_H1) phenotype, showing mainly positivity for tumor necrosis factor (TNF) and, to a lesser extent, for CD107a and IFN-γ/TNF, and were negative for the T_H2 marker interleukin-4 (IL-4) comparably with SARS-CoV-2-specific T cells in convalescent donors (Fig. 3B-D and Fig. S5A). A significantly increased frequency of TNF^+CD4^+ T cells was observed for the mRNA-vaccinated cohort compared with the vector- and heterologous-vaccinated groups and for $TNF^+IFN\text{-}\gamma^+CD4^+$ T cells compared with the vector-vaccinated group. $CD8^+$ T cell responses, in terms of frequencies of cytokine-producing cells and the ability to produce multiple cytokines, also showed a similar profile in vaccinated donors and convalescent individuals with particular positivity for IFN-γ. Prepandemic donors had lower frequencies of cytokine producing cells, significantly reduced for IFN-γ compared with vector and mRNA vaccinated donors (Fig. 3E-G). No significant differences could be observed between $CD8^+$ T cell responses and functionality in individuals vaccinated with different vaccination regimens or in convalescent donors.

Comparable frequencies of vaccine-induced memory $CD45RO^+TNF^+CD4^+$ T cells were observed in the mRNA and heterologous vaccine cohort and the convalescent cohort (86% for mRNA-vaccinated, 70% for heterologous-vaccinated, and 58% for convalescents), whereas no $CD45RO^+TNF^+CD4^+$ T cells could be detected in donors vaccinated with a vector-based vaccine regimen (Fig. S5B). Cytokine-positive $CD8^+$ memory T cells ($CD45RO^+IFN\text{-}\gamma^+CD8^+$ T cells) were observed to a much lower extent (21% for mRNA-vaccinated, 43% for vector-vaccinated, 0% for heterologous-vaccinated, and 0% for convalescents, 0%; Fig S5C).

In conclusion, no significant differences could be observed between $CD4^+$ and $CD8^+$ T cell responses in individuals vaccinated with different vaccination regimens and in convalescent donors. However, the ability of vector-vaccinated donors to produce several cytokines was reduced compared to the other vaccination regimens.

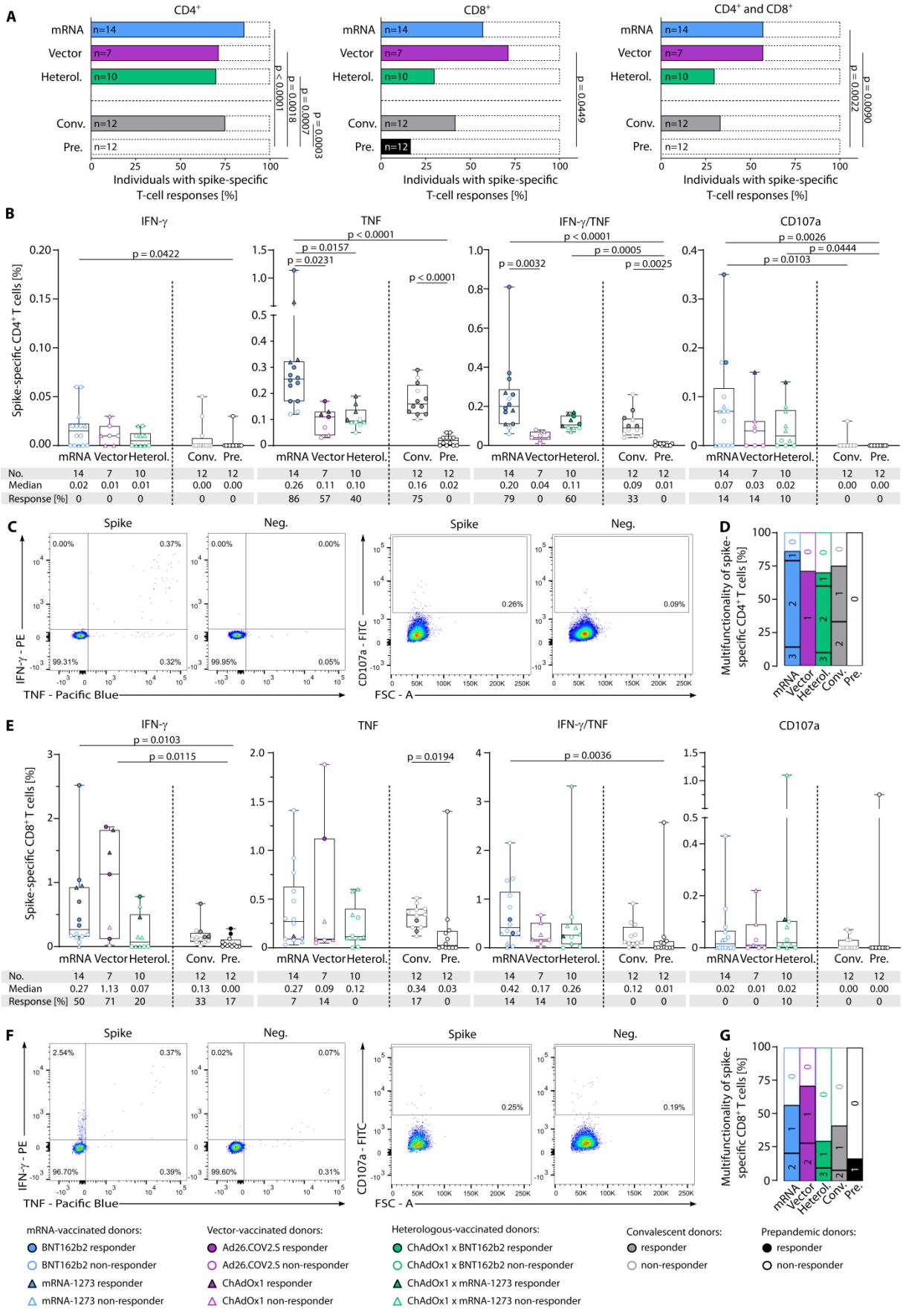

Figure 3: *Ex vivo* characterization of spike-specific T cell responses after complete vaccination. Spike-specific T cell responses after complete vaccination (two doses of BNT162b2, mRNA-1273 or ChAdOx1; one dose of Ad26.COV2.S; or one dose of the vector vaccine ChAdOx1 followed by one dose of an mRNA vaccine for heterologous (Heterol.) vaccine regimens) were characterized *ex vivo* by intracellular cytokine (IFN-γ and TNF) and surface marker (CD107a) staining. **A,** Percentage of

individuals with *ex vivo* $CD4^+$ (left), $CD8^+$ (middle) as well as both $CD4^+$ and $CD8^+$ (right) T cell responses to the SARS-CoV-2 spike-specific peptide pools. **B,** Frequencies of spike-specific $CD4^+$ T cells after complete vaccination assessed *ex vivo*. **C,** Exemplary flow cytometry data of indicated cytokines and surface marker shown for $CD4^+$ T cells for one donor after complete vaccination (BNT162b2 x BNT162b2) with an mRNA vaccine. **D,** Proportion of samples with non-functional (0), mono-functional (1), bi-functional (2), or tri-functional (3) spike-specific $CD4^+$ T cells after complete vaccination. **E,** Frequencies of spike-specific $CD8^+$ T cells after complete vaccination assessed *ex vivo*. **F,** Exemplary flow cytometry data of indicated cytokines and surface marker shown for $CD8^+$ T cells for one donor after complete vaccination (BNT162b2 x BNT162b2) with an mRNA vaccine. **G,** Proportion of samples with non-functional (0), mono-functional (1), bi-functional (2), or tri-functional (3) spike-specific $CD8^+$ T cells after complete vaccination. T cell responses were considered positive if the detected frequency of cytokine-positive $CD4^+$ or $CD8^+$ T cells was ≥ 3-fold higher than the frequency in the negative control and at least 0.1% of total $CD4^+$ or $CD8^+$ T cells. Responders are represented by colored symbols, and nonresponders are represented by clear symbols. Symbol shapes indicate the different vaccine products received by the donors. **A,** Fisher's exact test. **B,E,** Box plots show the median with the 25th and 75th percentiles, and whiskers represent minimum and maximum; Kruskal-Wallis test was used. If P values are not shown, then the results were not significant. FSC, forward scatter; Neg., negative control.

Effects of Booster Vaccination on Spike-Specific Immune Responses to mRNA and Heterologous Vaccination Regimens

Spike-specific antibody and T cell responses were assessed over time, at baseline before vaccination (V0), 1 month after the first (V1), after complete vaccination, 6 months after complete vaccination, and 1 month after the booster vaccination for mRNA- and heterologous-vaccinated donors. Booster vaccination induced a significant (up to eightfold) increase in spike-specific antibody levels, with immunoglobulin G (IgG) titers similarly enhanced from a median of 19 to 100 for mRNA-vaccinated individuals and from a median of 12 to 100 for heterologous-vaccinated donors compared with the time point 6 months after complete vaccination (Fig. 4A,B and Fig. S6A). Spike-specific T cell responses were assessed by IFN-γ ELISpot assays *ex vivo* (Fig. 4C,D) and after 12-day T cell expansion (Fig. S6C,D) for different time points after vaccination. *Ex vivo* IFN-γ T cell responses peaked comparably after complete vaccination for both vaccination regimens (median mRNA, 71; heterologous, 69), being about two- to threefold higher compared with 6 months after complete vaccination (median mRNA, 39; heterologous, 19; Fig. 4C,D and Fig S6B). In contrast to antibody responses, the increase in T cell response intensity through boost vaccination, in terms of calculated spot counts, did not reach levels of significance, neither *ex vivo* nor after 12-day T cell expansion (Fig. 4A-D and Fig. S6A-D). No correlations could be observed between IFN-γ T cell response intensity and BMI, age, sex, and donor-reported side effects after booster vaccination (Fig. S2I-L). The number of different spike-derived peptide pools that resulted in an *ex vivo* detectable T cell response (pool recognition rate) was highest after complete vaccination for both vaccination regimens and was not altered or increased by the booster vaccination. Spike-specific T cells showed potent expandability, resulting in T cell responses against all three spike peptide pools after 12-day T cell expansion at all time points after vaccination (Fig. S6C-F, Fig. S7). Cross-recognition of the Omicron BA.1- and BA.2-mutated regions of the spike protein after booster vaccination in donors vaccinated with mRNA (45 and 91% for BA.1 and 45 and 91% for BA.2 donors with T cell response) or heterologous regimen (64 and 91% for BA.1 and 55 and 82% for BA.2 donors with T cell response) *ex vivo* and after 12-day T cell expansion, respectively, was comparable with the results after complete vaccination (Fig. 4E,F and Fig. S6G,H).

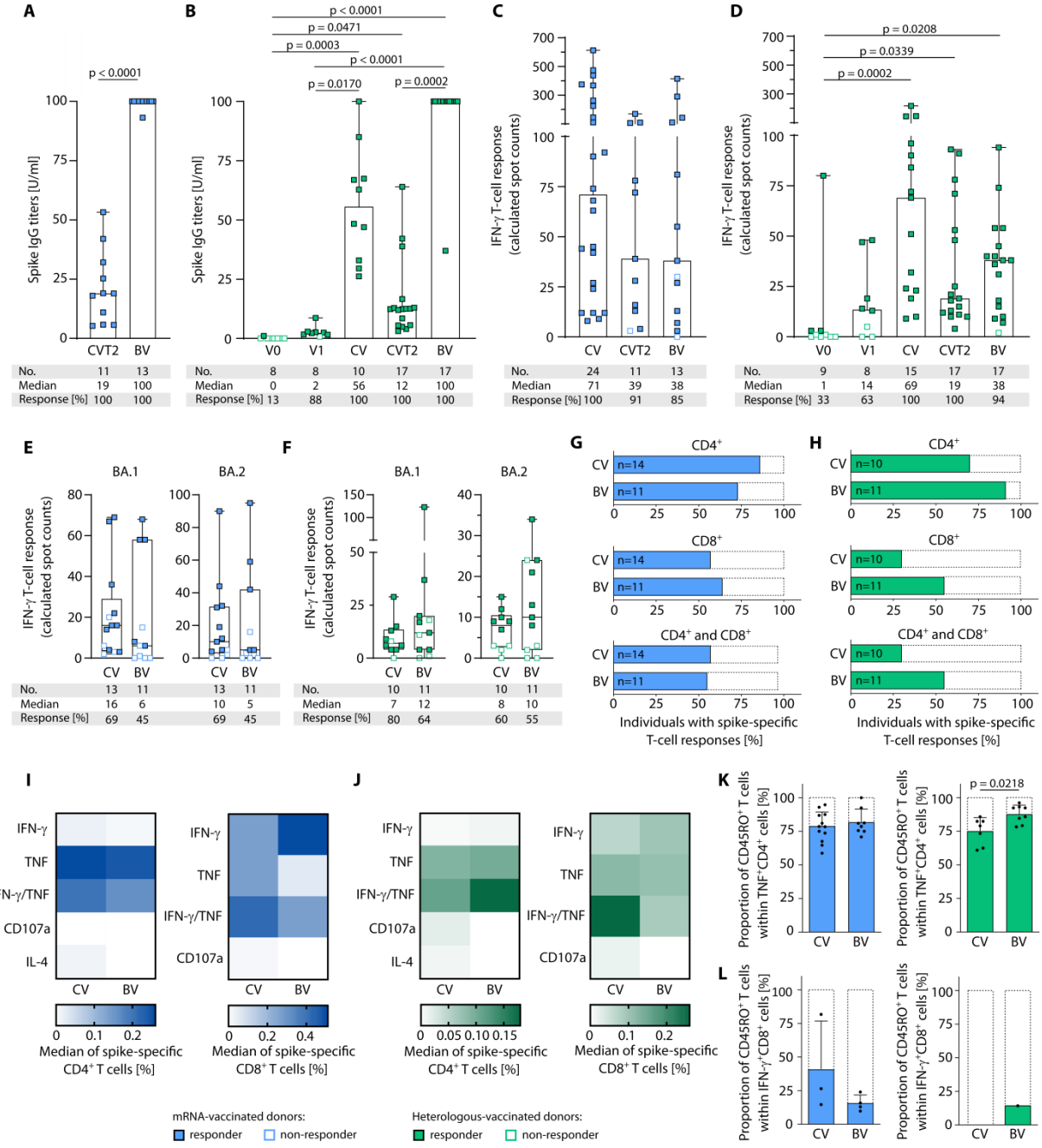

Figure 4: T cell and antibody responses of mRNA- and heterologous-vaccinated individuals after booster vaccination. A-D, Time course of spike antibody titers (**A,B**), and intensities of *ex vivo* IFN-γ T cell responses in terms of calculated spot counts were assessed by IFN-γ ELISpot assays targeting spike-specific peptide pools (**C,D**) after mRNA (**A,C**) and heterologous (**B,D**) vaccination before (V0), 1 month after the first (V1) and complete vaccination (CV), 6 months after CV (CVT2) and 1 month after boost vaccination (BV). For results of paired samples from the same donors at each time point please refer to Fig. S9 (paired samples n = 8 for heterologous vaccination, n = 2 for mRNA vaccination). **E,F,** Intensities of *ex vivo* IFN-γ T cell responses against the SARS-CoV-2 BA.1 and BA.2 mutation pools at complete vaccination and boost vaccination for mRNA and heterologous vaccinated donors, respectively. Responders are represented by colored symbols, and nonresponders are represented by clear symbols. **G-L,** T cell responses were characterized by *ex vivo* intracellular cytokine and surface marker staining. T cell responses were considered positive if the detected frequency of cytokine-positive $CD4^+$ or $CD8^+$ T cells was ≥ 3-fold higher than the frequency in the negative control and minimum of 0.1% of total $CD4^+$ or $CD8^+$ T cells. **G,H,** Percentage of individuals with $CD4^+$ (top), $CD8^+$ (middle), and both $CD4^+$ and $CD8^+$ (bottom) *ex vivo* T cell responses to spike-specific peptide pools during the course of mRNA (**G**) and heterologous (**H**) vaccination. **I,J,** Heatmaps showing the percentages of cytokine- and surface marker-expressing $CD4^+$ and $CD8^+$ T cells *ex vivo* after complete vaccination and boost vaccination after mRNA (**I**) and heterologous (**J**) vaccination. **K,** Proportion of TNF^+CD4^+ spike-specific T cells expressing the T cell memory marker CD45RO after complete (n = 12, n = 7) and boost vaccination (n = 8, n = 8) for mRNA- and heterologous-vaccinated donors, respectively. **L,** Proportion of $INF\text{-}\gamma^+CD8^+$ spike-specific T cells expressing the T cell memory marker CD45RO after complete (n = 3, n = 0) and boost vaccination (n = 4, n = 1) for mRNA- and heterologous-vaccinated donors, respectively. **A,B,**

Antibody titers are shown in units per milliliter (1 U/ml corresponds to 21.80 binding antibody units/ml). **A-D,** Data are presented as scatter dot plots with the median, whiskers show maximum. **E,F,** box plots show the median with the 25th and 75th percentiles, and whiskers represent minimum and maximum. **K,L,** Data are presented as scatter dot plots with the mean, error bars indicates SD. **A,K,L,** Mann-Whitney test was used. **B-F,** Kruskal-Wallis test was used. **G,H,** Fisher's exact test was used. If P values are not shown, then results were not significant.

Comparison of vaccine-induced T cell phenotypes and functionality after complete vaccination and booster vaccination using *ex vivo* intracellular cytokine and surface marker staining showed no differences in the proportion of donors developing $CD4^+$ and $CD8^+$ T cell responses for the two vaccination cohorts (mRNA: $CD4^+$ T cells 86% versus 73% and $CD8^+$ T cells 57% versus 64%, respectively), with a nonsignificant increase in donors with vaccine-induced $CD4^+$, $CD8^+$, and $CD4^+$ and $CD8^+$ T cells after booster vaccination in the heterologous-vaccinated cohort (heterologous: $CD4^+$ T cells 70% versus 91% and $CD8^+$ T cells 30% versus 55%, respectively; Fig. 4, G and H; and Fig. S8). Booster vaccination-induced $CD4^+$ T cells in the mRNA and heterologous vaccine cohorts displayed a T_H1 phenotype, showing mainly positivity for TNF and, to a lesser extent, for CD107a and IFN-γ/TNF, and were negative for the T_H2 marker IL-4, comparable with the T cell responses observed after complete vaccination (Fig. S9A,B). $CD8^+$ T cell responses, in terms of frequencies of cytokine-producing cells and the ability to produce multiple cytokines, also showed a similar profile in both vaccination cohorts after complete and booster vaccination with particular positivity for IFN-γ (Fig. 4I,J and Fig. S8). Within the vaccine-induced TNF-producing spike-specific T cells, the proportion of $CD45RO^+CD4^+$ memory T cells showed a slight increase after booster vaccination compared with complete vaccination in both vaccination cohorts (mRNA: 78% versus 82%, heterologous: 75% versus 88%; Fig. 4K and Fig. S9C-F). For vaccine-induced INF-γ-producing spike-specific $CD8^+$ T cells, this increase in memory T cell response is only detected after heterologous vaccination (mRNA: 41% vs. 16%, heterologous: 0% vs. 14%; Fig. 4L).

In summary, the booster vaccination led to a significant increase of anti-spike IgG responses, which show a marked decline 6 month after complete vaccination. In contrast, anti-spike T cell responses remained stable over time after complete vaccination, with no significant effect of booster vaccination on the total intensity and frequency of T cell responses or on cross-recognition of Omicron BA.1 and BA.2 mutations within the spike protein.

Discussion

T cell immunity is central for the control of viral infections. Although the role of antiviral T cell response is extensively studied during acute SARS-CoV-2 infection and COVID-19 (*13, 15, 19, 20*), the induction of T cells upon vaccination with the different approved COVID-19 vaccines is studied less extensively (*12, 17*). This study reports on T cell immunity after complete and booster vaccination regimens in comparison to SARS-CoV-2 T cell responses in convalescents and prepandemic donors.

In line with previous reports (*21, 22*), the frequency and intensity of spike-specific T cell responses were lower in vector-vaccinated donors compared with mRNA- and heterologous-vaccinated individuals, who showed comparable T cell responses. Of note, the observed difference between vaccination regimens vanished after *in vitro* T cell expansion, indicating potent expandability of vaccine-induced T cells upon virus encounter. Besides the expandability of virus-specific T cells (*23*), the diversity of T cell responses, *i.e,.* recognition of multiple T cell epitopes, is shown to be central to combat viral disease, including SARS-CoV-2 (*15, 24*). We showed that vaccine-induced T cells responded to different peptide pools covering the whole spike protein, indicating highly diverse T cell immunity by the different vaccination regimens. Our data on the expandability and broadness of vaccine-induced T cell responses indicated that mRNA, vector, and heterologous vaccination regimens can be recommended in the future to induce protective T cell immunity.

Comparison with spike-specific T cell responses induced in non-hospitalized convalescent individuals revealed similar frequency and intensity of T cells induced by different vaccination regimens. Of note, the phenotype and functionality of vaccine-induced $CD4^+$ and $CD8^+$ T cells also resembled those after natural infection (*25*). The induction of both $CD4^+$ and $CD8^+$ T cells has been shown to be central for effective T cell immunity in infectious and malignant disease (*26*).

Cross-reactivity of T cells for different virus species or even amongst different pathogens is a well-known phenomenon postulated to enable heterologous immunity to a pathogen after exposure to a nonidentical pathogen (*27*). In SARS-CoV-2, cross-reactive T cells are associated with protection against infection in COVID-19 contacts (*28*) and with enhanced immune responses upon infection and vaccination (*18*). Here, we showed high frequencies of spike-specific T cell responses in a cohort of prepandemic, unexposed donors after *in vitro* T cell expansion. In line with previous reports (*18, 20*), the intensity and diversity of these preexisting T cell responses were significantly lower than in convalescent and vaccinated individuals. In contrast to previous reports (*18*), we could also show cross-reactive T cell responses against the Prot_S1 peptide pool covering the complete N-terminal part of the S1 domain of the spike protein, which is described as less HCoV homologous than the C-terminal section covered by the Prot_S peptide pool, indicating that cross-reactivity is not only based on sequence similarity but also on physiochemical and human leukocyte antigen (HLA)-binding properties (*29, 30*).

Application of a booster vaccination after complete vaccination shows beneficial effects in terms of protection from SARS-CoV-2 infection and severe courses of COVID-19 (*31, 32*). In line with previous reports, we showed a significant increase in IgG titers after booster vaccination for both mRNA and heterologous vaccination (*33*). In contrast, the frequency and intensity of T cell responses were not significantly boosted by the additional vaccination; however, T cell responses also did not exhibit such a marked decline after the complete vaccination compared with antibody responses. This is in line with

reports after SARS-CoV-2 infection, showing a rapid antibody decline and the persistence of T cell immunity (*9*). No differences between mRNA and heterologous vaccination were observed in terms of T cell frequency, intensity and ability of $CD4^+$ T cell to produce multiple cytokines after booster vaccination. Of note, cytokine production in $CD8^+$ T cells was only boosted in donors who received three doses of mRNA vaccine. These data indicated that boost vaccination is of particular relevance for the amelioration of antiviral antibody activity, whereas robust T cell immunity is already established after complete vaccination.

We further observed cross-recognition of the Omicron BA.1- and BA.2-mutated regions of the spike protein by vaccine-induced T cells after complete and booster vaccination for most of the donors in the mRNA- and heterologous-vaccinated cohorts. This is in line with the cross-reactivity potential of SARS-CoV-2-specific T cells to HCoV (*18, 28*) and provides the basis for the reported conservation of vaccine-induced T cell responses against different SARS-CoV-2 variants (*12, 17*). This cross-reactivity is suggested to balance the lack of neutralizing antibodies targeting newly arising VOCs (*34*) and thus to prevent severe COVID-19 in vaccinees. These data on the cross-recognition potential of vaccine-induced T cells indicate that robust T cell immunity toward Omicron variants is also induced from complete vaccination.

There are several limitations to our study. We had a limited number of samples available, which particularly affected the vector-vaccinated group because vector-based vaccines stopped being recommended by German governments in mid-2021 (*35*). The other main limitation is the restricted number of paired samples for the analysis over time.

Together, our work shows that complete vaccination against COVID-19 induces broad spike-specific $CD4^+$ and $CD8^+$ T cell immunity by different vaccination regimens that resemble T cell responses after natural SARS-CoV-2 infection. Moreover, booster vaccination seems to be of particular relevance for the amelioration of antiviral antibody activity, because T cell responses are not markedly boosted by a third vaccination.

Materials and Methods

Study Design

This prospective cohort study was initiated in 2021 and describes T cell responses in donors vaccinated with different COVID-19 vaccines after complete and booster vaccination (regimens described in more detail below), compared to convalescent and prepandemic donors. Starting January 2021, the German population was recommended to get vaccinated with the approved COVID-19 vaccines (BNT162b2, mRNA-1273, ChAdOx1 or Ad26.COV2.S), and volunteers were asked to participate in our study, which aimed to identify differences in T cell responses after the different vaccination regimens. T cell responses against the whole spike protein and against the Omicron BA.1 and BA.2 variant mutations

were assessed. The control groups included samples collected from volunteer convalescents in 2020 after positive polymerase chain reaction (PCR) test and prepandemic samples collected before March 2017. No randomization was performed, and blinding was not appropriate for this study. The methods and assays used were standardized to prevent batch effects. Data for the time point before and after first and complete vaccination of the same donor were obtained in the same assay and data before and after booster vaccination were obtained in the same assay.

Donors and Blood Samples

Peripheral blood mononuclear cells (PBMCs) from vaccinated donors, COVID-19 convalescents, and from prepandemic healthy volunteers, collected between August 2015 and March 2017 at the University Hospital Tübingen and the Cancer Research Department Rhein-Main (Hospital Nordwest), were isolated by density gradient centrifugation and stored at -80°C for short term storage or in liquid nitrogen until further use for subsequent T cell-based assays. Informed consent was obtained in accordance with the Declaration of Helsinki protocol. The study was performed according to the guidelines of the local ethics committees (179/2020/BO2, MC 288/2015, 2021-2305-evBO).

Donors Vaccinated with Different COVID-19 Vaccination Regimens

To assess spike-specific immune responses after vaccination, we collected blood samples from donors vaccinated with three different COVID-19 vaccine regimens. The mRNA-based vaccine cohort includes healthy volunteers vaccinated two (complete vaccination) to three times (booster vaccination) either with mRNA-1273 or with BNT162b2. The heterologous vaccination group received one dose of ChAdOx1 followed by one (complete vaccination) or two doses (booster vaccination) of either mRNA-1273 or BNT162b2. Donors of the vector-based vaccine group either received two doses of AZD1222 or one dose of Ad26.COV2.S for complete vaccination. Donor characteristics and side effects after vaccination of the cohorts (n = 61) are provided in Table 1 and were assessed by questionnaire. Donors reporting headache, fever or shivering after vaccination were classified as donors with side effects.

SARS-CoV-2 Convalescent Individuals

To delineate differences of SARS-CoV-2 immune responses in vaccinated participants to immune responses after natural infection, we used a reference group of COVID-19 convalescent individuals, described previously (*20*) for comparison. SARS-CoV-2 infection was confirmed by real-time PCR after nasopharyngeal swab. Sample collection for human COVID-19 convalescents (n = 16) was performed in July 2020, 94 – 130 days (median 117 days) after positive PCR. By the time of sample collection, the wildtype SARS-CoV-2 was circulating, and VOCs emerged at a later time point. Donor characteristics and COVID-19 symptoms were assessed by questionnaire. Details are provided in Table 2. Written

informed consent was obtained in accordance with the Declaration of Helsinki protocol (179/2020/BO2).

IFN-γ ELISpot Assay

ELISpot assays were performed *ex vivo* or following 12-day *in vitro* expansion. For *in vitro* expansion, PBMCs were pulsed with overlapping 15-mer peptide pools covering the entire spike protein (Miltenyi, PepTivator® SARS-CoV-2 Prot_S, PepTivator® SARS-CoV-2 Prot_S+, PepTivator® SARS-CoV-2 Prot_S1, Fig. 1A) or the Omicron BA.1 and BA.2 mutated regions (Miltenyi, PepTivator® SARS-CoV-2 Prot_S B.1.1.529/BA.1 Mutation Pool and PepTivator® SARS-CoV-2 Prot_S B.1.1.529/BA.2 Mutation Pool) (0.02 nmol/peptide per milliliter) and cultured for 12 days, adding IL-2 (20 U/ml; Novartis) on days 3, 5, and 7. Peptide-stimulated (*in vitro* expanded) or freshly thawed (*ex vivo*) PBMCs were analyzed by IFN-γ ELISpot assay, as described previously (20). In brief, 100,000 - 300,000 cells per well were incubated in 96-well ELISpot plates coated with anti-IFN-γ antibody (2 µg/ml; clone 1-D1K, MabTech, catalog no. 3420-3-250, RRID: AB_907283) with peptide pools (0.01 nmol/peptide per milliliter). Phytohemagglutinin (Sigma-Aldrich) served as positive control. An irrelevant HLA-DR-restricted control peptide (ETVITVDTKAAGKGK, FLNA_HUMAN1669−1683) in double-distilled water served as negative controls. After 24 hours of incubation, spots were revealed with anti-IFN-γ biotinylated detection antibody (0.3 µg/ml; clone 7 B6 1, MabTech, Catalog no. 3420-6-250, RRID: AB_907273), ExtrAvidin-Alkaline Phosphatase (1:1,000 dilution, Sigma-Aldrich), and bromochloroindolyl phosphate/nitro-blue tetrazolium (Sigma-Aldrich). Spots were counted using an ImmunoSpot S6 analyzer (CTL). T cell responses were considered positive, and donors as responders, if the mean spot count of the technical replicates normalized to 300,000 cells was at least three spots *ex vivo* and six spots after 12-day *in vitro* expansion and threefold higher than the mean spot count of the negative control normalized to 300,000 cells (*15, 36*). The intensity of T cell responses is depicted as calculated spot counts, which represent the sum of mean spot count normalized to 300,000 cells for all three tested spike-specific peptide pools subtracting the normalized mean spot count of the respective negative control.

Intracellular Cytokine and Cell Surface Marker Staining

Peptide-specific T cells were characterized by cell surface marker and intracellular cytokine staining (ICS) as previously described (*20*). In brief, 250,000 to 1,000,000 PBMCs were incubated over 12 to 14 hours with the 15-mer peptide pools covering the entire spike protein or the negative control peptide, brefeldin A (Sigma-Aldrich), and GolgiStop (BD Biosciences). Phorbol 1-myristate 13-acetate and ionomycin (Sigma-Aldrich, Catalog no.L1668) served as positive control, for the *ex vivo* ICS, staphylococcal enterotoxin B (SEB) (Sigma-Aldrich, Catalog no.S4881) was used as an additional positive control. Staining was performed using Cytofix/Cytoperm solution (BD), Zombie Aqua (for *ex vivo* samples, 1:200 dilution, BioLegend), allophycocyanin (APC)/Cy7 anti-human CD4 (1:100 dilution,

BioLegend, Catalog no.300518, RRID: AB_314086), phycoerythrin (PE)/Cy7 anti-human CD8 (1:400 dilution, Beckman Coulter, Catalog no.737661, RRID: AB_1575980), Pacific Blue anti-human TNF (1:120 dilution, BioLegend, Catalog no.502920, RRID: AB_528965), fluorescein isothiocyanate anti-human CD107a (1:100 dilution, BioLegend, Catalog no.328606, RRID: AB_1186036), PE anti-human IFN-γ monoclonal antibodies (1:200 dilution, BioLegend, Catalog no.506507, RRID: AB_315440), APC anti-human CD45RO (1:100 dilution, BioLegend, Catalog no.304210 , RRID: AB_314426), PE-Dazzle 594 anti-human IL-4 (1:25 dilution, BioLegend, Catalog no.500832, RRID: AB_2564036). *Ex vivo* samples were analyzed on a FACS LSRFortessa (BD; gating strategy; Fig. S10). In this study, a T helper 1 (T_H1) response was defined as cells producing IFN-γ and tumor necrosis factor, and a T_H2 response as cells producing IL-4. T cell responses were considered positive if the detected frequency of cytokine-positive $CD4^+$ or $CD8^+$ T cells was ≥ 3-fold higher than the frequency in the negative control and minimum 0.1%. The frequency of cytokine-positive cells was corrected for background by subtraction of the respective negative control values. Negative values were set to zero.

SARS-CoV-2 Anti-Spike and Anti-Nucleocapsid Antibody Testing

The Siemens SARS-CoV-2 IgG (SCOVG) assay was performed on an automated ADVIA Centaur XPT system (Siemens Healthineers) according to the manufacturer's instructions. The immunoassay detects anti-SCOVG antibodies directed against the S1 domain of the viral spike protein (including the immunologically relevant receptor binding domain). The Elecsys assay from Roche detecting high-affinity antibodies (including IgG) directed against the nucleocapsid protein of SARS-CoV-2 was performed according to the manufacturer's instructions for samples collected at the University Hospital Tübingen. Results are reported in index values for the Roche assay and the SCOVG assay. For the latter, an index value of 1 corresponds to one U/ml, 1 U/ml can be converted to 21.80 binding antibody units/ml according to the manufacturer. The final interpretation of positivity is determined by an antibody titer ≥ 1.0 U/ml given by the manufacturer. Values < 0.1 were set to 0.1. One hundred was the highest measurable index value with the SCOVG assay. Quality control was performed following the manufacturer's instructions on each day of testing.

Software and Statistical Analysis

Flow cytometric data was analyzed using FlowJo 10.7.1 (BD). Graphs were plotted using Inkscape 1.1 and GraphPad Prism 9.2.0. Statistical analyses were conducted using GraphPad Prism 9.2.0. Data are displayed as mean ± SD, and box plots are displayed as median with 25 or 75% quantiles and minimum/maximum whiskers. Continuous data were tested for distribution, and individual groups were tested by the use of two-sided Fisher's exact test, unpaired t-test, unpaired Mann-Whitney-U-test, Kruskal-Wallis test, or paired Wilcoxon signed rank test and Friedman test, all performed as two-

sided tests. Correlation was tested using Spearman test and linear regression. P values of < 0.05 were considered statistically significant.

Acknowledgements

We thank U. Schmidt, H. Zug, R. Schaad, J. Rieth, I. Schäfer, C. Gouttefangeas and J. Heitmann for technical support and project coordination.

Funding

This work was supported by the Ministry of Science, Research and the Arts Baden-Württemberg, Germany (MWK, Sonderfördermassnahme COVID-19, TÜ17) (J.S.W.), the Federal Agency of Science, Research and the Arts, Germany (BMBF, FKZ:01KI20130 and FKZ:16LW0004K) (J.S.W.), the Deutsche Forschungsgemeinschaft (DFG, German Research Foundation, Grant WA 4608/1-2) (J.S.W.), the Deutsche Forschungsgemeinschaft under Germany's Excellence Strategy (Grant EXC2180 390900677) (J.S.W.), the German Cancer Consortium (DKTK) (J.S.W.), the Wilhelm Sander Stiftung (Grant 2016.177.2) (J.S.W.) and the José Carreras Leukämie-Stiftung (Grant DJCLS 05 R/2017) (J.S.W.).

Author Contributions

Y.M., A.N. and J.S.W. were involved in the design of the overall study and strategy. Y.M. performed the T cell experiments. Spike-specific IgG were analyzed by S.H., A.P.. S.S., J.K., E.J, J.S.W. conducted donor data and sample collection. Y.M., A.N., J.S. and J.S.W. analyzed the data. Y.M., A.N. and J.S.W. drafted the manuscript. All authors supported the creation of the manuscript by review and editing. J.S.W. supervised the study.

Competing Interests

Authors declare that they have no competing interests.

Data and Materials Availability

All data necessary to evaluate the conclusions in this study are present in the manuscript or the Supplementary Materials.

List of Supplementary Materials

Table S1: Raw data file

Table S2: Mutations described for the BA.1 and BA.2 Omicron variants of concern (VOC) affecting the spike protein and spike-derived peptide pools

Fig. S1: Index values of nucleocapsid antibodies in vaccinated donors

Fig. S2: Spike-specific T cell responses after vaccination and in convalescents according to demographics and symptoms

Fig. S3: Immune responses to the SARS-CoV-2 spike-specific peptide pools after complete vaccination following 12-day *in vitro* expansion

Fig. S4: IFN-γ responses to SARS-CoV-2 BA.1 and BA.2 mutation pools following 12-day *in vitro* expansion

Fig. S5: *Ex vivo* characterization of spike-specific T cell responses after complete vaccination

Fig. S6: T cell responses following mRNA and heterologous vaccination

Fig. S7: Spike-specific peptide pool recognition during the course of mRNA and heterologous vaccination

Fig. S8: Characterization of *ex vivo* spike-specific T cell responses following complete and booster vaccination with mRNA and heterologous vaccination regimens

Fig. S9: Characterization of *ex vivo* spike-specific T cell responses after complete vaccination

Fig. S10: Gating strategy for *ex vivo* flow cytometry-based evaluation of surface marker and intracellular cytokine staining on a FACS LSRFortessa.

References and Notes

1. M. N. Ramasamy, A. M. Minassian, K. J. Ewer, A. L. Flaxman, P. M. Folegatti, D. R. Owens, M. Voysey, P. K. Aley, B. Angus, G. Babbage, S. Belij-Rammerstorfer, L. Berry, S. Bibi, M. Bittaye, K. Cathie, H. Chappell, S. Charlton, P. Cicconi, E. A. Clutterbuck, R. Colin-Jones, C. Dold, K. R. W. Emary, S. Fedosyuk, M. Fuskova, D. Gbesemete, C. Green, B. Hallis, M. M. Hou, D. Jenkin, C. C. D. Joe, E. J. Kelly, S. Kerridge, A. M. Lawrie, A. Lelliott, M. N. Lwin, R. Makinson, N. G. Marchevsky, Y. Mujadidi, A. P. S. Munro, M. Pacurar, E. Plested, J. Rand, T. Rawlinson, S. Rhead, H. Robinson, A. J. Ritchie, A. L. Ross-Russell, S. Saich, N. Singh, C. C. Smith, M. D. Snape, R. Song, R. Tarrant, Y. Themistocleous, K. M. Thomas, T. L. Villafana, S. C. Warren, M. E. E. Watson, A. D. Douglas, A. V. S. Hill, T. Lambe, S. C. Gilbert, S. N. Faust, A. J. Pollard, C. V. T. G. Oxford, Safety and immunogenicity of ChAdOx1 nCoV-19 vaccine administered in a prime-boost regimen in young and old adults (COV002): a single-blind, randomised, controlled, phase 2/3 trial. *Lancet* **396**, 1979-1993 (2021).
2. F. P. Polack, S. J. Thomas, N. Kitchin, J. Absalon, A. Gurtman, S. Lockhart, J. L. Perez, G. Perez Marc, E. D. Moreira, C. Zerbini, R. Bailey, K. A. Swanson, S. Roychoudhury, K. Koury, P. Li, W. V. Kalina, D. Cooper, R. W. Frenck, Jr., L. L. Hammitt, O. Tureci, H. Nell, A. Schaefer, S. Unal, D. B. Tresnan, S. Mather, P. R. Dormitzer, U. Sahin, K. U. Jansen, W. C. Gruber, C. C. T. Group, Safety and Efficacy of the BNT162b2 mRNA Covid-19 Vaccine. *N Engl J Med* **383**, 2603-2615 (2020).
3. L. R. Baden, H. M. El Sahly, B. Essink, K. Kotloff, S. Frey, R. Novak, D. Diemert, S. A. Spector, N. Rouphael, C. B. Creech, J. McGettigan, S. Khetan, N. Segall, J. Solis, A. Brosz, C. Fierro, H. Schwartz, K. Neuzil, L. Corey, P. Gilbert, H. Janes, D. Follmann, M. Marovich, J. Mascola, L. Polakowski, J. Ledgerwood, B. S. Graham, H. Bennett, R. Pajon, C. Knightly, B. Leav, W. Deng, H. Zhou, S. Han, M. Ivarsson, J. Miller, T. Zaks, C. S. Group, Efficacy and Safety of the mRNA-1273 SARS-CoV-2 Vaccine. *N Engl J Med* **384**, 403-416 (2021).
4. J. Sadoff, G. Gray, A. Vandebosch, V. Cardenas, G. Shukarev, B. Grinsztejn, P. A. Goepfert, C. Truyers, H. Fennema, B. Spiessens, K. Offergeld, G. Scheper, K. L. Taylor, M. L. Robb, J. Treanor, D. H. Barouch, J. Stoddard, M. F. Ryser, M. A. Marovich, K. M. Neuzil, L. Corey, N. Cauwenberghs, T. Tanner, K. Hardt, J. Ruiz-Guinazu, M. Le Gars, H. Schuitemaker, J. Van Hoof, F. Struyf, M. Douoguih, E. S. Group, Safety and Efficacy of Single-Dose Ad26.COV2.S Vaccine against Covid-19. *N Engl J Med* **384**, 2187-2201 (2021).
5. C. f. D. C. a. Prevention. U.S. COVID-19 Vaccine Administration by Vaccine Type. https://covid.cdc.gov/covid-data-tracker/#vaccinations_vacc-people-additional-dose-totalpop. (2022).

6. G. o. Canada. Cumulative number of COVID-19 vaccine doses administered in Canada by accine product and dose number, as of October 9, 2022. https://health-infobase.canada.ca/covid-19/vaccine-administration/. (2022).
7. O. W. i. Data. COVID-19 vaccine doses administered by manufacturer, European Union. https://ourworldindata.org/covid-vaccinations#which-vaccines-have-been-administered-in-each-country. (2022).
8. A. Greinacher, T. Thiele, T. E. Warkentin, K. Weisser, P. A. Kyrle, S. Eichinger, Thrombotic Thrombocytopenia after ChAdOx1 nCov-19 Vaccination. *N Engl J Med* **384**, 2092-2101 (2021).
9. E. G. Levin, Y. Lustig, C. Cohen, R. Fluss, V. Indenbaum, S. Amit, R. Doolman, K. Asraf, E. Mendelson, A. Ziv, C. Rubin, L. Freedman, Y. Kreiss, G. Regev-Yochay, Waning Immune Humoral Response to BNT162b2 Covid-19 Vaccine over 6 Months. *N Engl J Med* **385**, e84 (2021).
10. N. Barda, N. Dagan, C. Cohen, M. A. Hernan, M. Lipsitch, I. S. Kohane, B. Y. Reis, R. D. Balicer, Effectiveness of a third dose of the BNT162b2 mRNA COVID-19 vaccine for preventing severe outcomes in Israel: an observational study. *Lancet* **398**, 2093-2100 (2021).
11. D. S. Khoury, D. Cromer, A. Reynaldi, T. E. Schlub, A. K. Wheatley, J. A. Juno, K. Subbarao, S. J. Kent, J. A. Triccas, M. P. Davenport, Neutralizing antibody levels are highly predictive of immune protection from symptomatic SARS-CoV-2 infection. *Nat Med* **27**, 1205-1211 (2021).
12. A. Tarke, C. H. Coelho, Z. Zhang, J. M. Dan, E. D. Yu, N. Methot, N. I. Bloom, B. Goodwin, E. Phillips, S. Mallal, J. Sidney, G. Filaci, D. Weiskopf, R. da Silva Antunes, S. Crotty, A. Grifoni, A. Sette, SARS-CoV-2 vaccination induces immunological T cell memory able to cross-recognize variants from Alpha to Omicron. *Cell* **185**, 847-859 e811 (2022).
13. A. T. Tan, M. Linster, C. W. Tan, N. Le Bert, W. N. Chia, K. Kunasegaran, Y. Zhuang, C. Y. L. Tham, A. Chia, G. J. D. Smith, B. Young, S. Kalimuddin, J. G. H. Low, D. Lye, L. F. Wang, A. Bertoletti, Early induction of functional SARS-CoV-2-specific T cells associates with rapid viral clearance and mild disease in COVID-19 patients. *Cell Rep* **34**, 108728 (2021).
14. D. Geers, M. C. Shamier, S. Bogers, G. den Hartog, L. Gommers, N. N. Nieuwkoop, K. S. Schmitz, L. C. Rijsbergen, J. A. T. van Osch, E. Dijkhuizen, G. Smits, A. Comvalius, D. van Mourik, T. G. Caniels, M. J. van Gils, R. W. Sanders, B. B. Oude Munnink, R. Molenkamp, H. J. de Jager, B. L. Haagmans, R. L. de Swart, M. P. G. Koopmans, R. S. van Binnendijk, R. D. de Vries, C. H. GeurtsvanKessel, SARS-CoV-2 variants of concern partially escape humoral but not T-cell responses in COVID-19 convalescent donors and vaccinees. *Sci Immunol* **6**, (2021).
15. T. Bilich, A. Nelde, J. S. Heitmann, Y. Maringer, M. Roerden, J. Bauer, J. Rieth, M. Wacker, A. Peter, S. Horber, D. Rachfalski, M. Marklin, S. Stevanovic, H. G. Rammensee, H. R. Salih, J. S. Walz, T cell and antibody kinetics delineate SARS-CoV-2 peptides mediating long-term immune responses in COVID-19 convalescent individuals. *Sci Transl Med* **13**, (2021).
16. R. Rose, F. Neumann, O. Grobe, T. Lorentz, H. Fickenscher, A. Krumbholz, Humoral immune response after different SARS-CoV-2 vaccination regimens. *BMC Med* **20**, 31 (2022).
17. C. H. GeurtsvanKessel, D. Geers, K. S. Schmitz, A. Z. Mykytyn, M. M. Lamers, S. Bogers, S. Scherbeijn, L. Gommers, R. S. G. Sablerolles, N. N. Nieuwkoop, L. C. Rijsbergen, L. L. A. van Dijk, J. de Wilde, K. Alblas, T. I. Breugem, B. J. A. Rijnders, H. de Jager, D. Weiskopf, P. H. M. van der Kuy, A. Sette, M. P. G. Koopmans, A. Grifoni, B. L. Haagmans, R. D. de Vries, Divergent SARS-CoV-2 Omicron-reactive T and B cell responses in COVID-19 vaccine recipients. *Sci Immunol* **7**, eabo2202 (2022).
18. L. Loyal, J. Braun, L. Henze, B. Kruse, M. Dingeldey, U. Reimer, F. Kern, T. Schwarz, M. Mangold, C. Unger, F. Dorfler, S. Kadler, J. Rosowski, K. Gurcan, Z. Uyar-Aydin, M. Frentsch, F. Kurth, K. Schnatbaum, M. Eckey, S. Hippenstiel, A. Hocke, M. A. Muller, B. Sawitzki, S. Miltenyi, F. Paul, M. A. Mall, H. Wenschuh, S. Voigt, C. Drosten, R. Lauster, N. Lachman, L. E. Sander, V. M. Corman, J. Rohmel, L. Meyer-Arndt, A. Thiel, C. Giesecke-Thiel, Cross-reactive CD4(+) T cells enhance SARS-CoV-2 immune responses upon infection and vaccination. *Science* **374**, eabh1823 (2021).
19. J. Braun, L. Loyal, M. Frentsch, D. Wendisch, P. Georg, F. Kurth, S. Hippenstiel, M. Dingeldey, B. Kruse, F. Fauchere, E. Baysal, M. Mangold, L. Henze, R. Lauster, M. A. Mall, K. Beyer, J.

Rohmel, S. Voigt, J. Schmitz, S. Miltenyi, I. Demuth, M. A. Muller, A. Hocke, M. Witzenrath, N. Suttorp, F. Kern, U. Reimer, H. Wenschuh, C. Drosten, V. M. Corman, C. Giesecke-Thiel, L. E. Sander, A. Thiel, SARS-CoV-2-reactive T cells in healthy donors and patients with COVID-19. *Nature* **587**, 270-274 (2020).

20. A. Nelde, T. Bilich, J. S. Heitmann, Y. Maringer, H. R. Salih, M. Roerden, M. Lubke, J. Bauer, J. Rieth, M. Wacker, A. Peter, S. Horber, B. Traenkle, P. D. Kaiser, U. Rothbauer, M. Becker, D. Junker, G. Krause, M. Strengert, N. Schneiderhan-Marra, M. F. Templin, T. O. Joos, D. J. Kowalewski, V. Stos-Zweifel, M. Fehr, A. Rabsteyn, V. Mirakaj, J. Karbach, E. Jager, M. Graf, L. C. Gruber, D. Rachfalski, B. Preuss, I. Hagelstein, M. Marklin, T. Bakchoul, C. Gouttefangeas, O. Kohlbacher, R. Klein, S. Stevanovic, H. G. Rammensee, J. S. Walz, SARS-CoV-2-derived peptides define heterologous and COVID-19-induced T cell recognition. *Nat Immunol* **22**, 74-85 (2021).
21. T. Schmidt, V. Klemis, D. Schub, J. Mihm, F. Hielscher, S. Marx, A. Abu-Omar, L. Ziegler, C. Guckelmus, R. Urschel, S. Schneitler, S. L. Becker, B. C. Gartner, U. Sester, M. Sester, Immunogenicity and reactogenicity of heterologous ChAdOx1 nCoV-19/mRNA vaccination. *Nat Med* **27**, 1530-1535 (2021).
22. D. Hillus, T. Schwarz, P. Tober-Lau, K. Vanshylla, H. Hastor, C. Thibeault, S. Jentzsch, E. T. Helbig, L. J. Lippert, P. Tscheak, M. L. Schmidt, J. Riege, A. Solarek, C. von Kalle, C. Dang-Heine, H. Gruell, P. Kopankiewicz, N. Suttorp, C. Drosten, H. Bias, J. Seybold, E. C. S. Group, F. Klein, F. Kurth, V. M. Corman, L. E. Sander, Safety, reactogenicity, and immunogenicity of homologous and heterologous prime-boost immunisation with ChAdOx1 nCoV-19 and BNT162b2: a prospective cohort study. *Lancet Respir Med* **9**, 1255-1265 (2021).
23. T. M. Wilkinson, C. K. Li, C. S. Chui, A. K. Huang, M. Perkins, J. C. Liebner, R. Lambkin-Williams, A. Gilbert, J. Oxford, B. Nicholas, K. J. Staples, T. Dong, D. C. Douek, A. J. McMichael, X. N. Xu, Preexisting influenza-specific CD4+ T cells correlate with disease protection against influenza challenge in humans. *Nat Med* **18**, 274-280 (2012).
24. A. C. Tan, N. L. La Gruta, W. Zeng, D. C. Jackson, Precursor frequency and competition dictate the HLA-A2-restricted CD8+ T cell responses to influenza A infection and vaccination in HLA-A2.1 transgenic mice. *J Immunol* **187**, 1895-1902 (2011).
25. L. B. Rodda, J. Netland, L. Shehata, K. B. Pruner, P. A. Morawski, C. D. Thouvenel, K. K. Takehara, J. Eggenberger, E. A. Hemann, H. R. Waterman, M. L. Fahning, Y. Chen, M. Hale, J. Rathe, C. Stokes, S. Wrenn, B. Fiala, L. Carter, J. A. Hamerman, N. P. King, M. Gale, Jr., D. J. Campbell, D. J. Rawlings, M. Pepper, Functional SARS-CoV-2-Specific Immune Memory Persists after Mild COVID-19. *Cell* **184**, 169-183 e117 (2021).
26. D. J. Shedlock, H. Shen, Requirement for CD4 T cell help in generating functional CD8 T cell memory. *Science* **300**, 337-339 (2003).
27. G. Petrova, A. Ferrante, J. Gorski, Cross-reactivity of T cells and its role in the immune system. *Crit Rev Immunol* **32**, 349-372 (2012).
28. R. Kundu, J. S. Narean, L. Wang, J. Fenn, T. Pillay, N. D. Fernandez, E. Conibear, A. Koycheva, M. Davies, M. Tolosa-Wright, S. Hakki, R. Varro, E. McDermott, S. Hammett, J. Cutajar, R. S. Thwaites, E. Parker, C. Rosadas, M. McClure, R. Tedder, G. P. Taylor, J. Dunning, A. Lalvani, Cross-reactive memory T cells associate with protection against SARS-CoV-2 infection in COVID-19 contacts. *Nat Commun* **13**, 80 (2022).
29. O. Y. Borbulevych, K. H. Piepenbrink, B. E. Gloor, D. R. Scott, R. F. Sommese, D. K. Cole, A. K. Sewell, B. M. Baker, T cell receptor cross-reactivity directed by antigen-dependent tuning of peptide-MHC molecular flexibility. *Immunity* **31**, 885-896 (2009).
30. Y. Yin, R. A. Mariuzza, The multiple mechanisms of T cell receptor cross-reactivity. *Immunity* **31**, 849-851 (2009).
31. N. Andrews, J. Stowe, F. Kirsebom, S. Toffa, R. Sachdeva, C. Gower, M. Ramsay, J. Lopez Bernal, Effectiveness of COVID-19 booster vaccines against COVID-19-related symptoms, hospitalization and death in England. *Nat Med* **28**, 831-837 (2022).

32. Y. M. Bar-On, Y. Goldberg, M. Mandel, O. Bodenheimer, L. Freedman, N. Kalkstein, B. Mizrahi, S. Alroy-Preis, N. Ash, R. Milo, A. Huppert, Protection of BNT162b2 Vaccine Booster against Covid-19 in Israel. *N Engl J Med* **385**, 1393-1400 (2021).
33. J. Yu, A. Y. Collier, M. Rowe, F. Mardas, J. D. Ventura, H. Wan, J. Miller, O. Powers, B. Chung, M. Siamatu, N. P. Hachmann, N. Surve, F. Nampanya, A. Chandrashekar, D. H. Barouch, Neutralization of the SARS-CoV-2 Omicron BA.1 and BA.2 Variants. *N Engl J Med* **386**, 1579-1580 (2022).
34. W. H. Organization. Tracking SARS-CoV-2 variants. https://www.who.int/activities/tracking-SARS-CoV-2-variants. (2022).
35. Bundesregierung. AstraZeneca vaccine primarily for over-60s. https://www.bundesregierung.de/breg-en/news/astrazeneca-vaccine-primarily-for-over-60s-1884412. (2021).
36. I. Cassaniti, F. Bergami, E. Percivalle, E. Gabanti, J. C. Sammartino, A. Ferrari, K. M. G. Adzasehoun, F. Zavaglio, P. Zelini, G. Comolli, A. Sarasini, A. Piralla, A. Ricciardi, V. Zuccaro, F. Maggi, F. Novazzi, L. Simonelli, L. Varani, D. Lilleri, F. Baldanti, Humoral and cell-mediated response against SARS-CoV-2 variants elicited by mRNA vaccine BNT162b2 in healthcare workers: a longitudinal observational study. *Clin Microbiol Infect* **28**, 301 e301-301 e308 (2022).

General Discussion and Perspective

Malignant and infectious diseases pose regular threats to the human body. The immune system defends the body by orchestrating a synergistic response mediated by the innate and adaptive immunity and can therefore prevent disease development (*1, 2*). For centuries, vaccines have been used to train the immune system to recognize pathogens and thus successfully prevent infectious diseases (*3*). Research advances in the field of tumor immunology, within the last decades, have established immunotherapy as treatment option for malignant disease, showing durable clinical responses (*4*). Peptide-based vaccines represent one immunotherapeutic approach, that relies on comparable principles as vaccination for infectious diseases, *i.e.*, to specifically train the adaptive immune system to recognize and target tumor cells, however focusing primarily on the activation of tumor-specific T cells. This low side-effect approach has been used in trials for the treatment of solid and hematological malignancies showing promising immunogenicity, nevertheless, clinical efficacy is still very limited. For successful peptide-based vaccination, several aspects play a role: i) selection of relevant tumor antigens, ii) time point of vaccine administration, iii) the correct combinatorial drug and iv) selection of the right adjuvant (*5*).

Using CLL as a representative low mutational burden tumor entity, we here presented a novel workflow for the immunopeptidomics-guided design of peptide warehouses (Chapter 1). The warehouse preselection included relevant HLA class I- and HLA class II-restricted peptides found on tumor samples that were highly frequent, non-mutated and tumor-associated. To further determine if the latter were good candidates for vaccination, peptide immunogenicity was assessed. Peptides either needed to show preexisting or *de novo* inducible T cell responses for inclusion in the final peptide warehouse.

As an outlook, this CLL-derived peptide warehouse is currently being evaluated in a phase I clinical trial (iVAC-XS15-CLL01, NCT04688385) that aims to address all mentioned aspects that are relevant for successful peptide-based vaccination. This includes the optimal timing of vaccine administration (*6, 7*): Patients receive a personalized peptide cocktail selected from the warehouse that include the HLA-matched peptides once the state of minimal residual disease is achieved, after remission induction with Bruton's tyrosine kinase inhibitors. This allows for an optimal effector to target cell ratio and can thus improve vaccine efficacy (*8*). Bruton's tyrosine kinase inhibitors that are administered throughout the trial, have more over been shown to have a positive effect on T cell functionality (*9-11*) and should therefore not interfere but rather support the peptide-based vaccines. With regard to adjuvants the synthetic toll-like receptor 1/2 ligand XS15 (*12*) is used in this trial. XS15 has already shown the ability

to induce strong and long-lasting T cell responses when administered as adjuvant for peptide-based vaccination (*13*), even in immunocompromised patients suffering from B-cell deficiency, including CLL patients (*14*). With this peptide warehouse design workflow, we performed the preliminary work required for the iVAC-XS15-CLL01 clinical trial, and showed a concept of peptide warehouse definition easily transferrable to other tumor entities that enables time- and cost-effective personalized T cell-based immunotherapy approaches.

As depicted in the first chapter of this thesis, immunogenicity screening represents an important requirement for the selection of peptides to be applied in immunotherapeutic approaches. The HLA class II-restricted peptides for the CLL warehouse were selected solely based on the ability of recall activation of preexisting peptide-specific $CD4^+$ T cells. The unavailability of a functional method to prove *de novo* peptide-specific $CD4^+$ T cell inducibility represents a possible hinderance for the definition of future peptide warehouses for other tumor entities. Since commercially available HLA class II monomers are restricted to a limited number of alleles and represent a significant cost factor, aAPCs were not suited for priming experiments of HLA-class II restricted peptides. An available preliminary autologous MoDC priming protocol for $CD4^+$ T cells was tested several times without success. Therefore, the second aim of this thesis was the optimization of this method (Chapter 2). Adjustments made to the protocol included i) the maturation cocktail used for MoDC maturation, ii) duration of MoDC coincubation with peptides and iii) the general stimulation setting. i) The maturation cocktail for MoDCs was changed from TNF, Prostaglandin E2 and Resiquimod to LPS, since it allowed for higher expression of costimulatory molecules required for successful T cell activation and is widely used for DC maturation (*15-19*). ii) After the start of the maturation process, MoDCs have an improved ability of antigen presentation that is lost 20 to 40h later (*20*), this phenomenon was not considered in the preliminary protocol. MoDCs have also been shown to induce T cell activation already 1 h after MoDC and peptide coincubation (*21*), therefore the optimized protocol comprises a MoDC and peptide coincubation step of 2 hours instead of the 24 h in the preliminary protocol. iii) As we do for the aAPC priming, many groups perform their MoDC assays in round-bottom 96-well plates (*22-24*), which allows for better cell-cell interactions due to the shape and reduced volume. This was also the final modification to the protocol, that enabled the successful priming of specific $CD4^+$ T cells for all tested peptides and donors and concluded the MoDC priming optimization. This method optimization will allow to prove peptide immunogenicity for HLA class II-restricted peptides without detectable preexisting T cell responses and will therefore facilitate the final step of peptide selection for the definition of novel peptide warehouses for clinical application.

T cell responses also play a vital role in protecting the body from infectious diseases (*3*). The outbreak of SARS-CoV-2 in 2019 that initiated the COVID-19 pandemic had an immense impact on the world and

led to the rapid development of several vaccines to reduce transmission and infection rates. The most widely approved and administered vaccines in Europe and North America (*25-27*) mostly targeted the spike protein of SARS-CoV-2 and included the vector vaccines, ChAdOx1 and Ad26.COV2.S (*28, 29*), and the first ever approved mRNA vaccines BNT162b2 and mRNA-1273 (*30, 31*). For complete vaccination status, the vaccination schedules comprise two doses of ChAdOx1, BNT162b2 and mRNA-1273 and one dose of Ad26.COV2.S (*28-31*). The heterologous vaccination scheme, comprised of one dose of ChAdOx1 followed by one dose of mRNA vaccine, was the result of reports of thromboembolic events after vector vaccination (*32*). Within the third part of this thesis, we analyzed differences in T cell responses after vaccination depending on vaccination regimen and the number of received vaccination doses in healthy volunteers. We could show that complete vaccination with all vaccine regimens induces broad spike-specific $CD4^+$ and $CD8^+$ T cell responses that were comparable with T cell responses in convalescents after natural infection and significantly increased compared to prepandemic donors. With a convalescent and prepandemic group as reference, we could confirm the observations made by Jordan *et al.* for mRNA-vaccinated donors (*33*). In general, mRNA- and heterologous-vaccinated individuals appeared to have an advantage in intensity and multifunctionality of spike-specific T cells compared with vector-vaccinated donors, which was in line with previous reports (*34, 35*). We could also confirm the significant increase in anti-spike IgG after booster vaccination for mRNA- and heterologous-vaccinated donors (*36, 37*). This booster vaccination-induced increase was not seen for T cell responses, that remained rather constant for all time points after complete vaccination for mRNA- and heterologous-vaccinated individuals. The results obtained while testing the BA.1 and BA.2 Omicron mutation pools showed cross recognition of the mutated spike regions for most mRNA- and heterologous-vaccinated donors but not for vector-vaccinated donors. However, this observation does not generally mean that donors with no cross-recognition of mutated regions have no T cell protection against VOCs, to assess that, experiments would have to be performed using peptide pools containing peptides covering the whole BA.1 and BA.2 spike protein. In general, this shown cross-recognition may also lead to protection against newly arising variants of concern. While further analyses of the effects of vaccination several months after the booster dose would have been of interest, the number of donors suitable for analyses kept decreasing due to either the application of a fourth vaccine dose or infection with COVID-19. Increased infection rates were due to the ease of restrictions, such as social distancing, the wearing of facial masks and travel restrictions used to contain COVID-19 spread (*38*).

As demonstrated in this thesis, $CD4^+$ and $CD8^+$ antigen-specific T cell responses can be induced both, *in vitro* by aAPC and MoDC primings as shown for tumor-associated antigens, and *in vivo* through vaccination approaches as demonstrated for SARS-CoV-2. In general, the induction of both $CD4^+$ and $CD8^+$ is of great importance for the therapeutic aspect in malignant disease as well as for the

prophylactic aspect in infectious disease. Whereas the role of $CD8^+$ cytotoxic T cells has been considered as highly relevant for a long time, the role of $CD4^+$ T cells has been gaining importance (*39*). Over the past years, $CD4^+$ T cells have also been shown to directly induce cell death, either through cytotoxic abilities by secreting granzyme B and perforin (*40*), or by orchestrating inflammatory cell death together with tumoricidal myeloid cells (*41*). Considering the growing knowledge on the direct roles of $CD4^+$ T cells, the concept of including HLA class II-restricted peptides in peptide-based approaches, or using other vaccines able to induce $CD4^+$ T cells appears to be of relevance. One attractive option for peptide-based therapeutic approaches consists in using HLA class II-restricted peptides that contain elongated HLA class I-restricted epitopes for the activation of both $CD4^+$ as well as $CD8^+$ T cells with only one administrated peptide (*5*). Using peptide vaccine cocktails including several elongated peptides allow for broader patient treatment due to HLA class II promiscuity while still including epitopes for several HLA class I allotypes. This approach was used in a clinical Phase I/II trial of CoVac-1, a peptide-based COVID-19 T-cell activator, including six SARS-CoV-2 derived HLA-DR epitopes with embedded HLA class I sequences, that showed successful and strong induction of mostly $CD4^+$ T cell responses in patients with B cell deficiency unable to mount antibody responses (*14*).

In this thesis antigen-specific T cell responses were characterized in the context of prophylactic and therapeutic vaccination against infectious and malignant disease. Aside from the herein performed T cell response characterization, additional TCR sequencing allows to determine individual TCR repertoires, sequences and clonalities (*42*). It is a suitable tool for comparative analysis of different study cohorts, for example to analyze the TCR repertoires of vaccinated donors and of unvaccinated donors, or to assess the development of T cell responses for the prediction of immunotherapy activity and efficacy by analyzing TCR repertoire and clonality before and after vaccination. After priming and expanding antigen-specific T cells, the latter can be analyzed by combining single cell RNA sequencing with TCR sequencing which allows for the direct identification of epitope-specific TCR sequences from the antigen-stimulated T cells with highest expression levels of activation markers (*43*). The identified TCRs can be further engineered for improved expression, stability and affinity for potential TCR-based adoptive therapy approaches. T cells for TCR-based therapy approaches are generated by using lentiviral or retroviral vectors for gene delivery (*44*). TCR-based therapies have been arising over the past years, with first clinical trials showing treatment efficacy for the treatment of cytomegalovirus infection after allogeneic hematopoietic stem cell transplantation (*45*) and clinical response was also seen in trials treating patients of several cancer entities, including melanoma and synovial cell sarcoma (*43, 46*).

In the future, combining peptide-based vaccination with other approaches such as TCR-based therapy could be of great interest, by first inducing antigen-specific T cell responses in the patients, sequencing

the most potent TCRs to then use the latter for subsequent TCR-based therapy for a boost of antigen-specific T cell responses.

References

1. D. D. Chaplin, Overview of the immune response. *J Allergy Clin Immunol* **125**, S3-23 (2010).
2. H. Gonzalez, C. Hagerling, Z. Werb, Roles of the immune system in cancer: from tumor initiation to metastatic progression. *Genes Dev* **32**, 1267-1284 (2018).
3. K. Murphy, P. Travers, M. Walport, C. Janeway, *Janeway's immunobiology*. (Garland Science, New York, ed. 8th, 2012), pp. xix, 868 p.
4. Y. Zhang, Z. Zhang, The history and advances in cancer immunotherapy: understanding the characteristics of tumor-infiltrating immune cells and their therapeutic implications. *Cell Mol Immunol* **17**, 807-821 (2020).
5. A. Nelde, H. G. Rammensee, J. S. Walz, The Peptide Vaccine of the Future. *Mol Cell Proteomics* **20**, 100022 (2021).
6. J. Nakata, Y. Nakae, M. Kawakami, S. Morimoto, D. Motooka, N. Hosen, F. Fujiki, H. Nakajima, K. Hasegawa, S. Nishida, A. Tsuboi, Y. Oji, Y. Oka, A. Kumanogoh, H. Sugiyama, Wilms tumour 1 peptide vaccine as a cure-oriented post-chemotherapy strategy for patients with acute myeloid leukaemia at high risk of relapse. *Br J Haematol* **182**, 287-290 (2018).
7. T. A. Brown, 2nd, E. A. Mittendorf, D. F. Hale, J. W. Myers, 3rd, K. M. Peace, D. O. Jackson, J. M. Greene, T. J. Vreeland, G. T. Clifton, A. Ardavanis, J. K. Litton, N. M. Shumway, J. Symanowski, J. L. Murray, S. Ponniah, E. A. Anastasopoulou, N. F. Pistamaltzian, C. N. Baxevanis, S. A. Perez, M. Papamichail, G. E. Peoples, Prospective, randomized, single-blinded, multi-center phase II trial of two HER2 peptide vaccines, GP2 and AE37, in breast cancer patients to prevent recurrence. *Breast Cancer Res Treat* **181**, 391-401 (2020).
8. R. Le Dieu, D. C. Taussig, A. G. Ramsay, R. Mitter, F. Miraki-Moud, R. Fatah, A. M. Lee, T. A. Lister, J. G. Gribben, Peripheral blood T cells in acute myeloid leukemia (AML) patients at diagnosis have abnormal phenotype and genotype and form defective immune synapses with AML blasts. *Blood* **114**, 3909-3916 (2009).
9. Q. Yin, M. Sivina, H. Robins, E. Yusko, M. Vignali, S. O'Brien, M. J. Keating, A. Ferrajoli, Z. Estrov, N. Jain, W. G. Wierda, J. A. Burger, Ibrutinib Therapy Increases T Cell Repertoire Diversity in Patients with Chronic Lymphocytic Leukemia. *J Immunol* **198**, 1740-1747 (2017).
10. C. Cubillos-Zapata, J. Avendano-Ortiz, R. Cordoba, E. Hernandez-Jimenez, V. Toledano, R. Perez de Diego, E. Lopez-Collazo, Ibrutinib as an antitumor immunomodulator in patients with refractory chronic lymphocytic leukemia. *Oncoimmunology* **5**, e1242544 (2016).
11. I. Sagiv-Barfi, H. E. Kohrt, L. Burckhardt, D. K. Czerwinski, R. Levy, Ibrutinib enhances the antitumor immune response induced by intratumoral injection of a TLR9 ligand in mouse lymphoma. *Blood* **125**, 2079-2086 (2015).
12. H. G. Rammensee, K. H. Wiesmuller, P. A. Chandran, H. Zelba, E. Rusch, C. Gouttefangeas, D. J. Kowalewski, M. Di Marco, S. P. Haen, J. S. Walz, Y. C. Gloria, J. Bodder, J. M. Schertel, A. Tunger, L. Muller, M. Kiessler, R. Wehner, M. Schmitz, M. Jakobi, N. Schneiderhan-Marra, R. Klein, K. Laske, K. Artzner, L. Backert, H. Schuster, J. Schwenck, A. N. R. Weber, B. J. Pichler, M. Kneilling, C. la Fougere, S. Forchhammer, G. Metzler, J. Bauer, B. Weide, W. Schippert, S. Stevanovic, M. W. Loffler, A new synthetic toll-like receptor 1/2 ligand is an efficient adjuvant for peptide vaccination in a human volunteer. *J Immunother Cancer* **7**, 307 (2019).
13. J. S. Heitmann, T. Bilich, C. Tandler, A. Nelde, Y. Maringer, M. Marconato, J. Reusch, S. Jager, M. Denk, M. Richter, L. Anton, L. M. Weber, M. Roerden, J. Bauer, J. Rieth, M. Wacker, S. Horber, A. Peter, C. Meisner, I. Fischer, M. W. Loffler, J. Karbach, E. Jager, R. Klein, H. G. Rammensee, H. R. Salih, J. S. Walz, A COVID-19 peptide vaccine for the induction of SARS-CoV-2 T cell immunity. *Nature* **601**, 617-622 (2022).

14. J. S. Heitmann, C. Tandler, M. Marconato, A. Nelde, T. Habibzada, S. M. Rittig, C. M. Tegeler, Y. Maringer, S. U. Jaeger, M. Denk, M. Richter, M. T. Oezbek, K. H. Wiesmuller, J. Bauer, J. Rieth, M. Wacker, S. M. Schroeder, N. Hoenisch Gravel, J. Scheid, M. Marklin, A. Henrich, B. Klimovich, K. L. Clar, M. Lutz, S. Holzmayer, S. Horber, A. Peter, C. Meisner, I. Fischer, M. W. Loffler, C. A. Peuker, S. Habringer, T. O. Goetze, E. Jager, H. G. Rammensee, H. R. Salih, J. S. Walz, Phase I/II trial of a peptide-based COVID-19 T-cell activator in patients with B-cell deficiency. *Nat Commun* **14**, 5032 (2023).
15. L. Castiello, M. Sabatino, P. Jin, C. Clayberger, F. M. Marincola, A. M. Krensky, D. F. Stroncek, Monocyte-derived DC maturation strategies and related pathways: a transcriptional view. *Cancer immunology, immunotherapy : CII* **60**, 457-466 (2011).
16. I. Baltathakis, O. Alcantara, D. H. Boldt, Expression of different NF-kappaB pathway genes in dendritic cells (DCs) or macrophages assessed by gene expression profiling. *J Cell Biochem* **83**, 281-290 (2001).
17. K. Abdi, N. J. Singh, P. Matzinger, Lipopolysaccharide-activated dendritic cells: "exhausted" or alert and waiting? *J Immunol* **188**, 5981-5989 (2012).
18. P. Jin, T. H. Han, J. Ren, S. Saunders, E. Wang, F. M. Marincola, D. F. Stroncek, Molecular signatures of maturing dendritic cells: implications for testing the quality of dendritic cell therapies. *J Transl Med* **8**, 4 (2010).
19. F. Granucci, E. Ferrero, M. Foti, D. Aggujaro, K. Vettoretto, P. Ricciardi-Castagnoli, Early events in dendritic cell maturation induced by LPS. *Microbes Infect* **1**, 1079-1084 (1999).
20. A. Alloatti, F. Kotsias, J. G. Magalhaes, S. Amigorena, Dendritic cell maturation and cross-presentation: timing matters! *Immunol Rev* **272**, 97-108 (2016).
21. R. A. Rosalia, E. D. Quakkelaar, A. Redeker, S. Khan, M. Camps, J. W. Drijfhout, A. L. Silva, W. Jiskoot, T. van Hall, P. A. van Veelen, G. Janssen, K. Franken, L. J. Cruz, A. Tromp, J. Oostendorp, S. H. van der Burg, F. Ossendorp, C. J. Melief, Dendritic cells process synthetic long peptides better than whole protein, improving antigen presentation and T-cell activation. *Eur J Immunol* **43**, 2554-2565 (2013).
22. H. Tanaka, C. E. Demeure, M. Rubio, G. Delespesse, M. Sarfati, Human monocyte-derived dendritic cells induce naive T cell differentiation into T helper cell type 2 (Th2) or Th1/Th2 effectors. Role of stimulator/responder ratio. *J Exp Med* **192**, 405-412 (2000).
23. K. Schlienger, N. Craighead, K. P. Lee, B. L. Levine, C. H. June, Efficient priming of protein antigen-specific human CD4(+) T cells by monocyte-derived dendritic cells. *Blood* **96**, 3490-3498 (2000).
24. M. A. Verkade, C. J. van Druningen, C. T. Op de Hoek, W. Weimar, M. G. Betjes, Decreased antigen-specific T-cell proliferation by moDC among hepatitis B vaccine non-responders on haemodialysis. *Clin Exp Med* **7**, 65-71 (2007).
25. C. f. D. C. a. Prevention. U.S. COVID-19 Vaccine Administration by Vaccine Type. https://covid.cdc.gov/covid-data-tracker/#vaccinations_vacc-people-additional-dose-totalpop. (2022).
26. G. o. Canada. Cumulative number of COVID-19 vaccine doses administered in Canada by accine product and dose number, as of October 9, 2022. https://health-infobase.canada.ca/covid-19/vaccine-administration/. (2022).
27. O. W. i. Data. COVID-19 vaccine doses administered by manufacturer, European Union. https://ourworldindata.org/covid-vaccinations#which-vaccines-have-been-administered-in-each-country. (2022).
28. M. N. Ramasamy, A. M. Minassian, K. J. Ewer, A. L. Flaxman, P. M. Folegatti, D. R. Owens, M. Voysey, P. K. Aley, B. Angus, G. Babbage, S. Belij-Rammerstorfer, L. Berry, S. Bibi, M. Bittaye, K. Cathie, H. Chappell, S. Charlton, P. Cicconi, E. A. Clutterbuck, R. Colin-Jones, C. Dold, K. R. W. Emary, S. Fedosyuk, M. Fuskova, D. Gbesemete, C. Green, B. Hallis, M. M. Hou, D. Jenkin, C. C. D. Joe, E. J. Kelly, S. Kerridge, A. M. Lawrie, A. Lelliott, M. N. Lwin, R. Makinson, N. G. Marchevsky, Y. Mujadidi, A. P. S. Munro, M. Pacurar, E. Plested, J. Rand, T. Rawlinson, S. Rhead, H. Robinson, A. J. Ritchie, A. L. Ross-Russell, S. Saich, N. Singh, C. C. Smith, M. D. Snape, R. Song,

R. Tarrant, Y. Themistocleous, K. M. Thomas, T. L. Villafana, S. C. Warren, M. E. E. Watson, A. D. Douglas, A. V. S. Hill, T. Lambe, S. C. Gilbert, S. N. Faust, A. J. Pollard, C. V. T. G. Oxford, Safety and immunogenicity of ChAdOx1 nCoV-19 vaccine administered in a prime-boost regimen in young and old adults (COV002): a single-blind, randomised, controlled, phase 2/3 trial. *Lancet* **396**, 1979-1993 (2021).

29. J. Sadoff, G. Gray, A. Vandebosch, V. Cardenas, G. Shukarev, B. Grinsztejn, P. A. Goepfert, C. Truyers, H. Fennema, B. Spiessens, K. Offergeld, G. Scheper, K. L. Taylor, M. L. Robb, J. Treanor, D. H. Barouch, J. Stoddard, M. F. Ryser, M. A. Marovich, K. M. Neuzil, L. Corey, N. Cauwenberghs, T. Tanner, K. Hardt, J. Ruiz-Guinazu, M. Le Gars, H. Schuitemaker, J. Van Hoof, F. Struyf, M. Douoguih, E. S. Group, Safety and Efficacy of Single-Dose Ad26.COV2.S Vaccine against Covid-19. *N Engl J Med* **384**, 2187-2201 (2021).
30. F. P. Polack, S. J. Thomas, N. Kitchin, J. Absalon, A. Gurtman, S. Lockhart, J. L. Perez, G. Perez Marc, E. D. Moreira, C. Zerbini, R. Bailey, K. A. Swanson, S. Roychoudhury, K. Koury, P. Li, W. V. Kalina, D. Cooper, R. W. Frenck, Jr., L. L. Hammitt, O. Tureci, H. Nell, A. Schaefer, S. Unal, D. B. Tresnan, S. Mather, P. R. Dormitzer, U. Sahin, K. U. Jansen, W. C. Gruber, C. C. T. Group, Safety and Efficacy of the BNT162b2 mRNA Covid-19 Vaccine. *N Engl J Med* **383**, 2603-2615 (2020).
31. L. R. Baden, H. M. El Sahly, B. Essink, K. Kotloff, S. Frey, R. Novak, D. Diemert, S. A. Spector, N. Rouphael, C. B. Creech, J. McGettigan, S. Khetan, N. Segall, J. Solis, A. Brosz, C. Fierro, H. Schwartz, K. Neuzil, L. Corey, P. Gilbert, H. Janes, D. Follmann, M. Marovich, J. Mascola, L. Polakowski, J. Ledgerwood, B. S. Graham, H. Bennett, R. Pajon, C. Knightly, B. Leav, W. Deng, H. Zhou, S. Han, M. Ivarsson, J. Miller, T. Zaks, C. S. Group, Efficacy and Safety of the mRNA-1273 SARS-CoV-2 Vaccine. *N Engl J Med* **384**, 403-416 (2021).
32. A. Greinacher, T. Thiele, T. E. Warkentin, K. Weisser, P. A. Kyrle, S. Eichinger, Thrombotic Thrombocytopenia after ChAdOx1 nCov-19 Vaccination. *N Engl J Med* **384**, 2092-2101 (2021).
33. S. C. Jordan, B. H. Shin, T. M. Gadsden, M. Chu, A. Petrosyan, C. N. Le, R. Zabner, J. Oft, I. Pedraza, S. Cheng, A. Vo, N. Ammerman, J. Plummer, S. Ge, M. Froch, A. Berg, M. Toyoda, R. Zhang, T cell immune responses to SARS-CoV-2 and variants of concern (Alpha and Delta) in infected and vaccinated individuals. *Cell Mol Immunol* **18**, 2554-2556 (2021).
34. D. Hillus, T. Schwarz, P. Tober-Lau, K. Vanshylla, H. Hastor, C. Thibeault, S. Jentzsch, E. T. Helbig, L. J. Lippert, P. Tscheak, M. L. Schmidt, J. Riege, A. Solarek, C. von Kalle, C. Dang-Heine, H. Gruell, P. Kopankiewicz, N. Suttorp, C. Drosten, H. Bias, J. Seybold, E. C. S. Group, F. Klein, F. Kurth, V. M. Corman, L. E. Sander, Safety, reactogenicity, and immunogenicity of homologous and heterologous prime-boost immunisation with ChAdOx1 nCoV-19 and BNT162b2: a prospective cohort study. *Lancet Respir Med* **9**, 1255-1265 (2021).
35. T. Schmidt, V. Klemis, D. Schub, J. Mihm, F. Hielscher, S. Marx, A. Abu-Omar, L. Ziegler, C. Guckelmus, R. Urschel, S. Schneitler, S. L. Becker, B. C. Gartner, U. Sester, M. Sester, Immunogenicity and reactogenicity of heterologous ChAdOx1 nCoV-19/mRNA vaccination. *Nat Med* **27**, 1530-1535 (2021).
36. J. Yu, A. Y. Collier, M. Rowe, F. Mardas, J. D. Ventura, H. Wan, J. Miller, O. Powers, B. Chung, M. Siamatu, N. P. Hachmann, N. Surve, F. Nampanya, A. Chandrashekar, D. H. Barouch, Neutralization of the SARS-CoV-2 Omicron BA.1 and BA.2 Variants. *N Engl J Med* **386**, 1579-1580 (2022).
37. P. Naaber, L. Tserel, K. Kangro, M. Punapart, E. Sepp, V. Jurjenson, J. Karner, L. Haljasmagi, U. Haljasorg, M. Kuusk, E. Sankovski, A. Planken, M. Ustav, E. Zusinaite, J. M. Gerhold, K. Kisand, P. Peterson, Protective antibodies and T cell responses to Omicron variant after the booster dose of BNT162b2 vaccine. *Cell Rep Med* **3**, 100716 (2022).
38. F. D. F. Freitas, A. C. Q. de Medeiros, F. A. Lopes, Effects of Social Distancing During the COVID-19 Pandemic on Anxiety and Eating Behavior-A Longitudinal Study. *Front Psychol* **12**, 645754 (2021).
39. D. E. Speiser, O. Chijioke, K. Schaeuble, C. Munz, CD4(+) T cells in cancer. *Nat Cancer* **4**, 317-329 (2023).

40. A. Takeuchi, T. Saito, CD4 CTL, a Cytotoxic Subset of CD4(+) T Cells, Their Differentiation and Function. *Front Immunol* **8**, 194 (2017).
41. B. Kruse, A. C. Buzzai, N. Shridhar, A. D. Braun, S. Gellert, K. Knauth, J. Pozniak, J. Peters, P. Dittmann, M. Mengoni, T. C. van der Sluis, S. Hohn, A. Antoranz, A. Krone, Y. Fu, D. Yu, M. Essand, R. Geffers, D. Mougiakakos, S. Kahlfuss, H. Kashkar, E. Gaffal, F. M. Bosisio, O. Bechter, F. Rambow, J. C. Marine, W. Kastenmuller, A. J. Muller, T. Tuting, CD4(+) T cell-induced inflammatory cell death controls immune-evasive tumours. *Nature* **618**, 1033-1040 (2023).
42. L. Mazzotti, A. Gaimari, S. Bravaccini, R. Maltoni, C. Cerchione, M. Juan, E. A. Navarro, A. Pasetto, D. Nascimento Silva, V. Ancarani, V. Sambri, L. Calabro, G. Martinelli, M. Mazza, T-Cell Receptor Repertoire Sequencing and Its Applications: Focus on Infectious Diseases and Cancer. *Int J Mol Sci* **23**, (2022).
43. E. Baulu, C. Gardet, N. Chuvin, S. Depil, TCR-engineered T cell therapy in solid tumors: State of the art and perspectives. *Sci Adv* **9**, eadf3700 (2023).
44. P. Shafer, L. M. Kelly, V. Hoyos, Cancer Therapy With TCR-Engineered T Cells: Current Strategies, Challenges, and Prospects. *Front Immunol* **13**, 835762 (2022).
45. G. Liu, H. Chen, X. Cao, L. Jia, W. Rui, H. Zheng, D. Huang, F. Liu, Y. Liu, X. Zhao, P. Lu, X. Lin, Efficacy of pp65-specific TCR-T cell therapy in treating cytomegalovirus infection after hematopoietic stem cell transplantation. *Am J Hematol* **97**, 1453-1463 (2022).
46. P. F. Robbins, S. H. Kassim, T. L. Tran, J. S. Crystal, R. A. Morgan, S. A. Feldman, J. C. Yang, M. E. Dudley, J. R. Wunderlich, R. M. Sherry, U. S. Kammula, M. S. Hughes, N. P. Restifo, M. Raffeld, C. C. Lee, Y. F. Li, M. El-Gamil, S. A. Rosenberg, A pilot trial using lymphocytes genetically engineered with an NY-ESO-1-reactive T-cell receptor: long-term follow-up and correlates with response. *Clin Cancer Res* **21**, 1019-1027 (2015).

Abbreviations

aa	amino acid
aAPC	artificial antigen-presenting cells
BCIP/NBT	5-bromo-4-chloro-3-indolyl-phosphate/nitro-blue tetrazolium chloride
Benda	Bendamustine
BTK	Bruton's tyrosine kinase
BV	booster vaccination
CAR	chimeric antigen receptor
CD	cluster of differentiation
CLB	Chlorambucil
CLL	chronic lymphocytic leukemia
CTLA4	cytotoxic T lymphocyte-associated molecule 4
CV	complete vaccination
Conv.	Convalescents
COVID-19	Coronavirus Disease 2019
DKFZ	German Cancer Research Center
DKTK	German Cancer Consortium
DNA	deoxyribonucleic acid
ELISpot	enzyme-linked immunospot
FACS	fluorescence-activated cell sorting
FC	Fludarabine and Cyclophosphamide
FDR	false discovery rate
Freq.	frequency
FSC	forward scatter
GMP	good manufacturing practice
HCoV	common cold human coronaviruses
Heterol.	Heterologous
HLA	human leukocyte antigen
HV	healthy volunteers
ICI	Immune checkpoint inhibitors
ICS	intracellular cytokine staining
IDs	identifications
IFN-γ	interferon-gamma
IL	interleukin
LC-MS/MS	liquid chromatography-tandem mass spectrometry
LPS	lipopolysaccharide
lympho.	lymphocytes
mAB	monoclonal antibody
MACS	magnetic-activated cell sorting
MassSpec	mass spectrometer
MEK	mitogen-activated protein kinase kinase
MoDC	monocyte-derived dendritic cell
MRD	minimal residual disease
mRNA	messenger ribonucleic acid
MS	mass spectrometry
n	number
n.a.	not available
Neg.	negative
n_{pep}	number of peptides

No.	number
n.s.	not significant
PARP	poly ADP-ribose polymerase
PBMCs	peripheral blood mononuclear cells
PCR	polymerase chain reaction
PD-1	programmed cell death receptor-1
PE	R-phycoerythrin
PHA	phytohemagglutinin
PMA	phorbol myristate acetate
Pos.	positive
Pre.	Prepandemic
RBD	receptor binding domain
R-Benda	Rituximab - Bendamustin
R-CHOP	Rituximab – Cyclophosphamide- Hydroxydaunorubicin- Oncovin - Prednisone
SARS-CoV-2	severe acute respiratory syndrome coronavirus 2
SSC	side scatter
TAA	Tumor-associated antigen
T_H cells	helper T cells
TLR	Toll-like receptor
TNF	tumor-necrosis factor
T_H	helper T cell
T_{reg}	regulatory T cell
UPN	uniform patient number
V	vaccination
VOC	variant of concern
Vs.	versus
WBC	white blood cell count

Acknowledgments

First, I want to thank Juliane Walz for the opportunity of doing my PhD in her amazing group and for the supervision. I watched the group grow and am absolutely impressed by your drive. I would like to thank Hans-Georg Rammensee for also being my supervisor and the great input through the years in our T cell clubs.

I want to thank the AG Walz for making me happy to go to work (almost) every day: Tati, Annika, Jens, Ulrike, Jonas R., Malte, Marcel, Naomi, Marissa, Lenam, Jonas, Sarah, Jonas, Richard, Melek, Anna, Maxifee, Steffen, Claudi, Iris. I am very grateful to Tati, for teaching me how to be a T cell mom and for always having an open ear, even after moving to another continent. A special thanks also to Annika and Jens for their support during all this time.

I want to specially thank my “PhD survival camp” colleagues and dear friends, Franci, Anna and Felix, for supporting me through the years.

I thank Beate and Claudia for the kind technical support. Thank you to Cécile, Juliane, Anna, Ana and Valero from the AG Gouttefangeas for always helping out with open questions on T cell assays.

I would like to thank all my friends in Tübingen helping me get my mind off after work and the amazing time we had together, specially Alexi, Lisa, Melli, Anna, Annika and Lissi.

To my friends from the time at university, I want to specially thank Charlotte, Togo, Timon, Freddy, Anais, Johanna, Cansu, Sinja, for the great time we still spend together and for having my back! Thank you, Jakob, for having spent the last years by my side, pushing me and being there for me.

Finally, I want to thank my unbelievable and amazing family for being my pillar and my safety net every day. Your love and support are everything.

Supplement of Chapter 1

Supplementary Figures

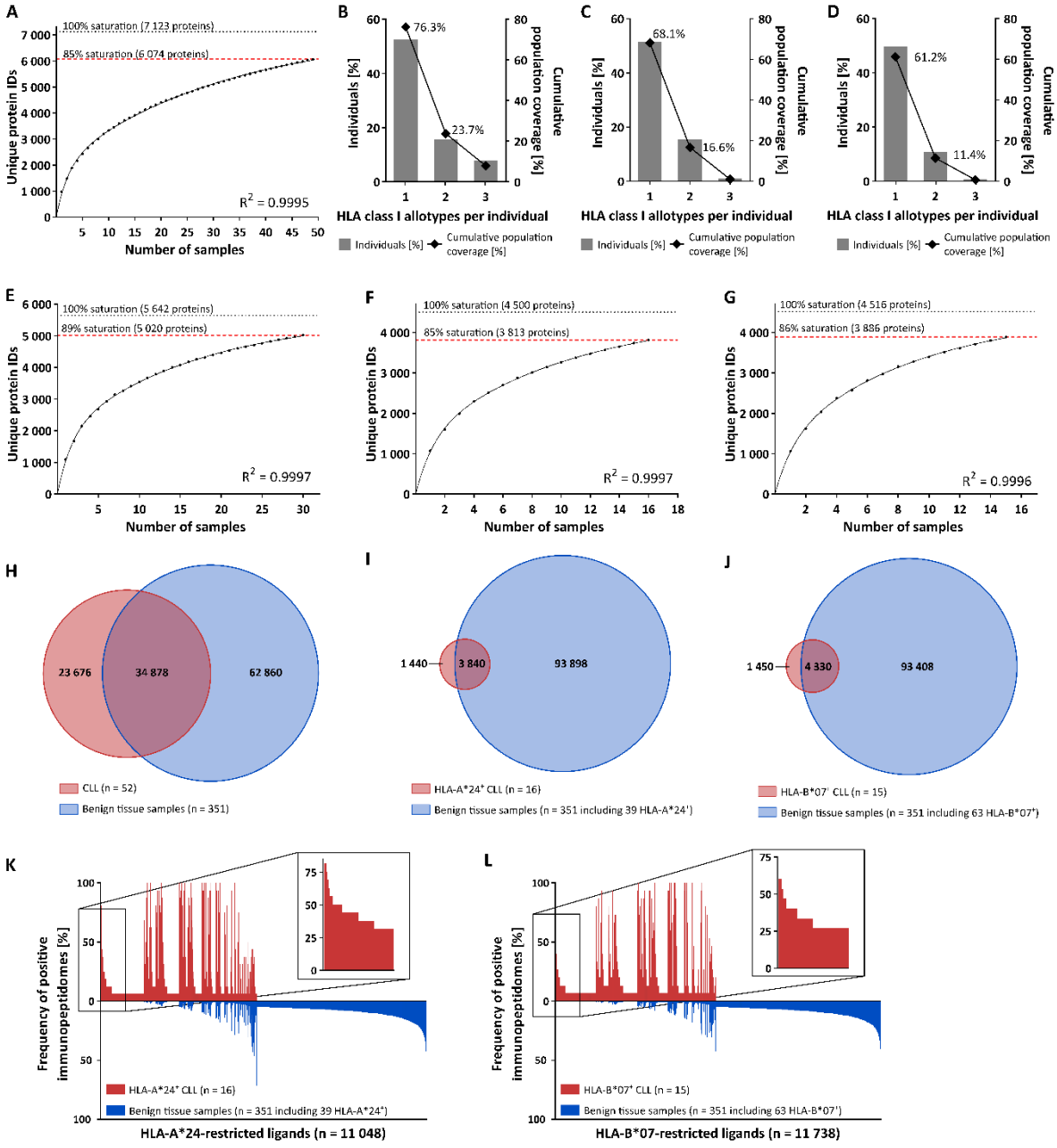

Figure S1: **Saturation analysis, population coverage and comparative immunopeptidome profiling**. (**A**) Saturation analysis of HLA class II-restricted peptide source proteins of the CLL patient cohort. Number of unique source protein identifications shown as a function of cumulative immunopeptidome analysis of CLL samples (n = 49). Exponential regression allowed for the robust calculation of the maximum attainable number of different source protein identifications (dotted lines). The dashed red line depicts the source proteome coverage achieved in the CLL patient cohort. (**B-D**) HLA-A*02, HLA-A*24, and HLA-B*07 allotype coverage within (**B**) the CLL patient cohort of a previous peptide vaccination trial (NCT02802943) as well as within (**C**) the European population and (**D**) the world population (calculated by the IEDB population coverage tool, www.iedb.org). The frequencies of individuals within the respective cohort carrying up to three HLA allotypes (x-axis) are

indicated as gray bars on the left y-axis. The cumulative percentage of population coverage is depicted as black dots on the right y-axis. (**E-G**) Saturation analysis of (**E**) HLA-A*02-, (**F**) HLA-A*24-, and (**G**) HLA-B*07-restricted peptide source proteins of the CLL patient cohort. Number of unique source protein identifications shown as a function of cumulative immunopeptidome analysis of CLL samples (E, n = 30; F, n = 16; G, n = 15). Exponential regression allowed for the robust calculation of the maximum attainable number of different source protein identifications (dotted lines). The dashed red lines depict the source proteome coverage achieved in the respective CLL patient cohort. (**H-J**) Overlap analysis of (**H**) HLA class I-, (**I**) HLA A*24-, and (**J**) HLA-B*07-restricted peptides of HLA-matched CLL samples (H, n = 52; I, n = 16; J, n = 15) and benign tissue samples (n = 351; I, including 39 HLA-A*24+; J, including 63 HLA B*07+). (**K, L**) Comparative profiling of (**K**) HLA-A*24- and (**L**) HLA-B*07-presented ligands based on the frequency of presentation in allotype-matched CLL and benign tissue immunopeptidomes. Frequencies of positive immunopeptidomes for the respective HLA ligands (x-axis) are indicated on the y axis. HLA ligands identified on < 5% of the respective cohort were not depicted. Boxes on the left side highlight CLL-associated antigens that show CLL-exclusive high-frequent presentation. IDs, identifications.

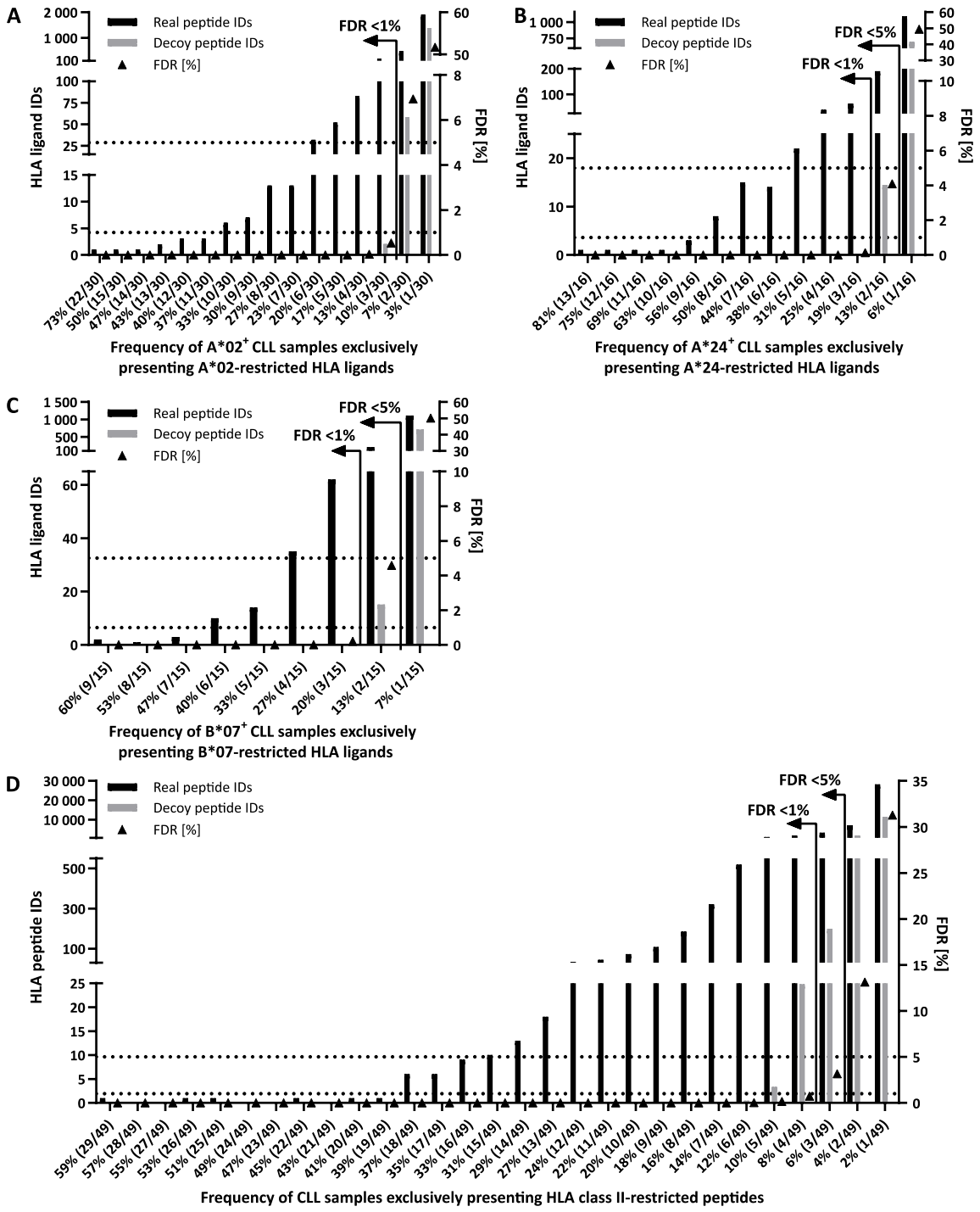

Figure S2: Statistical analysis of the proportion of false-positive CLL-associated antigen identifications at different representation frequencies. The numbers of identified (**A**) HLA-A*02-, (**B**) HLA-A*24-, (**C**) HLA-B*07-, and (**D**) HLA class II-restricted peptides based on the analysis of the CLL and benign tissue cohorts were compared with random virtual (HLA-matched) CLL-associated peptides (left y-axis), respectively. Virtual ligandomes of CLL samples and benign tissue samples were generated in silico based on random weighted sampling from the entirety of peptide identifications in both original cohorts. These randomized virtual ligandomes were used to define CLL-associated antigens based on simulated cohorts of CLL versus benign tissue samples. The process of peptide randomization, cohort assembly, and CLL-associated antigen identification was repeated 1,000 times and the mean value of resultant virtual CLL-associated antigens was calculated and

plotted for the different threshold values. The corresponding false discovery rates (right y-axis) for any chosen threshold (x-axis) were calculated and the 1% and 5% false discovery rates are indicated within the plot (dotted lines and arrows). IDs, identifications; FDR, false discovery rate.

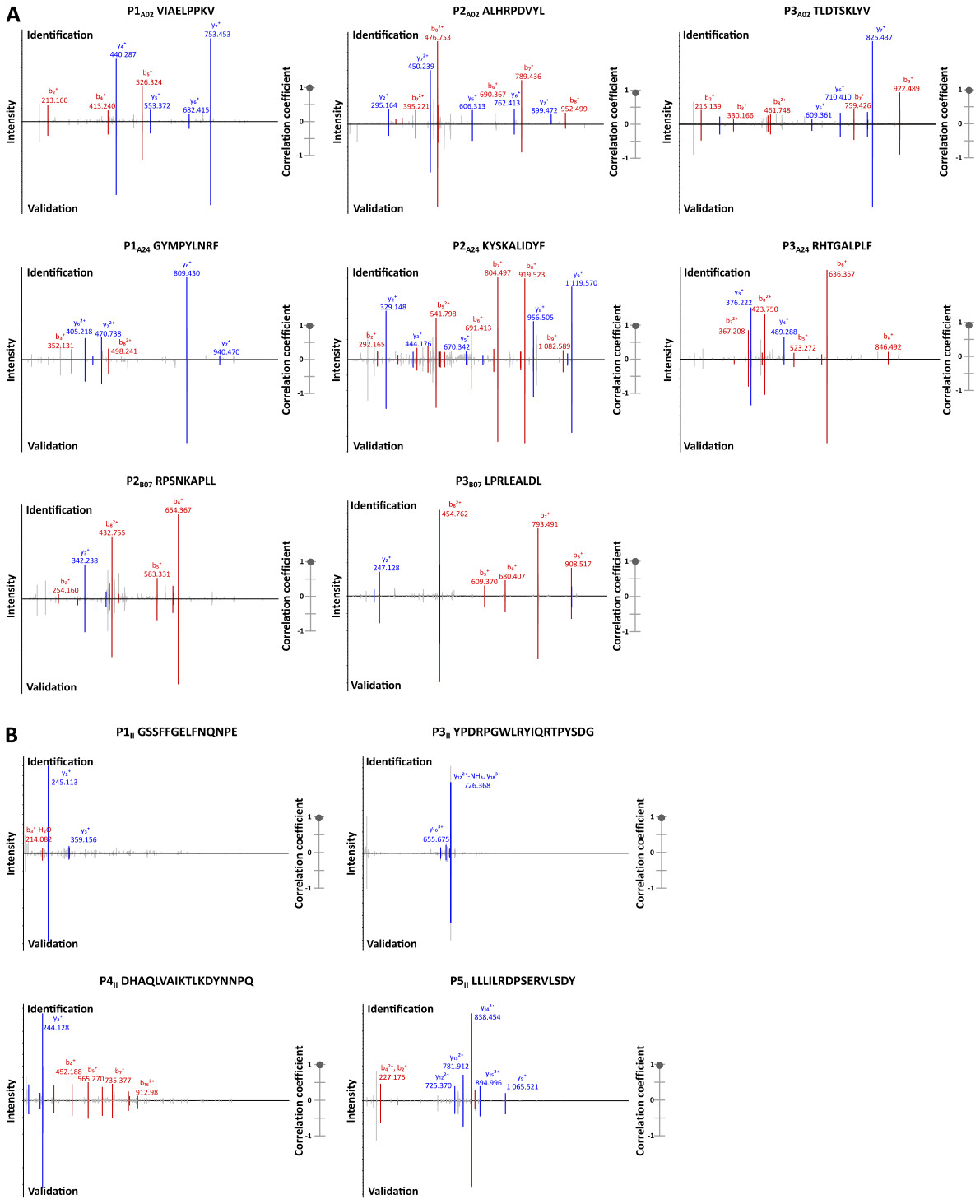

Figure S3: Validation of experimentally eluted peptides by synthetic peptides. Comparison of fragment spectra (m/z on the x-axis) of (**A**) HLA class I and (**B**) class II-restricted peptides eluted from primary CLL samples (identification) to their corresponding synthetic peptides (validation, mirrored on x-axis). Identified b- and y-ions are marked in red and blue, respectively. The calculated spectral correlation coefficients are depicted on the right graphs.

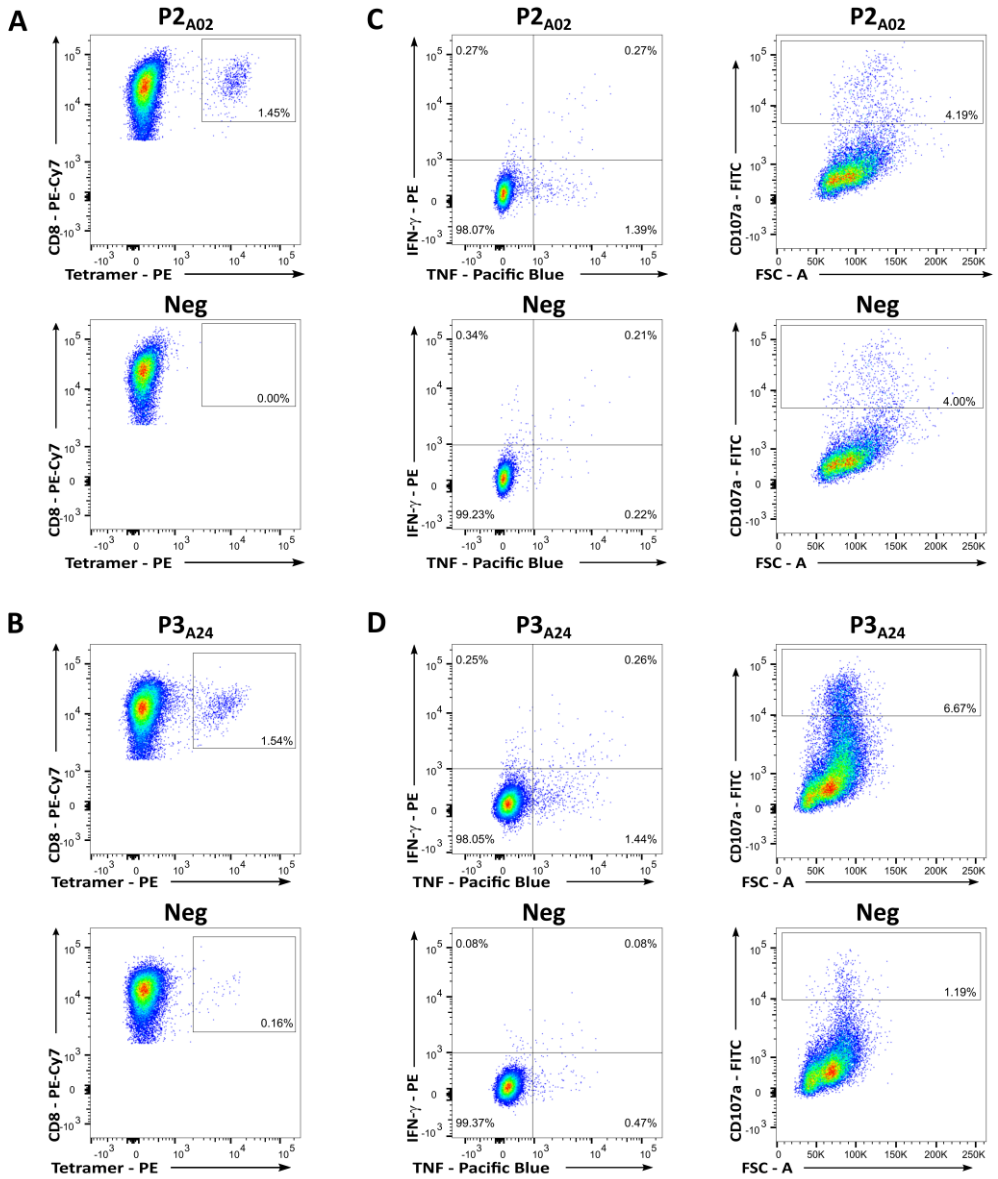

Figure S4: Immunogenicity confirmation of HLA-A*02- and HLA-A*24-restricted peptides by *de novo* T cell induction in HVs. (**A, B**) Tetramer staining of $CD8^+$ T cells derived from HVs after 4 cycles of aAPC stimulation with the peptides (**A**) $P2_{A02}$ and (**B**) $P3_{A24}$. (**C, D**) Representative intracellular cytokine (IFN-γ, TNF) and degranulation marker (CD107a) staining of peptide-specific $CD8^+$ T cells after 4 cycles of *in vitro* aAPC-based primings following stimulation with the peptides (**C**) $P2_{A02}$ and (**D**) $P3_{A24}$. Neg, negative control; FSC, forward scatter.

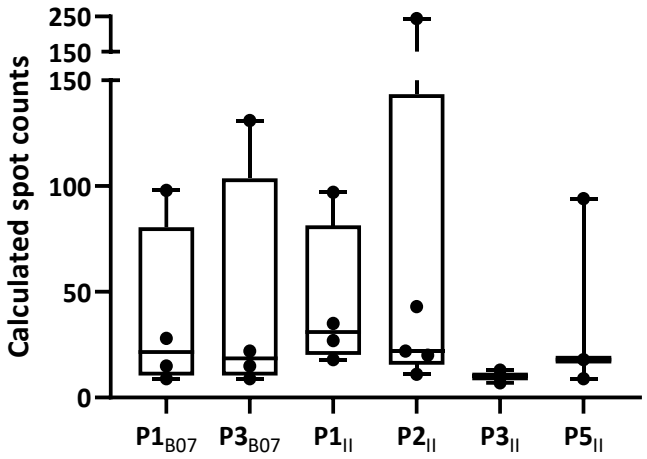

Figure S5: Intensity of preexisting T cell responses. Overview of all detected preexisting T cell responses against the respective CLL-associated antigens evaluated by IFN-γ ELISpot assays after 12-day *in vitro* expansion using peripheral blood mononuclear cells (PBMCs) of CLL patients. Intensity is depicted as calculated spot counts, which were calculated as the mean spot count of duplicates normalized to 5×10^5 cells minus the normalized mean spot count of the respective negative control. Each dot represents an individual donor. Boxes represent median and 25th to 75th percentiles, whiskers are minimum to maximum.

Supplementary Tables

Table S1: Patient characteristics of immunopeptidome samples

UPN	HLA type	Time point sample collection	Therapy prior to sample collection (1st line | 2nd line |…)	WBC [per µl]	Lympho. [%]
UPN001	A*02:01, A*11:01, B*39:01, B*40:01, C*03:04, C*12:03	diagnosis	no	245 200	71
UPN002	A*02:01, B*35:01, B*39:01, C*04:01, C*12:03	relapse	yes (FC | R-Benda | FC | R-Benda | CLB)	151 690	n.a.
UPN003	A*25:01, A*26:01, B*18:01, B*38:01, C*12:03	relapse	yes (CLB)	53 020	56
UPN004	A*01:01, A*24:02, B*08:01, B*27:05, C*02:02, C*07:02	diagnosis	no	103 000	75
UPN005	A*02:01, A*03:01, B*18:01, B*35:01, C*04:01, C*05:01	diagnosis	no	103 800	77
UPN006	A*03:01, A*30:01, B*07:02, B*13:02, C*06:02, C*07:02	relapse	yes (CLB)	130 450	97
UPN007	A*02:01, A*03:01, B*07:02, B*55:01, C*01:02, C*07:02	relapse	yes (Trofosfamide)	72 080	84
UPN008	A*01:01, A*02:01, B*27:05, B*37:01, C*02:02, C*06:02	diagnosis	no	111 000	86
UPN009	A*01:01, A*02:01, B*27:02, B*37:01, C*02:02, C*06:02	diagnosis	no	111 800	79
UPN010	A*23:01, B*49:01, C*03:04, C*07:02	relapse	yes (R-Benda | Benda)	37 800	88
UPN011	A*01:01, A*68:01, B*08:01, B*44:02, C*07:01, C*07:04	diagnosis	no	40 990	59
UPN012	A*02:01, A*03:01, B*40:01, C*03:04	diagnosis	no	35 400	86
UPN013	A*01:01, A*03:01, B*08:01, B*51:01, C*01:02, C*07:01	diagnosis	no	54 360	84
UPN014	A*02:01, A*03:01, B*07:02, B*44:02, C*05:01, C*07:02	diagnosis	no	61 760	64
UPN015	A*02:05, A*24:02, B*35:01, B*50:01, C*04:01, C*06:02	relapse	yes ("Knospe protocol" | R-Benda | Benda | FC | CLB | Benda)	56 360	67
UPN016	A*11:01, B*15:01, B*52:01, C*04:01, C*12:02	relapse	yes (R-Benda)	83 390	81
UPN017	A*01:01, A*02:01, B*08:01, B*13:02, C*06:02, C*07:02	diagnosis	no	67 410	78
UPN018	A*32:01, A*68:01, B*07:02, B*27:05, C*07:01, C*07:02	relapse	yes (R-Benda)	76 840	88
UPN019	A*01:01, A*26:01, B*07:02, B*37:01, C*02:02, C*07:02	diagnosis	no	220 710	n.a.
UPN020	A*01:01, A*32:01, B*07:02, B*44:02, C*07:01, C*07:02	relapse	yes (R-Benda | CLB)	770 400	n.a.
UPN021	A*02:01, A*24:02, B*51:01, B*57:01, C*14:02	relapse	yes (Fludarabine | R-Benda)	110 300	71
UPN022	A*02:01, A*03:01, B*40:01, B*44:02, C*02:02, C*03:04	diagnosis	no	46 170	80
UPN023	A*02:01, A*03:01, B*35:01, C*04:01	diagnosis	no	160 600	77
UPN024	A*01:01, A*02:01, B*08:01, B*51:01, C*02:02, C*07:02	diagnosis	no	123 700	85
UPN025	A*02:01, A*24:02, B*51:01, B*57:01, C*01:02, C*06:02	relapse	yes (CLB)	259 750	95
UPN026	A*01:01, A*03:01, B*07:02, B*44:02, C*05:01, C*07:02	diagnosis	no	171 510	90
UPN027	A*01:01, A*02:01, B*08:01, B*27:02, C*02:02, C*07:01	diagnosis	no	335 730	94
UPN028	A*02:01, B*15:01, B*56:01, C*01:02, C*03:04	relapse	yes (R-Benda)	58 260	87
UPN029	A*24:02, A*26:01, B*27:05, B*39:01, C*01:02, C*07:02	diagnosis	no	68 610	86
UPN030	A*02:01, B*07:02, B*18:01, C*03:04, C*06:02	diagnosis	no	31 950	n.a.
UPN031	A*02:01, A*11:01, B*35:01, B*40:01, C*03:04, C*04:01	diagnosis	no	537 370	96
UPN032	A*01:01, A*24:02, B*07:02, B*08:01, C*07:02	diagnosis	no	146 810	92
UPN033	A*02:01, A*68:01, B*38:01, B*51:01, C*12:03, C*14:02	diagnosis	no	38 680	88
UPN034	A*02:01, A*29:02, B*44:02, C*05:01, C*16:01	diagnosis	no	170 420	97
UPN035	A*01:01, A*26:01, B*07:02, B*40:01, C*02:02, C*07:02	diagnosis	no	81 510	87
UPN036	A*02:01, A*11:01, B*35:01, B*40:01, C*03:04, C*04:01	diagnosis	no	27 340	73
UPN037	A*02:01, A*24:02, B*15:01, B*44:02, C*03:04, C*16:01	diagnosis	no	438 060	97
UPN038	A*24:02, A*25:01, B*18:01, B*49:01, C*07:02, C*12:03	diagnosis	no	227 910	96
UPN039	A*03:01, A*24:02, B*35:01, C*04:01	diagnosis	no	79 010	92
UPN040	A*02:01, A*24:02, B*07:02, B*44:02, C*05:01, C*07:02	diagnosis	no	147 340	92

UPN	HLA type	Time point sample collection	Therapy prior to sample collection (1st line | 2nd line |…)	WBC [per µl]	Lympho. [%]
UPN041	A*02:01, A*11:01, B*07:02, B*15:01, C*03:04, C*07:02	diagnosis	no	127 100	94
UPN042	A*02:01, A*24:02, B*07:02, B*13:02, C*06:02, C*07:02	diagnosis	no	259 550	94
UPN043	A*01:01, A*68:01, B*44:02, B*55:01, C*03:04, C*05:01	diagnosis	no	253 100	97
UPN044	A*01:01, A*24:02, B*08:01, B*35:01, C*04:01, C*07:02	diagnosis	no	129 080	99
UPN045	A*03:01, A*24:02, B*51:01, C*14:02, C*16:01	diagnosis	no	198 200	97
UPN046	A*02:01, A*24:02, B*13:02, B*44:02, C*05:01, C*06:02	diagnosis	no	401 080	91
UPN047	A*02:01, A*26:01, B*07:02, B*40:01, C*03:04, C*07:02	diagnosis	no	115 000	63
UPN048	A*02:01, A*11:01, B*40:01, B*44:02, C*03:04, C*05:01	diagnosis	no	79 800	35
UPN049	A*02:01, B*08:01, B*40:01, C*03:04, C*07:02	diagnosis	no	95 200	55
UPN050	A*11:01, A*68:01, B*08:01, B*35:01, C*04:01, C*07:02	diagnosis	no	166 000	59
UPN051	A*01:01, A*24:02, B*15:01, B*40:01, C*02:02, C*07:02	diagnosis	no	123 500	78
UPN052	A*01:01, A*24:02, B*07:02, B*08:01, C*07:01, C*07:02	diagnosis	no	51 850	91
UPN053	A*02:01, A*30:01, B*13:02, B*35:01	diagnosis	no	52 350	79
UPN054	A*02:01, B*40:01, B*51:01, C*03:04, C*15:02	diagnosis	no	238 570	94
UPN055	A*02:01, B*55:01, B*57:01	relapse	yes (R-CHOP*)	83 560	n.a.
UPN056	A*30:01, A*33:01, B*14:02, B*40:01, C*03:04, C*08:02	diagnosis	no	20 000	61
UPN057	A*02:01, A*03:01, B*27:05, B*57:01	diagnosis	no	43 000	78
UPN058	A*02:01, A*24:02, B*07:02, B*51:01, C*01:02, C*07:02	diagnosis	no	27 300	90
UPN059	A*03:01, A*26:01, B*07:02, B*38:01, C*07:02, C*12:03	diagnosis	no	36 870	89
UPN060	A*01:01, A*02:01, B*51:01, B*57:01, C*06:02, C*15:02	diagnosis	no	20 300	69
UPN061	A*02:01, A*11:01, B*39:06, C*06:02	diagnosis	no	131 400	98

UPN, uniform patient number; WBC, white blood cell count; lympho., lymphocytes; n.a., not available; Benda, Bendamustine; FC, Fludarabine and Cyclophosphamide; R-CHOP, Rituximab - Cyclophosphamide - Hydroxydaunorubicin - Oncovin - Prednisone; R-Benda, Rituximab - Bendamustine; CLB, Chlorambucil; "Knospe protocol", Chlorambucil and Prednisone; *, individualized therapy concept due to high risk disease (TP53 mutation).

Table S2: Sample characteristics of immunogenicity cohort

UPN	Lymphocyte count [per µl]	$CD3^+$ cells [% of lymphocytes]
UPN005	147 970	2.7
UPN007	1 340	71.3
UPN012	11 580	n.a
UPN017	148 270	3.9
UPN018	67 680	n.a
UPN019	99 140	2.6
UPN022	14 820	n.a
UPN026	202 240	2.6
UPN029	59 040	3.6
UPN035	71 020	7.7
UPN038	219 200	2.4
UPN039	72 730	4.2
UPN040	136 130	1.8
UPN041	119 420	7.2
UPN042	243 070	4.0
UPN045	192 360	n.a
UPN047	72 200	n.a
UPN051	77 810	n.a
UPN052	47 410	n.a
UPN057	61 570	3.7
UPN058	24 530	6.3
UPN062	730	n.a
UPN063	28 890	n.a
UPN064	1 830	n.a
UPN066	66 010	n.a
UPN069	55 530	n.a
UPN070	3 720	44.5
UPN071	2 850	n.a
UPN073	38 400	7.9
UPN074	31 569	n.a
UPN075	106 370	n.a
UPN077	68 940	7.9
UPN078	172 680	1.8
UPN080	580	n.a
UPN082	1 660	n.a
UPN083	100 260	6.1
UPN085	153 520	2.5
UPN087	19 850	4.9
UPN088	176 120	n.a
UPN089	193 260	n.a
UPN090	136 130	1.8
UPN091	129 840	3.7
UPN092	510	36.0
UPN093	121 150	n.a
UPN095	34 650	4.2
UPN096	329 310	1.6
UPN097	13 550	12.2
UPN098	17 370	99.2
UPN099	5 630	31.8
UPN100	6 430	9.8
UPN102	2 100	70.7

Table S3: Recurrent CLL-associated mutations

Frameshift mutations		
Gene	**Protein**	**Mutation [protein sequence]**
BIRC3	BIRC3	Q547Nfs*21
NFKBIE	IKBE	Y254Sfs*13
NOTCH1	NOTC1	P2514fsRVP*
Missense mutations		
Gene	**Protein**	**Mutation [protein sequence]**
ADGRF5	ADGRF5	S765F
ASB10	ASB10	H227L
ATM	ATM	L1222P, R3008C
BIRC6	BIRC6	L3687R
BNC2	BNC2	V771I
BRAF	BRAF	G469A, V600E
CALCRL	CARL1	Q33H
CARMIL1	CARMIL1	L283H
CCDC185	CC185	R380W
CCND3	CCND3	P199S
CD3G	CD3G	D35G
CEP250	CP250	Q2041H
COL3A1	CO3A1	G741S
DNASE2	DNS2A	R62W
EDEM2	EDEM2	V39F
EGR2	EGR2	E356K, H384N
EIF2A	EIF2A	D359N
ERBB4	ERBB4	R50H
GLB1L2	GLBL2	G366S
HOXC11	HXC11	E202D
IKZF3	IKZF3	L162R
IRF4	IRF4	S114R
JAK2	JAK2	V617F
KCTD9	KCTD9	P199S
KIAA1211	CRAD	A1035V
KIAA1217	SKT	R1188W
LGI3	LGI3	W341R
LRP1B	LRP1B	N1754K
LRRD1	LRRD1	P735S
LRRIQ4	LRIQ4	V225I
MDGA2	MDGA2	R53W
MED12	MED12	E33K, L36R, G44D, G44S
MYO5B	MYO5B	T846I
NFE2L3	NF2L3	C595Y
NID1	NID1	G562S
NRAS	RASN	Q61K, Q61R
PADI3	PADI3	T335I
PAPPA	PAPPA	G438R
PCDHA13	PCDAD	D376Y
PENK	PENK	R229W
PLCG2	PLCG2	S707F, D993H, M1141R, M1141K
RIMS1	RIMS1	E658A
RYR3	RYR3	D4710N
SBNO1	SBNO1	V1132A
SECISBP2	SEBP2	K15R
SF3B1	SF3B1	E622D, Y623C, N626Y, H662D, H662Q, T663I, K666E, K666N, K666T, K700E, I704F, I704N, G740E, G742D
SLC7A13	S7A13	V407M
SNX16	SNX16	W171L
STAMBPL1	STALP	P48R
TLR2	TLR2	D327V

Gene	Protein	Mutation [protein sequence]
TMEM131	T131L	S1256C
TP53	P53	R175H, H179L, Y220C, Y234C, S241F, G244D, R248Q, R248W, R273C, R273H, R337C
TRAPPC10	TPC10	A301S
TSPAN12	TSN12	E301K
UGT2B4	UD2B4	I331V
UTF1	UTF1	R108L
VPS13D	VP13D	A4248V
XPO1	XPO1	E571A, E571G, E571K, E571Q, E571V

Table S4: HLA class I and HLA class II peptide yields

UPN	Mass spec	HLA class I		HLA-A*02		HLA-A*24		HLA-B*07		HLA class II	
		Ligand IDs	Protein IDs	Ligand IDs	Protein IDs	Ligand IDs	Protein IDs	Ligand IDs	Protein IDs	Peptide IDs	Protein IDs
UPN001	XL	1 554	1 432	201	265					997	327
UPN002	XL	852	929	251	358					706	473
UPN003	XL	1 230	1 199							n.a.	n.a.
UPN004	XL	1 921	1 800			509	614			1 075	470
UPN005	XL	1 349	1 375	201	280					575	363
UPN006	XL	1 407	1 563					486	557	n.a.	n.a.
UPN007	XL	2 555	2 196	919	1 016			1 263	1 212	n.a.	n.a.
UPN008	XL	1 121	1 198	299	387					n.a.	n.a.
UPN009	XL	1 492	1 457	666	736					944	441
UPN010	XL	679	771							n.a.	n.a.
UPN011	XL	1 228	1 203							n.a.	n.a.
UPN012	XL	1 157	1 173	247	336					n.a.	n.a.
UPN013	XL	1 243	1 288							627	331
UPN014	XL	1 182	1 206	177	250			466	500	n.a.	n.a.
UPN015	XL	632	759	174	256	199	303			n.a.	n.a.
UPN016	XL	800	849							n.a.	n.a.
UPN017	XL	1 060	1 130	533	665					691	326
UPN018	XL	678	729					223	257	631	360
UPN019	XL	1 308	1 247					794	783	n.a.	n.a.
UPN020	XL	759	786					239	266	1 651	643
UPN021	XL	728	784	159	220	319	391			1 066	551
UPN022	XL	2 457	1 992	511	632					728	379
UPN023	XL	1 231	1 221	266	364					n.a.	n.a.
UPN024	XL	849	969	82	93					725	388
UPN025	XL	527	676	99	177	134	201			745	405
UPN026	XL	1 860	1 714					658	692	3 029	877
UPN027	Lumos	8 561	4 741	2 811	2 312					7 865	1 393
UPN028	Lumos	7 957	4 912	3 723	2 845					7 010	1 406
UPN029	Lumos	3 082	2 599			1 505	1 499			4 096	664
UPN030	Lumos	5 976	3 820	2 500	2 125			1 815	1 642	2 586	815
UPN031	Lumos	8 622	4 610	2 198	1 936					7 397	1 430
UPN032	Lumos	4 928	3 570			1 679	1 636	1 990	1 781	6 488	1 411
UPN033	Lumos	5 298	3 568	1 594	1 542					6 748	1 411
UPN034	Lumos	9 530	5 046	2 134	1 865					9 570	1 789
UPN035	Lumos	3 055	2 436					651	720	2 603	842
UPN036	Lumos	2 003	1 725	456	574					3 316	928
UPN037	Lumos	3 412	2 593	731	853	973	1 040			3 470	896
UPN038	Lumos	1 992	1 822			533	639			8 922	1 649
UPN039	Lumos	4 393	3 285			1 515	1 550			8 954	1 799
UPN040	Lumos	8 816	4 917	2 182	1 938	1 926	1 866	2 933	2 361	10 392	1 626
UPN041	Lumos	7 539	4 644	1 908	1 749			2 568	2 166	7 016	1 531

UPN	Mass spec	HLA class I		HLA-A*02		HLA-A*24		HLA-B*07		HLA class II	
		Ligand IDs	Protein IDs	Ligand IDs	Protein IDs	Ligand IDs	Protein IDs	Ligand IDs	Protein IDs	Peptide IDs	Protein IDs
UPN042	Lumos	4 558	3 296	2 042	1 850	1 447	1 439	1 235	1 197	4 272	1 104
UPN043	Lumos	2 696	2 284							4 524	999
UPN044	Lumos	3 608	2 943			1 264	1 305			7 258	1 558
UPN045	Lumos	1 186	1 247			536	609			1 264	509
UPN046	Lumos	7 643	4 461	2 969	2 439	1 775	1 742			7 031	1 491
UPN047	Lumos	2 490	2 135	927	1 032			508	588	2 569	832
UPN048	Lumos	3 002	2 347	1 077	1 131					4 246	1 039
UPN049	Lumos	2 877	2 316	1 599	1 544					4 490	1 196
UPN050	Lumos	4 358	3 238							6 192	1 551
UPN051	Lumos	5 292	3 554			1 439	1 405			5 673	1 337
UPN052	Lumos	3 073	2 598			916	978	1 267	1 236	2 624	870
UPN053	XL	n.a.	n.a.							606	357
UPN054	XL	n.a.	n.a.							873	474
UPN055	XL	n.a.	n.a.							935	489
UPN056	Lumos	n.a.	n.a.							603	306
UPN057	Lumos	n.a.	n.a.							4 505	1 280
UPN058	Lumos	n.a.	n.a.							4 584	1 286
UPN059	Lumos	n.a.	n.a.							5 343	1 530
UPN060	Lumos	n.a.	n.a.							6 233	1 697
UPN061	Lumos	n.a.	n.a.							3 814	1 103

UPN, uniform patient number; Mass spec, mass spectrometer; ID, identification; n.a., not available.

Table S5: HLA-A*02-restricted CLL-associated antigens

Sequence	Source protein	Peptide length	Allotype-specific presentation frequency	Sequence	Source protein	Peptide length	Allotype-specific presentation frequency
KLLESVASA	PACER	9	73%	**LLFHGMLLL**	ZDH24	9	23%
GIIDGSPRL	PACER	9	50%	**QLYNSLIFL**	RNFT2	9	23%
VIAELPPKV	IGHM	9	47%	**SLASITVPL**	GGA1	9	23%
SLFSHLLEI	WDFY4	9	43%	**SLLAELHVLTV**	FCRL3	11	23%
VLTNLVVFL	ABCA6	9	43%	**SLMLEVPAL**	DMD	9	23%
ALHRPDVYL	IGHM	9	40%	**SLPELVHAV**	SESN3	9	23%
YLLDQSFVM	RGRF1	9	40%	**SLTSLLILV**	TM243	9	23%
YLTVVIFTA	LOX5	9	40%	**VLRELCEEL**	SYNE2	9	23%
ILDEKPVII	ABCA6	9	37%	**YILTFPLYL**	MET7A	9	23%
RLLYQLVFL	IL4RA	9	37%	**AIPPSFASIFL**	IGHM	11	20%
TLDTSKLYV	RGRF1	9	37%	**ALHWFLNQV**	UBP34	9	20%
FLTDLEDLTL	NAT9	10	33%	**ALMGLSAQL**	DNMBP	9	20%
LIWPLLSTV	NUP88	9	33%	**ALWIPEVSI**	JADE1, JADE2, JADE3	9	20%
LLDAMNYHL	KLH14	9	33%	**ATMPVVPSV**	SHLB2	9	20%
SLASHIQSL	WDFY4	9	33%	**FAIPPSFASI**	IGHM	10	20%
VMLQINPKL	GRDN	9	33%	**FLNFNSFNL**	CC14B, CC14C	9	20%
YLVEDVLLL	KLH14	9	33%	**FLYIGDIVSL**	ITPR2	10	20%
ALPEILFAKV	CXCR5	10	30%	**FVDEGIKTL**	DPOLB	9	20%
AVAIIVVSV	SCIMP	9	30%	**FVFEAPYTL**	DOC11	9	20%
FLSAMDWHL	CNPD1	9	30%	**GLLRASFLL**	TLR9	9	20%
LLHEIENHL	PKHG1	9	30%	**GLYFGMLLL**	CD37	9	20%
LLLPDVIKV	TBCD9	9	30%	**HLANIVERL**	TRI34	9	20%
VLTDIVAKC	DOC10	9	30%	**HLIDTNKIQL**	DOC10	10	20%
YLGGFALSV	KSYK	9	30%	**IIQSYIINI**	PCDBI	9	20%
ALGIFSFTL	SGPP1	9	27%	**ILSLSIASV**	CYAC3	9	20%
ALPTLIPSV	ZEP1	9	27%	**KQSEEIPEV**	LONF1	9	20%
ALVDELEWEI	CNPY2	10	27%	**KVIGFLEEV**	RGRF1	9	20%
ALYLTEVFL	BANK1	9	27%	**NLWSVDGEVTV**	SNX29	11	20%
AVGAFLIYI	MAT2B	9	27%	**RVLEALWEL**	BAIP3	9	20%
FLIDGSFNI	COCH	9	27%	**SLAHVAGCEL**	PACER	10	20%
FTLPEVAEC	HNRPU	9	27%	**SLASIHVPL**	GGA3	9	20%
GLLDGVFNV	CRNS1	9	27%	**SLDLTTTCV**	FOXP1	9	20%
IINGIIISV	HVCN1	9	27%	**SLMGTVFLL**	SAMD8	9	20%
QLIPKLIFL	WDFY4	9	27%	**SLMSVGFLL**	NUBP2	9	20%
SLFDLDGPKV	PHF23	10	27%	**SVASVLLYL**	PRKDC	9	20%
SLFLGILSV	CD20	9	27%	**SVWEKEIEI**	AKAP9	9	20%
SLLAELHVL	FCRL3	9	27%	**VLLSIPFVSV**	ORML3	10	20%
ATPMPTPSV	SBNO1	9	23%	**YLFEEAISM**	WDFY4	9	20%
GLGELAGLTV	STRN	10	23%	**YLMAAEDLEL**	CK5P2	10	20%
HVLEEVQQV	CKAP4	9	23%	**YLVNFLHKL**	TEAD2	9	20%
KLTEENTTL	PEG10	9	23%	**YQFDSALLPAV**	SPIB	11	20%

Table S6: HLA-A*24-restricted CLL-associated antigens

Sequence	Source protein	Peptide length	Allotype-specific presentation frequency	Sequence	Source protein	Peptide length	Allotype-specific presentation frequency
TYTDVTPRQF	STAR7	10	81%	**LYQTFVVQL**	IL2RG	9	31%
IYQQNHMVL	IKZF3	9	75%	**LYSQLQVFF**	TRM7	9	31%
KYGVFEESL	TRI34	9	69%	**MYPVWKSFL**	FCSD2	9	31%
VYNENLVHM	SPF27	9	63%	**PYPQYLAVI**	MED29	9	31%
GYMPYLNRF	SWP70	9	56%	**QYILIHQAL**	PTPRC	9	31%
KYVGAVQML	SNX29	9	56%	**RYVRKFVLM**	CHM2A	9	31%
RFPPTPPLF	BC11A	9	56%	**SYGYQFPGF**	MSI2H	9	31%
FYVGHIDAF	ICE2	9	50%	**TYDAHHSAF**	IRF8	9	31%
IFPPVINITW	DOA	10	50%	**TYIKVFVPSW**	ZC12D	10	31%
IFPPVVNITW	DQA2	10	50%	**VFKLWPLSF**	PIGQ	9	31%
KYSKALIDYF	AFF3	10	50%	**VWSDIAPLNF**	MMP17	10	31%
KYTEGVQSL	SP16H	9	50%	**VYPTLSQQL**	TPC10	9	31%
RHTGALPLF	SI1L3	9	50%	**YFISHILAF**	RIR2B	9	31%
VHIPEVYLI	WDFY4	9	50%	**AYPTAYPSF**	SMAP2	9	25%
VYHSDIPKW	SIAT1	9	50%	**DYLEWPEYF**	DCTD	9	25%
AFPEIFYTF	PI3R4	9	44%	**EFKQFAQLF**	TRAF5	9	25%
EYSRFVNQI	KHDC4	9	44%	**EWPKHWPTF**	XPO1	9	25%
FYIENMQYL	ABCA6	9	44%	**EYGENFPML**	ZN121	9	25%
FYTLIPHDF	PARP1	9	44%	**FYTQLLQEL**	SMG7	9	25%
GYPGRQYYF	RHBL4	9	44%	**GYPVPPYAFF**	RARA	10	25%
IFLTKSTKL	IGHM	9	44%	**HYFNTPFQL**	PPTC7	9	25%
IYGKDVFEAF	CUL4B	10	44%	**IFNGFSVTL**	MPCP	9	25%
IYNGETLVF	PCYOX	9	44%	**IYGSVPYLL**	GANC	9	25%
IYSPDHTNNSF	ITF2	11	44%	**IYNHITTRV**	ADDA	9	25%
IYWDGPLAL	IRF4	9	44%	**IYQKPFQTL**	ATLA2	9	25%
KLPTEWNVL	AKP13	9	44%	**KYAATSQVL**	IGHM	9	25%
SYLPRIVLL	GRP3	9	44%	**KYIEYYLVL**	ADA28	9	25%
TYKALNTFI	CLPT1	9	44%	**KYLSDNVHL**	CDC37	9	25%
VFSNVSIILF	GNA13	10	44%	**KYSFLPYQL**	BFAR	9	25%
YFYLFPNRL	ARBK1	9	44%	**KYVKVFDKF**	ZN107	9	25%
DWPLTQVTF	FCRLA	9	38%	**LYQHAVEYF**	VPS4A	9	25%
DYTGALAVF	HAP40	9	38%	**LYVPALSALW**	GNA12	10	25%
EYTRYLFAL	FARP2	9	38%	**NWGRLVAFF**	B2CL2, BCL2	9	25%
IFTDIFHYL	XRN1	9	38%	**NYTDRIQVL**	PDE4B	9	25%
IYSQLETLI	S11IP	9	38%	**QYVVDLTSF**	NTPCR	9	25%
KYPASTVQI	NOP56	9	38%	**RYKEENNDHL**	UBP8	10	25%
LFKNDPLFF	LACTB	9	38%	**SEYADTHYF**	CLNK	9	25%
PYAKPIPAQF	WDR33	10	38%	**SYILDTLVF**	TNPO2	9	25%
RYGLPAAWSTF	IGFR1	11	38%	**TFTDHVMLF**	DDX27	9	25%
RYNGGLLEF	DZIP3	9	38%	**TYSEDTYRL**	NR2C2	9	25%
RYPLLLMEL	DNMBP	9	38%	**TYSSSYEQF**	SRPK2	9	25%
TYDSVTISW	IGHM	9	38%	**TYVKEIEVW**	RN213	9	25%
VFIIVPAIF	GPAT4	9	38%	**VAAGSYQRF**	PMF1	9	25%
VYRQDCETF	PPHLN	9	38%	**VFIEGADAETF**	SYEP	11	25%
AYVVFVTTL	HTR5B	9	31%	**VFTPYSAAFLL**	KCNH2, KCNH6	11	25%
EFLTKTAKF	P4R3A, P4R3B	9	31%	**VYERAVEFF**	CRNL1	9	25%
IYGGTYML	GDIA, GDIB	8	31%	**VYNIPVRF**	BLNK	8	25%
IYHFNSELL	PKHG1	9	31%	**VYPYKLYRL**	ZBT38	9	25%
IYKDLPFETL	RM39	10	31%	**VYQVGGVTAYF**	MFRN2	11	25%
IYVIPQPHF	KNL1	9	31%	**YLLDQSFVM**	RGRF1	9	25%
KYDDNVKAYF	AIP	10	31%	**YWPDVIHSF**	RNT2	9	25%
LYGKVQEI	GMDS	8	31%	**YYTVAHAI**	SMCA2	8	25%
LYPGQLVQL	RHG09	9	31%				

Table S7: HLA-B*07-restricted CLL-associated antigens

Sequence	Source protein	Peptide length	Allotype-specific presentation frequency	Sequence	Source protein	Peptide length	Allotype-specific presentation frequency
IPSIHIEL	RHG44	8	60%	**MPLLSRLDL**	KDM2A	9	27%
SPRSWIQVQI	FCRL5	10	60%	**NPRYPNYMF**	ROR1	9	27%
SPRVYWLGL	CL17A	9	53%	**RPCDISRQL**	PAX1/2/5/8/9	9	27%
APQHKGHTTAL	TRI38	11	47%	**RPHVSPRHSF**	RELB	10	27%
RPKENVTIM	LY9	9	47%	**SAAHSRQAL**	LFNG	9	27%
RPSNKAPLL	EHMT1	9	47%	**SLASHIQSL**	WDFY4	9	27%
GPGPLRESL	PRAG1	9	40%	**SPDATRESM**	SNX17	9	27%
GPMAYARAFL	DOC10	10	40%	**SPKGRFVML**	FBX7	9	27%
IPASHPVL	FCRL5	8	40%	**SPRKSSSI**	ACINU	8	27%
IPRRQEHDISL	SYMPK	11	40%	**SPSGNHQSSF**	BMI1	10	27%
IPVSHPVL	FCRL3	8	40%	**TIRAIIAVL**	YTDC2	9	27%
LPRLEALDL	TLR9	9	40%	**TPKGETRQL**	ABR	9	27%
RAAENRQGTL	NCF1	10	40%	**VPSPKVVL**	CPSF2	8	27%
RPALPRSEL	M3K14	9	40%	**ALMGLSAQL**	DNMBP	9	20%
SPGGAHSNL	ARHGI	9	40%	**APARGLLL**	SPAST	8	20%
VPRNLPSSL	TLR9	9	40%	**APEAKKQKV**	NUCL	9	20%
AAAAGRIAI	PTBP1	9	33%	**APESKHKSSL**	STT3B	10	20%
APSFRAGAQL	DOP2	10	33%	**APLLKDIL**	PACER	8	20%
APSLQAKL	TEAD2	8	33%	**APNTGRANQQM**	BFAR	11	20%
ISRPKGVAL	IGHM	9	33%	**APRDGRVVF**	SIPA1	9	20%
KPFSQTPFTL	TEAD2	10	33%	**APREPFAHSL**	ZC12D	10	20%
NPSADRNLL	GGA2	9	33%	**APRGNVTSLSL**	TLR9	11	20%
QPKGGHVTSM	KMT2D	10	33%	**ASRKSTAAL**	ARHG7	9	20%
RAAKETISL	3BP5	9	33%	**EPAVRSSEL**	SH2D3	9	20%
RPAVGHSGL	ZC3H3	9	33%	**EPQPERSSV**	IER5	9	20%
RPNTTSSTGM	WIPF2	10	33%	**GPDHNRSFI**	DHX9	9	20%
RPQKISGNPSL	FOXP1	11	33%	**GPLVRQISL**	ZEP1	9	20%
SPFHRNLFL	WDR34	9	33%	**IPSIRNSILAI**	USP9Y	11	20%
VPEQRTVTL	DEPD5	9	33%	**KAKPVTTNL**	RBIS	9	20%
VPSEPGGVL	PTN6	9	33%	**KPAENDVKL**	UBCP1	9	20%
APKPKWTQL	ALKB6	9	27%	**KPASKKERI**	CHD2	9	20%
APKPRLNQL	SYF1	9	27%	**KPDFKELTV**	RINI	9	20%
APPQIPDTRREL	EAF6	12	27%	**KPEIRVTSL**	PWP2	9	20%
APQPAKPRL	HDAC6	9	27%	**KPGAAMVEM**	HNRPL	9	20%
APRGNVTSL	TLR9	9	27%	**KPGAPLQAF**	DEN1C	9	20%
APRWGNPRAL	OAS1	10	27%	**KPIEPRRELL**	HSH2D	10	20%
APSFGSLVAL	TLR9	10	27%	**KPKPLSQAEM**	AIM2	10	20%
APTIVGKSSL	OST48	10	27%	**KPRVTPVEVM**	PAF1	10	20%
APTPRIKAEL	TLE1/2/4	10	27%	**KPSEERKTI**	ARI5B	9	20%
FPKEPVEL	DPA1	8	27%	**KPYNNHSEM**	DCP2	9	20%
HPKPSEASTTL	IFIX	11	27%	**KVKNVGIFL**	SP16H	9	20%
HPRFLVALI	SAC2	9	27%	**LPAPSWNVL**	OAS2	9	20%
IPVSRPIL	FCRL1	8	27%	**LPRHSFGRNAL**	GBRB2	11	20%
IYSPDHTNNSF	ITF2	11	27%	**LPRPQGAAA**	PSRC1	9	20%
KIRPHIATL	PUM1	9	27%	**MPSSRAYGL**	NCOA3	9	20%
KPGKAPKL	KV133, KV105, KVD33, KV139	8	27%	**NPDWRRLPREL**	RPC7L	11	20%
KPIGGAAEL	VP13B	9	27%	**QPEKSKKEL**	NOL9	9	20%
KPIPLPRF	BLNK	8	27%	**QPFRDRSNTL**	SYNRG	10	20%
KPTDEKLREL	SMC1A	10	27%	**QPSWSIRTAL**	UB2J1	10	20%
KPYHAHKEEM	GLYR1	10	27%	**RAAKKKASL**	FOXO1	9	20%
LPDSDKAIL	CAR11	9	27%	**RPEDQRSSF**	HPS5	9	20%
LPSSHVARL	SMHD1	9	27%	**RPENRAPGAGL**	EMD	11	20%
RPGAHPLSF	UHRF2	9	20%	**SPSLSGLKL**	PRI2	9	20%
RPHTLNSTSM	KMT2D	10	20%	**SVASVLLYL**	PRKDC	9	20%

Sequence	Source protein	Peptide length	Allotype-specific presentation frequency	Sequence	Source protein	Peptide length	Allotype-specific presentation frequency
RPKGLGVFF	VP13D	9	20%	**TPRDLAVPAAL**	PO210	11	20%
RPNLLLGL	PHF3, DIDO1	8	20%	**TPRPGQEL**	ZC12A	8	20%
RPPGGHSNL	SMBT1	9	20%	**TPRPSSPGGL**	RBG1L	10	20%
RPRSNSAWQIYL	MINK1	12	20%	**VPENSRPAT**	SH3L1	9	20%
RVASPKLVM	RTCB	9	20%	**VPNWHRDL**	RAN	8	20%
SLASITVPL	GGA1	9	20%	**VPRSKPLML**	ADNP	9	20%
SPASLARTL	TOX2	9	20%	**VPSKRQEAL**	KTN1	9	20%
SPGGHNRPGTL	GPS2	11	20%	**WASPPGRWL**	PTCA	9	20%
SPISSNSHRSL	BIRC6	11	20%	**YPRSVAVL**	PKHG1	8	20%
SPRSSSRMEERL	P66B	12	20%				

Table S8: HLA class II-restricted CLL-associated antigens

Sequence	Source protein	Peptide length	Freq.	Sequence	Source protein	Peptide length	Freq.
GSSFFGELFNQNPE	CHST2	14	59%	**DDHDAVLRFNGAPTANFQQDVG**	SIAT1	22	27%
SGSSFFGELFNQNPE	CHST2	15	53%	**DYGNFLANEASPL**	VA0D1	13	27%
VQGFESATFLGYFKSG	GELS	16	51%	**GNEFWSALLEKAY**	CAN1/8	13	27%
FPEEFDKTSFHKVR	GNPTA	14	45%	**IPGSSYTVEIFAQVG**	PTPRJ	15	27%
WIGLRWTAYEKINKWT	LY75	16	41%	**KGNFNYIEFTRIL**	ML12A/B	13	27%
GKYFLWVVKFNSLN	GRB2	14	39%	**KPGIVYASLNHSVIG**	BTLA	15	27%
EDHLFRKFHYLPFLPS	DRA	16	37%	**MPGPLPRSLRELHLDHNQISRVPN**	FMOD	24	27%
FQVLKSLGKLAMG	SIAT1	13	37%	**QQRLKSQDLELSWN**	FCER2	14	27%
HHWLLFEMSRHSLE	HG2A	14	37%	**RRWRFTFSHFVVDPD**	I17RA	15	27%
INEFSISSFCTVVD	FMOD	14	37%	**SDMFNYEEYCTANAV**	SPIT2	15	27%
TGSMSIIFFLPLK	PEDF	13	37%	**TDQFSGQHWLWIG**	LY75	13	27%
WNFEKFLVGPDG	GPX1/3/5/6	12	37%	**YPDRPGWLRYIQRTPYSDG**	SGCE	19	27%
HAFFRYIDWEKLERK	KPCB	15	35%	**YPRKNLFLVEVTQLTESDSGVY**	FAIM3	22	27%
IPPFHPFHPFPALPENEDTQPE	APLP2	22	35%	**YPRKNLFLVEVTQLTESDSGVYA**	FAIM3	23	27%
KFLFVREPFERLVS	CHSTB	14	35%	**AKPEASFQVWNKDSSSKNLIPR**	SIAT1	22	25%
LNEDLRSWTAADTAAQITQ	HLAB, HLAC	19	35%	**APIDKKGNFNYIEFTRIL**	ML12A/B	18	25%
SGSSFFGELFNQNPEV	CHST2	16	35%	**DGRRLAVRFTALDLGFG**	LRP10	17	25%
TIQFIQSYFVTDYDPT	RRAS2	16	35%	**DGTFQKWAAVVVPSGEEQ**	HLAA/C/E/G/H	18	25%
ATPLLMQALPMGALPQGPMQ	HG2A	20	33%	**DHAQLVAIKTLKDYNNPQ**	ROR1	18	25%
DNVLYMEIRARLLPV	CECR1	15	33%	**DKNLIKYDLQNLKPY**	PTPRC	15	25%
ETIDWKVFESWM	HG2A	12	33%	**DQFSGQHWLWIGLN**	LY75	14	25%
GPSLLPIMWQLYPDG	TCL1A	15	33%	**DYIALNEDLRSWTAADTAAQITQ**	HLAB, HLAC	23	25%
IKDAMVATFFDIYEDG	TIP	16	33%	**EDLRSWTAVDTAAQ**	HLAE	14	25%
NPPPTIRWFKNDAPVVQ	ROR1	17	33%	**EPDPKGIPEFWFTIFRNVD**	NP1L4	19	25%
SAYKWKETLFSVMPGL	ITIH4	16	33%	**EPNKKFFELVGRTFDWH**	HS3S1	17	25%
TDQFSGQHWLWIGLN	LY75	15	33%	**EQNEIIDDLANLVE**	STX8	14	25%
VPERVYSMNPSIRLL	HS3S1	15	33%	**FGLIKLDLKTKSENG**	VDAC1	15	25%
AEQQRLKSQDLELSWNLNG	FCER2	19	31%	**GDGTFQKWAAVVVPSGEEQR**	HLAA/C/E/G/H	20	25%
DRATWKSNYFLKIIQ	RLA0, RLA0L	15	31%	**GGTFKLELFLPEE**	UBE2N	13	25%
DVLPKYILDFSL	CHSTE	12	31%	**GKSTLINSLFLTDLYSPE**	SEPT7	18	25%
EQNFQWSIYLPSSPE	IGSF3	15	31%	**GKYFLWEEKFNSLNEL**	GRAP	16	25%
FRSYVWDPLLIL	SYS1	12	31%	**GSSFFGELFNQNPEV**	CHST2	15	25%
KSTLINSLFLTDLYSPE	SEPT7	17	31%	**HPAENGKSNFLNCYVSGFHPS**	B2MG	21	25%
LKTIDWVAFAEIIPQ	ATP5H	15	31%	**KRRLNWIQWASL**	S35A5	12	25%
LPHSGDIIATVFAPL	XPR1	15	31%	**LLLILRDPSERVLSDY**	HS3S1	16	25%
MRMATPLLMQALPM	HG2A	14	31%	**LLLWHWDTTQSLK**	FCER2	13	25%
TGRFMWIKFSSDEE	NETO2	14	31%	**LNLKWSRFARVVL**	NRAM2	13	25%
AVRRLIWEKNLKF	CATS	13	29%	**MPGPLPRSLRELHLDHNQISR**	FMOD	21	25%
EQQRLKSQDLELSWNLNG	FCER2	18	29%	**QQRLKSQDLELSW**	FCER2	13	25%
GFMTTAFQYIIDNK	CATS	14	29%	**REIDDHDAVLRFNGAPTANFQQDVG**	SIAT1	25	25%
GGDKKRKGQVIQF	RL36A, RL36L	13	29%	**RFSVIWQLVDRQNRR**	IGSF3	15	25%
GKSTLINSLFLTDLYPE	SEPT2	17	29%	**SGSSFFGELFNQNPEVF**	CHST2	17	25%
GKYFLWVVKFNSL	GRB2	13	29%	**SPSPQDWRDTLFYGVF**	SEM4B	16	25%
IPEFWLTVFKNVD	NP1L1	13	29%	**TKEFQVLKSLGKLAM**	SIAT1	15	25%
LLLWHWDTTQSLKQLE	FCER2	16	29%	**TPQGPPEIYSDTQFPSLQ**	CDV3	18	25%
LLWHWDTTQSLK	FCER2	12	29%	**VPRPYIAARFSVLPPTFHPG**	PTPRS	20	25%
NKGIDSDASYPYK	CATS	13	29%	**VPSRMKYVYFQNNQ**	FMOD	14	25%
QPPDWLQGHYLVVRYEDL	CHST2	18	29%	**AGQPLWPPVFVNL**	I27RA	13	22%
TKQLFEVLHFLAEN	SL9A7	14	29%	**ARLTESLFLDLLG**	IL4RA	13	22%
TPKIQVYSRHPAENGKSNF	B2MG	19	29%	**ARNFERNKAIKVIIAV**	CCR7	16	22%
AEQQRLKSQDLELSWNLNGLQ	FCER2	21	27%	**DGIIMIQTL**	CD79B	9	22%
AGKYFLWVVKFNSL	GRB2	14	27%	**DLEFMNEQKLNRYPA**	TMM59	15	22%
AKFALNGEEFMNFD	FCGRN	14	27%	**DLRSWTAVDTAAQ**	HLAE	13	22%
ATPLLMQALPM	HG2A	11	27%	**DQFSGQHWLWIG**	LY75	12	22%
EDLRSWTAADTAAQITQRKWE	HLAB, HLAC	21	22%	**EGQGFHILIPTIL**	FAIM3	13	20%
EEVVEIDGKQVQQKD	GINM1	15	22%	**EPLVVKVEEGDNAVL**	CD19	15	20%
EFQVLKSLGKLAMG	SIAT1	14	22%	**EQQRLKSQDLELSW**	FCER2	14	20%
GDGLTYNDFLILPG	IMDH2	14	22%	**EQQRLKSQDLELSWNL**	FCER2	16	20%

Sequence	Source protein	Peptide length	Freq.	Sequence	Source protein	Peptide length	Freq.
GDGTFQKWAAVVVPSGEEQ	HLAA/C/E/G/H	19	22%	**FLETHFLDEEV**	FRIL	11	20%
GKKELQVSLFQTL	CUL4B	13	22%	**GLGVTKQDLGPVPM**	HG2A	14	20%
GPLPRSLRELHLDHNQI	FMOD	17	22%	**GPLPRSLRELHLDHNQISRVPN**	FMOD	22	20%
GSSLKILSKGKRGG	CXCR4	14	22%	**GPPIPQNQRFIPINGYPIPPG**	ROR1	21	20%
GTKVVLDDKDYFLFR	CH10	15	22%	**GPPKLDIRKEEKQIMIDIFHPS**	INGR1	22	20%
HFELGGDKKRKGQVIQF	RL36A, RL36L	17	22%	**GVFEWEAFARGTK**	PGK1	13	20%
IGVKFRNDLFKLFK	CCR7	14	22%	**HAFFRYIDWEKL**	KPCB	12	20%
IHEHMVITDRIENIDHLG	ITM2B	18	22%	**HGNQITSDKVGRKV**	FMOD	14	20%
KAVLLGATFLIDYM	PLS3	14	22%	**HWLLFEMSRHSLE**	HG2A	13	20%
KEIHLYQTFVVQLQDPREPR	IL2RG	20	22%	**IGVKFRNDLFKLFKD**	CCR7	15	20%
KFLFVREPFERLVSA	CHSTB	15	22%	**IPTSSFVVDKFAGDIL**	DDX60	16	20%
KQLFEVLHFLAE	SL9A7	12	22%	**ISHPFFNDFTFDYD**	ST14	14	20%
LLWHWDTTQSLKQLE	FCER2	15	22%	**IVSIKTENTDASWNL**	TM87B	15	20%
NPILYAFLGAKFKTSAQHA	CXCR4	19	22%	**KGDDVKFEEFVAYLIDPH**	CHSTB	18	20%
QARNFERNKAIKVIIA	CCR7	16	22%	**KKVLHMDRNPYYG**	GDIA/B	13	20%
QQILHSEEFLSFFD	DC1I2	14	22%	**KPEASFQVWNKDSSSKNLIPR**	SIAT1	21	20%
RLWAWEKFVYLDEK	TCL1A	14	22%	**LATFSTDQELRFVL**	IDD	14	20%
RMATPLLMQALPMGALPQGPM	HG2A	21	22%	**LKNTMETIDWKVF**	HG2A	13	20%
RNLKYLPFVPSRMK	FMOD	14	22%	**LLLLWHWDTTQSLKQ**	FCER2	15	20%
RPGLRDVAYQYVKKG	SSBP	15	22%	**LMQALPMGALPQ**	HG2A	12	20%
RSWTAADTAAQIT	HLAB, HLAC	13	22%	**LPDQSFLWNVFQRVD**	PDCD6	15	20%
SFEPPEFEIVGFT	INAR2	13	22%	**LPGNATISKAGKLPYHH**	PAR14	17	20%
SFKLQTKEFQVLKSL	SIAT1	15	22%	**LWVVKFNSLNEL**	GRB2	12	20%
SFKLQTKEFQVLKSLG	SIAT1	16	22%	**MTIEPSTFLAVPT**	TLR9	13	20%
SMRYFYTAVSRPGRGEPR	HLAC	18	22%	**NKGIDSDASYPYKAM**	CATS	15	20%
SRSYYWIGIRKIGGIW	LYAM1	16	22%	**NKIFLPTIYSIIF**	CXCR4	13	20%
TGSMSIIFFLPLKVT	PEDF	15	22%	**NRRTFETARHNLIIN**	SGCE	15	20%
VAREFGVNVFIVSVAKPIP	COCH	19	22%	**NVFLRHERFERFR**	TOM1	13	20%
VATMNSEEFVLVPQYA	RBG1L	16	22%	**QARNFERNKAIKVII**	CCR7	15	20%
VGSFVGSGLLAL	S15A4	12	22%	**QQRLKSQDLELSWNLN**	FCER2	16	20%
VGYVDDTLFVRFDSD	HLAB	15	22%	**RKLFSSHRFQVII**	HVCN1	13	20%
VKKMMKDNNLVRH	AT2B1/2/3/4	13	22%	**RPAGDRTFQKWAAVVVPSGEEQRYT**	HLAB	25	20%
WNFEKFLVGPD	GPX1/3/5/6	11	22%	**RVTLKQYPRKNLFLV**	FAIM3	15	20%
AGLGRAYALAFAERGAL	DHB4	17	20%	**SDGLNSLTYQVLDVQRYPLY**	B4GT1	20	20%
APLDFRGMLRKLFS	HVCN1	14	20%	**SDLSFSKDWSFYLL**	B2MG	14	20%
ASILATAANLLRHYP	TM127	15	20%	**SELIKIIRRRLQLNAN**	MLP3B/2	16	20%
AVGYVDDTQFVRFDSDA	HLAA/B/C	17	20%	**SFFKISYLTFLPS**	DQA2	13	20%
AYDGKDYIALNEDLRSWTA	HLAA/C/E/G/H	19	20%	**SPNELVDDLFKGAKEHG**	NSF1C	17	20%
DGLNSLTYQVLDVQRYPLY	B4GT1	19	20%	**SPPPEFSFNTPGKNVNPV**	ZNT6	18	20%
DGQKFSVTAYSEWIE	TMEM2	15	20%	**SPSPGVYRLFIQNVAVQDSGTY**	IGSF3	22	20%
DGTFQKWAAVVVPSGE	HLAA/C/E/G/H	16	20%	**SSWYEVDSFTPFR**	INAR1	13	20%
DGTFQKWAAVVVPSGQ	HLAA/B/C	16	20%	**TSADLFLDQTELAAIN**	TICN2	16	20%
DGTFQKWAAVVVPSGQE	HLAA/B/C	17	20%	**VARLSRDATFHYGEQ**	IGSF3	15	20%
DLRSWTAADTAA	HLAB/C/G	12	20%	**VDDTQFVRFDSDAASQRMEPRAPWI**	HLAA	25	20%
DNKGIDSDASYPY	CATS	13	20%	**VGQFIQDVKNSRSTD**	CAND1	15	20%
DPTLDHHWHLWKKTYGKQYKEKNE	CATS	24	20%	**VGRKVFSKLRHLER**	FMOD	14	20%
DQPTIRKENFNNVP	CHP3	14	20%	**VLRFNGAPTANFQ**	SIAT1	13	20%
DRLWAWEKFVYLDE	TCL1A	14	20%	**VNLIEKVASYGVKPRYG**	CFAB	17	20%
DRLWAWEKFVYLDEK	TCL1A	15	20%	**VPRKVIIDDQLPVDHKG**	CAN7	17	20%
DYGIVADLFKVVP	ETFA	13	20%	**VPSRMKYVYFQNNQITSIQ**	FMOD	19	20%
EDYLSVVLNQL	ALBU	11	20%	**YKIVNFDPKLLE**	GL8D1	12	20%

Supplement of Chapter 2

Supplementary Figures

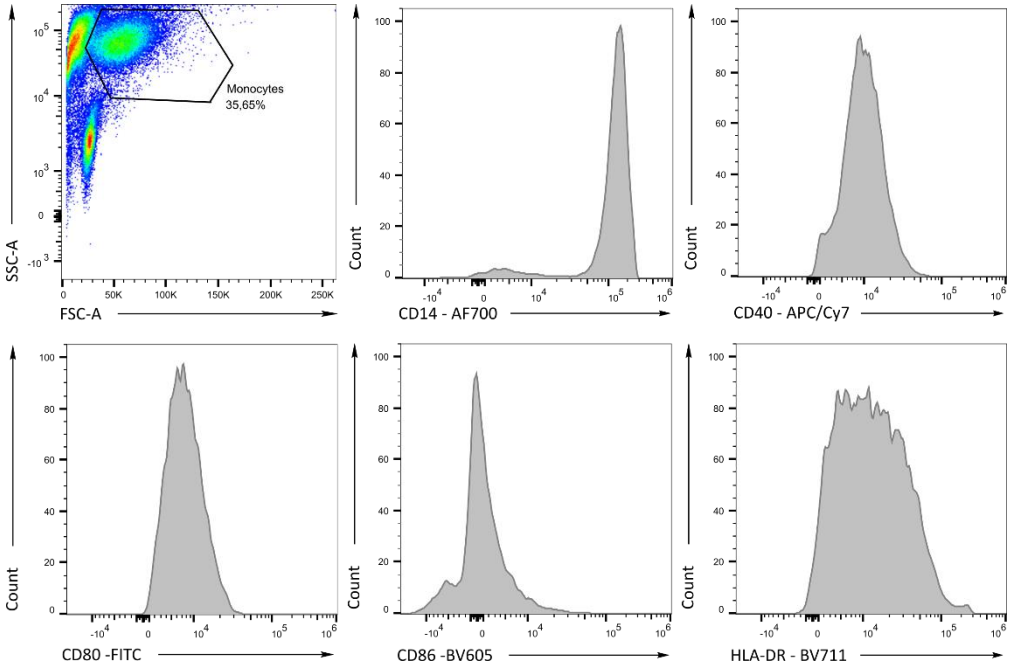

Figure S1: Gating strategy for flow cytometry-based evaluation of surface marker expression on monocyte-derived dendritic cells (MoDCs) on a FACS LSRFortessa. Representative example showing the gating strategy used for the evaluation of flow cytometry-acquired surface marker expression data. The first gate identifies the MoDCs (FSC-A vs. SSC-A), which were further analyzed for the expression of the markers CD14 (CD14-AF700 cs. count), CD40 (CD40-APC/Cy7 vs. count) CD80 (CD80-FITC vs. count), CD86 (CD86-BV605), and HLA-DR (HLA-DR-BV711 vs. count). This gating strategy was applied for the data presented in Fig. 3.

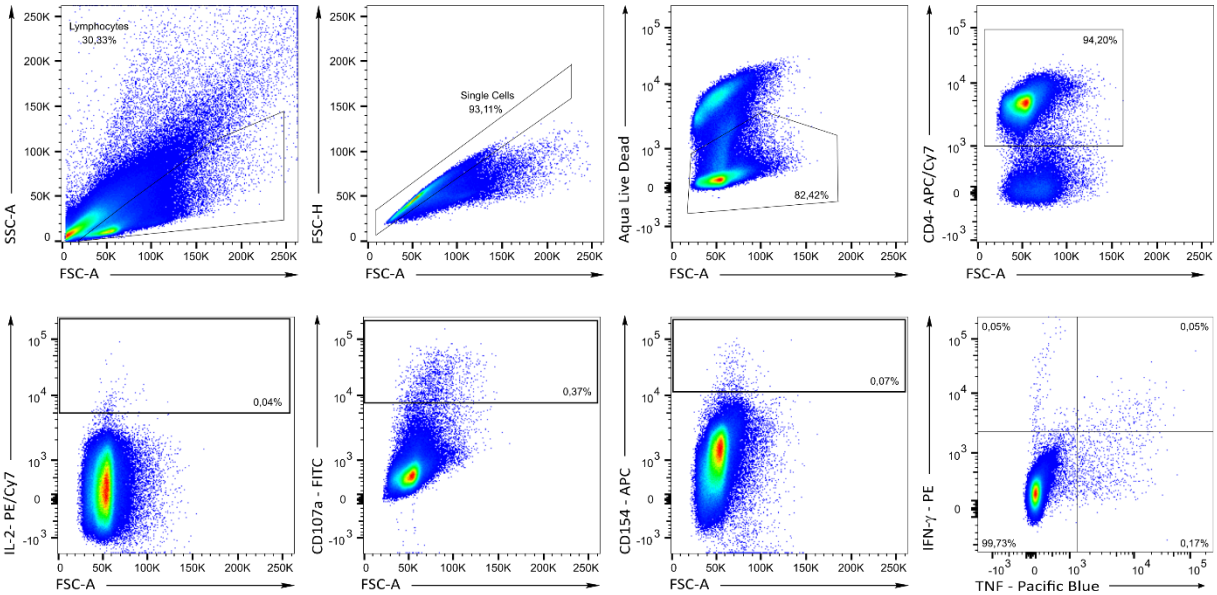

Figure S2: Gating strategy used for intracellular cytokine and cell surface marker staining evaluation of MoDC-based CD4⁺ T cell priming. Exemplary flow-cytometry-based sample analysis showing the gating strategy for the evaluation of intracellular cytokine and surface marker stainings of MoDC-based CD4⁺ T cell priming. The first gate identifies the lymphocytes (FSC-A vs. SSC-A), which are further gated for single cells (FSC-A vs. FSC-H), viable cells (FSC-A vs. Aqua Live Dead), and CD4⁺ cells (FSC-A vs. CD4-APC/Cy7). The CD4⁺ T cell population was analyzed for IL-2 (FSC-A vs. IL-2-PE-Cy7), CD107a (FSC-A vs. CD107a-FITC), CD154 (FSC-A vs. CD154-APC) and TNF as well as IFN-γ (TNF-Pacific Blue vs. IFN-γ-PE) expression and production. This gating strategy was applied for the data presented in Fig. 2, Fig. 4, Fig. 5, Fig. 6, Fig. 8, Fig. 9 Fig. S3 and Fig. S4.

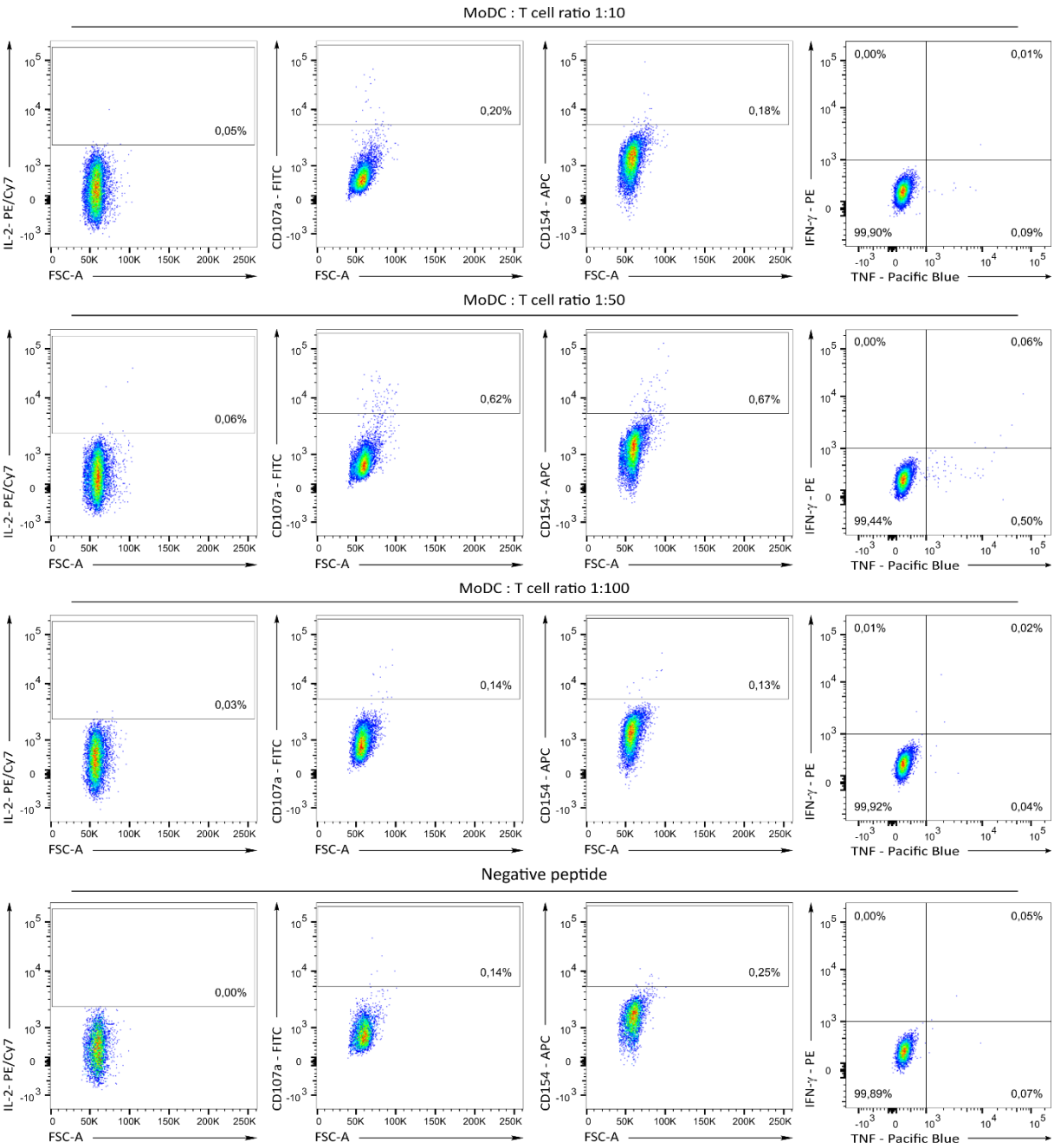

Figure S3: Intracellular cytokine and surface marker staining of a MoDC priming with the peptide KLKKMWKSPNGTIQNILGGTVF using the optimized protocol and 100.000 CD4⁺ T cells. Representative example of the flow cytometry-based analysis of CD4⁺ T cells from a healthy volunteer primed with MoDCs loaded with KLKKMWKSPNGTIQNILGGTVF (upper three panels stimulated with indicated MoDC to T cell ratios) using the optimized priming protocol and using 100.000 CD4⁺ T cells per well in a 96-well plate. The lower panels show the negative controls consisting of KREIFDRYGEEVKEFLAKAKED-primed CD4⁺ T cells stimulated with a negative peptide.

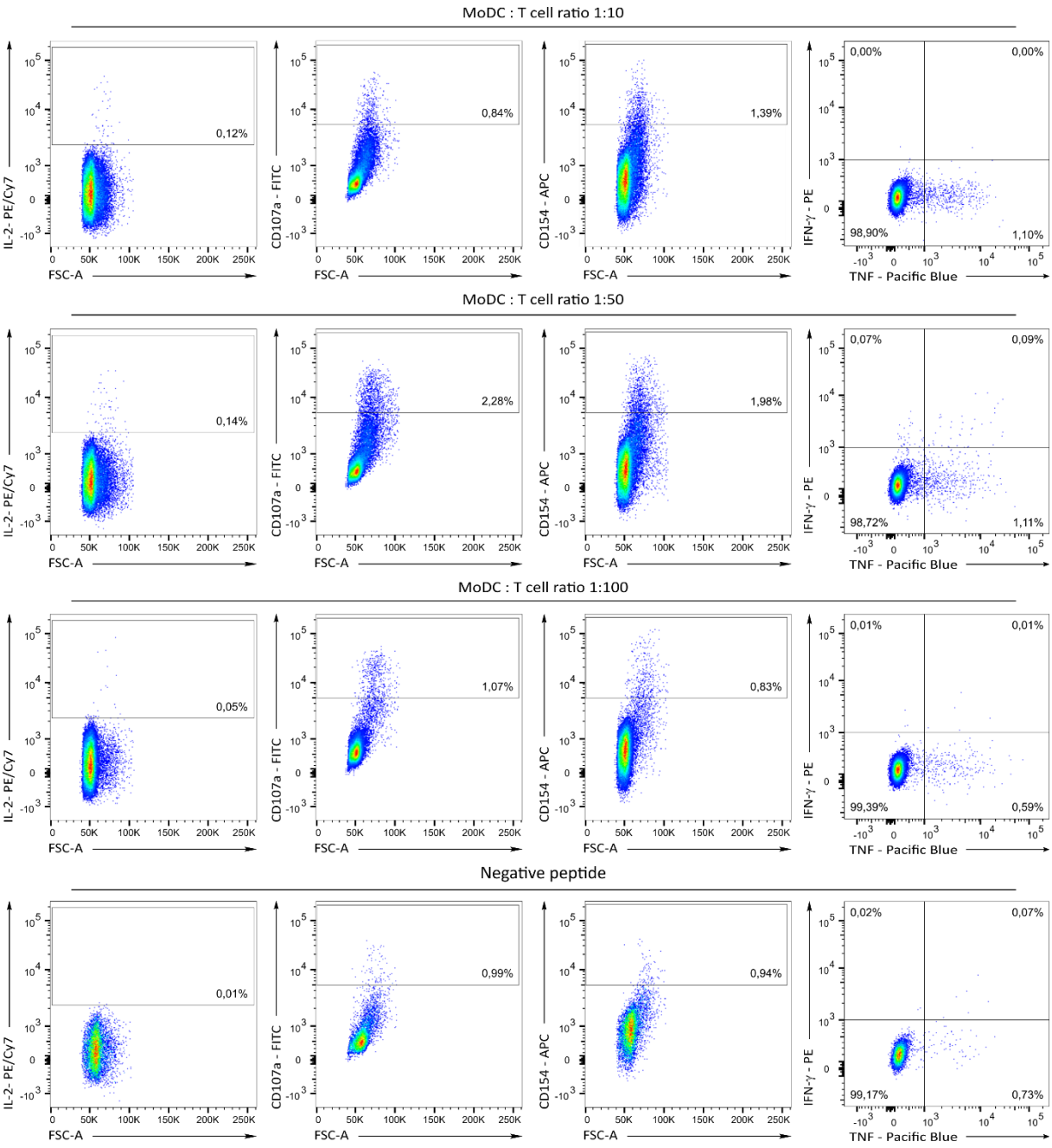

Figure S4: Intracellular cytokine and surface marker staining of a MoDC priming with the peptide KLKKMWKSPNGTIQNILGGTVF using the optimized protocol and 500.000 CD4⁺ T cells. Representative example of the flow cytometry-based analysis of CD4⁺ T cells from a healthy volunteer primed with MoDCs loaded with KLKKMWKSPNGTIQNILGGTVF (upper three panels stimulated with indicated MoDC to T cell ratios) using the optimized priming protocol and using 500.000 CD4⁺ T cells per well in a 96-well plate. The lower panels show the negative controls consisting of KREIFDRYGEEVKEFLAKAKED-primed CD4⁺ T cells stimulated with a negative peptide.

Supplement of Chapter 3

Supplementary Figures

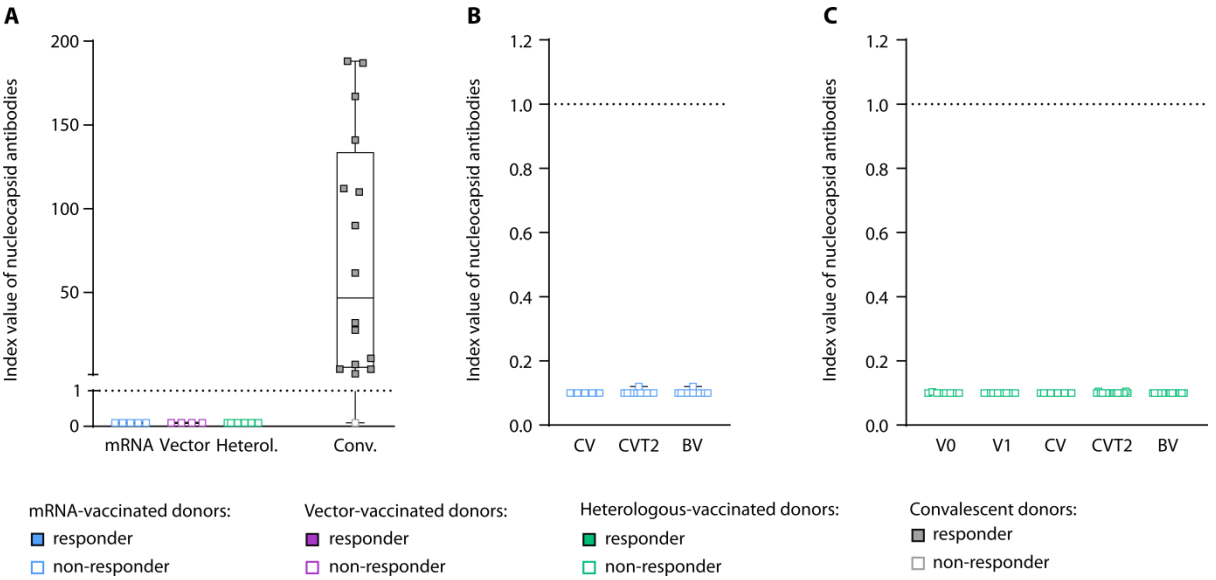

Figure S1: Index values of nucleocapsid antibodies in vaccinated donors. Index values of nucleocapsid antibodies were assessed after complete vaccination (CV) for mRNA- (n = 5), vector- (n = 4) and heterologous- (n = 10) vaccinated donors (**A**), for the mRNA cohort after CV (n = 5), six months after CV (CVT2, n = 11) and after boost vaccination (BV, n = 12) (**B**), as well as for the heterologous cohort before vaccination (V0, n = 8), after first vaccination (V1, n = 8), after CV (n = 10), after CVT2 (n = 17) and after BV (n = 17) (**C**). The dashed line marks the nucleocapsid index value threshold for positivity. Responders are represented by colored symbols, non-responders by clear symbols. Results are represented as box plots showing median with 25th and 75th percentiles, whiskers represent minimum and maximum.

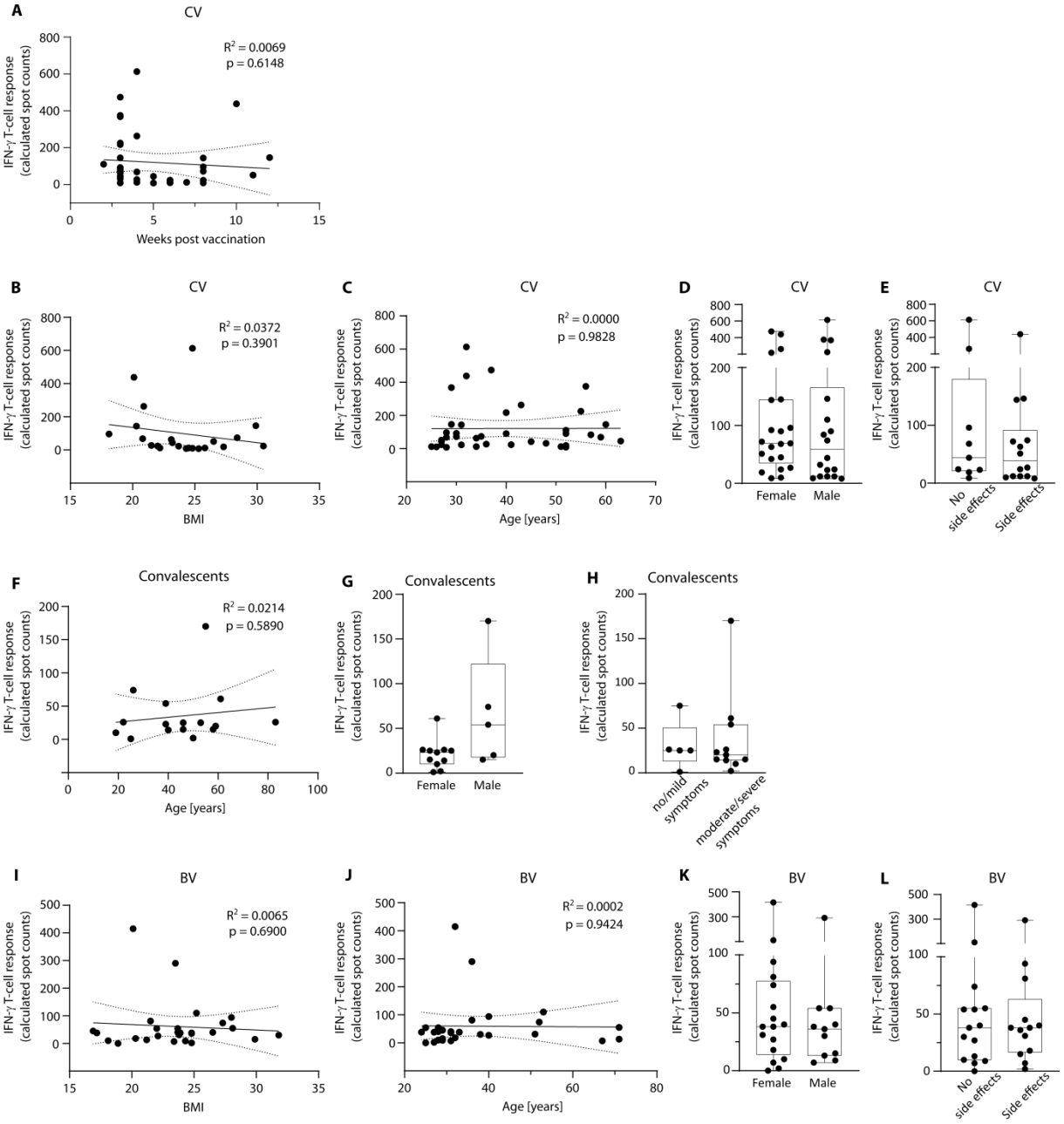

Figure S2: Spike-specific T cell responses after vaccination and in convalescents according to demographics and symptoms. **A-L,** Interferon-gamma (IFN-γ) T cell responses were assessed using *ex vivo* ELISpot assays. Intensities of T cell responses are depicted in terms of calculated spot counts. **A,** Correlation of the intensity of spike-specific IFN-γ T cell responses after complete vaccination (CV, two doses of either BNT162b2 or mRNA-1273, or one dose of the vector vaccine ChAdOx1 followed by one dose of an mRNA vaccine) with time post vaccination (n = 39). **B,C**, Correlation of the intensity of spike-specific IFN-γ T cell responses after complete vaccination (CV) with BMI (**B**, n = 22) and age (**C**, n = 39). **D,E**, Comparison of the intensity of spike-specific IFN-γ T cell responses after CV according to gender (**D**, n = 39) and side effects (headache, fever, shivering) after vaccination (**E**, n = 23). **F**, Correlation of the intensity of spike-specific IFN-γ T cell responses with age for COVID-19 convalescents (n = 16). **G,H,** Comparison of the intensity of spike-specific IFN-γ T cell response in convalescent donors according to gender (**G**, n = 16) and to clinical symptoms (no/mild vs. moderate/severe) during COVID-19 (**H**, n = 16). **I,J**, Correlation of the intensity of spike-specific IFN-γ T cell responses after boost vaccination (BV) with BMI (**I**, n = 27) or age (**J**, n = 28). **K,L**, Comparison of the intensity of spike-specific IFN-γ T cell responses after BV according to gender (**K**, n = 28) and side effects (headache, fever, shivering) after vaccination (**L**, n = 28). **A-C,F,I,J**, dotted lines show the 95% confidence level, R^2

and p value for linear regression are shown. **D,E,G,H,K,L,** box plots show median with 25th and 75th percentiles, whiskers represent minimum and maximum. **D,E,G,H,K,L,** Kruskal-Wallis test was used; if no p values are shown results were not significant.

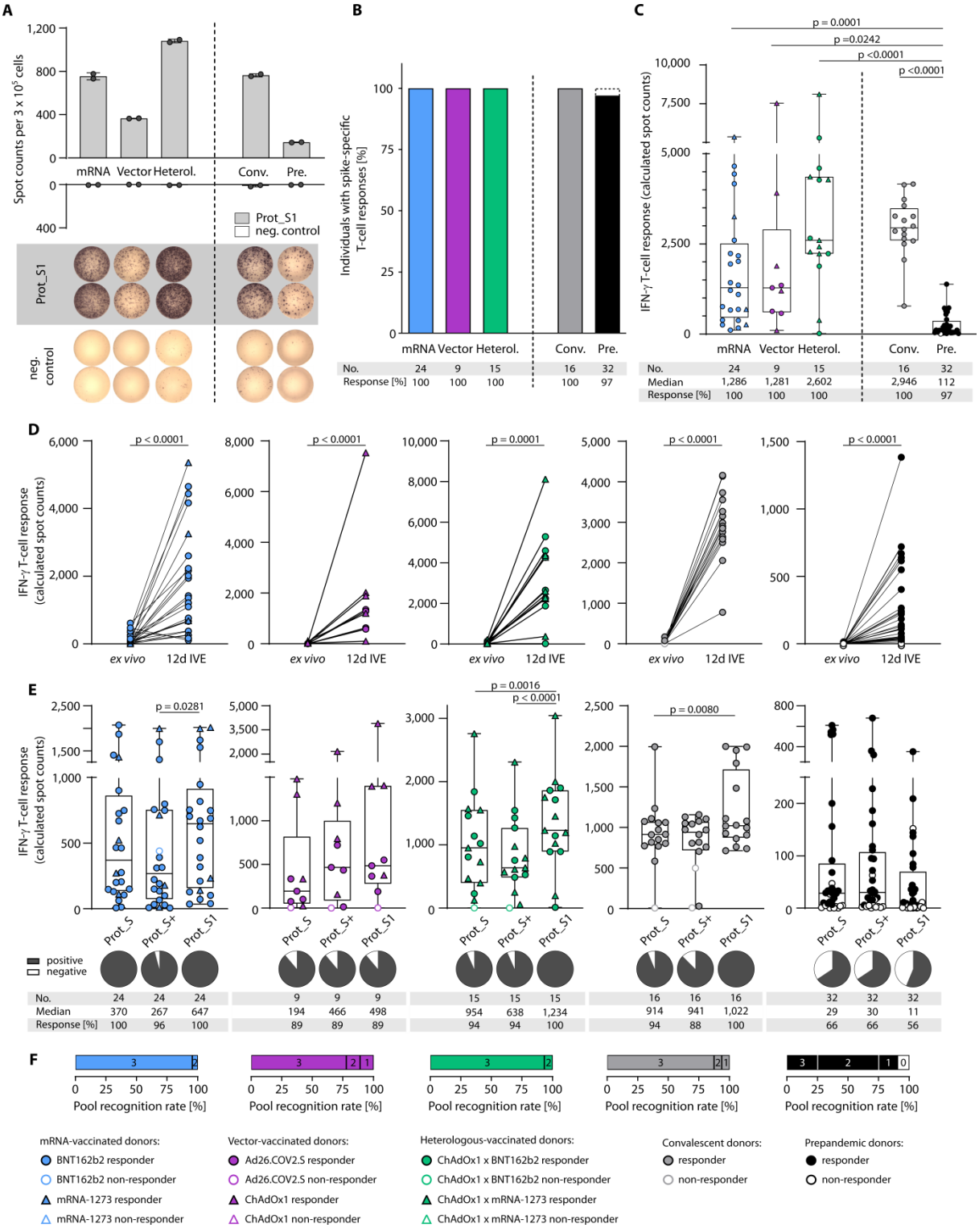

Figure S3: Immune responses to the SARS-CoV-2 spike-specific peptide pools after complete vaccination following 12-day *in vitro* expansion. A, Representative example of interferon-gamma (IFN-γ) T cell responses to the Prot_S1 peptide pool compared to a negative (neg.) control peptide, evaluated by IFN-γ ELISpot following 12-day *in vitro* T cell expansion after complete vaccination (two doses of either BNT162b2, mRNA-1273 or ChAdOx1, one dose of Ad26.COV2.S, or one dose of the vector vaccine ChAdOx1 followed by one dose of an mRNA vaccine for heterologous vaccine regimens), showing the duplicates for one donor of each cohort. **B,C,** Percentage of individuals with IFN-γ T cell responses (**B**), and intensities of T cell responses in terms of calculated spot counts (**C**) targeting the spike peptide pools after 12-day *in vitro* T cell expansion

following mRNA, vector or heterologous (heterol.) vaccination, in comparison to COVID-19 convalescents (Conv.) and prepandemic (Pre.) donors. **D,** Spike-specific IFN-γ T cell responses assessed in the different cohorts *ex vivo* and after 12-day *in vitro* expansion (IVE). **E,** Intensities of IFN-γ T cell response shown separately for the distinct spike-specific peptide pools. **F,** Proportion of individuals with responses to all three, two, one or none of the spike peptide pools. Responders are represented by colored symbols, non-responders by clear symbols. Symbol shapes indicate the different vaccine products received by the donors. In **B,C,** box plots represent median with 25th and 75th percentiles with minimum and maximum whiskers. **B,** Fisher's exact test was used, **C,** Kruskal-Wallis test was used, **D,** Wilcoxon test was applied, **E,** Friedman test was used, if no p values are shown results were not significant.

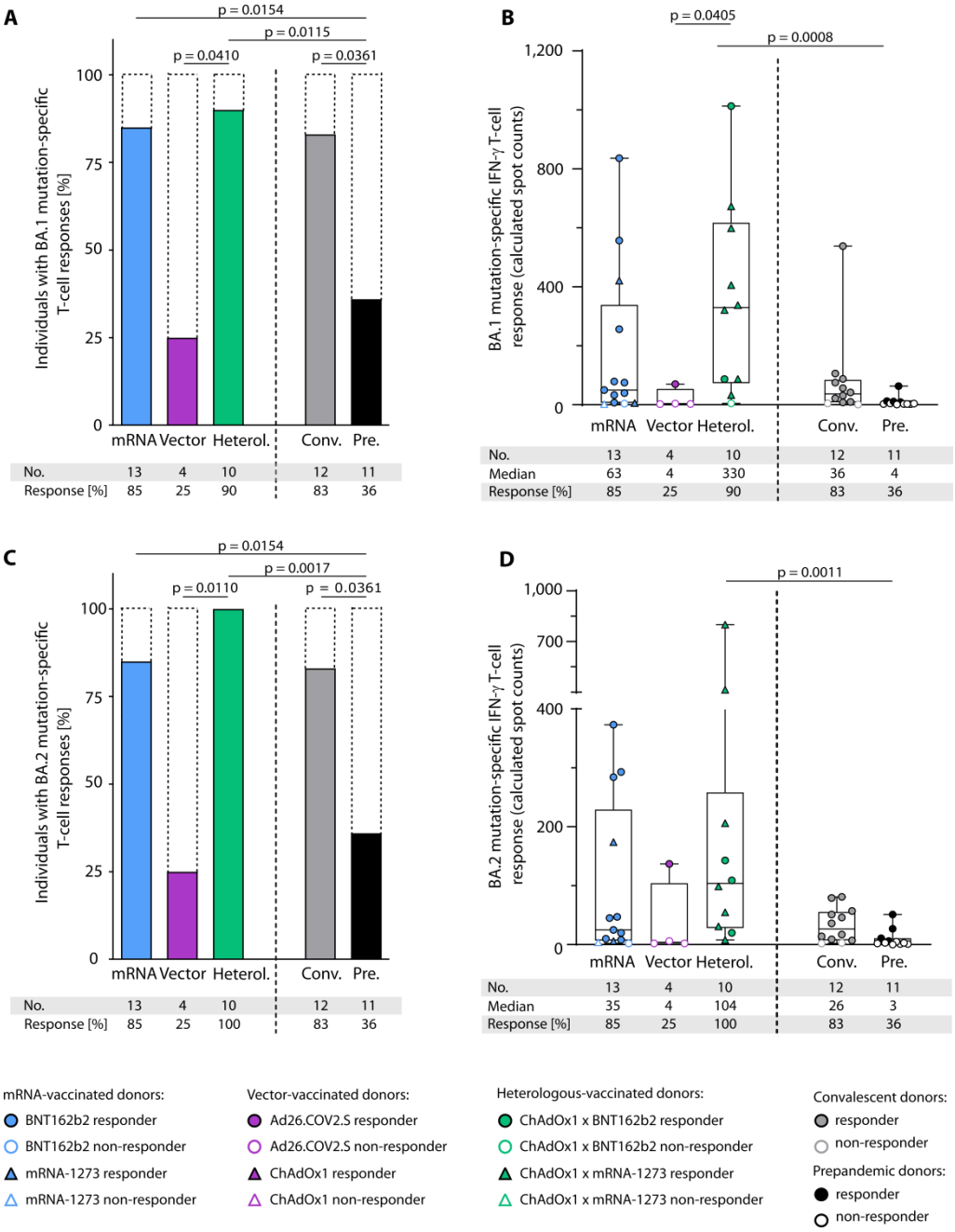

Figure S4: IFN-γ responses to SARS-CoV-2 BA.1 and BA.2 mutation pools following 12-day *in vitro* expansion. A-D, T cell responses after complete vaccination (two doses of either BNT162b2, mRNA-1273 or ChAdOx1, one dose of Ad26.COV2.S, or one dose of the vector vaccine ChAdOx1 followed by one dose of an mRNA vaccine for heterologous vaccine regimens), were assessed by interferon-gamma (IFN-γ) enzyme-linked immunospot (ELISpot) assays after 12-day *in vitro* T cell expansion against the SARS-CoV-2 BA.1 and BA.2 mutation pools. **A,** Percentage of individuals with IFN-γ ELISpot T cell responses after 12-day expansion, and **B,** intensities of IFN-γ T cell responses in terms of calculated spot counts against the spike BA.1 mutation pool, after mRNA, vector or heterologous (heterol.) vaccination, compared to COVID-19 convalescents (Conv.) and prepandemic (Pre.) donors. **C,** Percentage of individuals with IFN-γ ELISpot T cell responses after 12-day T cell expansion, and **D,** intensities of IFN-γ T cell responses in terms of calculated spot counts against the spike BA.2 mutation pool. Responders are represented by colored symbols, non-responders by clear symbols. Symbol shapes indicate the different vaccine products received by the donors. **B,D,** box plots represent the median with 25th and 75th percentiles with minimum and maximum

whiskers. **A,C,** Fisher's exact test was used. **B,D**, Kruskal-Wallis test was used, if no p values are shown results were not significant. No., number.

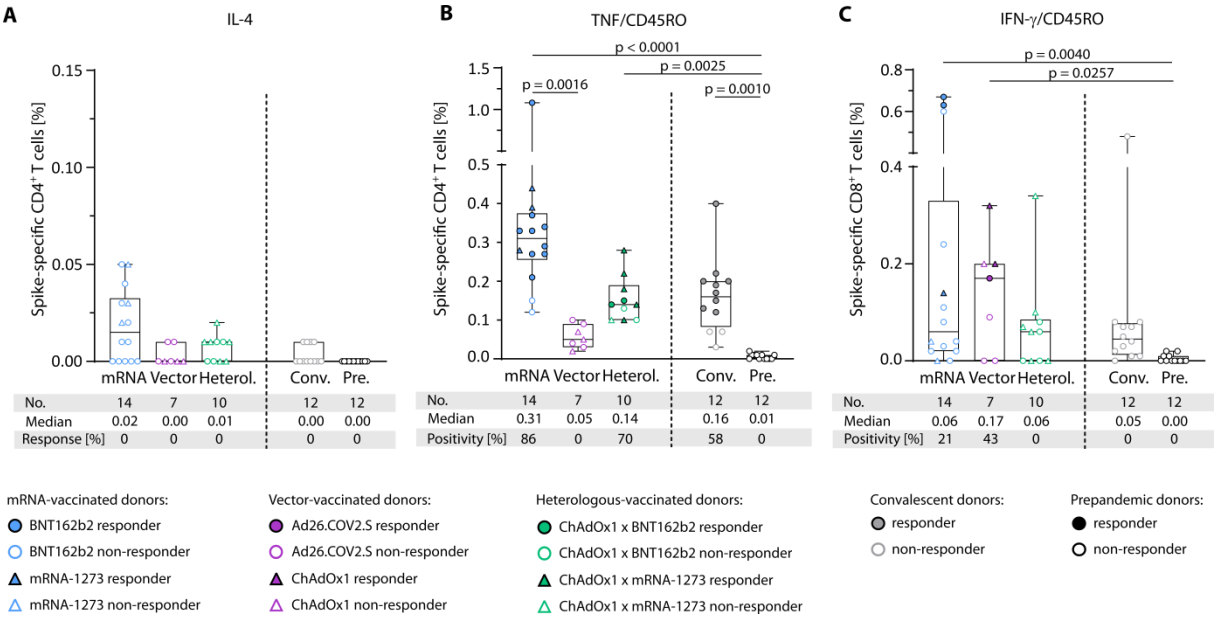

Figure S5: ***Ex vivo*** **characterization of spike-specific T cell responses after complete vaccination. A-C,** Spike-specific T cell responses after complete vaccination (two doses of either BNT162b2, mRNA-1273 or ChAdOx1, one dose of Ad26.COV2.S, or one dose of the vector vaccine ChAdOx1 followed by one dose of an mRNA vaccine for heterologous vaccine regimens) were characterized *ex vivo* by intracellular cytokine (interferon-gamma (IFN-γ), interleukin-4 (IL-4), tumor necrosis factor (TNF)) and surface marker (CD45RO) staining. **A,** Frequency of spike-specific IL-4 expressing $CD4^+$ T cells. **B,** Frequency of $TNF^+CD45RO^+CD4^+$ T cells. **C,** Frequency of $IFN\text{-}\gamma^+CD45RO^+CD8^+$ T cells. T cell responses were considered positive if the detected frequency of cytokine- and surface marker positive $CD4^+$ or $CD8^+$ T cells was ≥ 3-fold higher than the frequency in the negative control and minimum 0.1% of total $CD4^+$ or $CD8^+$ T cells. Responders are represented by colored symbols, non-responders by clear symbols. Symbol shapes indicate the different vaccine products received by the donors. Box plots show the median with 25^{th} and 75^{th} percentiles, whiskers represent minimum and maximum; Kruskal-Wallis test was used, if p values are not shown the results were not significant. FSC, forward scatter; Neg., negative control.

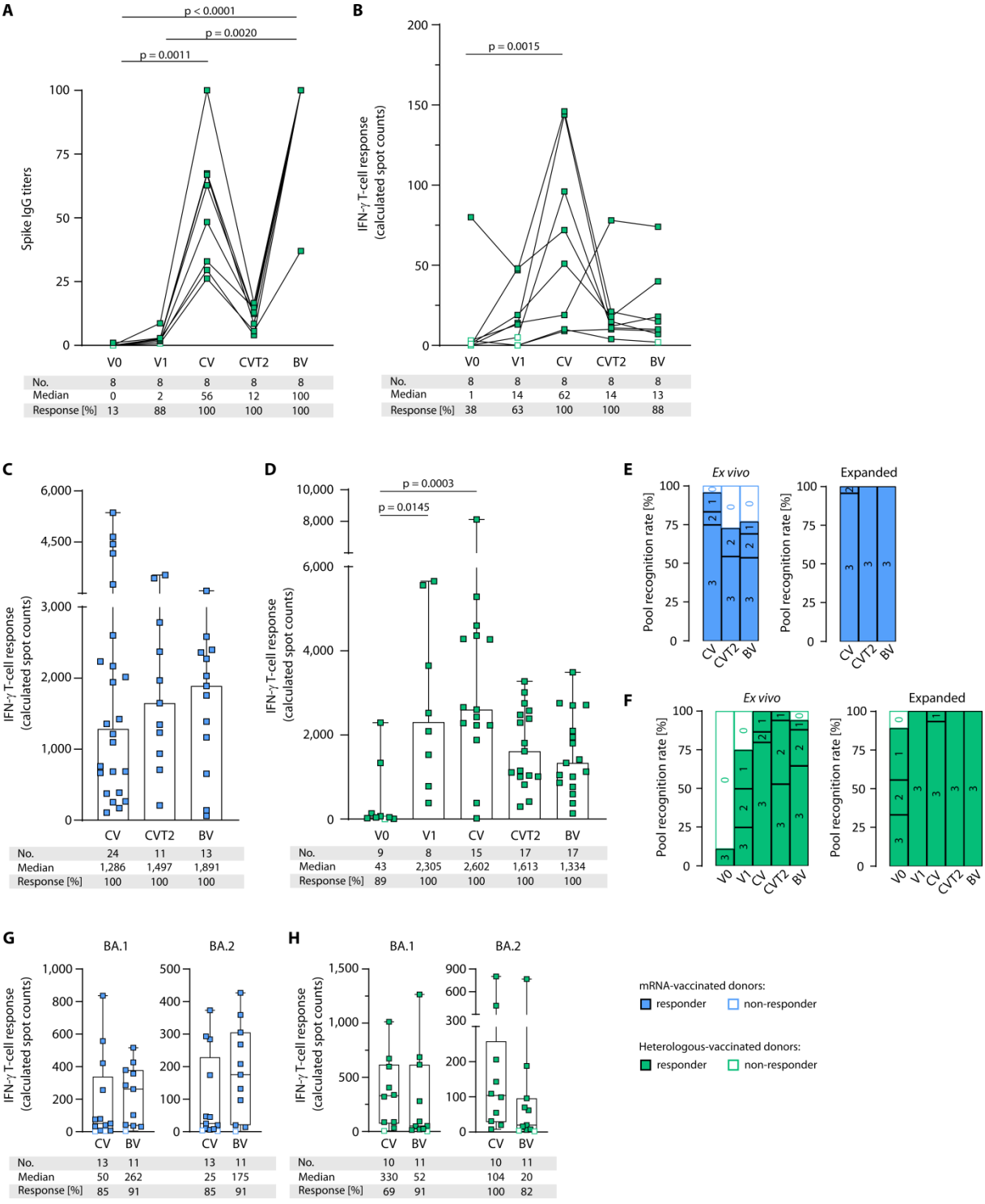

Figure S6: T cell responses following mRNA and heterologous vaccination. A,B, Paired spike antibody titers (**A**), and intensities of *ex vivo* interferon-gamma (IFN-γ) T cell responses in terms of calculated spot counts targeting spike-specific peptide pools (**B**) after heterologous vaccination, either before (V0), one month after first (V1) and complete vaccination (CV), six months after complete vaccination (CVT2) and one month after boost vaccination (BV). **C,D,** Intensity of interferon-gamma (IFN-γ) T cell response against the spike peptide pools after 12-day *in vitro* T cell expansion following mRNA (**C**) and heterologous (heterol.) (**D**) vaccination. **E,F,** Proportion of mRNA- (**E**) or heterologous-vaccinated (**F**) individuals with responses *ex vivo* and after 12-day T cell expansion to all three, two, one or none of the spike peptide pools (Prot_S1, Prot_S+, Prot_S). **G,H,** Intensities of IFN-γ T cell responses against the SARS-CoV-2 BA.1 and BA.2 spike mutation pools, after CV and

BV for mRNA- and heterologous-vaccinated donors, respectively. Responders are represented by colored symbols, non-responders by clear symbols. **A,B,** Data are presented as scatter dot plots with median, whiskers show maximum. **A,B,** Friedman test was used, **C,D,G,H,** Kruskal-Wallis test was used. No., number.

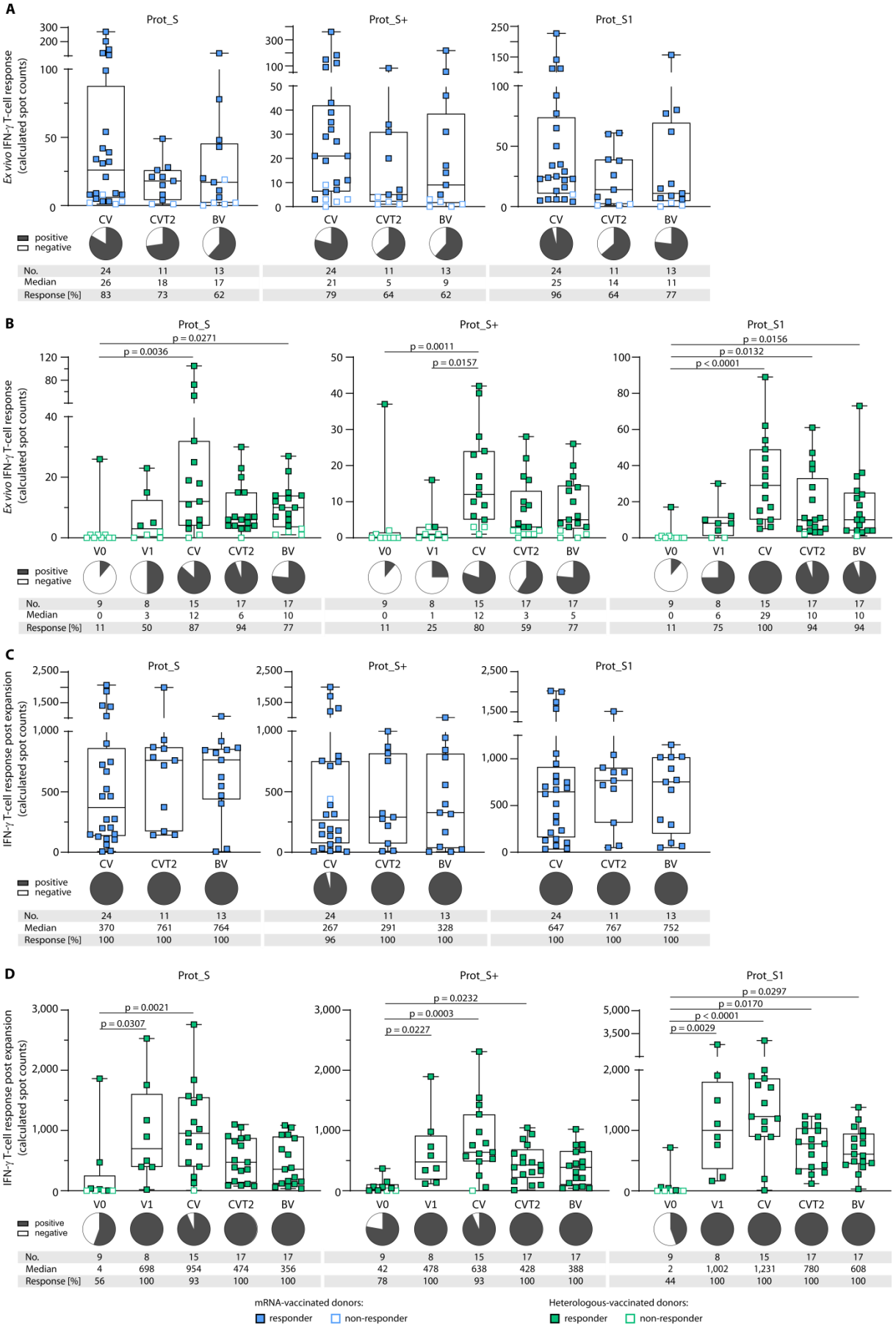
A
Prot_S
Prot_S+
Prot_S1
Ex vivo IFN-γ T-cell response (calculated spot counts)
CV
CVT2
BV
positive
negative
No. 24 11 13 | 24 11 13 | 24 11 13
Median 26 18 17 | 21 5 9 | 25 14 11
Response [%] 83 73 62 | 79 64 62 | 96 64 77
B
Prot_S
p = 0.0271
p = 0.0036
Prot_S+
p = 0.0011
p = 0.0157
Prot_S1
p = 0.0156
p = 0.0132
p < 0.0001
Ex vivo IFN-γ T-cell response (calculated spot counts)
V0
V1
CV
CVT2
BV
positive
negative
No. 9 8 15 17 17 | 9 8 15 17 17 | 9 8 15 17 17
Median 0 3 12 6 10 | 0 1 12 3 5 | 0 6 29 10 10
Response [%] 11 50 87 94 77 | 11 25 80 59 77 | 11 75 100 94 94
C
Prot_S
Prot_S+
Prot_S1
IFN-γ T-cell response post expansion (calculated spot counts)
CV
CVT2
BV
positive
negative
No. 24 11 13 | 24 11 13 | 24 11 13
Median 370 761 764 | 267 291 328 | 647 767 752
Response [%] 100 100 100 | 96 100 100 | 100 100 100
D
Prot_S
p = 0.0021
p = 0.0307
Prot_S+
p = 0.0232
p = 0.0003
p = 0.0227
Prot_S1
p = 0.0297
p = 0.0170
p < 0.0001
p = 0.0029
IFN-γ T-cell response post expansion (calculated spot counts)
V0
V1
CV
CVT2
BV
positive
negative
No. 9 8 15 17 17 | 9 8 15 17 17 | 9 8 15 17 17
Median 4 698 954 474 356 | 42 478 638 428 388 | 2 1,002 1,231 780 608
Response [%] 56 100 93 100 100 | 78 100 93 100 100 | 44 100 100 100 100
mRNA-vaccinated donors:
responder
non-responder
Heterologous-vaccinated donors:
responder
non-responder

Figure S7: Spike-specific peptide pool recognition during the course of mRNA and heterologous vaccination. A-D, Intensities of interferon-gamma (IFN-γ) T cell responses in terms of calculated spot counts *ex vivo* (**A,B**) and after 12-day T cell expansion (**C,D**), reflecting the course of mRNA- (**A,C**) and heterologous (heterol.)-vaccinated (**B,D**) individuals shown for the distinct spike protein peptide pools (Prot_S1, Prot_S+, Prot_S). Responses are shown either before (V0), one month after first (V1) and complete vaccination (CV), six months after complete vaccination (CVT2) and one month after third vaccination (BV). Responders are represented by colored symbols, non-responders by clear symbols. **A-D,** box plots represent the median with 25^{th} and 75^{th} percentiles with minimum and maximum whiskers. **A-D,** Friedman test was used. No., number.

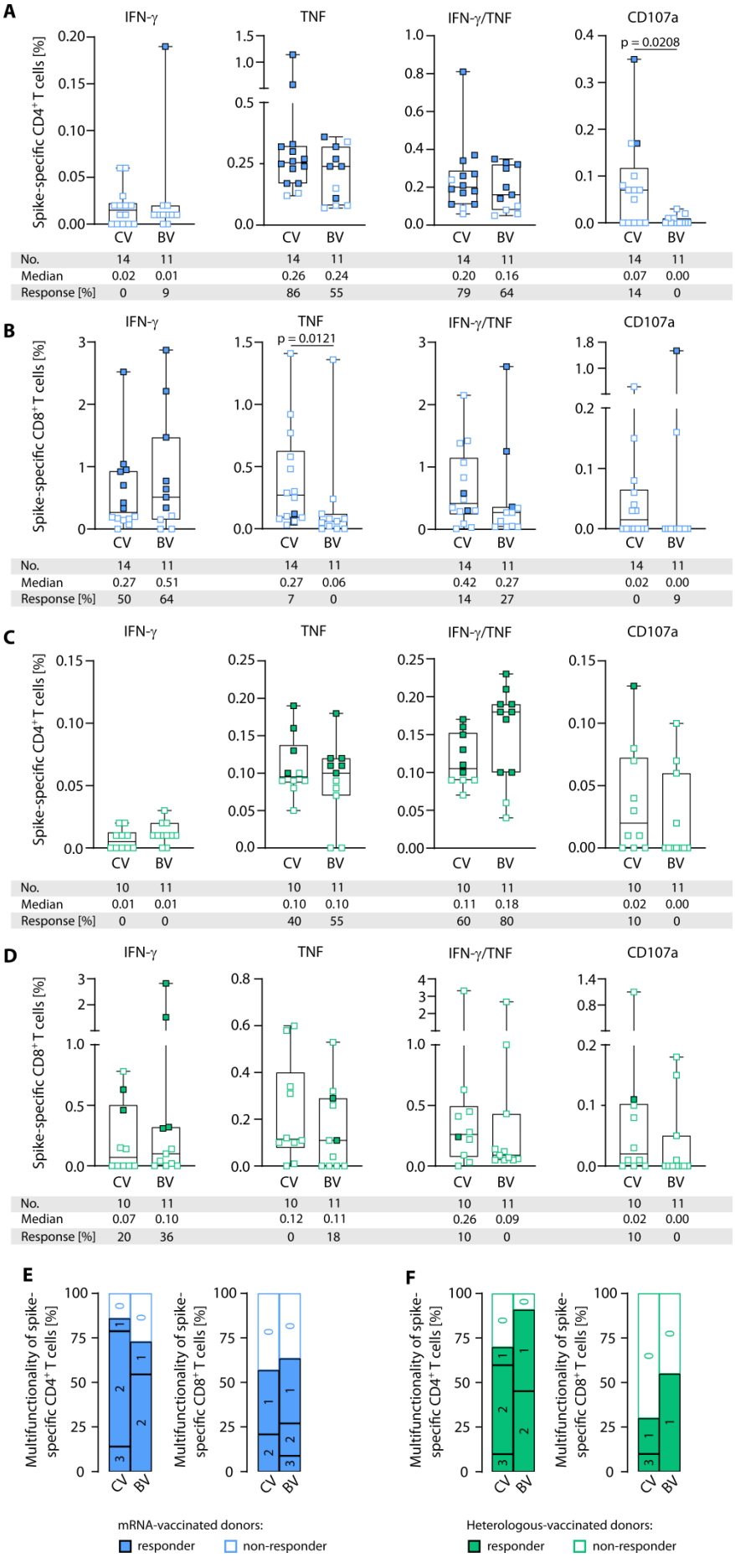
A
IFN-γ
TNF
IFN-γ/TNF
CD107a
Spike-specific CD4+ T cells [%]
p = 0.0208
CV BV
No. 14 11 14 11 14 11 14 11
Median 0.02 0.01 0.26 0.24 0.20 0.16 0.07 0.00
Response [%] 0 9 86 55 79 64 14 0
B
IFN-γ
TNF
IFN-γ/TNF
CD107a
Spike-specific CD8+ T cells [%]
p = 0.0121
CV BV
No. 14 11 14 11 14 11 14 11
Median 0.27 0.51 0.27 0.06 0.42 0.27 0.02 0.00
Response [%] 50 64 7 0 14 27 0 9
C
IFN-γ
TNF
IFN-γ/TNF
CD107a
Spike-specific CD4+ T cells [%]
CV BV
No. 10 11 10 11 10 11 10 11
Median 0.01 0.01 0.10 0.10 0.11 0.18 0.02 0.00
Response [%] 0 0 40 55 60 80 10 0
D
IFN-γ
TNF
IFN-γ/TNF
CD107a
Spike-specific CD8+ T cells [%]
CV BV
No. 10 11 10 11 10 11 10 11
Median 0.07 0.10 0.12 0.11 0.26 0.09 0.02 0.00
Response [%] 20 36 0 18 10 0 10 0
E
Multifunctionality of spike-specific CD4+ T cells [%]
Multifunctionality of spike-specific CD8+ T cells [%]
CV BV
mRNA-vaccinated donors:
responder
non-responder
F
Multifunctionality of spike-specific CD4+ T cells [%]
Multifunctionality of spike-specific CD8+ T cells [%]
CV BV
Heterologous-vaccinated donors:
responder
non-responder

Figure S8: Characterization of *ex vivo* spike-specific T cell responses following complete and booster vaccination with mRNA and heterologous vaccination regimens. Frequencies of spike-specific $CD4^+$ (**A**) and $CD8^+$ (**B**) T cells following complete vaccination (CV , two doses of either BNT162b2 and mRNA-1273) (one dose of the vector vaccine ChAdOx1 followed by one dose of an mRNA vaccine for heterologous vaccine regimens) and boost (BV) mRNA vaccination. Frequencies of spike-specific $CD4^+$ (**C**) and $CD8^+$ (**D**) T cells following CV (one dose of the vector vaccine ChAdOx1 followed by one dose of an mRNA vaccine) and BV with the heterologous vaccination regimen. Frequencies were assessed *ex vivo* by intracellular cytokine (interferon-gamma (IFN-γ), tumor necrosis factor (TNF)) and surface marker (CD107a) staining. T cell responses were considered positive if the detected frequency of cytokine-positive $CD4^+$ or $CD8^+$ T cells was ≥ 3-fold higher than the frequency in the negative control and at least 0.1%. Responders are represented by colored symbols, non-responders by clear symbols. **A-D,** box plots show median with 25^{th} and 75^{th} percentiles, whiskers represent minimum and maximum. No., number.

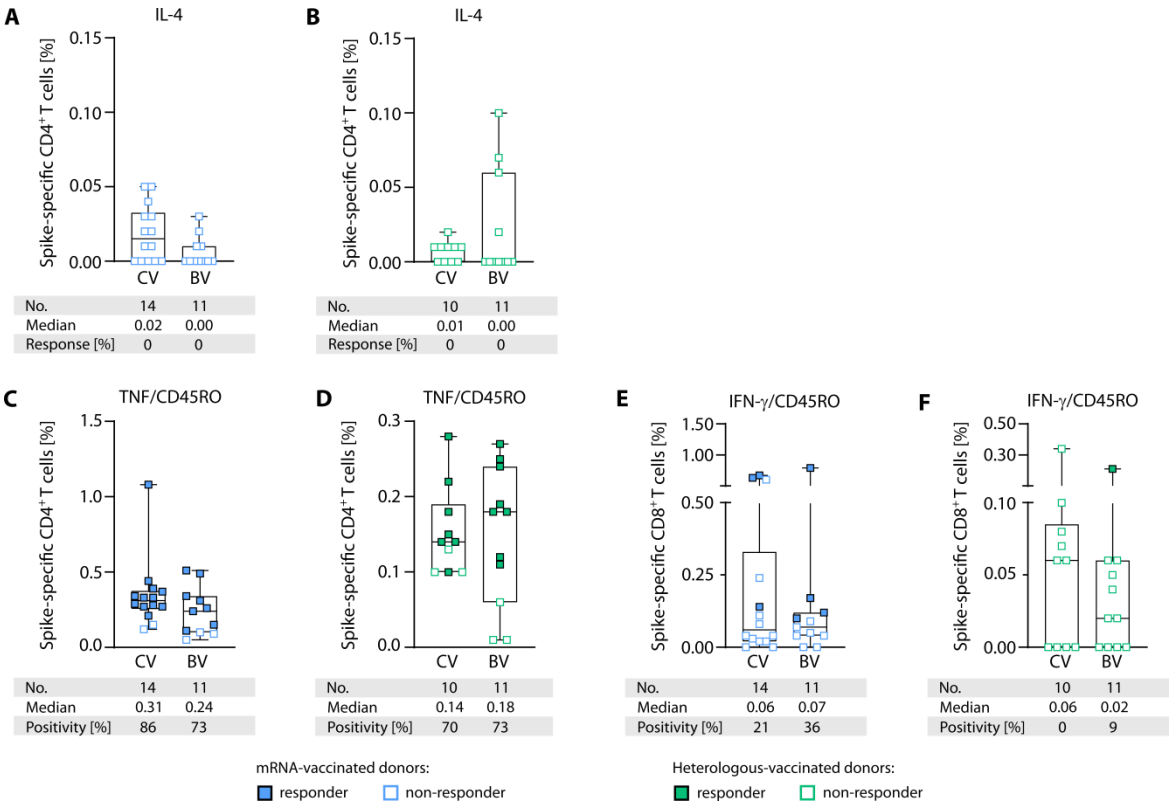

Figure S9: Characterization of *ex vivo* spike-specific T cell responses after complete vaccination. A,B, Frequencies of spike-specific IL-4 expressing $CD4^+$ T cells after complete vaccination (CV) and boost vaccination (BV) assessed *ex vivo* using intracellular cytokine and surface marker staining for mRNA- and heterologous-vaccinated donors, respectively. **C,D,** Frequency of $TNF^+CD45RO^+CD4^+$ T cells for mRNA- and heterologous-vaccinated donors, respectively. **E,F,** Frequency of IFN-$\gamma^+CD45RO^+CD8^+$ T cells for mRNA- and heterologous-vaccinated donors, respectively. T cell responses were considered positive if the detected frequency of cytokine- and surface marker positive $CD4^+$ or $CD8^+$ T cells was ≥ 3-fold higher than the frequency in the negative control and at least 0.1% of total $CD4^+$ or $CD8^+$ T cells. Responders are represented by colored symbols, non-responders by clear symbols. **A-F,** box plots show the median with 25th and 75th percentiles, whiskers represent minimum and maximum. **A-F,** Kruskal-Wallis test was used. FSC, forward scatter; Neg., negative control.

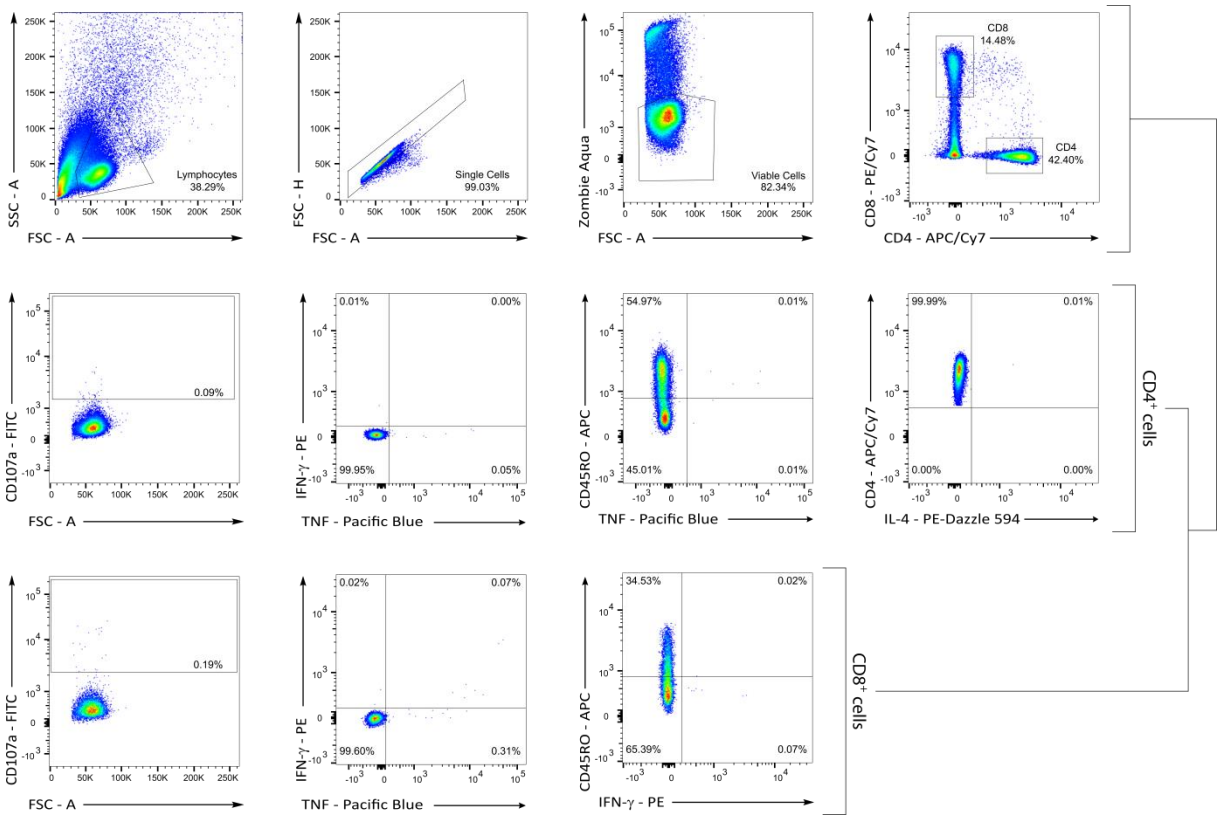

Figure S10: Gating strategy for *ex vivo* flow cytometry-based evaluation of surface marker and intracellular cytokine staining on a FACS LSRFortessa. Representative example showing the gating strategy for the evaluation of flow cytometry-acquired surface marker and intracellular cytokine staining *ex vivo* data. The first gate identifies the lymphocytes (FSC-A vs. SSC-A), which are further gated for single cells (FSC-A vs. FSC-H) and viable cells (FSC-A vs. Zombie Aqua). Populations of $CD4^+$ and $CD8^+$ T cells (CD4-APC/Cy7 vs. CD8-PE/Cy7) are analyzed separately for the degranulation marker CD107a (FSC-A vs. CD107a-FITC) and different cytokines (TNF-Pacific Blue vs. IFN-γ-PE; CD45RO-APC vs. TNF-Pacific Blue (only $CD4^+$ cells); CD4-APC/Cy7 vs. IL-4-PE-Dazzle 594 (only $CD4^+$ cells), CD45RO-APC vs. IFN-γ-PE (only $CD8^+$ cells)). This gating strategy was applied for the data presented in Fig. 3, Fig. 4G-L, Fig. S8 and Fig. S9A,B.